The University of Nottingham
Department of Civil Engineering
Nottingham Transportation Engineering Centre

Influence of Specimen Size and Orientation on the Mechanical Properties of Laboratory Compacted Asphalt Specimens

by

Masahiko Iwama

Thesis submitted to the University of Nottingham
for the degree of Master of Philosophy

July 2009

Abstract

It is always desirable for laboratory compaction to simulate actual site compaction in terms of the volumetric proportions, aggregate structure and mechanical properties of the compacted asphalt mixture, when specimens are manufactured, especially for mixture design. However, finding a laboratory compaction method that is able to achieve this requirement for all asphalt mixture types is in most cases extremely difficult. Some of the reasons for this lack of agreement between site and laboratory compaction include the influence of laboratory factors such as specimen geometry and size, mould confinement and compaction mechanism. Therefore, this study examines the effect of these factors on the volumetric proportions, aggregate matrix and mechanical properties of a typical UK continuously graded asphalt mixture with a maximum aggregate size of 28 mm.

Three types of laboratory asphalt mixture compaction (i.e. gyratory, vibratory and slab) were used to compact either 150 mm diameter cylindrical specimens or 300 mm by 300 mm slabs both to a height of 100 mm. Then, the volumetric proportions and mechanical properties were determined on the 150 mm diameter cylinders and 150 mm diameter cores taken from the slabs; and these proportions compared to those obtained on 100 mm diameter specimens cored from the original 150 mm specimens or cored directly from slabs. In addition, image analysis technique were applied to investigate the internal aggregate structure of these specimens as a function of compaction method, specimen size and specimen orientation.

The results proved that specimen size, especially for mould based compaction methods such as gyratory and vibratory, has a significant effect on volumetric proportions, aggregate orientation and mechanical properties. Also, slab specimens cored from the three orthogonal directions showed significant variation in mechanical properties. The reason for change in mechanical properties between the mould based 150 mm and cored 100 mm diameter specimens were related in part to change in combined effects such as aggregate volumetric composition, orientation and segregation. Finally, the image analysis results indicated that the variation in mechanical properties for the three orthogonal slab specimens may be associated with particle segregation.

Acknowledgements

This research project would not have been completed without the support of many people. In particular, I would like to thank the following people and organisations:

First and foremost, I gratefully acknowledge the supervision provided by Professor Gordon Airey. Gordon has always encouraged and supported my research work, even on his sabbatical term in the United States. He has gone out of his way to make pavement engineering materials interesting to a relatively inexperienced Civil Engineer. In addition, he has constantly been on hand to provide guidance and advice through e-mails and telephone calls, and helped me prepare for conference presentation. I am very fortunate to have met such a good supervisor in Nottingham.

Secondly, without the assistance provided by the staff and technicians at Nottingham Transportation Engineering Centre, NTEC (former NCPE), I could not have conducted the laboratory testing and analysis. Their excellent work has made the NTEC a world leader in pavement engineering research. I am particularly grateful to Dr. Alistair Hunter whose development of Image Analysis Methodology was used in this research. Without his work, I could not have fully appreciated the essence of compaction work in asphalt mixtures. My thanks also go to my friends, Jay (Sanjaya) and Jed (Jiantao Wu). I will never forget the time I spent with them at both the NTEC and school.

Thirdly, I am grateful to the members of NIPPO Corporation for giving me the opportunity to study and conduct research in both the UK and Japan. Without their assistance, I could not have continued this study.

Also, I am most grateful to the International Road Federation (IRF) and Japan Road Association which provided me with a one-year fellowship and funding.

Last, but not least, I would like to say a big “thank you” to my parents for their love and encouragement. Without their support, I could not have met such wonderful people from all parts of the world.

Declaration

The work described in this thesis was conducted at the University of Nottingham, School of Civil Engineering between July 2005 and September 2006. I declare that the work is my own and has not been submitted for a degree of another university.

Table of Contents

Page

List of Figures

List of Tables

List of Pictures

CHAPTER 1

Introduction

1.1 BACKGROUND

Compaction is one of the major parts of pavement construction and has a direct effect on pavement life and performance. In addition, compaction is important in the laboratory where many kinds of compaction equipment are used to manufacture asphalt mixture specimens. However, research has shown that different compaction methods produce specimens with different mechanical properties. Brown and Gibb (1999) carried out mechanical testing using specimens which were compacted using different types of compaction method and showed differences in the permanent deformation characteristics of the specimens. However, it was not understood why these differences occurred and which factors affect mechanical properties.

Hunter et al. (2004) investigated aggregate orientation and segregation of laboratory compacted asphalt mixture samples by using image analysis to look at aggregate orientation within the cross sections of samples. As a result of image analysis, it was found that circumferential particle orientation occurred in mould

based compaction methods such as gyratory and vibratory. Moreover, in terms of segregation, there were some remarkable differences between each compaction method. However, the relationship between mechanical property and aggregate orientation was not understood. To look at these relationships in more detail, it is required to investigate the influence of specimen geometry size and orientation. By looking at these properties, the relationship between aggregate orientation and mechanical properties will be made clearer. The aim of this study is therefore to compare three laboratory compaction methods and to identify the differences of aggregate orientation as a function of changing specimen size and orientation for each compaction method.

1.2 SCOPE OF PROJECT

This thesis consists of seven parts. In Chapter 2, a literature review related to the general area of laboratory compaction will be presented. Firstly, laboratory compaction methods will be introduced and explained followed by a description of mechanical property tests used to evaluate of compacted asphalt samples. Thirdly, the internal structure of asphalt mixtures will be described based on previous research in this area and an evaluation method for aggregate orientation will be introduced. Finally, the research methodology for this project will be presented.

Preparation work for the experiment part of the work, such as mix design, mixing and measurement of density is highlighted in Chapter 3. Moreover, specimen manufacture using the three compaction methods will be described. Trimming

techniques for asphalt mixture specimens needed for mechanical testing will be presented and, finally, the results of measurement of density and air void content for all of specimen will be highlighted.

Results of mechanical testing will be discussed in Chapter 4. The Nottingham Asphalt Tester (NAT) was used to perform the Indirect Tensile Stiffness Modulus (ITSM) and Repeated Load Axial (RLA) tests to compare the differences in terms of mechanical property between asphalt mixtures as a function of specimen size and orientation. The influence of specimen size related to mechanical properties was analysed using 150 mm and 100 mm diameter specimens.

Image analysis techniques were used to analyze the internal structure of asphalt mixture specimens. These procedures and techniques used to quantify the images will be shown in Chapter 5.

Chapter 6 will concentrate on particle orientation and discussion on observed mechanical properties of asphalt specimens will be presented together with a comparison of the results from the image analysis. Chapter 7 will address the issue of aggregate distribution and segregation with the relationship between mechanical properties and image analysis being highlighted in these two chapters.

Finally, Chapter 8 will provide a summary of the main findings and conclusions from the study and recommendations for further research.

CHAPTER 2

Literature Review

2.1 INTRODUCTION

Many studies related to asphalt mixture compaction have been carried out over the years. This literature review provides information on various laboratory compaction methods, mechanical testing of asphalt mixtures and the evaluation of the internal structure of asphalt mixtures. The chapter is divided into the following sections:

- Laboratory compaction methods
- Mechanical testing of asphalt mixtures
- Measurement of aggregate matrix
- Internal structure of asphalt mixture
- Research methodology

2.2 LABRATORY COMPACTION METHODS

2.2.1 Gyratory Compactor

Gyratory compaction is used to manufacture asphalt mixture specimens. In general, the gyratory compactor has been widely used in practice. Harman (2002) stated that 2000 gyratory compacters, which were specified by U.S. Strategic Highway Research Program (SHRP) project, have been applied to both mixture design and site control. Also, according to the Asphalt Institute (2007), the gyratory compactors, which were manufactured in Texas, enable simulation of actual compaction conducted in the field.

Using a gyratory compactor, compaction is governed by three major factors: vertical pressure, angle of gyration and gyratory speed (Figure 2.1). In order to achieve 4% air voids with the SHRP gyratory compacter, vertical pressure, angle of gyration and gyratory speed were specified as 1.25°, 0.6 MPa and 30 revolutions per minutes, respectively. However, Brown et al. (1996) recommended that a different gyratory level should be specified to achieve 4% air voids. Bucher (1998) investigated these three factors and found that air void content of the specimen decreased significantly as vertical pressure increased. However, rotational speed has no effect on void content. In addition, he recommended that angle of gyration in the range of two degrees or above, is applied because compaction state was less sensitive within this range, and the vertical pressure should be within the range of 400 kPa to 600 kPa.

Masad et al. (1999, 2004) examined the difference in air voids distribution between Superpave Gyratory Compacted (SGC) specimen and Linier Kneading Compacted (LKC) specimen. Through image analysis, they found that compaction within the

middle part of the SGC specimen is consistent compared with the top and bottom parts (Figure 2.2). Alternatively, other types of compaction namely the LKC specimen showed non-uniform void distribution. The percent void content at the top is lower than at the bottom which means that the top part is compacted more than the bottom. Gyratory compaction can therefore be considered to produce asphalt mixture specimens having relatively uniform air-void distribution.

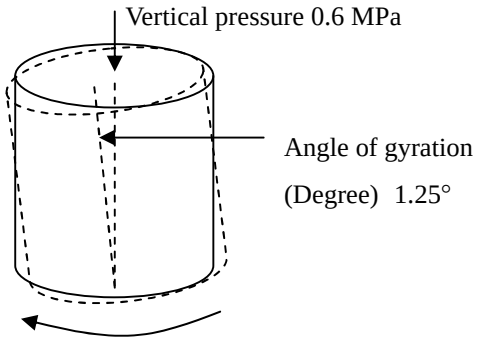

Figure 2.1: Schematic diagram of gyratory motion (after Read and Whiteoak 2003)

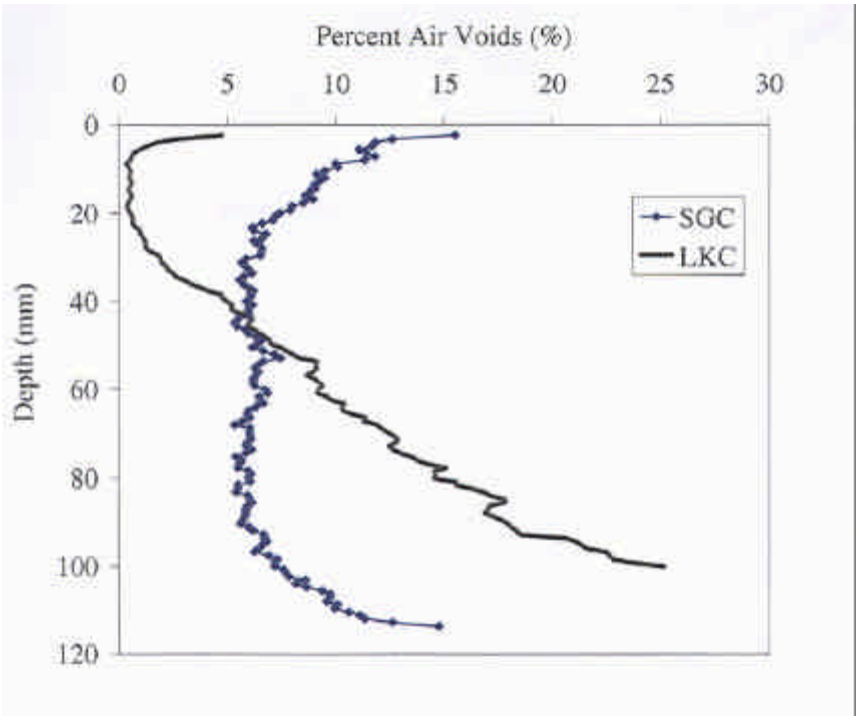

Figure 2.2: Distribution of void content in gyratory compacted specimen (Masad et al. 1999, 2004)

2.2.2 Vibratory Compactor

Vibratory compaction is also used to produce laboratory asphalt mixture specimens. Cooper et al. (1985, 1991) used a vibratory hammer to develop the new Hot-Mix Asphalt mixture design method, which aims to be more efficient than previous methods. The vibratory hammer was applied as a compaction method in the Percentage Refusal Density test (Figure 2.3). From their research, it was found that the specimens manufactured by the percentage density equipment were similar to cores taken from field, in terms of density. In addition, Brown and Gibb (1999) suggested that the use of the vibrating hammer is a very effective way to simulate actual site compaction, although values of permanent deformation are lower than actual site cores. Hunter et al. (2004) described that the vibrating hummer is often used in place of the Marshall compactor because it is easier to achieve target bulk density and void contents.

However, the disadvantage of this compaction method is that the quality of compaction depends on the operator.

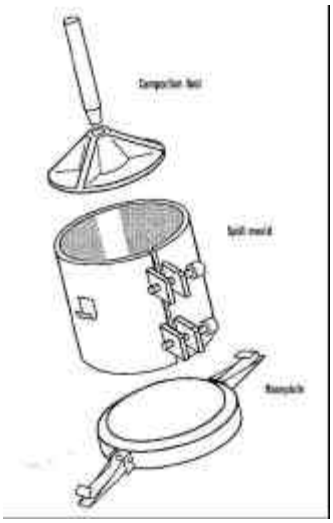

Figure 2.3: Schematic of vibratory compactor (Brown et al. 1991)

2.2.3 Slab 'Roller' Compactor

To make slab type specimens, slab 'roller' compactors are widely used. The advantage of roller compaction is that this equipment can manufacture two or four cores whose size is 150 mm in diameter or 100 mm in diameter respectively at the same time. In addition, Consuegra et al. (1989) suggested that the movement of a roller compactor on the surface of a slab is similar to site compaction, in terms of aggregate orientation. Scholz et al. (1993) and Lai & Shami (1995) also stated that rolling compaction is similar to field compaction.

A typically used roller compactor can be seen in Figure 2.4 (a). In this study, a roller compactor was used to produce slabs with dimensions of 300 mm by 300 mm by 120 mm in height (Figure 2.4 (b)). Cores were taken in both vertical and horizontal directions. This will be explained in more detail in Chapter 4.

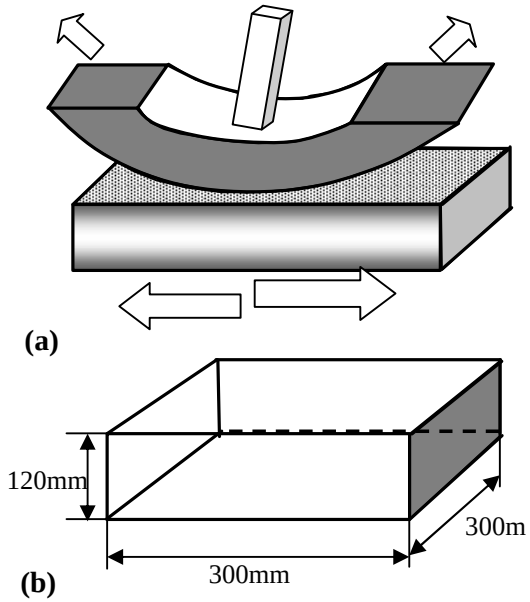

Figure 2.4: Schematic representation of roller compactor equipment (a) Compactor (b) Slab

2.2.4 Past Compaction Studies

It is always desirable for laboratory compacted specimens to have the same properties as field compacted cores (McRae, 1957). To achieve this purpose, the equipment for laboratory compaction is manufactured to simulate field conditions as closely as possible. However, it has long been recognized that different laboratory compaction methods create differences in terms of mechanical properties (Vallerga, 1951; Brown and Cooper 1980; Sousa et al. 1991; Hopman et al. 1992; Renkin, 2000). Nevitt (1959) indicated that the properties of specimen are dependent on compaction techniques such as magnitude, direction and duration of force applied. Therefore, several studies, which compared laboratory compacted specimens with site cores, were conducted over the years. These are analyzed in the following sections.

2.2.4.1 Von Quintus et al. (1991)

Von Quintus et al. (1991) investigated the differences between laboratory compaction methods as a part of the Asphalt-Aggregate Mixture Analysis System (AAMAS) study in the NCHRP project. Five laboratory compaction methods namely Texas gyratory compactor, ASTM kneading compactor, Arizona vibratory/kneading compactor, Marshall hammer and a steel roller were examined to decide the method, which most closely simulates actual site condition. From their report, it was found that the specimens compacted by the Texas gyratory compactor showed similar behaviour to actual site cores in terms of mechanical properties.

It should be noted that although the research of Von Quintus et al. successfully compared five laboratory compaction methods, the cores taken from sites showed relatively higher air-voids than the laboratory compacted specimens.

2.2.4.2 Sousa et al. (1991)

Sousa et al. (1991) investigated the permanent deformation characteristics of laboratory compacted specimens in the SHRP project. In this study, three compaction methods namely Texas gyratory, kneading and rolling-wheel compactor were compared to analyse the differences of compaction methods. In addition to this, three types of mechanical test were performed in order to examine fundamental mixture properties among three types of compacted specimen.

From their research, it was found that rolling-wheel compaction represents most closely field cores in terms of aggregate structure. Also, their research indicated that the kneading compactor produces specimen with the strongest aggregate structure, while gyratory compaction produces the weakest specimens.

2.2.4.3 Button et al. (1994)

Button et al. (1994) examined the correlation between field cores and laboratory compacted specimens. They also looked at compaction methods most like actual site compaction. In their study, field cores were obtained from five different sites, whereas specimens were manufactured using four laboratory compaction methods (i.e. Texas gyratory, Exxon rolling wheel, Elf kneading and Marshall hammer). These were examined through both mechanical tests and statistical analysis. Their

research concluded that the Texas gyratory compactor is the most suitable compaction method to simulate site compaction. The Exxon rolling compactor and Elf linear kneading compactor often simulate the behaviour of actual site cores, whereas the Marshall hammer did not show any similarities to site cores. However, specimens compacted by Exxon rolling-wheel compactor did not have similar air void contents to other laboratory compacted specimens. Therefore, the specimens were not comparable with field cores.

2.2.4.4 Harvey et al. (1994)

Harvey et al. (1994) examined the performance of laboratory compacted specimens. In order to evaluate the differences of compaction methods, they compared field cores with five types of laboratory compaction method: Texas gyratory, rolling wheel, kneading, SHRP gyratory and Marshall hammer compaction. In their study, the specimens with the same air-voids were compared as this parameter significantly affects the behaviour. In addition, repetitive shear tests were performed on the specimens.

As a result, they concluded that rolling-wheel compacted specimens most nearly simulated field cores. While kneading compaction tends to create stiffer specimens than field cores, gyratory compaction leads to the production of the weaker specimens in terms of permanent deformation.

2.2.4.5 Brown et al. (1999)

Brown et al. (1999) studied the influence of compaction method looking at the

mechanical properties of asphalt mixtures. They examined four types of cores: field cores, cores taken from large slabs, cores from a laboratory roller compactor and cores compacted by vibratory hammer. After manufacturing specimens with the same air-void, Repeated Load Axial Tests were conducted to compare permanent deformation properties of these specimens. The results showed that the vibratory hammer provided similar specimens to field cores with respect to mechanical behaviour.

It should be noted that although this research compared several types of compaction methods, the gyratory compacter, which is a popular equipment in the laboratory, was not examined. Therefore, further research including gyratory compaction would be required.

2.2.4.6 Airey et al. (2006)

Airey et al. (2006) compared field cores with specimens compacted by three types of compactor: gyratory, vibratory and roller compactor. In their research, four types of asphalt mixture were also examined. In order to compare these specimens, both field and laboratory cores were assessed with approximately the same volumetric properties (i.e. size, air-voids and VMA). From mechanical test results, it was found that the roller compacted specimens are similar to the field cores.

It is interesting to note that the cores taken from the field showed considerably lower stiffness modulus and permanent deformation resistance, despite the fact that they have the same air voids.

2.2.4.7 Summary

To sum up, past compaction studies were reviewed in this section. Although differences of compaction method were examined using several types of compaction equipment, these results are inconclusive. In particular, the properties of three compaction methods: gyratory, vibratory and roller compaction were not understood clearly, as many researchers recommended different compaction methods, as representative of field compaction. This research, therefore, focuses on the three compaction methods and will examine the factors affecting the mechanical properties of the specimens.

2.3 MECHANICAL TESTING OF ASPHALT MIXTURES

2.3.1 Indirect Tensile Stiffness Modulus

The Indirect Tensile Stiffness Modulus (ITSM) test is used to determine the stiffness modulus of asphalt mixture specimens (Figure 2.5). The ITSM test is usually performed in accordance with British Standard BS 213 (1993). During the test a load pulse is applied along the vertical diameter of a cylindrical specimen and the resultant peak transient deformation measured along the horizontal diameter. The stiffness modulus is then calculated as a function of load, deformation, specimen dimensions and an assumed Poisson's ratio of 0.35.

During the ITSM test, five conditioning pulses are followed by five test pulses, which are averaged to obtain the stiffness modulus for that test. The test is then repeated after rotating the specimen through 90° and the mean stiffness from the

two tests is recorded as the stiffness modulus of the asphalt mixture specimen.

Horizontal deformation: 5 μm, 7 μm

Rise time: 124 ms

Specimen diameter: 100 mm, 150 mm

Specimen height: 60 mm

Test temperature: 20°C

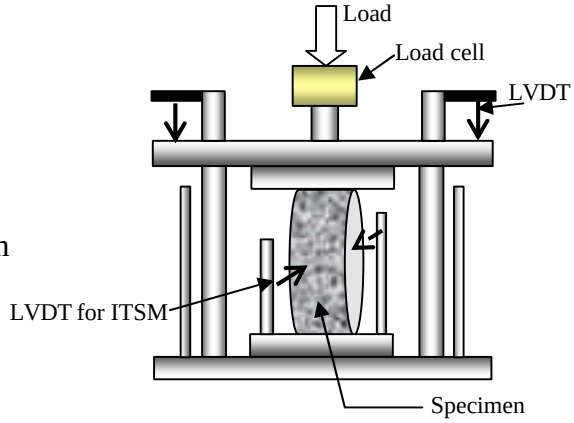

Figure 2.5: Schematic of ITSM test

The ITSM stiffness is calculated using equation 2.1.

$$S_m = \frac{P(c_5 - uc_6)}{d_h t} \quad (2.1)$$

Where S_m = Stiffness modulus, P = applied related load, n = Poisson's ratio, d_h = resilient total horizontal deformation, t = thickness of specimen, c_5 and c_6 = constants depending on specimen diameter and loading strip width.

2.3.2 Repeated Load Axial Test

The Repeated Load Axial Test (RLAT) is widely used to determine the permanent deformation resistance of asphalt mixtures using a direct uniaxial compression configuration as shown in Figure 2.6. The RLA tests are usually performed in accordance with British Standard BS185 (1996).

The permanent deformation performance of asphalt mixtures can be quantified in terms of the ultimate percentage strain after 3600 cycles and by the rate of strain (microstrain per cycle) over the linear phase of the deformation response calculated by linear regression between 1800 and 3600 load cycles (Brown and Gibb 1996).

Test temperature: 30°C

Test duration: 7200 seconds (3600 cycles)

Repeated pulse of 1sec. duration and 1 sec. rest

Axial stress: 100 kPa

Conditioning stress: 10 kPa for 120 s

Diameter of sample: 150 mm

Thickness of sample: 70 mm

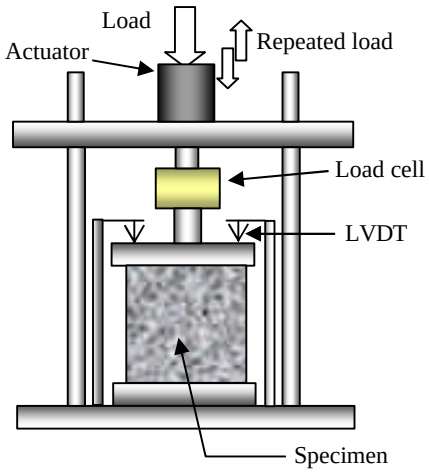

Figure 2.6: Schematic of RLAT test

2.4 MEASURMENT OF AGGREGATE MATRIX

Image analysis techniques have been widely used in order to evaluate the internal structure of an asphalt mixture specimen. Also, it has been recognized that image analysis is an efficient way to evaluate the influence of internal structure on the mechanical properties of asphalt mixture (Seo et al. 2002; Fletcher et al. 2003).

Masad et al. (1999, 2004) utilized a digital imaging process to compare gyratory and linear kneading compacted asphalt mixtures in terms of internal structure

(Figure 2.7). To evaluate the effect of orientation, they used two equations which are shown below:

$$D = \frac{100}{N}\sqrt{(\Sigma \sin 2q_k)^2 + \left(\sqrt{\Sigma \cos 2q_k}\right)^2} \quad (2.2)$$

$$q = \frac{\Sigma |q_k|}{N} \quad (2.3)$$

where Δ is a vector magnitude, q is the angle of inclination from the horizontal direction, q_k is the orientation of individual aggregates and N is number of aggregates.

The range of value D is from 0 to 100. $D = 0$ means that the direction of all aggregates is completely different, whereas $D = 100$ means that all the aggregates arranged themselves in the same direction. Their research is described further in Section 2.5.2.

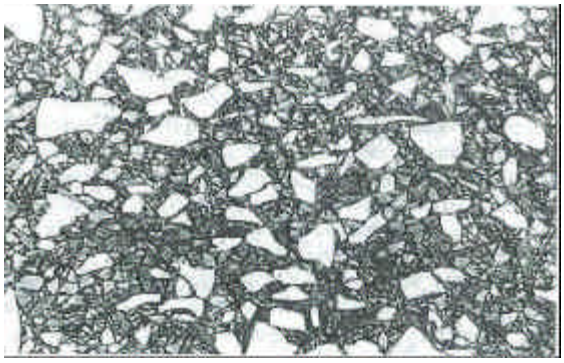

Figure 2.7: Optical image of internal structure of asphalt concrete (Masad et al. 1999)

Similarly, Hunter et al. (2004) described an image analysis technique conducted using analysis software. This software produces monochrome images (Figure 2.8) which are then subjected to thresholding carried out in the software to provide information on the contrast of different objects in the image (Figure 2.9).

Image analysis is most effective where the objects of interest have distinct colour / lightness phases when compared to their surroundings. In this type of image analysis, the monochrome contrast between the two materials, bitumen and aggregate, is critical to the success of the results.

The image analysis software enables the user to automatically select light coloured objects. In this instance the software uses an algorithm based on the threshold data to make a judgment of what constitutes a light coloured object, or in this instance aggregate particles. Once the thresholding process has been undertaken, the user may perform a number of 'count & measure' operations on the objects selected. Virtually any measurement of a recognised particle can be made, for example area, particle orientation, centre of area, perimeter.

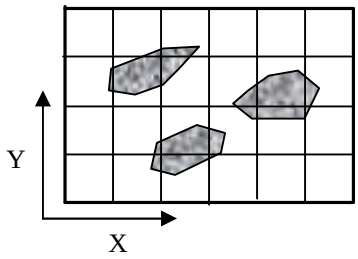

Figure 2.8: Coordinate for internal structure of specimen in image analysis

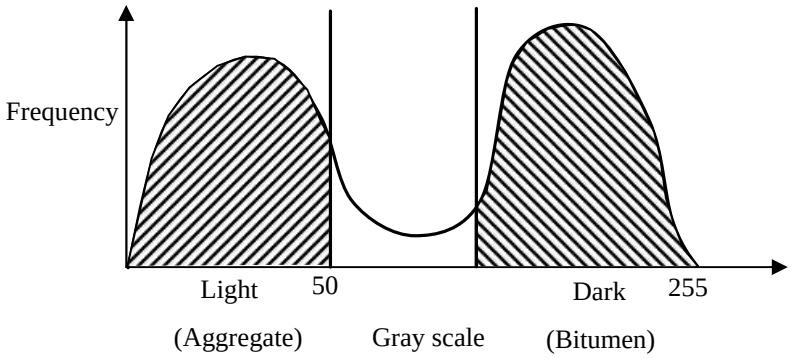

Figure 2.9: Schematic image of threshold plot (Hunter et al. 2004)

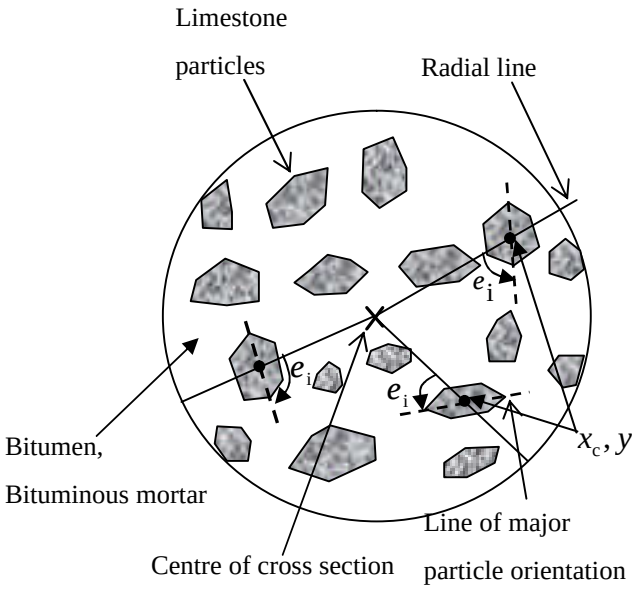

Figure 2.10: Schematic diagram of image analysis (after Hunter et al. 2004)

By using these functions, they quantified aggregate orientation using a central particle angle, e_i (Figure 2.10). The angle of e_i is expressed as the angle between the radial line and the line of major particle orientation. This parameter is represented as an angle between the centre of the specimen line and vertical particle angle ß. The range of angle e_i is from 0° to 90°. The angle e_i = 0° means distributions of particles are in a radial direction, whereas e_i = 90° means all particles lie in a circumferential direction. Moreover, if angle e_i is 45°, then the distribution of particles is random. This will be explained in more detail in Chapter 5.

However, a disadvantage of the image analysis system is that fine particles are not recognized in this process due to the limitation of the software and cutting process. Therefore, only approximately 88% of the total visible cross-sectional area of the specimen is recognized by the image analysis system. However, according to their report, this will not significantly affect the image analysis study as the image

analysis system still captures about 3,000 aggregate particles per cross-section which is sufficient to evaluate the internal structure of the specimen.

In the image analysis, useful information to evaluate the internal structure of specimens can be provided through the following parameters:

- Visible particle cross sectional area (VSA)
- The vertical particle angle (b) which is the angle between the major axis length of aggregate and the vertical axis. The vertical axis is provided by the image.
- Centre of VSA (x_c, y_c) of the aggregate.
- The maximum length of the aggregate particle.
- The maximum width of the aggregate particle.

In this study, image analysis techniques will be applied for the evaluation of internal structure in asphalt mixtures.

2.5 INTERNAL STRUCTURE OF ASPHALT MIXTURE

2.5.1 Aggregate orientation

Past studies indicate that performance of asphalt mixture depends on its internal structure (Yue et al. 1995; Masad et al. 1999; Vavrik et al. 1999; Nukunya et al. 2002; Tashman et al. 2001, 2002; Hunter et al. 2004; Airey et al. 2006). Brown & Gibb (1999) stated that aggregate orientation is affected by the method of

compaction and this has a significant influence on the properties of the asphalt mixture. The internal structure of an asphalt mixture is therefore a very important factor when considering different compaction methods. In addition, as mentioned in the previous section, aggregate orientation can be quantified thanks to the recent development of image analysis techniques. This section considers the internal structure of asphalt mixtures reviewing four studies: Masad et al. (1999, 2004), Tashman et al. (2001), Hunter et al. (2004) and Airey et al. (2006).

2.5.2 Masad et al. (1999, 2004)

Masad et al. (1999) studied the aggregate orientation of asphalt mixtures comparing two compaction methods: Superpave Gyratory Compactor (SGC) and Linear Kneading Compactor (LKC). They measured the angle between the aggregate axis and horizontal axis utilizing digital image analysis techniques. To avoid any problem about boundary effects, they did not count aggregates, which were located around the boundaries. Aggregate orientation was then calculated to express the distribution of aggregate using two parameters in the form of a vector magnitude D (Equation 2.2) and an average angle of inclination from the horizontal q (Equation 2.3).

Also, they examined the internal structure of the asphalt mixture divided it into three categories: aggregate orientation, aggregate contact and air void distribution. The results are shown in Figure 2.11. According to their results, the angle of inclination of linear kneading compacted specimens shows higher values than gyratory compacted specimens, while the vector magnitude of gyratory specimens

indicates larger values than linear kneading compaction. As a result, they concluded that the arrangement of aggregate in linear kneading compacted specimens is more random than in specimens compacted by means of gyration.

With respect to the contact between aggregates, they stated that the number of contacts for linear kneading compacted specimens is greater than for gyratory compacted specimens. They therefore deduced that the shear strength of asphalt mixture specimens, which are compacted by kneading action, is closely related to the number of contacts among aggregates. This was confirmed as kneading compacted specimens tend to have relatively higher resistance to permanent deformation compared with gyratory compacted specimens.

With regard to air void distribution, significant features of each specimen are shown. The compaction state in the middle part of the gyratory compacted specimen shows lower void content compared with its bottom and top. On the other hand, the linear kneading compacted specimen has the void content at the top much lower than the bottom which means the top part is compacted better in comparison to the bottom (Figure 2.2).

As a result, they concluded that the mechanical properties of a specimen are affected by non-uniformity of the void distribution. It is therefore estimated that if two specimens are compared which have different air void distributions from each other, these specimens would show different mechanical behaviour.

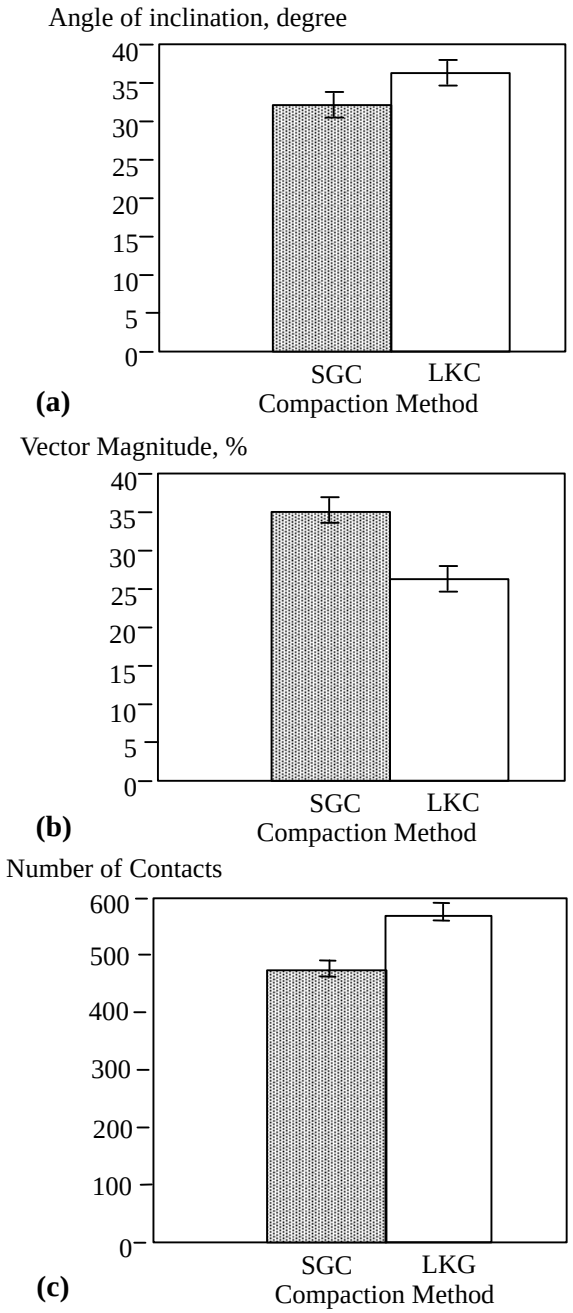

Figure 2.11: Properties of SGC and LKG specimen (a) Average angle (b) Vector magnitude (c) Number of contacts (after Masad et al. 1999)

2.5.3 Tashman et al. (2001)

Tashman et al. (2001) studied the factors affecting the internal structure of asphalt mixtures using the specimens compacted by Superpave Gyratory Compactor (SGC) and field cores taken from three different sites. The asphalt mixtures were compacted changing four factors: gyratory angle, pressure, height and temperature, while the field pavements were constructed with different compaction methods. These specimens were examined through both mechanical tests and image analysis.

The results suggested that the internal structure of the gyratory compacted specimen is affected by two factors: the angle of gyration and specimen height. In addition, they found that larger aggregate tends to move to the mould boundary during the compaction process. Furthermore, it was understood that a gyratory angle of 1.5° and a specimen height of 50 mm to 75 mm are preferable to simulate the internal structure of field cores. Finally, they concluded that the gyratory pressure does not influence the internal structure of laboratory compacted specimens.

It should be noted that although the field cores were compacted with different compaction methods, these specimens showed similar internal structure. In contrast, the internal structure of specimens compacted by SGC, was significantly affected by the two factors: gyratory angle and specimen height.

2.5.4 Hunter et al. (2004); Airey et al. (2006)

Hunter et al. (2004) undertook research on the aggregate orientation and

segregation of asphalt mixture using laboratory compacted specimens. To examine factors affecting the compaction property of asphalt mixture, they looked at three laboratory compaction methods: gyratory, vibratory and roller compaction. In order to assess the specimens, both image analysis and mechanical tests such as the Indirect Tensile Stiffness Modulus (ITSM) test and Repeated Load Axial Test (RLAT), were performed.

As a result, it was concluded that significantly more aggregate orientation was obtained in mould based specimens, gyratory and vibratory compacted specimens, whereas roller compacted specimens showed random particle orientation. Furthermore, the results of RLAT tests indicated that the gyratory and vibratory compacted specimens have higher permanent deformation resistance than the roller compacted specimens.

It should be noted that Hunter et al. (2004) suggested the effect of mould confinement through the image analysis and mechanical tests. However, it is not clear how this phenomenon influences the mechanical performance of laboratory compacted specimens.

Airey et al. (2006) also studied the aggregate orientation of laboratory compacted specimens (i.e. gyratory, vibratory, roller compactor). Their research was conducted to understand differences between field and laboratory compacted specimens in terms of the internal structure of an asphalt mixture. The research followed the same procedure as Hunter et al. (2004); the internal structures of laboratory and

field compacted cores were assessed through mechanical tests (i.e. Indirect Tensile Stiffness Modulus (ITSM) test, Indirect Tensile Fatigue Test (ITFT) and Repeated Load Axial Test (RLAT)) and image analysis.

The results indicated that mould based compaction methods such as gyratory and vibratory compaction tend to produce specimens with circumferential orientation. Moreover, it was found that this trend is more pronounced for specimens with larger particle size. However, a similar aggregate matrix to field cores was shown in roller compacted specimens. Considering the results of previous researches, differences of compaction method should be investigated by looking at the aggregate orientation for each compaction method.

2.5.5 Aggregate Segregation

The segregation of aggregate often occurs in both field and laboratory. In general, aggregate segregation results in non-uniform distribution of aggregate particles (Brock, 1986). In other words, the segregation phenomenon is defined as the separation between larger and smaller aggregates in asphalt mixtures (Tashman et al. 2001; The Asphalt Institute, 2007). Stroup-Gardiner and Brown (2000) suggested that asphalt mixture subjected to segregation would lead to the failure of the surface layer. In addition, Hunter et al. (2004) stated that an ideal specimen, which consists of a continuous graded mixture, is difficult to produce in the laboratory due to segregation. Aggregate segregation is, therefore, a crucial parameter in order to evaluate the internal structure of the asphalt mixture.

Tashman et al. (2001) examined aggregate segregation of both gyratory compacted specimens and field cores using an image analysis technique. The cross section of specimens was divided into two regions on an image: an outer region and an inner region (Figure 2.12 (a)). In their studies, the segregation was defined as the ratio of average aggregate diameter in the outer and inner regions.

Despite the fact that they tried to find differences in lateral segregation in both the field cores and gyratory specimens, there were no significant differences among the compaction methods. However, comparing the gyratory compacted specimens to the field cores, more random aggregate distribution was found in the field cores. In contrast, the segregation phenomenon, in which larger aggregate tends to be displaced to the outer region, was confirmed in the gyratory compacted specimens (Figure 2.12 (b)).

Hunter et al. (2004) also divided the segregation into two aspects: peripheral segregation and regional segregation. Peripheral segregation refers to the ratio of aggregate distribution in different sectors of the asphalt mixture cross section. Peripheral segregation ratio is defined by maximum aggregate percent and minimum aggregate percent in different quarters. Regional segregation was represented by the ratio between the outer and inner regions of the cross sectional area.

From the image analysis, they concluded that the segregation tends to occur more in vibratory and gyratory compaction than in roller compaction. In addition, they

suggested that each segregation will represent differences due to the different compaction methods. Therefore, it was expected that these segregations account for influences of specimen geometry size and orientation and affect the mechanical properties of the compacted asphalt mixture.

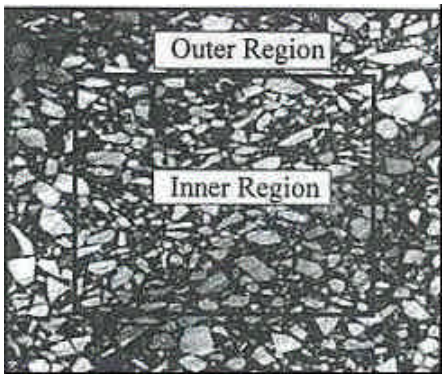

(a)

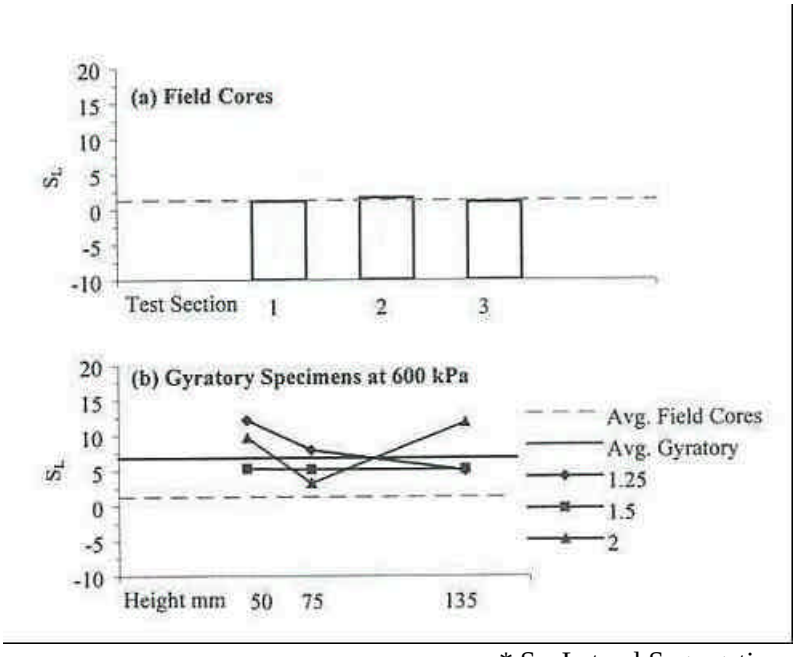

(b)

Figure 2.12: Lateral segregation of asphalt mixture (a) Outer and inner region (b) Lateral segregation of field cores and gyratory specimens (Tashman et al. 2001)

2.6 RESEARCH METHODOLOGY

This section describes the experimental programme for this study. The influence of specimen size and orientation as a function of three different laboratory compaction methods will be examined in this study using the procedure shown in Figure 2.13.

Firstly, specimens are made using gyratory, vibratory and roller compactors. By comparing three compaction methods, differences of compaction method in terms of mechanical property might be understood. After making cylindrical specimens, the Indirect Tensile Stiffness Modulus (ITSM) test will be performed to investigate the stiffness of the compacted asphalt mixture.

Secondly, cores are taken from the original specimen after measuring stiffness. In the case of gyratory specimens, cores are taken from cylindrical specimens whose diameter is 150 mm (Figure 2.14), whereas specimens with 100 mm diameter made by roller compactor are taken in the X-direction (side), Y-direction (roller direction) and Z-direction (top) (Figure 2.15).

Thirdly, before conducting mechanical tests, density and void content are measured in each specimen as it is required that specimens using gyratory compaction, vibratory compaction and roller compaction have almost the same density to compare the differences of compaction method. Specimens that did not meet this requirement were remanufactured.

In the next step, mechanical testing will be conducted in the form of ITSM tests. Also, for the specimens, which were cored out from slab, the Repeated Load Axial Test (RLAT) will be carried out to examine the difference of permanent deformation characteristics in terms of specimen orientation.

Finally, image analysis will be carried out by using a digital camera and image analysis software. Part of this work will be conducted before mechanical testing as well as after mechanical testing.

In the following chapters, detailed information for each experiment will be described in more detail.

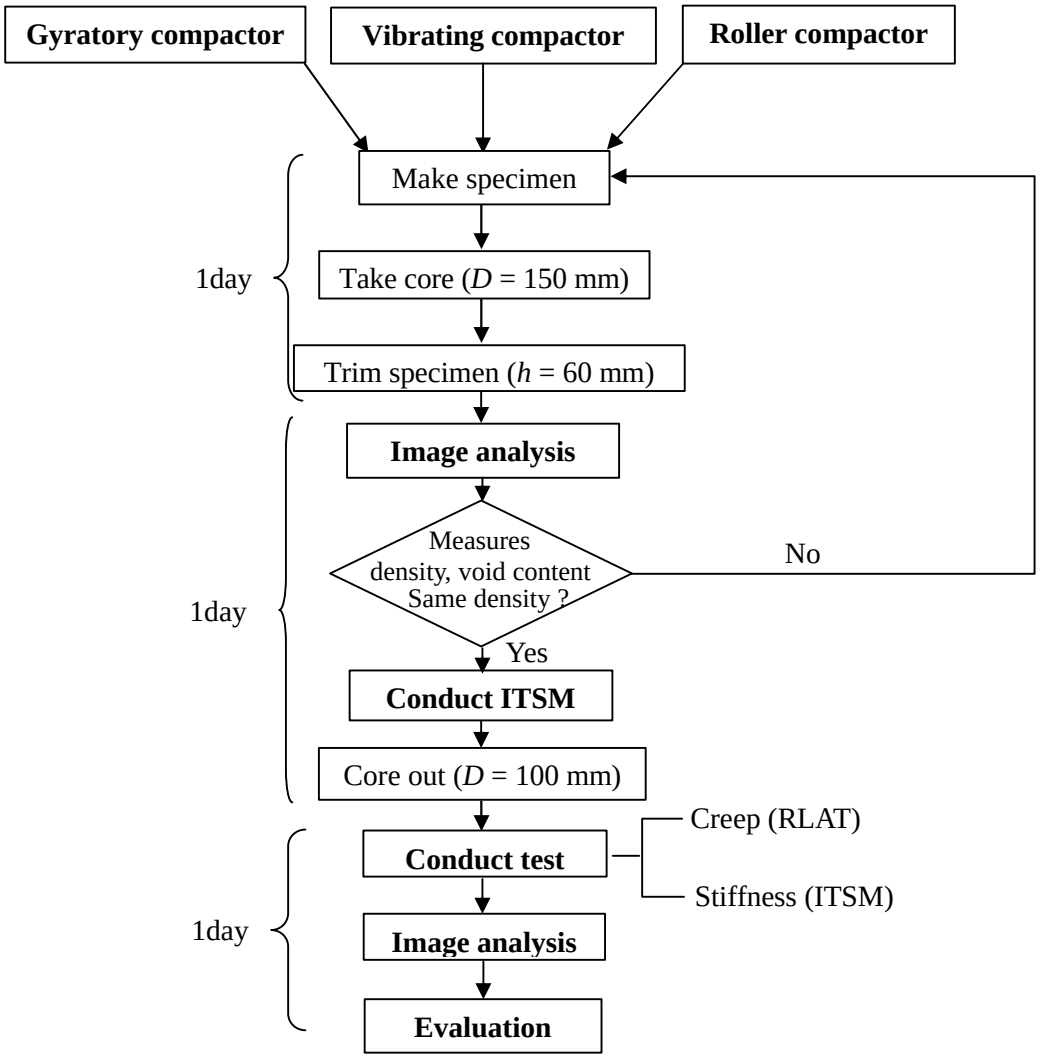

Figure 2.13: Flow of experiment

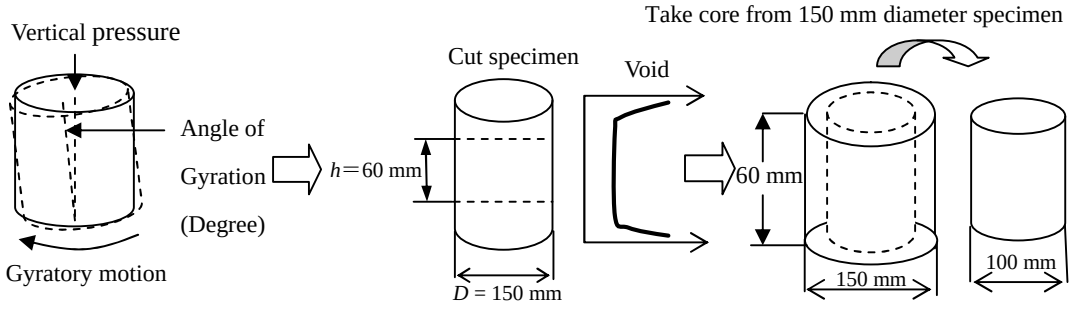

Figure 2.14: Coring out procedure for gyratory compaction specimens

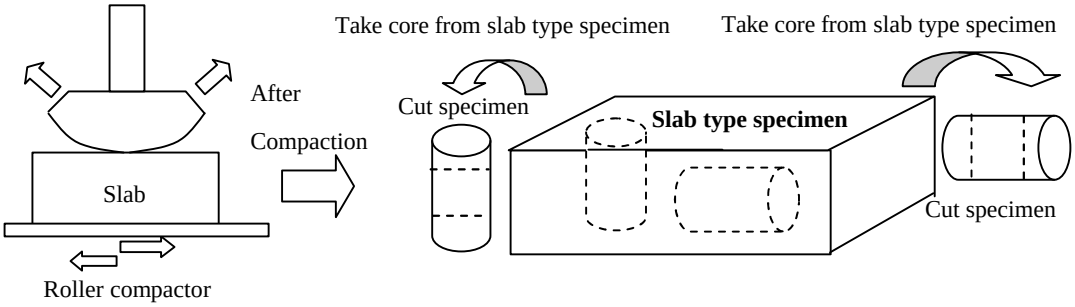

Figure 2.15: Sampling procedure for slab type specimens

CHAPTER 3

Preparation of Specimens

3.1 INTRODUCTION

In order to compare the influence of different laboratory compaction methods, a series of asphalt mixture specimens were needed. Moreover, to compare specimens, it is necessary to prepare specimens which have the same air void content. Also, when considering the image analysis process, the selection of aggregate type is very important in terms of discriminating between aggregate and bitumen. The aim of this chapter is to describe the procedures used for the mixing design, manufacture of specimens and measurement of air voids content for specimens produced using three different compaction methods.

3.2 MIX DESIGN

As stated above, mix design is an important process in pavement engineering both on site and in the laboratory due to pavement performance, such as rutting resistance and durability, being dependant on the type of asphalt mixture as well as degree of compaction. Therefore, mix design was carried out according to the

recipe design for dense bitumen macadam (DBM) detailed in Clause 929 (Highways Agency 1998) and British Standard 4987 (BSI 2001). For this image analysis based study, the mix design consisted of three parts; binder content, choice of aggregate, and asphalt mixture grading. The following sections describe the mixture design for specimen manufacture and the reasons for material selection.

3.2.1 Choice of Aggregate

In this study, 28 mm Dense Bitumen Macadam (DBM) is used as the selected asphalt mixture. The reason for the 28 mm DBM is that it is used as a standard UK base material. Also, since this study is related to previous research which was conducted by Hunter et al. (2004), the same aggregate as in their study is required in this project. Moreover, according to Hunter et al. (2004), segregation is more marked in larger aggregate sizes. Therefore, a large aggregate size (28 mm) was chosen in this study.

In terms of image analysis, it is required that aggregate has a distinct colour contrast with bitumen to allow the clear recognition of aggregate in the image. By considering the above factors, a carboniferous limestone was used in this study as it tends to have a whitish colour which is an advantage for image analysis.

Factors for selection of aggregate are summarized below.

- The most common material in the UK is needed.
- To look at aggregate segregation, larger particle size is preferred.
- Considering image analysis, colour contrast with bitumen is required.

3.2.2 Aggregate Grading

Aggregate grading was carried out by following British Standard 4987 (BSI 2001). According to the specification, there are upper and lower limits in each aggregate size. The target grading is required to be close to the centre line of the limits. In this study, aggregate batches with sizes 28 mm, 20 mm, 14 mm, 10 mm, 6 mm and dust were used. In usual work, filler is also applied to the asphalt mixture. However, as this study needs to follow previous research, filler was not used in this study. The aggregate grading which was followed by Hunter et al. (2004) is shown in Figure 3.1.

Particle distribution and aggregate grading in each size is depicted in Figure 3.1 and Table 3.1 respectively.

Table 3.1: Aggregate composition and binder content

Material	Percentage
40 mm	0
28 mm	19
20 mm	11
14 mm	11
10 mm	11
6 mm	10
Dust	38
Filler	0
Total	100
Binder (50pen)	4.0

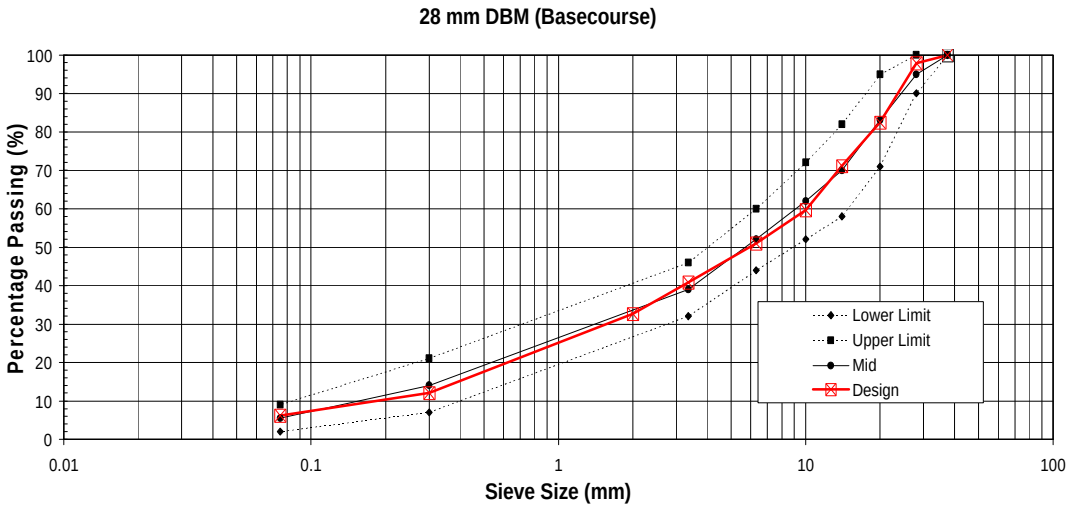

Figure 3.1: Aggregate grading curve (for this study)

3.2.3 Bitumen Content

Bitumen is another important material in an asphalt mixture as mechanical performance depends on binding between aggregate as well as aggregate interlocking. In the UK, binder content is dictated by recipe which is specified in the British Standard (Read and Whiteoak 2003). According to BS 4987, the range of binder contents for 28 mm size dense road base is between 4% +/- 0.6% and 6.8% +/- 0.6%. Considering site cores, 50 penetration grade bitumen is widely used in practice. Moreover, Hunter et al. (2004) also used 50 pen bitumen in their study. Therefore, in this study, 50 pen bitumen was selected as the binder. In the case of 50 pen bitumen with limestone, the corresponding binder content is 4.0% +/- 0.6%. The lower level of 4% was therefore chosen as the binder content in this study. The specific gravity of the bitumen was assumed to be 1.02.

3.3 MAXIMUM DENSITY

In the case of mix design, the maximum density, so-called rice density, is an important parameter used to manufacture specimens as the target air voids and density, which are necessary for mix design as well as specimen manufacture, are derived from maximum density. Therefore, a test for the determination of maximum density of bituminous mixtures was carried out in this study. The testing method followed the British Standard, BS EN12697-5:2002. Testing procedures for this method are as follows:

Procedure A: Volumetric procedure

1. Mix aggregate and bitumen for manufacture of bituminous bulk sample. (prEN12697-35).
2. After mixing, separate sample using 6 mm sieve. Mixed particles separated either over 6 mm or under 6 mm. Then, leave until cool.
3. After cooling, mix these two materials together into one container.
4. Measure mass of empty pyknometer and head piece of it. (m_1)
5. Measure mass of empty pyknometer and head piece and dry test sample. (m_2)
6. Fill pyknometer with de-aired water up to a maximum of 30 mm below the head joint
7. Evacuate entrapped air by applying a partial vacuum of a residual pressure of 4 kPa or less for 15 +/- 1 minutes.

8. Place the pyknometer filled with water up to head piece, into a water-bath for 30 minutes.
9. After 30 minutes, take pyknometer from bath, then cover the pyknometer with head piece.
10. Wipe carefully the outside of the mould dry and weight it immediately. (m_3)

After carrying out the measurements, maximum density is determined by the following equation:

$$r_{mv} = \frac{m_2 - m_1}{1000 \times V_p - (m_3 - m_2)/r_w} \quad (3.1)$$

where r_{mv} is the maximum density of the bituminous mixture, V_p is the volume of the pyknometer, r_w is the density of the water. The maximum density was calculated as 2500 kg/m^3.

To manufacture specimens, it is necessary to set target density and target air voids content. As Hunter et al. (2004) set target air voids as 4.2%, this number is used as target air voids content in this study as well. The void content was calculated as follows:

$$V_v = \frac{100(g_{max} - g_m)}{g_{max}} \quad (3.2)$$

where V_v is the voids content (target air voids content), g_{max} is the maximum density (rice density), g_m is the target density. Now, since air voids content and maximum density are determined, target density is calculated. As a result, target air voids content and density are set to 4.2% and 2395 kg/m^3, respectively.

3.4 MIXING WORK

In order to coat aggregate with bitumen, adequate mixing must be conducted. In terms of mixing, coating of the aggregate is governed by time and temperature. Before starting mixing, aggregate and binder are heated up to a target mixing temperature. Usually, both aggregate and binder are put into the oven at 160°C. In case of aggregate, minimum preparation time in the oven is 4 hours, while binder must be kept in the oven between 3 and 5 hours. If storage time exceeds 5 hours, ageing of the binder will occur.

In terms of equipment, mixing was undertaken using a sun and planet mixer (Picture 3.1). The mixer is covered with an oil jacket around the steel drum to avoid any heat loss and subsequent changes in viscosity of the bitumen during mixing. In the mixing operation, each batch of aggregate and binder was mixed for 3 minutes. If aggregate was not sufficiently coated, the mixing operation was carried out for a further few minutes. After coating the aggregate with bitumen, the mixture is stored in an oven until the mixture reaches compaction temperature. According to the British Standard for manufacture of 28 mm DBM, mixing temperature and compaction temperature is determined as 160°C and 150°C respectively.

Picture 3.1: Laboratory asphalt mixer

3.5 LABORATORY COMPACTION WORK

3.5.1 Gyratory Compaction

In case of gyratory compaction, there are three important factors to compact specimens properly. These are gyratory pressure, gyratory angle, and gyratory motion. Usually, 0.6 MPa and 1.25° were applied as gyratory pressure and gyratory angle, respectively. However, in order to satisfy target density and air voids content which were used in the previous study (Hunter et al., 2004), 0.8 MPa and 2.0° were applied in this study. According to Masad et al. (2004), anisotropy of specimens developed as angle of gyration was increased from 1.25° to 1.5°. However, specimen anisotropy decreased, when gyratory angle was raised to 2.0°. Gyratory speed was applied at 30 rev/min in this study.

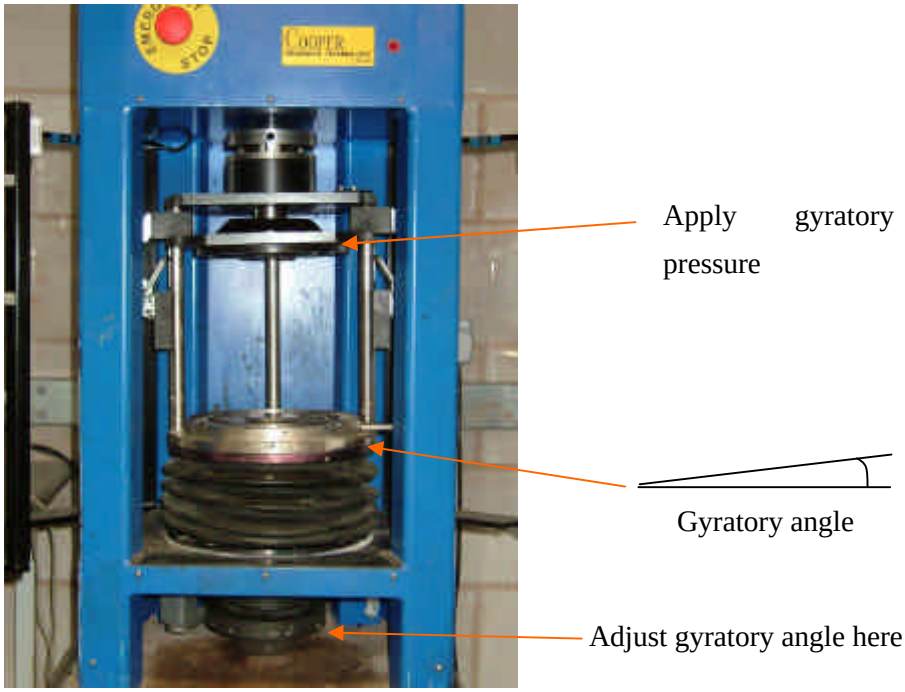

Picture 3.2: Gyratory compactor

3.5.2 Vibratory compaction

In case of vibratory compaction, the Kango hummer was applied in this study. Specimens were compacted both on top and on the bottom of the specimen. Firstly, the specimen was compacted using a small diameter compaction head at 8 parts of the surface. Compaction time in each part was for 4~5 seconds. After that compaction work was conducted using a large diameter compaction head. By doing this procedure in 8 parts, the specimen was compacted properly. The same sequence was repeated on the bottom surface.

(a)

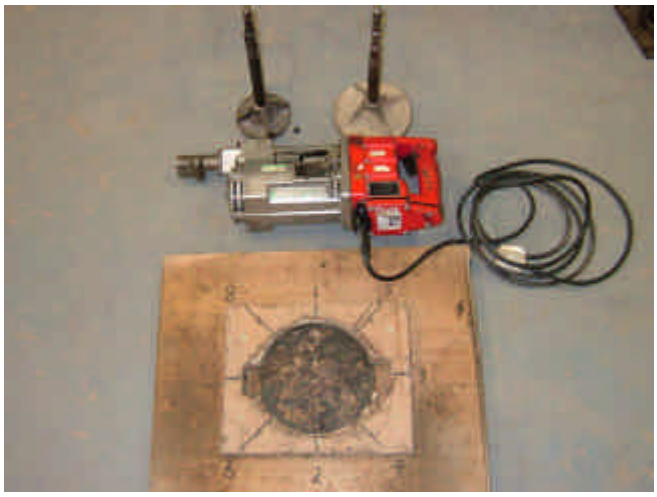

(b)

Picture 3.3: Vibratory compaction (a) Kango hammer, jig and plate (b) Compaction work

3.5.3 Slab 'Roller' Compactor

In order to manufacture slab specimens, a laboratory roller compactor was used. The mixture was put into a mould after finishing the mixing work. When the specimen reached the compaction temperature, the specimen was compacted using a roller compactor operated by pneumatic pressure. Specimens were compacted in both roller direction and transverse direction. The number of roller passes was ten times in each direction. As a final compaction, specimens were compacted in the roller direction.

(a)

(b)

Picture 3.4: Slab 'Roller' compactor (a) Mixture in the mould (b) Laboratory roller compaction work

3.6 TRIMMING AND CORING WORK FOR THE MECHANICAL TESTING

Before conducting mechanical testing, cylinder type specimens, which were compacted by gyratory compactor and vibratory compacter, were trimmed to 60 mm in height for the ITSM test. These specimens were cut by using a diamond edged circular saw. Schematic images of core section and surface are shown in Figure 3.2. After conducting ITSM tests with 150 mm diameter specimens, 100 mm diameter cores were taken out from the 150 mm diameter specimens. By comparing these two different diameter specimens, the influence of specimen size was investigated.

For the slab, coring work was carried out from the sides as well as the top of the slab to produce 100 mm diameter cores. To produce specimens for the ITSM test, the slab size was chosen as 305 mm by 305 mm by 110 mm in height. In total, 20 cores were taken from slabs (4 cores from X-direction, 4 cores from Y-direction and 12 cores from Z-direction). The cores from the x-direction and y-direction were then divided into 3 specimens (see Picture 3.5). By doing that, 12 specimens in each direction were prepared from the slab, and the influence of specimen orientation examined through the ITSM test, RLAT and image analysis.

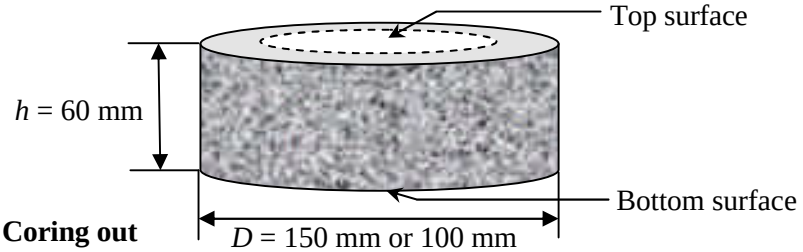

Figure 3.2: Coring out

(a)

(b)

Picture 3.5: Coring work (a) Coring out from slab (b) Cylindrical type specimens cored out from Y (roller direction) and X (side of slab) direction

3.7 MEASURMENT OF BULK DENSITY AND AIR VOIDS

In order to compare specimens, it was required to manufacture specimens which had the same air void contents in each specimen as the stiffness of asphalt mixtures depends on air voids content. If air voids content difference between different specimens were too large, then the mechanical properties between them would be different. Therefore, it was necessary to get as close to the same density and air voids as possible.

Measurement of bulk density and air voids was carried out by following BS EN 12697-6:2003. Firstly, specimen weight was measured after manufacturing the specimen. Secondly, its weight in water was measured by soaking the specimen in a water bath. Finally, the bulk density and air voids were calculated. After trimming and coring, bulk density and air voids were measured by following the same sequence. Testing results are shown in Appendix 1. In this stage, it is very important to produce specimens with similar densities for each compaction method. According to Appendix 1, density and air voids for each compaction method have similar averages. Also, comparing with previous research, differences are very small. Therefore, it could be concluded that specimens which were compacted by different types of compaction method had almost the same density. As a result, comparisons of the mechanical properties in each specimen are possible.

3.8 PARTICLE DISTRIBUTION AND SEGREGATION DURING MIXING AND COMPACTION PROCESS

3.8.1 Mixing Process

There are some concerns about particle segregation when specimens are manufactured in the laboratory. Although engineers try to make specimens with the same conditions found in the field, inevitably particle segregation does occur in the laboratory. In this section, some possible reasons for material segregation in the laboratory are described.

As shown in Section 3.4, mixing was conducted using a laboratory asphalt mixer (see Picture 3.1). Aggregate and bitumen are mixed in this equipment. However, aggregate segregation may be occurring in this process. In the mixing process, aggregate alone is mixed for 30 seconds prior to mixing with bitumen. This state is depicted in Picture 3.6. From this process, it is found that aggregate segregation occurs since bigger particles tend to be located towards the outside, whereas smaller particles are likely to be distributed in the inside.

After the mixing process, the mixture is put into moulds as shown in Picture 3.4 (a). However, aggregate segregation can occur in this process as well. Although both larger and smaller particles fall at the same rate under gravity, a cluster of the particles may be dropped as shown in Figure 3.3. Because of that, it is assumed that the particles are located with segregation in the moulds, when conducting compaction.

In case of site batching, it could be difficult for this phenomenon to occur because the pugmill mixer is often used in site batching plants (see Picture 3.7). In the case of pugmill mixing, both larger and smaller aggregates tend to be uniformly mixed so that aggregate segregation would not occur on site. Therefore, differences of mixing type may cause different types of mechanical properties between laboratory and site.

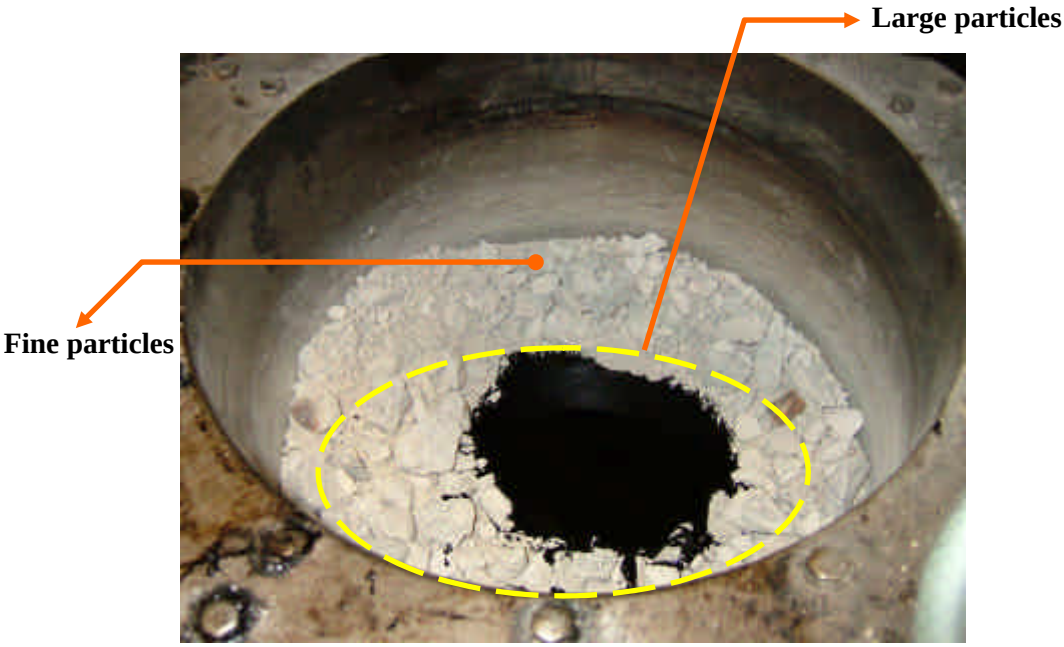

Picture 3.6: Aggregate segregation during dry mixing process

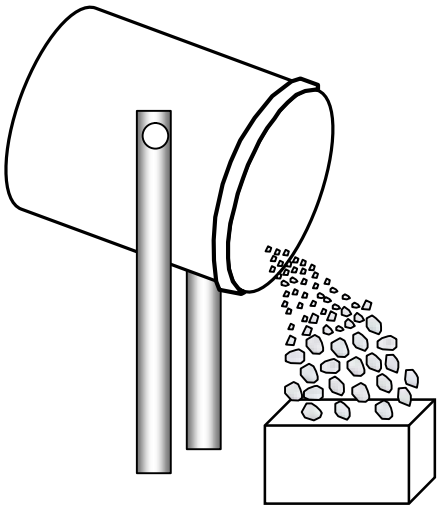

Figure 3.3: Aggregate segregation due to gravity (after Alexander et al. 2005)

(a)

(b)

Picture 3.7: Laboratory pugmill mixer (a) Whole image (b) Inside

3.8.2 Compaction Process

Aggregate segregation may occur in the compaction process. In this study, three types of compaction method were examined: gyratory, vibratory and slab (roller) compaction. In general, compaction process for the laboratory compacted asphalt specimen is classified into two categories: static compaction and dynamic compaction. Gyratory and slab compaction are recognised as static compaction, whereas vibratory compaction is identified as dynamic compaction.

In particular, it is assumed that vibratory compaction would cause aggregate segregation because of vibration. Also, vibration gives specimens good interlocking, particularly for larger particles. When vibration is applied to the specimen, bigger particles tend to move towards the bottom of the specimen, whereas smaller particles are more likely to move towards the surface of the specimen.

Similar phenomenon is seen in grain size analysis by the sedimentation method for the smaller particles. For the sedimentation method, the particle size is determined based on the application of Stokes's law for the settling velocity of special particles. In this case, bigger particles fall faster than smaller particles in the liquid clay. This phenomenon is also similar to "liquefaction", when earthquake occurs on sand.

Using this scenario, segregation during vibratory compaction may be explained as shown in Figure 3.4. Initially, vibration is applied to loose specimens. In this case, bitumen may behave like liquid, while bigger aggregate particles might fall to the bottom surface. Secondly, the specimen is turned over to compact the bottom

surface. However, at this stage, as the vibration is applied to dense specimen, bigger particles tend to fall slower than initial compaction so that the top surface may contain bigger particles, compared with the bottom surface. In addition, it is also assumed that bigger particles are located at the middle part of specimen after the second compaction. This might result in higher stiffness of the vibratory compacted specimens. In other words, this may lead to an overestimate of the stiffness of the asphalt mixture. It is, therefore, important to take into account this effect before mechanical testing of vibratory compacted specimens. This phenomenon will be examined and discussed further in Chapter 7.

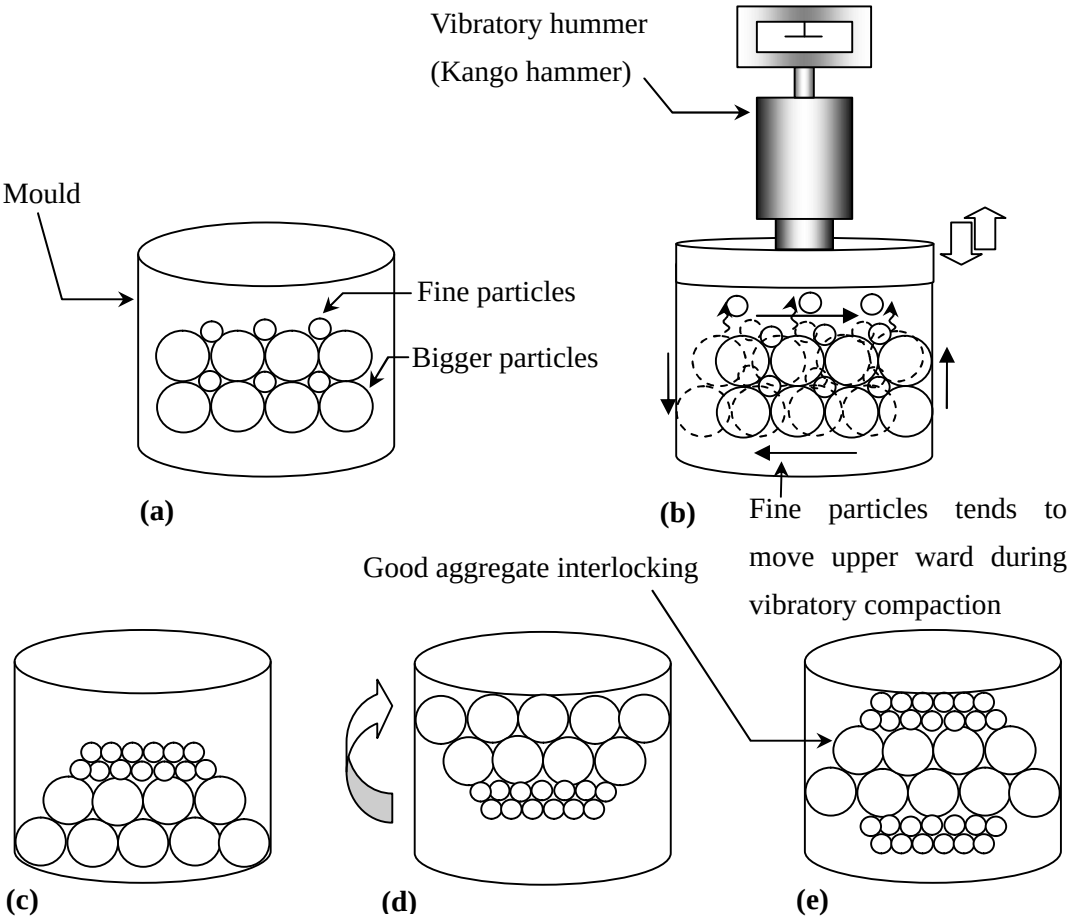

Figure 3.4: Assumed segregation during vibratory compaction process (a) After setting aggregate from mixer (b) During vibratory compaction process (c) After initial compaction (d) Turned over specimen (e) After second compaction

3.9 CONCLUSION

Three different types of compaction method were applied to manufacture specimens. Although there are slight differences between Hunter et al. (2004) and this study in terms of material and grading, almost the same specimens as in their research were made. Moreover, the same air void and density was achieved for each of the compaction types. As a result, it is possible to compare results between Hunter et al. (2004) and this study. Therefore, further investigations such as mechanical properties and image analysis were compared directly with results from the Hunter et al. (2004) study. These results are described in Chapter 4.

CHAPTER 4

Mechanical Properties of Specimens

4.1 INTRODUCTION

The mechanical properties of the different laboratory compacted specimens were evaluated in terms of their stiffness and permanent deformation characteristics. To achieve this, the Nottingham Asphalt Tester (NAT) was used to undertake standard stiffness modulus and permanent deformation tests. This chapter describes the procedures followed for these experiments and used to identify the influence of specimen size and orientation on the mechanical properties of laboratory compacted asphalt mixture specimens.

4.2 PRINCIPLE OF ITSM TEST

4.2.1 Measurement of Indirect Tensile Stiffness Modulus

The Indirect Tensile Stiffness Modulus (ITSM) test is conducted to determine the stiffness of an asphalt mixture. Originally, the ITSM testing facility was developed by Cooper and Brown (1989) as a part of development of the Nottingham Asphalt Tester (NAT). In addition to the ITSM procedure, there are several alternative

approaches to measure the stiffness of an asphalt mixture (Read and Whiteoak 2003). This section describes the principle of ITSM testing.

During the ITSM test, a vertical load is applied to the vertical diameter of a cylindrical specimen as indicated in Figure 4.1. This load generates horizontal tensile stress as well as vertical compressive stress in the specimen. As shown in Figure 4.1, the magnitude of the stress changes over the cross section of specimen. However, the maximum stress occurs in the centre of specimen (Read and Whiteoak 2003).

In order to conduct the ITSM test, the following conditions are assumed to calculate the strain (Read and Whiteoak 2003):

- The specimen is assumed as plane strain conditions $(s_z = 0)$.
- The material shows linear elastic behaviour.
- The material indicates isotropic behaviour.
- The material is homogeneous.
- Poisson's ratio (u) for the material is known.
- The vertical load (P) is applied as a line loading.

By using these assumptions, the elastic stiffness of the asphalt mixture specimens was calculated. In order to determine elastic stiffness, the stress applied to the specimen was calculated using the following equation:

$$\sigma_{x\max} = \frac{2P}{\pi dt} \tag{4.1}$$

$$\sigma_{y\max} = -\frac{6P}{\pi dt} \tag{4.2}$$

where P = applied vertical force (N), d = diameter of the specimen (m), t = thickness of the specimen (m), ν = Poisson's ratio, S_m = stiffness modulus of the specimen (Pa), $\sigma_{x\max}$ = maximum horizontal tensile stress at the centre of the specimen (N/m^2), $\sigma_{y\max}$ = maximum vertical compressive stress at the centre of the specimen (N/m^2) and $\varepsilon_{x\max}$ = maximum initial horizontal tensile strain at the centre of specimen.

Also, the strain is derived from Hooke's law,

$$\varepsilon_{x\max} = \frac{\sigma_{x\max}}{S_m} - \frac{\nu\sigma_{y\max}}{S_m} \tag{4.3}$$

Alternatively, equation 4.3 can be derived using equations 4.1 and 4.2.

$$\varepsilon_{x\max} = \frac{2P}{\pi dtS_m} + \frac{\nu 6P}{\pi dtS_m} \tag{4.4}$$

Combining equations 4.1 and 4.4 gives,

$$\varepsilon_{x\max} = \frac{\sigma_{x\max}}{S_m}(1+3\nu) \tag{4.5}$$

The target strain is given before testing. A compressive force is applied to the specimen taking into account the target strain. As the target strain is constant, the applied vertical force is also constant. Consequently, elastic stiffness is derived from the stress and strain relationship which is described in equation 4.5.

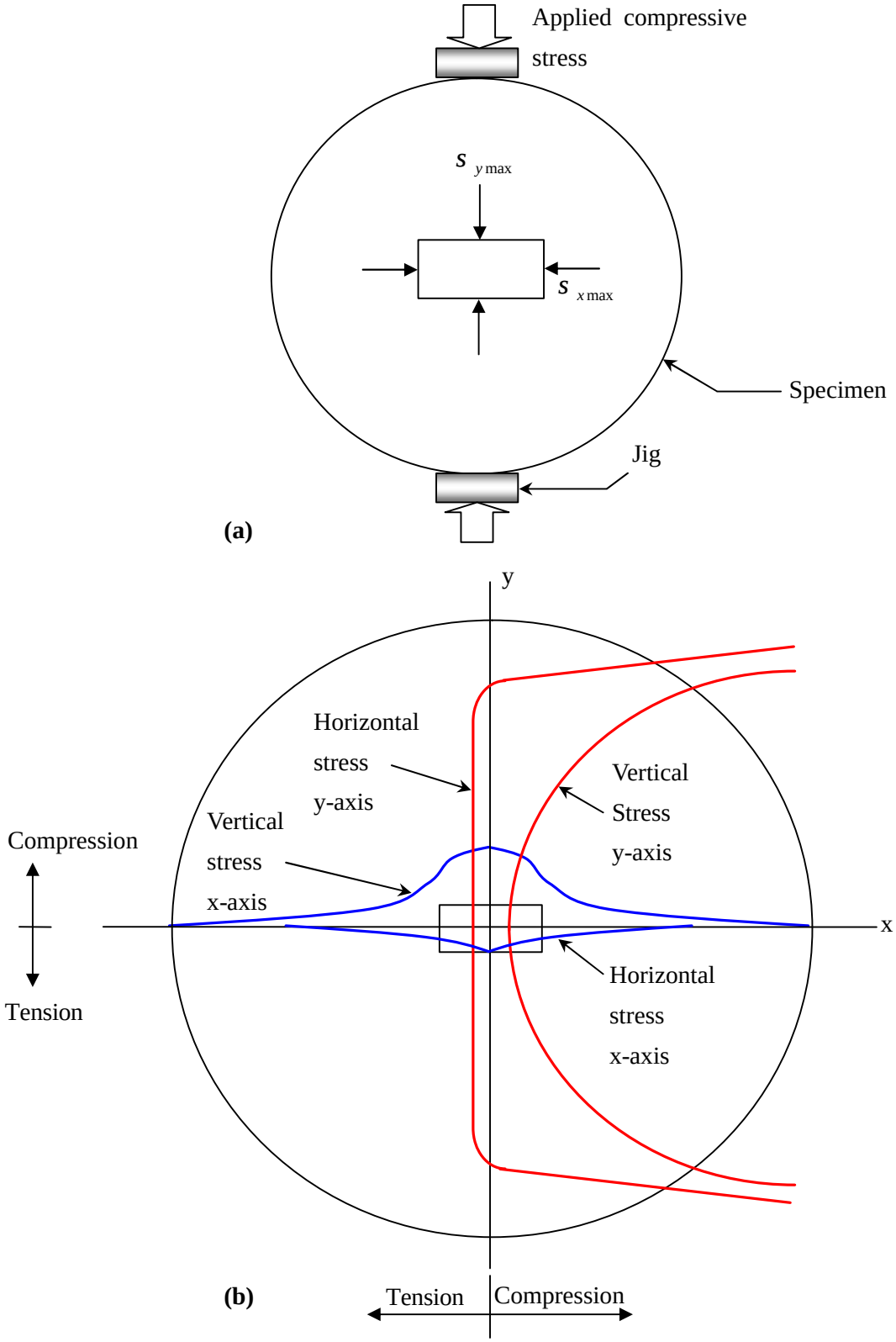

Figure 4.1: Stress distribution in the indirect tensile mode of test (after Read and Whiteoak 2003) (a) Testing state (b) Stress distribution

4.2.2 Comparison between NAT and ASTM Stiffness Modulus Methods

As described in the previous section, there are several ways to determine the stiffness of an asphalt mixture. In particular, two methods are used in practice in order to evaluate stiffness modulus. One of them is the Nottingham Asphalt Tester (NAT) method, the other is the ASTM method. This section compares the two methods and the reason for the application of the NAT equipment in this study.

In terms of application of vertical load, both methods apply a pulse load to the specimen. However, according to Nunn (1996), the two methods calculate the associated deformation differently as shown in Figure 4.2. The NAT method records a larger deformation compared to the two ASTM methods. The comparison between the NAT and ASTM methods is summarized in Table 4.1.

Table 4.1: Comparison of two methods (after Nunn 1996)

	NAT Method	ASTM Method
Advantages	1. Less sensitive to pulse shape. 2. Deformation components are more representative.	1. Established method
Disadvantages	1. Not defined in any standard.	1. More sensitive to pulse shape 2. Negative component of irrecoverable deformation.
Comments	1. A shorter pulse load would help to produce a deformation response more representative of a wheel load travelling at a realistic speed. 2. The negative component of irrecoverable deformation raises the question of what is the physical significance of the resultant stiffness deformation by the ASTM method.	

Also, Nunn (1996) compares the advantages and disadvantages of these methods. According to Table 4.1, the ASTM method is more sensitive to pulse load and has a negative component of irrecoverable deformation. The NAT method is not sensitive to pulse load and its deformation component is more representative than the ASTM method.

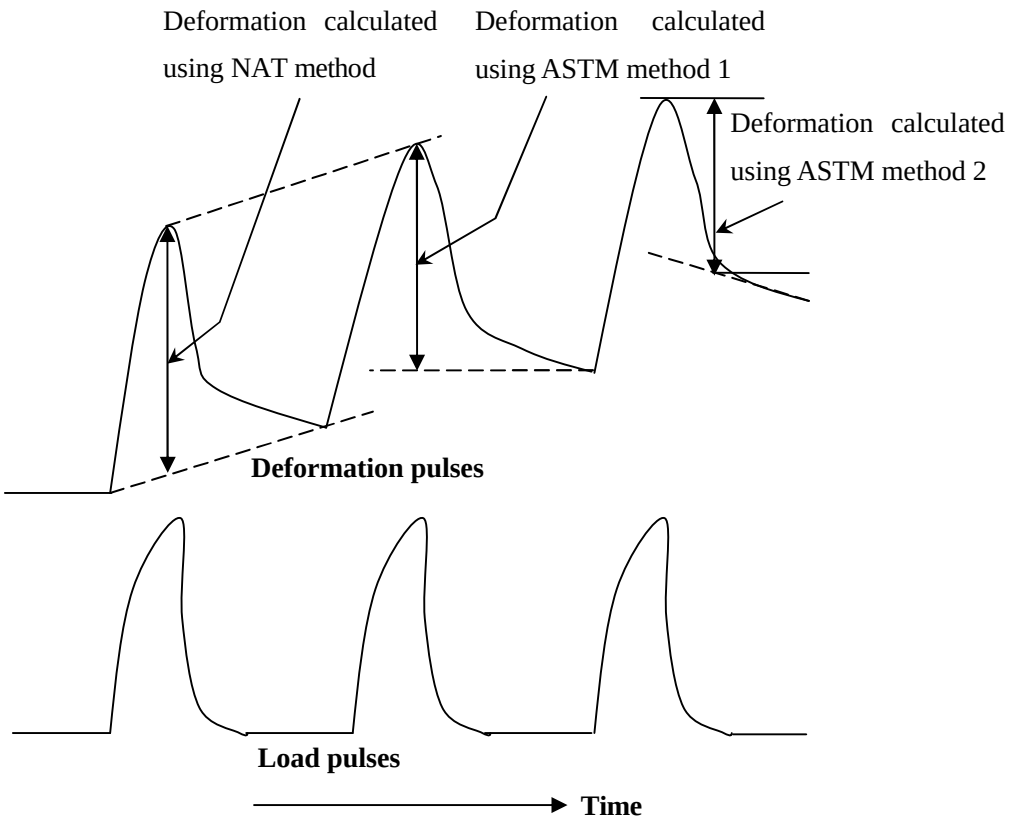

Figure 4.2: Differences of load pulse between NAT and ASTM (after Nunn 1996)

4.2.3 Effect of Pulse Shape

When the ITSM test is conducted, a vertical pressure is applied to the specimen by the pulse load at a particular rise time (rate of load application). The target deformation is then achieved by changing the loading force. However, according to

Nunn (1996), the shape of the pulse load is also one of factors affecting the stiffness of the asphalt mixture. He conducted two types of trials to investigate the effect of pulse shape using two types of pulse shape as shown in Figure 4.3.

In terms of the amplitude of the pulse, the rise time for pulse A is faster than that of pulse shape B. This results in a greater deformation for pulse A compared with that of pulse B. Moreover, Nunn (1996) suggested that the amplitude of the load pulse affects the irrecoverable deformation of the specimen.

Comparing pulse shapes A and B, pulse shape B has higher irrecoverable deformation than shape A at the end of the pulse cycle. These two factors (i.e. deformation and deformation response) affect the evaluation of stiffness modulus. Also, he concluded that the NAT method had 10% difference between pulse shape A and B, whereas the difference for the ASTM method was 20%.

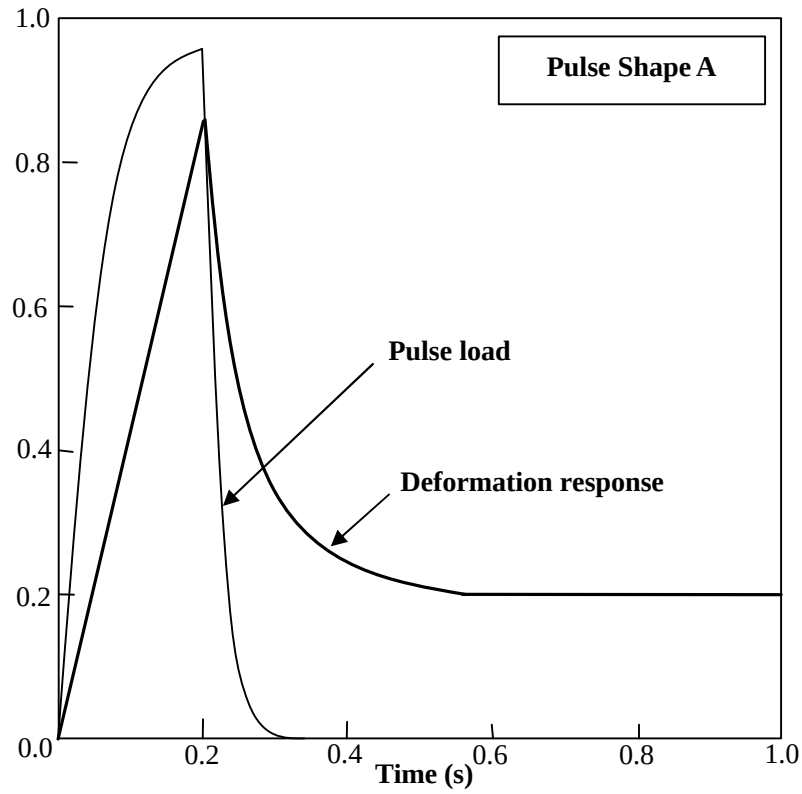

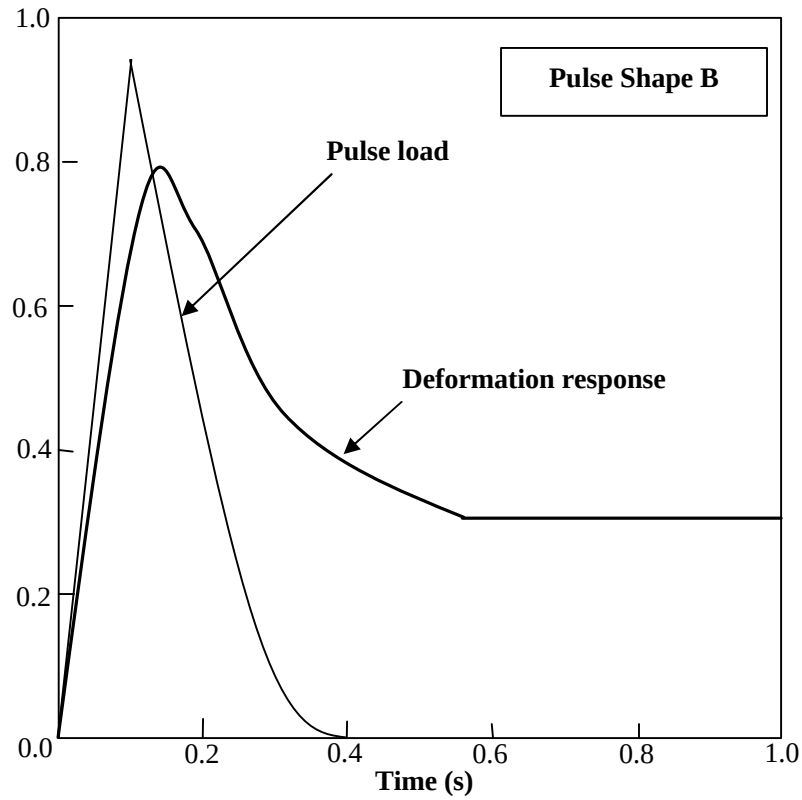

Figure 4.3: Comparison of load shape (after Nunn 1996)

4.3 TESTING PROCEDURE FOR THE ITSM

The Indirect Tensile Stiffness Modulus (ITSM) test was used to determine the stiffness of the asphalt mixtures manufactured using the three different laboratory compaction types carried out in this study. As stated Chapter 2, the ITSM test is conducted by applying vertical compressive load to the specimen. At the same time, resultant transient deformation is measured using linear variable differential transformers (LVDT). Using the stress and strain measurement, the stiffness modulus is calculated.

A picture of the ITSM testing facility is shown in Picture 4.1 and a schematic image of the ITSM apparatus in the Nottingham Asphalt Tester (NAT) is shown in Figure 4.4. A close up of the ITSM test equipment is shown in Picture 4.2. In terms of temperature conditioning, each specimen is put into the cabinet, which is set to 20°C, at least four hours prior to testing. After temperature conditioning, the specimen is placed in the ITSM testing equipment. A pneumatic actuator is used to apply a vertical force to the specimen and the resultant transient deformation is measured using LVDTs. The vertical pressure is adjusted in order to achieve the target deformation within the target rise time. By adjusting these parameters, an appropriate test is carried out with the actuator and data acquisition being controlled by a personal computer.

Picture.4.1: ITSM testing facilities

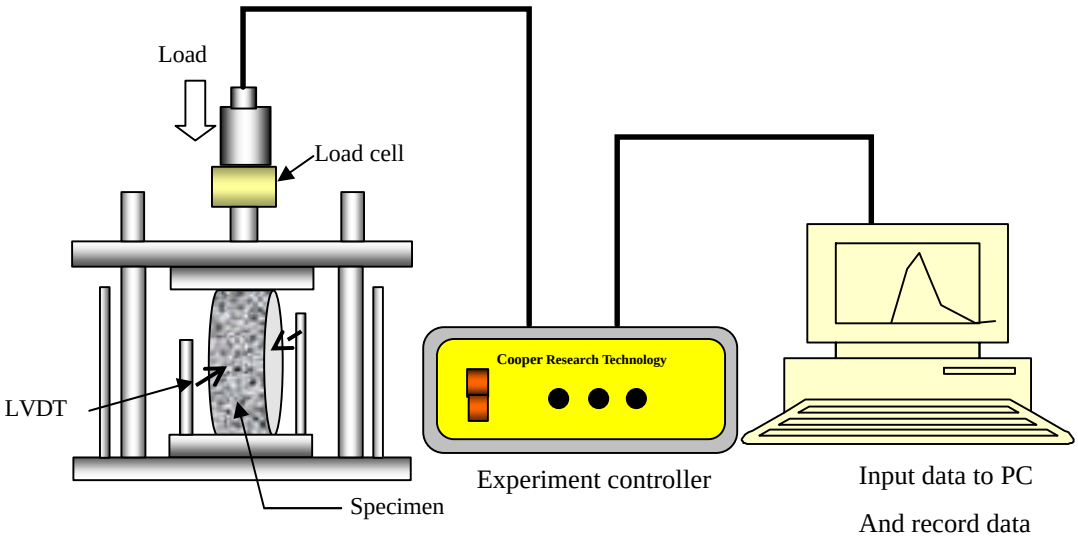

Figure 4.4: Schematic of whole ITSM test equipment

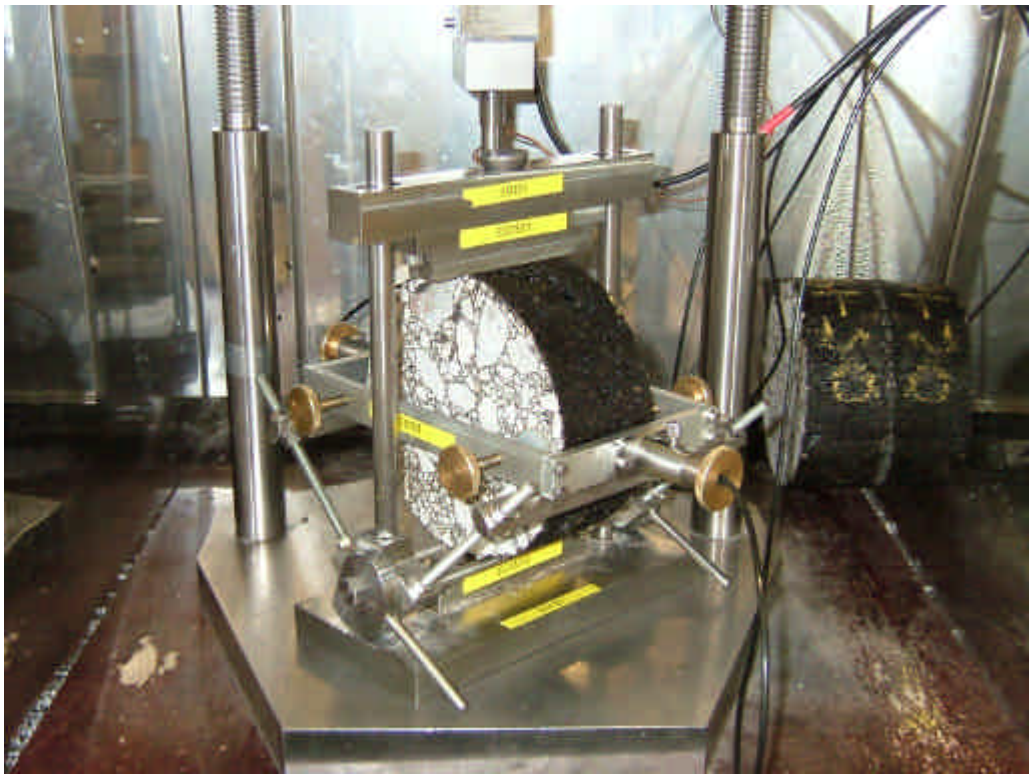

Picture 4.2: ITSM test equipment

Certain parameters need to be selected for the calculation of the elastic stiffness of the mixture. According to the British Standard DD 213, the Poisson's ratio of asphalt mixtures varies with temperature. In case of tests at 20°C, the appropriate value for Poisson's ratio is 0.35. The target horizontal deformation and target load pulse rise time is also needed for the measurement of stiffness. For 100 mm diameter specimens, the peak transient horizontal deformation is 5 μm and loading rise time is 124 milliseconds. For 150 mm diameter specimens, the target horizontal deformation is 7μm and target load pulse rise time is 124 milliseconds. Detailed information for ITSM testing for each diameter is summarized below.

- Specimen diameter; 100 mm 150 mm
- Rise time; 124 milliseconds 124 milliseconds
- Target horizontal deformation; 5 μm 7 μm
- Specimen thickness; 60 +/- 3 mm
- Test temperature; 20°C

The target horizontal deformation and rise time are achieved during five conditioning load pulses (Read and Whiteoak 2003). These conditioning pulses are also used to seat the specimen. After the five conditioning pulses, a further five load applications are recorded and used to determined the mean stiffness of the test specimen. In addition, the test is conducted along two perpendicular axes by rotating the specimen through 90° between tests. The stiffness is then taken as the average of the values determined in the two orientations. Eta (1991) concluded that these two values obtained from the ITSM test sometimes vary between the two

axes because of differences of aggregate matrix in each direction. According to the British Standard DD 213, tolerance between two testing results must be limited to +/- 10%.

4.4 STIFFNESS OF EACH SPECIMEN

4.4.1 Volumetric Proportions and Specimen Size

Asphalt mixture specimens were manufactured using the three compaction methods in this study. Many studies suggested that the mechanical properties of asphalt mixture specimens such as fatigue life and stiffness may be influenced by the air voids (Epps, 1969; Harvey et al. 1993, 1996). Therefore, before conducting mechanical tests for gyratory and vibratory specimens, the volumetric properties of the specimens (i.e. bulk density and air voids) were measured in three stages; before trimming (D = 150 mm by h = 100 mm), after trimming (D = 150 mm by h = 60 mm) and after coring specimens (D = 100 mm by h = 60 mm). The schematic of this process is shown in Figure 4.5. This section addresses the combined effects of compaction methods and specimen size on the volumetric proportions. The measurement results are shown in Tables 4.2 and 4.3.

Table 4.2 indicates the changes in volumetric proportion of gyratory compacted specimens. In general, the air voids of gyratory compacted specimens are decreased as the specimens are trimmed and cored. The air voids of gyratory compacted specimens were reduced by approx. 1% after trimming 20 mm in height on both top and bottom parts of the specimens. In contrast, the volumetric properties of

vibratory compacted specimens showed different trends from the gyratory compacted specimens (see Table 4.3). The vibratory compacted specimens did not show the reduction in air voids after trimming the top and bottom parts of the specimens. However, the specimens showed significant decrease in air voids after coring out D = 100 mm specimens from D = 150 mm specimens.

With regard to gyratory compacted specimens, the results show good agreement with the findings deduced from Masad et al. (1999, 2004), in terms of air void distribution. As described in Chapter 2, they found that the air voids of the middle part of gyratory specimens are smaller than the top and bottom parts (Figure 2.2). This trend is more pronounced as the number of gyrations increases. Since the air voids of middle parts showed significant decrease after trimming the top and bottom parts of specimens in this study, it seems that D = 150 mm by h = 60 mm gyratory compacted specimens have uniform air void distributions.

However, the specimens showed significant reduction in air voids after coring out D = 100 mm specimens from D = 150 mm specimens. This trend indicates some similarities with Harvey et al. (1994). They also observed the reduction in air voids, when the specimens were cored out from larger mass; they concluded that the mould wall affects the outer regions of the specimens, resulting in segregation of larger aggregate, in terms of internal structure; also they stated that this phenomenon leads to the creation of air voids. Considering their results, gyratory compaction may cause segregation of larger aggregate at the outer region of the specimens.

On the other hand, with respect to the vibratory compacted specimens, it seems that the specimens did not have the same air void distribution as the gyratory compacted specimens. The air void distribution did not change, despite trimming the top and bottom part of the specimens. However, the segregation may be caused in the vibratory compacted specimens, as the air voids of the specimens decreased after coring out. Furthermore, the degree of air void reduction for the vibratory compacted specimens was larger than that of the gyratory specimens.

The facts may strongly support that the mould boundary influences on the aggregate structure of mould based specimens. Therefore, it is essential to examine the effects using mechanical testings. It will be discussed further in the following sections.

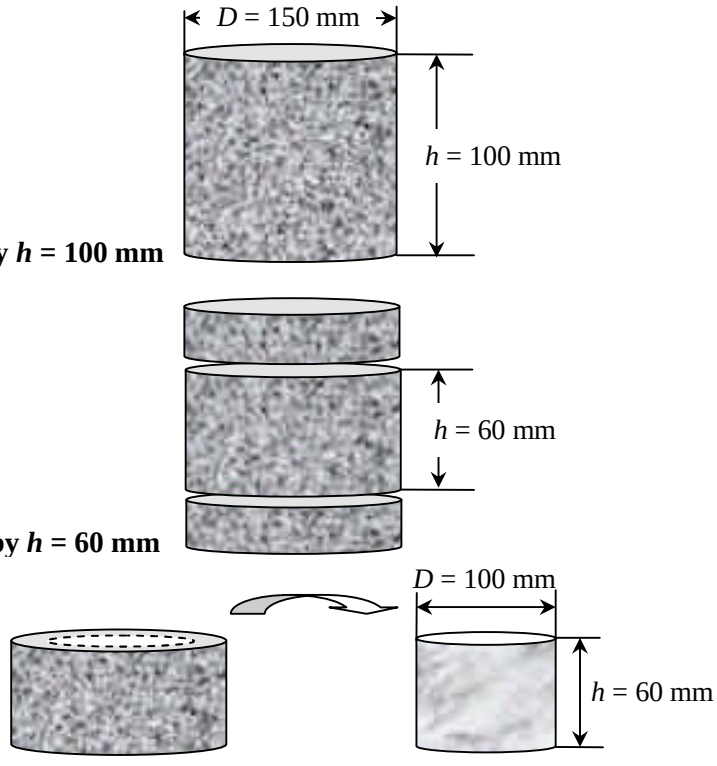

(a) *D* = 150 mm by *h* = 100 mm

(b) *D* = 150 mm by *h* = 60 mm

(c) *D* = 100 mm by *h* = 60 mm

Figure 4.5: Trimming and coring process (a) Before trimming (b) After trimming (c) After coring

Table 4.2: Volumetric proportions of gyratory compacted specimens

Specimen size	*D*=150mm by *h*=100mm	*D*=150mm by *h*=60mm	*D*=100mm by *h*=60mm
Density (kg/m^3)	2403	2432	2438
Air voids (%)	3.9	2.8	2.5

* 12 specimens were tested in each stage.

Table 4.3: Volumetric proportions of vibratory compacted specimens

Specimen size	*D*=150mm by *h*=100mm	*D*=150mm by *h*=60mm	*D*=100mm by *h*=60mm
Density (kg/m^3)	2422	2421	2433
Air voids (%)	3.1	3.1	2.7

* 12 specimens were tested in each stage.

4.4.2 Influence of Compaction Method on Asphalt Mixture Stiffness Modulus

Many studies regarding differences of compaction methods have been carried out with these results showing significant differences between compaction methods. Although the aim of this study is to investigate the influence of specimen geometry size and orientation, the effect of compaction method on stiffness modulus was also examined. The reasons for these comparisons are to understand the specific features of aggregate structure in each compaction method. By comparing stiffness modulus of each compaction method, some significant features could be identified. To achieve this aim, this section was divided into three phases.

Firstly, the differences of gyratory and vibratory compaction methods with 150 mm diameter specimens were examined using the ITSM test. Secondly, comparisons between this study and previous studies were carried out to confirm whether testing results and trends are comparative or not. Finally, three compaction methods with 100mm diameter specimens, namely gyratory, vibratory and roller compacted specimens, were compared with previous work. The aim of this section is to

confirm whether the trends of the testing results show the same as previous studies and to find some significant features.

Table 4.4 shows the average values from the 12 ITSM testing for 150mm diameter specimens. In the case of the gyratory compacted specimens, the standard deviation of air void contents for twelve specimens was 0.77. It means that air void contents of these twelve specimens are relatively consistent. If this data showed inconsistent scatter, these specimens would be unable to be compared because air voids of specimen affect mechanical properties of specimen as well as its performance. Therefore, before comparing each result, it was required to confirm whether these data are consistent or not. As stated above, since standard deviation for air void contents of 150 mm diameter specimen was 0.77, it is said that mean air voids and elastic stiffness were able to be used for the comparison with other specimens. Testing results showed that mean air void content for gyratory compacted specimens was 2.8, whereas its elastic stiffness was 6786 MPa.

In case of vibratory compacted specimens, the standard deviation for air void contents of 150 mm diameter specimens was 1.15. Normally, air void contents for vibratory compacted specimens tend to have more scatter as compaction is carried out by manual operation. Many factors such as compaction time, compaction force and place affect air void contents of specimens. However, these specimens were relatively consistent at a standard deviation of 1.15. Therefore, specimens were also able to be compared with each other. The mean air void content for 150 mm diameter specimens was 3.1 and mean elastic stiffness modulus was 8042 MPa.

Table 4.4: Result of the ITSM test for *D* = 150 mm specimens (This study)

Compaction Methods	Gyratory	Vibratory
Average Air Voids (%)	2.8	3.1
Average Stiffness (MPa)	6786	8042
Std Dev Air Voids (%)	0.77	1.15
Std Dev Stiffness (MPa)	566	670

* 12 specimens were tested in each compaction method.

Table 4.5: Result of the ITSM test conducted for *D* = 150 mm specimens (Hunter et al. 2004; Airey et al. 2006)

Compaction Methods	Gyratory	Vibratory
Average Air Voids (%)	3.1	2.8
Average Stiffness (MPa)	7906	10088
Std Dev Air Voids (%)	0.41	0.21
Std Dev Stiffness (MPa)	745	932

In terms of mean air void contents, the gyratory and vibratory compacted specimens showed values of 2.8 and 3.1, respectively. The difference between these values was 0.3. Therefore, it was considered that the physical state of these two types of specimens is almost the same; it was judged that comparison for elastic stiffness of both gyratory and vibratory compacted specimens was possible. Table 4.4 indicates that the mean elastic stiffness of gyratory compacted specimens with 150 mm diameter was 6786 MPa, and that the value for vibratory compacted specimens was 8042 MPa. The difference between these values was 1256 MPa. Despite the fact that these two types of specimen were manufactured using the same aggregate, binder (bitumen) and grading, stiffness of vibratory compacted specimens was significantly stiffer than gyratory compacted specimens. Masad et al. (2004) suggested that these differences were attributed to internal structure of the specimen.

Hunter et al. (2004) also conducted a similar study. They carried out experiments using three different types of compaction machine: gyratory, vibratory and roller compactor. Table 4.5 shows their ITSM testing results. In this case, the elastic stiffness of gyratory compacted specimens was 7906 MPa, whereas the elastic stiffness of vibratory compacted specimens was 10088 MPa. Average air void contents for gyratory and vibratory compacted specimens were 3.1% and 2.8%, respectively. As indicated at Table 4.5, the elastic stiffness of vibratory compacted specimens showed significantly stiffer value than gyratory compacted specimens. Therefore, it is clear that there are differences between gyratory and vibratory compacted specimens in terms of elastic stiffness.

Similar trends have appeared in this study as well. As stated above, the elastic stiffnesses of the gyratory and vibratory compacted specimens with 150 mm diameter were 6786 MPa and 8042 MPa, respectively. Therefore, it was found that the same trend which shows higher stiffness in vibratory compacted specimens was observed, although overall stiffness was lower than in the previous study.

In the case of 100 mm diameter specimens which were cored from 150 mm diameter specimens, the same trend was found. Table 4.6 shows the average values from the 12 ITSM testing results for 100 mm diameter specimens. Each specimen was manufactured by using gyratory, vibratory and slab ‘roller’ compacter. Standard deviation of air voids for each set of specimens was around 1.0. In particular, slab ‘roller’ compacted specimens showed 0.6 as a standard deviation. Mean air void contents for the gyratory, vibratory and slab ‘roller’ compacted

specimen were 2.5, 2.7 and 2.6, respectively. Since these are not big differences, the physical state of each specimen was identified as almost the same. The elastic stiffnesses of these specimens were 6304 MPa for the gyratory compacted specimens, 7435 MPa for the vibratory compacted specimens and 6577 MPa for the roller compacted specimens. Comparing with Hunter et al. (2004), trends between these specimens were almost the same, since vibratory compacted specimens showed the highest stiffness value for these three types of specimen (see Table 4.7). Moreover, stiffness of gyratory and vibratory compacted specimens were regarded as the same, since the difference was 273 MPa. Hunter et al (2004) also indicated similar trends. In this case, the difference in stiffness was 585 MPa. As a result, these differences were also not considered significant. Therefore, it is understood that there were no significant differences between gyratory and slab 'roller' compacted specimens in terms of elastic stiffness.

Table.4.6: Result of the ITSM test (for D = 100 mm)

Compaction Method	Gyratory	Vibratory	Slab(Z direction)
Average Air Voids (%)	2.5	2.7	2.6
Average Stiffness (MPa)	6304	7435	6577
Std Dev Air Voids (%)	1.05	1.00	0.60
Std Dev Stiffness (MPa)	597	642	794

* 12 specimens were tested in each compaction method.

Table.4.7: Result of the ITSM test conducted by Hunter et al. (2004) (Including slab compacted specimens)

Compaction Method	Gyratory	Vibratory	Slab(Z direction)
Average Air Voids (%)	3.1	2.8	3.0
Average Stiffness (MPa)	7906	10088	7321
Std Dev Air Voids (%)	0.41	0.21	0.42
Std Dev Stiffness (MPa)	745	932	753

4.4.3 Influence of Specimen Size on Stiffness Modulus

Two types of compaction method were examined to investigate the influence of specimen size in terms of elastic stiffness of the asphalt mixture. The testing programme for this part was divided into two phases. Firstly, specimens 150 mm in diameter were manufactured using gyratory and vibratory (kango) compaction. After manufacturing the specimens, they were trimmed to 60 mm in height, then 12 ITSM tests were carried out to determine the elastic stiffness modulus of each specimen. Testing results are shown in Figures 4.6 and 4.7. In terms of gyratory compacted specimens, the average elastic stiffness modulus of 150 mm diameter specimens was 6786 MPa. Although the range of air voids was between 1.8 and 4.8%, most air voids contents were relatively similar. Average air void was 2.8%.

Some significant trends were found when comparing with 100 mm diameter gyratory compacted specimens which were cored from 150 mm diameter specimens. ITSM test results indicate differences of elastic stiffness between 150 mm and 100 mm diameter specimens. Average values from the 12 ITSM tests suggest that elastic stiffness decreased slightly from 6786 MPa with 150 mm diameter specimens to 6304 MPa with 100 mm diameter specimens. Also, average air void content decreased to a certain extent. Moreover, in terms of stiffness modulus, each test result also shows the same trend except for sample number 05-1722 (see Appendix). In theory, specimens with high density have higher stiffness than specimens with lower density. However, actual ITSM testing results showed a different trend. Hunter et al. (2004) indicated that the mechanical properties of asphalt mixture would be related to particle orientation in the

aggregate matrix. Although they did not try to examine the influence of specimen size, they showed significant differences in the elastic stiffness of asphalt mixtures using image analysis. Therefore, it was expected that these results may be explained through image analysis. Results of the image analysis are described in Chapters 6 and 7.

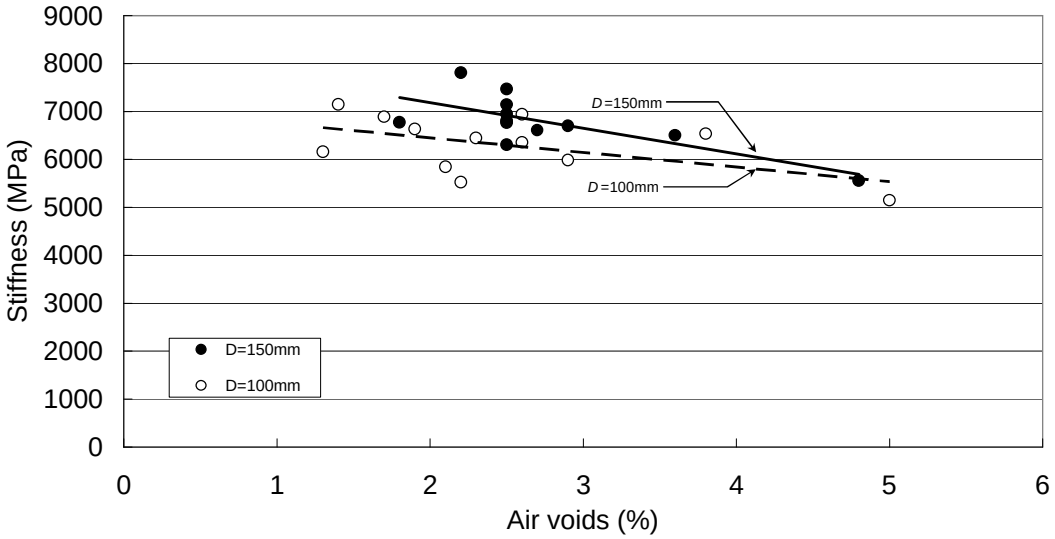

Figure 4.6: Relationship between stiffness and air voids for gyratory compacted specimens

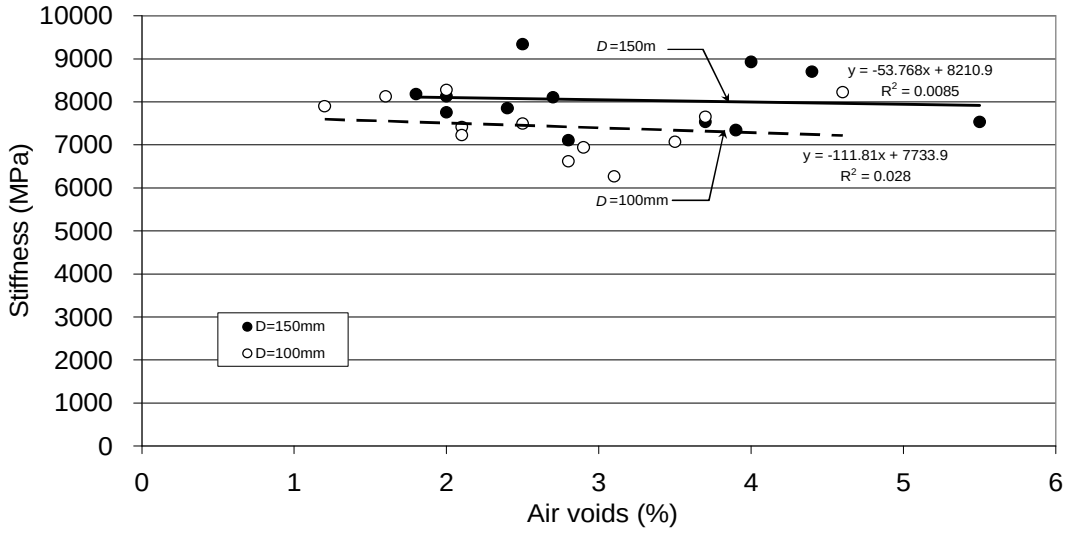

Figure 4.7: Relationship between stiffness and air voids for vibratory compacted specimens

Figure 4.6 shows the relationship between elastic stiffness modulus and air void contents of each specimen. The solid line and dotted line represent the results of linear regression analysis for both 150 mm and 100 mm diameter specimens, respectively. It seems that the slopes of both lines are similar within the range between 1.5% and 3.0% in air void content. However, the gap between the two lines decreases gradually from 1.5% to 5.0% in air void contents. Therefore, it is said that the influence of specimen size for the gyratory compacted specimens tends to be eliminated as air voids contents become high.

In terms of vibratory compacted specimens, the stiffness and trends between 150 mm and 100 mm diameter specimens were somewhat different compared with the gyratory compacted specimens. As stated in Section 4.4.2, vibratory compacted specimens showed higher stiffness than gyratory compacted specimens. Air void contents of vibratory compacted specimens were 3.1% on average. In addition to this, the standard deviation of these specimens was 1.1%. This means that air void contents of vibratory compacted specimens were consistent. Therefore, it is possible to compare these specimens in this study. With respect to 100 mm diameter specimens, the elastic stiffness is 7435 MPa as an average. The same trends for gyratory compacted specimens could be observed in this case as well. Despite the fact that 100 mm diameter specimens, which were cored out from 150 mm diameter specimens, have lower air voids contents, the elastic stiffnesses of these specimens were lower than 150 mm diameter specimens. These trends were found in each specimen except for specimen sample number 05-1930 (see Appendix 1).

With regard to the relationship between elastic stiffness and air voids, the trend lines were different from these for gyratory compacted specimens. Figure 4.7 shows the relationship between 150 mm and 100 mm diameter vibratory compacted specimens. Solid and dotted lines represent 150 mm and 100 mm diameter specimens, respectively. The slopes of these lines were calculated from the same linear regression analysis as was used for gyratory compacted specimen. The slope for 150 mm diameter specimens tends to be flat, whereas the slope for 100 mm diameter specimens decreases gradually as air void contents increase. Furthermore, the gap between the two lines increases steadily. These trends are different from these for gyratory compacted specimens.

In brief, two different types of compaction method have been compared looking at the influence of specimen size in this section. Through a series of the ITSM tests, some significant features were understood in this study. From the stiffness point of view, it is found that elastic stiffness of 100 mm diameter specimens decreases slightly compared with 150 mm diameter specimen, despite the fact that 100 mm specimens were denser than 150 mm specimens. These trends were observed from both gyratory and vibratory compacted specimens. Therefore, an investigation focused on the aggregate matrix is required, using image analysis. The image analysis methodology used in this study is described in Chapter 5.

With regard to the relationship between stiffness and air voids, the two types of compacted specimen showed contrasting trends. In the case of gyratory compacted specimens, the gap between the trend lines for 150 mm and 100 mm diameter

specimens decreased steadily as air void contents increased, whereas the gap between these lines for vibratory compacted specimen appears to be increasing gradually as air voids increased. The reason for the above mentioned phenomenon is not understood. Therefore, further investigations looking at aggregate matrix were carried out using the image analysis as described in Chapters 6 and 7.

4.4.4 Stiffness Modulus of the Slab in Three Orthogonal Directions

The mechanical properties of asphalt mixtures in the three dimensions tend to differ. However, the influence of specimen orientation in the Z, Y and X directions is difficult to quantify. This section compared the influence of specimen orientation on mechanical properties of asphalt mixture by coring specimens in the Z, Y and X directions from a slab. Usually, slab type specimens, which are compacted by roller compactor, are used for wheel tracking tests. Moreover, specimens which are cored out from the Z-direction have been used to determine the one dimensional mechanical properties of asphalt mixtures. The aim of this section is to compare specimen orientations and to understand the three dimensional behaviour of the pavement in terms of elastic stiffness. To achieve this aim, three slabs were manufactured using the laboratory roller compactor and then specimens were cored out from the Z, Y and X directions as shown in Figure 4.8. After that, these specimens were trimmed to 60 mm in height and the 12 ITSM tests were conducted in each cored direction.

Table 4.8 presents the air voids and ITSM testing results of specimens which were cored out from the Y-direction (direction of roller). The standard deviation for these

twelve specimens was 0.4%. It means that these air void contents are consistent; and therefore, these specimens should have almost the same physical properties. Mean air void content was 2.9%. Maximum air void content in these specimens was 3.4%, whereas minimum air void content was 2.0%. From these results, it was confirmed that differences between specimens were small and the air void distribution of the twelve specimens was relatively uniform.

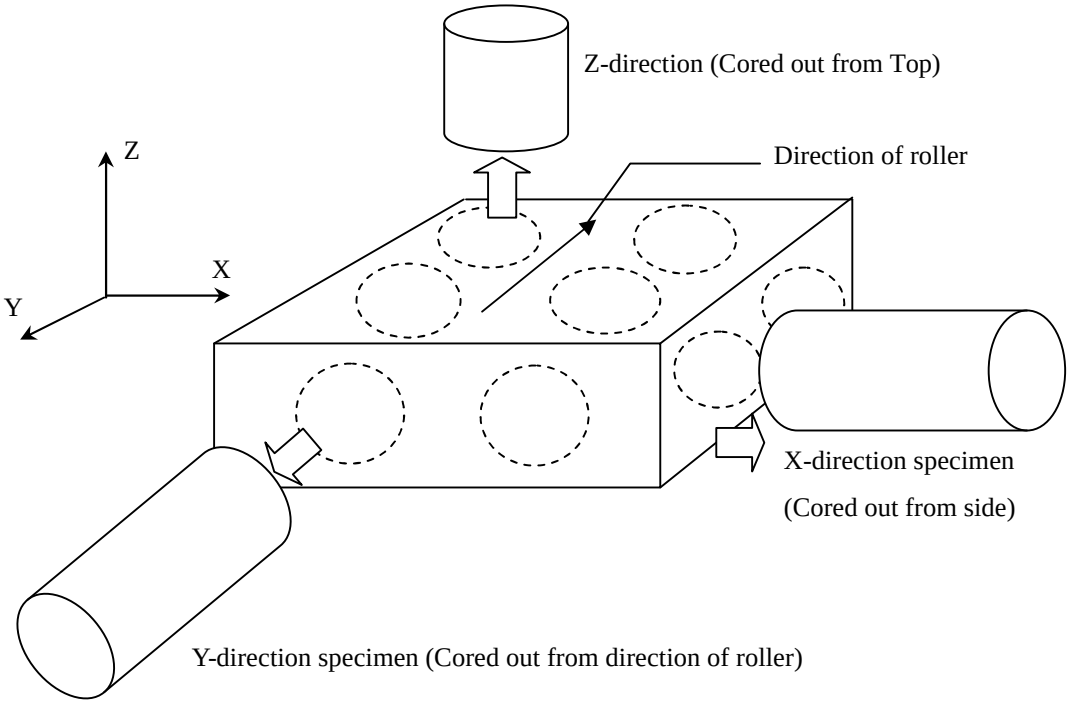

Figure 4.8: Schematic representation for specimens cored out from slab

With regard to the elastic stiffness, the mean elastic stiffness was 5868 MPa; maximum and minimum values of elastic stiffness were 6859 MPa and 5212 MPa, respectively. Therefore, the elastic stiffness can be considered to be closed.

In case of the X-direction, the trends for physical properties of each specimen are quite similar. Table 4.8 shows the mean air void content and elastic stiffness of specimens. The standard deviation for air void content was 0.6% which means the data are relatively consistent. Average air voids was 3.0%. With respect to elastic stiffness, mean elastic stiffness modulus was 4945 MPa. From the stiffness point of view, it seems that this value is relatively lower than for conventional specimens (Z direction) which are associated with the 28 mm DBM asphalt mixture.

Table 4.8 also shows the result of the ITSM test for specimens which were cored out in the Z-direction. According to these results, the air voids content of each specimen is almost the same with a standard deviation for these specimens of 0.6%. Therefore, it is possible to compare each specimen. Mean air void content and elastic modulus are 2.6% and 6577 MPa, respectively. The mean air voids of 2.6% is lower than for specimens which were cored out from the X and Y directions, whereas mean elastic stiffness showed a higher value compared with other the two directions. The relationships between stiffness and air voids for slab specimens are shown in Figure 4.9.

Table 4.8: Results of the ITSM test for slab specimens

	Specimen Direction (D = 100 mm)		
	Z-direction (Top)	Y-direction (Roller)	X-direction (Side)
Average Air Voids (%)	2.6	2.9	3.0
Average Stiffness (MPa)	6577	5868	4945
StDv Air Voids (%)	0.6	0.4	0.6
StDv Stiffness (MPa)	794.0	469.5	319.7

* 12 specimens were tested in each direction.

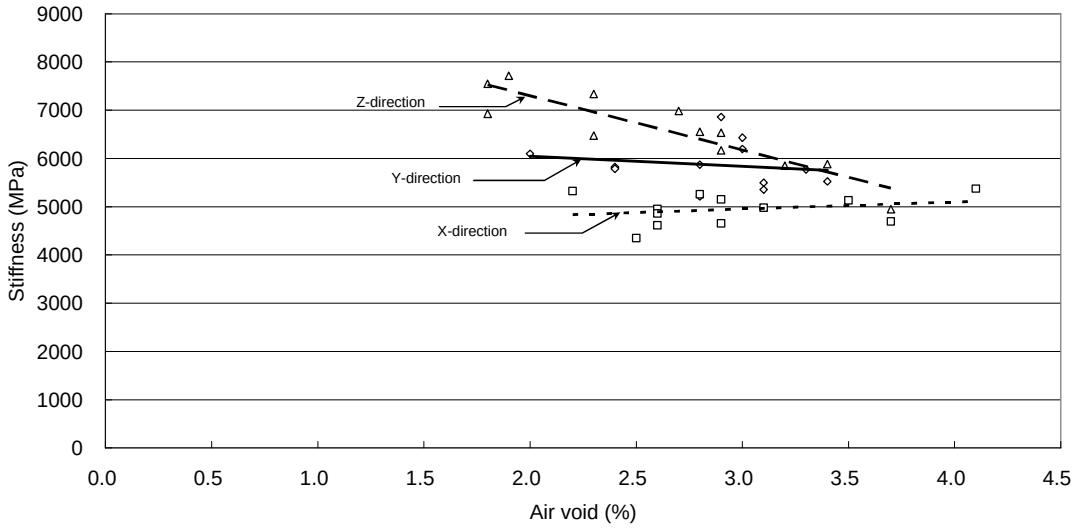

Figure 4.9: Relationship between stiffness and air voids for slab compacted specimens

4.4.5 Stiffness Properties for Slab Specimens

In order to examine the mechanical properties of slab specimens (12 specimens in each direction) in more detail, the density, air voids and ITSM test results shown in Tables 4.8 were re-analyzed in each cored and trimmed position. The schematic of this analysis is represented in Figure 4.10; the results are shown in Tables 4.9 to 4.12.

As shown in Table 4.9, the specimens indicated considerable variations in stiffness modulus, with respect to the effect of specimen orientation. The stiffest specimens were taken from Z direction, followed by the Y direction and X direction. However, in terms of Z direction, the results showed significant differences in stiffness in each position.

Tables 4.10 and 4.11 show the stiffness results in slab cores taken from Y and X directions. It is notable that the middle-part specimens indicate lower stiffness compared to these from the sides. This trend is consistent in both Y and X directions.

Table 4.12 shows in more detail the differences in stiffness in both core directions and positions. As would be expected, the cored specimens show considerable variations in stiffness in each position. Therefore, it seems that the mechanical properties of slab specimens are different in the three orthogonal coring directions. This is discussed further in the following sections.

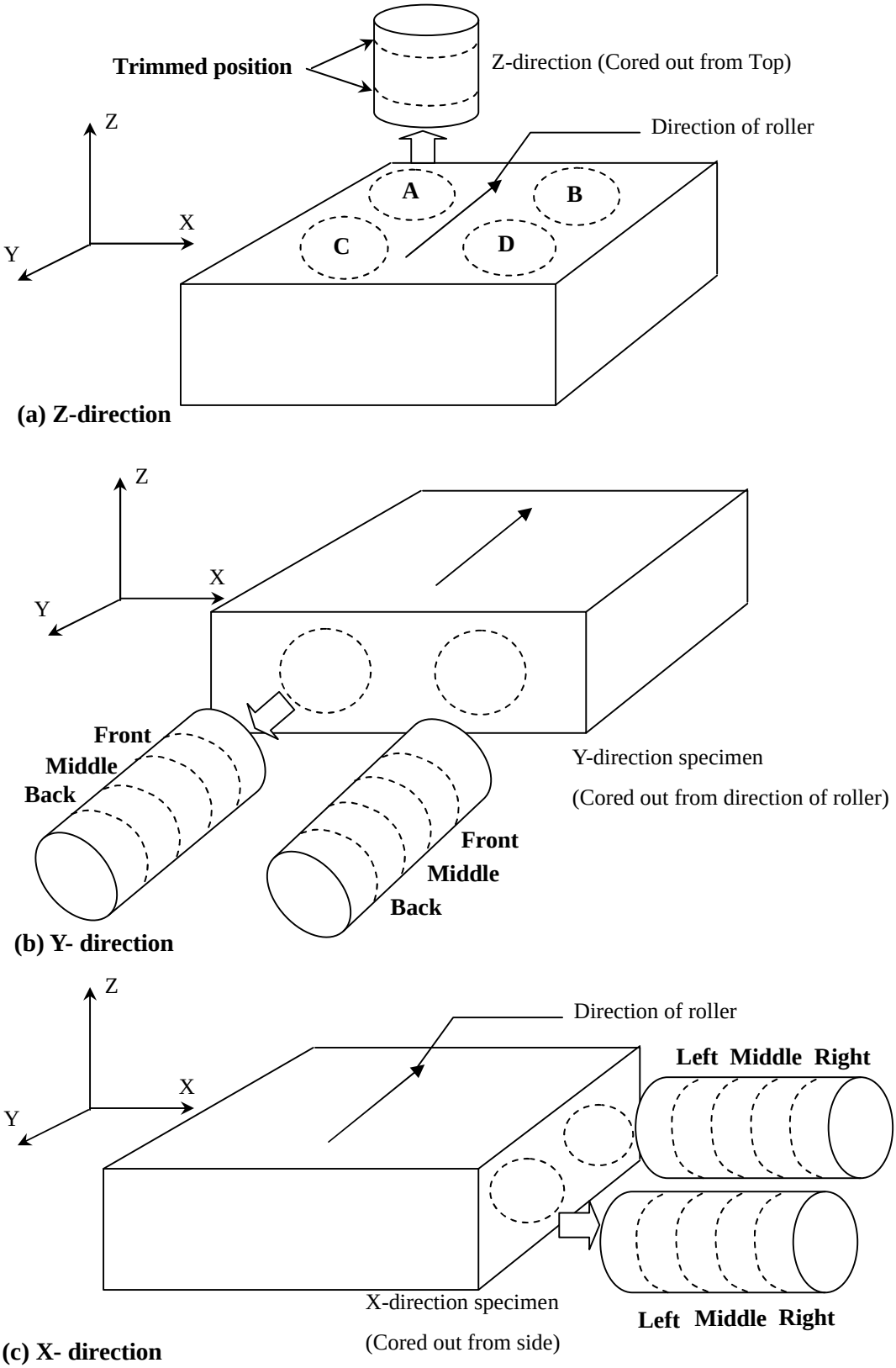

Figure 4.10: Schematic representation for trimmed positions of slab cores

Table 4.9: Differences of stiffness in each cored position (Z-direction)

Parameter	Slab Compaction 100 mm specimen (Z direction)			
Position	A	B	C	D
Density (kg/m^3)	2419	2424	2442	2450
Air voids (%)	3.3	3.0	2.3	2.0
Stiffness (MPa)	5778	6346	6651	7532

***** 3 specimens were tested in each position.

Table 4.10: Differences of stiffness in each trimmed part (Y direction)

Parameter	Slab Compaction 100 mm specimen (Y direction)		
Position	Front	Middle	Back
Density (kg/m^3)	2425	2434	2427
Air voids (%)	3.0	2.7	2.9
Stiffness (MPa)	6175	5684	5747

* 4 specimens were tested in each position.

Table 4.11: Differences of stiffness in each trimmed part (X direction)

Parameter	Slab Compaction 100 mm specimen (X direction)		
Position	Left	Middle	Right
Density (kg/m^3)	2423	2429	2426
Air voids (%)	3.1	2.9	2.9
Stiffness (MPa)	5184	4629	5021

* 4 specimens were tested in each position.

Table 4.12: Relationship of stiffness between cored directions and positions

Direction	Parameter	Position			
		A	B	C	D
Z[*1]	Air voids (%)	3.3	3.0	2.3	2.0
	Stiffness(MPa)	5778	6346	6651	7532
Y[*2]	Air voids (%)	3.1	3.0	2.9	2.9
	Stiffness (MPa)	5822	6529	5673	5821
X[*2]	Air voids (%)	2.8	2.7	3.5	3.2
	Stiffness (MPa)	5053	5151	5315	4891

*1: 3 specimens were tested in each position.

*2: 2 specimens were summarized in each position.

4.5 TESTING METHOD FOR RLAT

The repeated load axial test (RLAT) was carried out to confirm whether there are any significant differences in the permanent deformation characteristics of slab specimens in each direction. As stated in Chapter 3, cores were taken from the slab in each direction. Two cylindrical type cores were cored out in the X and Y directions, respectively. In addition, four cores were cored out in the Z-direction. After taking the cores from the slab, the specimens were trimmed to 60 mm in height. As a result, 12 specimens per direction were manufactured for RLAT as well as ITSM testing.

After finishing the non-destructive ITSM test, specimens were stored in a cabinet at 5°C to prevent ageing of the specimens. The specimens were then subjected to RLAT at a temperature of 50°C after conditioning the specimens at this temperature for 16 to 24 hours. The RLA test was therefore able to look at aggregate structure (matrix) rather than the effect of binder (bitumen) which has a greater influence when the RLA test is run at a temperature of 30°C. A close up of the RLA test equipment is shown in Picture 4.3.

The Nottingham Asphalt Tester (NAT) was used to evaluate the characteristics of permanent deformation of specimens cored from slabs. The testing load was applied to the specimen by applying compressed air pressure through a pneumatic actuator. The operation of compressive air pressure is controlled by a PC associated with an analogue converter which was produced by Cooper Research Technology.

If the specific parameters which are required to run the experiment are input into the PC, then the appropriate loads are applied automatically to the specimen through the pneumatic actuator. The resultant deformation is measured by LVDTs fixed to the top of specimen. Gibb (1996) states that this layout provides acceptable "mechanical averaging" for the measurement of overall strain and prevents the reading of local strain.

Measured strain and applied load are indicated on the interface of the PC. At the same time, these results were recorded to the hard disc of the PC. The operations for the implementation of the experiment and data collection are controlled simultaneously by the software. As a result, the experiment was conducted properly utilising the above mentioned system.

The RLA test was carried out to measure the permanent deformation characteristics of specimens cored from slabs in each direction. The testing procedure was divided into three phases. Firstly, a specimen was placed carefully into the testing equipment, then the LVDTs were installed at the top of the specimen. Secondly, a conditioning stress which is a static pressure of 10 kPa at a temperature of 50°C was applied to the specimen. The aim of this procedure is to seat the loading plate on the specimen prior to the experiment. The duration of conditioning was 600 seconds. After the elapsed 600 seconds, the RLA test was carried out by applying 3600 cycles of pneumatic pressure. The time of loading was one second followed by no-loading for one second in a square load pulse (Gibb, 1996). These repeated loads were applied to the specimen with a stress of 100 kPa and the permanent

deformation of each specimen was measured.

The testing conditions for RLA tests are summarized as:

- Test temperature : 50°C
- Axial stress : 100 kPa
- Conditioning stress : 10 kPa for 600 seconds
- Testing duration : 3600 cycles with 1 second of applied load followed by 1 second of no-load

Picture4.3: RLA test equipment

4.6 PERMAMENT DEFORMATION CHARACTERISTICS OF THE DIFFERENT SPECIMEN ORIENTATIONS

4.6.1 RLAT results

In order to understand the behaviour of the aggregate matrix, RLA testing was carried out using specimens cored out from Z, Y and X-directions of the slab. As stated above, 12 RLA testing in each direction was conducted at 50°C to look at the behaviour of aggregate under the repeated load. Moreover, to investigate three dimensional properties of aggregate structure, specimens were cored out from Z, Y and X-directions, then these were trimmed to 605 mm in height. After conditioning in a 50°C cabinet for 16~24 hours, RLA test was carried out. The results of the 12 RLA tests in each direction are shown in Table 4.13 and Figures 4.11 to 4.13.

Specimens cored out in the Y-direction (direction of roller) indicated a relatively small value of mean axial strain, despite of the fact that the RLA test was carried out at 50°C. The mean axial strain of those specimens was 1.04%, whereas the standard deviation was 0.18%. Therefore, it can be said that the axial strain in each specimen was consistent. Comparing with Hunter et al. (2004), it was understood that these values are small. They carried out RLA tests at 30°C and their specimens showed higher strain than 1.04%, although they used specimens cored out from Z-direction. They showed 1.33% as a mean axial strain, although the mean air void was 4.4%. As a result of this, it can be said that the permanent deformation characteristics for the specimens cored out from the Y-direction, were stiff compared with conventional specimens.

In the case of specimens cored out from X-direction (side), the data for those specimens showed similar results to those in the Y-direction. Maximum and minimum axial strains were 1.51% and 0.97%, respectively.

Table 4.13: RLA test results

Parameter	Slab Compaction D = 100 mm specimens		
Direction	Z	Y	X
Air voids (%)	2.6	2.9	3.0
Final axial strain (%)	1.52	1.04	1.15
Final strain rate ε* (%/cycle)	1.13E-04	9.24E-05	9.54E-05

* 12 specimens were tested in each direction.

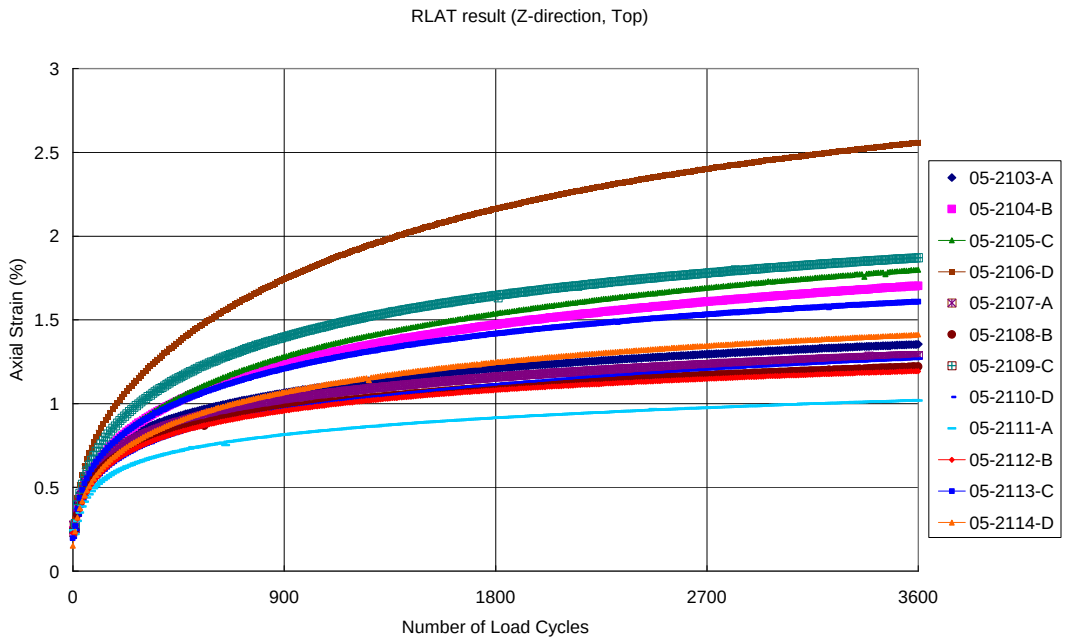

Figure 4.11: RLA test results (Z-direction, top)

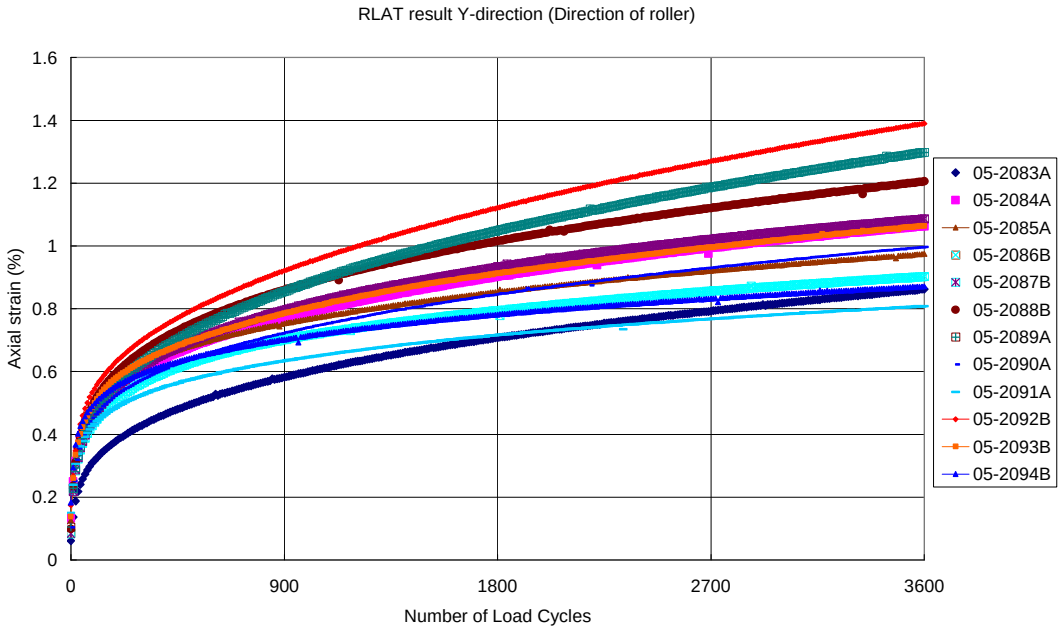

Figure 4.12: RLA test results (Y-direction, direction of roller)

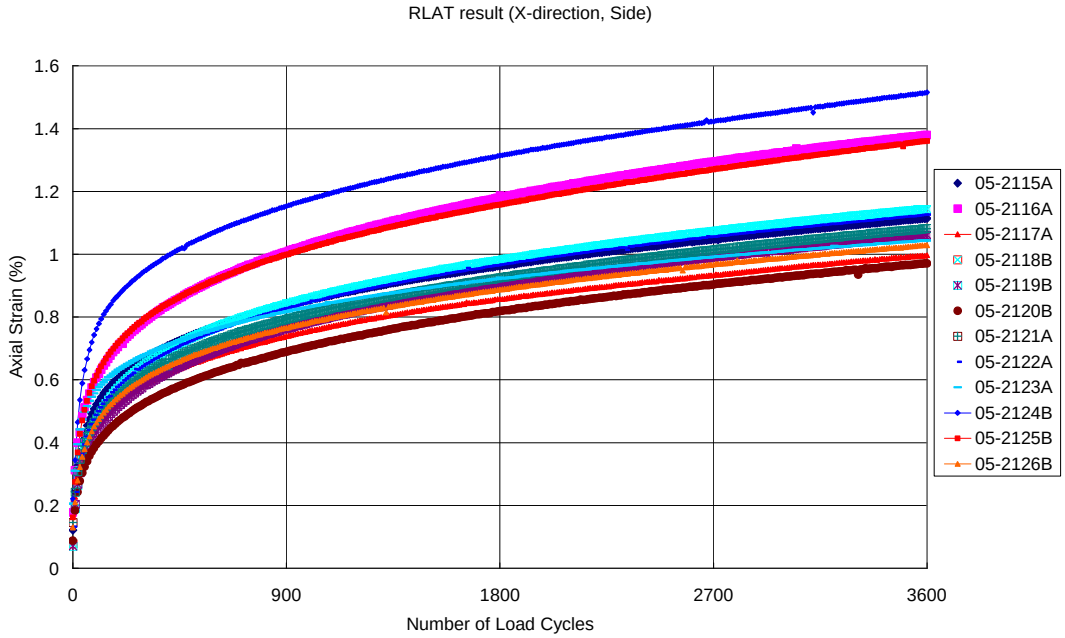

Figure 4.13: RLA test results (X-direction, side)

The standard deviation was 0.17 which was almost the same as for Y-direction specimens. Mean axial strain was 1.2%. However, the results for sample number 05-2124-B and 05-2125-B were not accurate because the bottom of the specimens indicated cutting error due to the trimming process (see Appendix). As a result, the LVDT measured this part of strain. Therefore, if those data were eliminated from the calculation, the mean axial strain is 1.1%. This value is similar to that in the Y-direction. Therefore, it can be said that specimens cored out from the Y-direction and X-direction have almost the same properties in terms of permanent deformation characteristics.

However, specimens cored out from the Z-direction showed a different trend. Table 4.13 also contains the results of RLA testing for those specimens. The standard deviation for those twelve datasets was 0.42. Maximum and minimum axial strains were 2.56% and 1.02% respectively, whereas mean axial strain was 1.52%. Compared with the other two directions, specimens cored out from the Z-direction showed slightly higher axial strain than those of the two other directions. It is difficult to explain why these differences occurred between these specimens. However, it is assumed that this is attributed to the aggregate orientation.

With respect to the deformation behaviour of specimens, a parameter called ε* is determined to characterize each specimen. ε* was defined as

$$e = \frac{e_{3600} - e_{1500}}{(3600 - 1500)} \tag{4.6}$$

where ε_{3600} and ε_{1500} were strains at the 3600^{th} and 1500^{th} cycle, respectively.

The mean slope of the strain curve (ε*) for Y-direction specimens was 9.24E-05, whereas ε* of X-directions specimen was 9.54E-05. As stated above, these two directions indicated similar axial strains; and ε* values in these two directions were also similar. Therefore, it can be said that specimens which were cored out from X-direction and Y-direction have almost the same properties in terms of strain.

On the other hand, the mean slope of the strain curve for Z-direction specimen was 1.13E-04. As axial strains for those specimens were higher than for the other two directions, the ε* value was higher as well. However, as stated above, some specimens indicated relatively higher values; others showed lower values in the Z-direction. Therefore, it is assumed that this scatter of data is attributed to the internal structure of the specimen. In particular, specimens which were cored out from the Z-direction showed relatively higher values in terms of standard deviation.

4.6.2 Normalized Strain Accumulation Plots

The axial strain of slab specimens produced from RLA tests was normalized to the final strain to examine the mechanical properties. The results are shown in Table 4.14; and the strain accumulation plots are presented in Figures 4.14 to 4.16. Although the specimens cored from the three orthogonal directions show similar strain accumulation curves, the normalized strain rates indicate slight differences in each direction. However, it is interesting to note that the strain curves obtained from RLA tests show significant variation, while the normalized accumulation plots indicate relatively similar curves.

Table 4.14: Normalized strain rate for slab specimens

Parameter	Slab Compaction D = 100 mm specimens		
Direction	Z	Y	X
Air voids (%)	2.6	2.9	3.0
Normalized strain rate* (%/cycle)	7.14E-05	8.66E-05	8.29E-05
StDv	1.16E-05	1.69E-05	6.00E-06

* Normalized to final axial strain

* 12 specimens were tested in each direction.

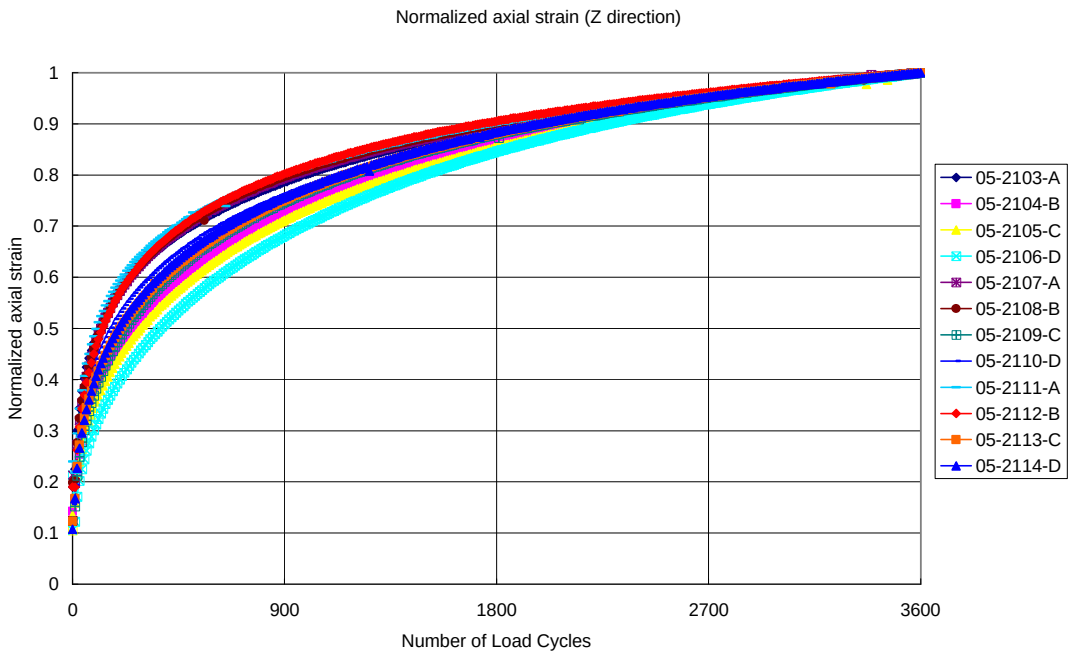

Figure 4.14: Normalized strain accumulation plots (Z direction)

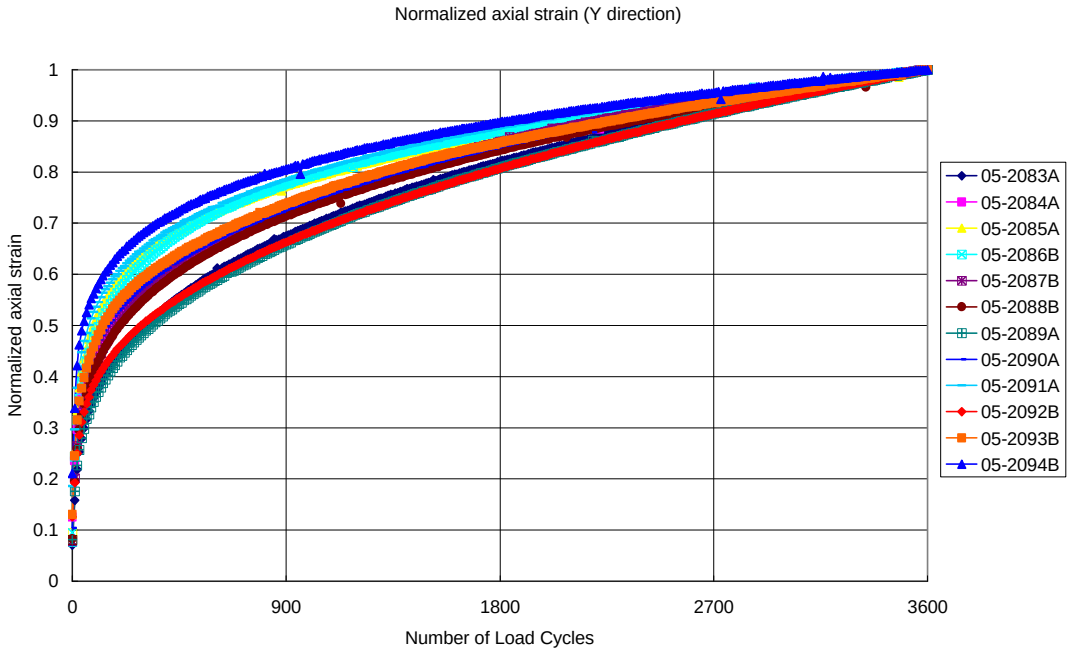

Figure 4.15: Normalized strain accumulation plots (Y direction)

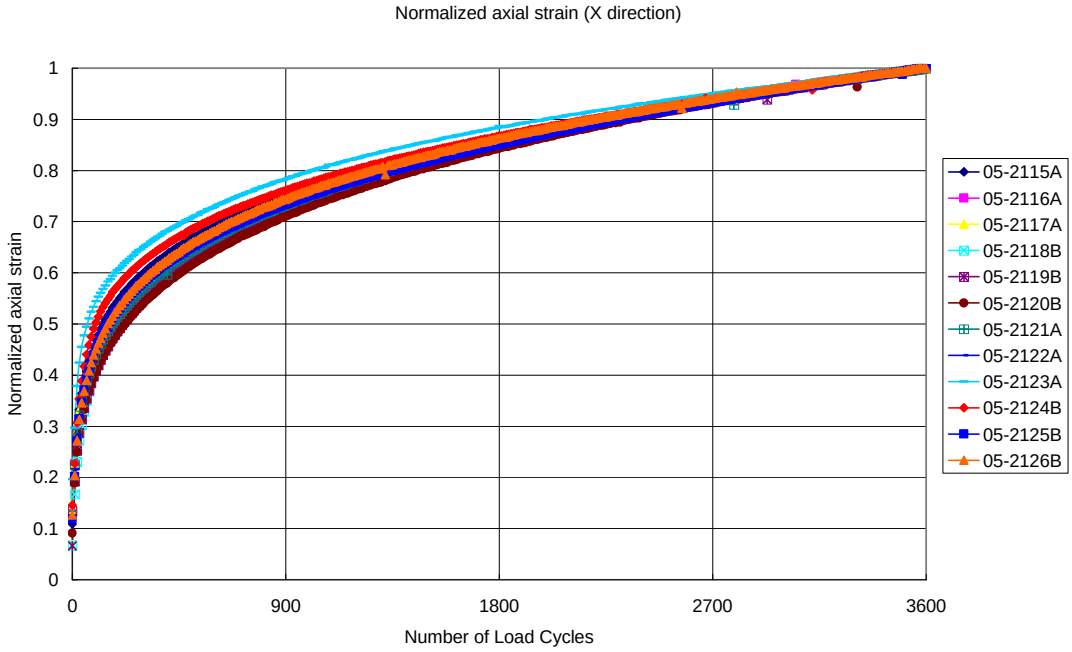

Figure 4.16: Normalized strain accumulation plots (X direction)

4.6.3 Permanent Deformation Properties

An interesting feature of slab specimen stiffness in the three orthogonal coring directions was described in Section 4.4.5. A more detailed investigation looking at axial strain was conducted using RLAT results.

Table 4.15 presents the summarized permanent deformation results for Z direction specimens cored from each position. The results show significant differences in both final axial strain and strain rate. It should be noted that the specimens with lower air voids (i.e. position C and D) tend to show lower permanent deformation resistance compared to the specimens with higher air voids (i.e. position A and B). Also, it is interesting to note that the Z specimens show lower permanent deformation resistance, despite the fact that the specimens have relatively higher stiffness than specimens cored from other directions as discussed in Section 4.4.5.

Tables 4.16 and 4.17 show the variation of permanent deformation with air voids for the specimens cored from Y and X directions. However, no significant differences are shown in middle part of specimens, despite the fact that the specimens indicate lower stiffness than specimens from other sides.

Table 4.18 shows the variation of axial strain with air voids looking at both cored directions and positions. Based on these results, it appears that the permanent deformation properties do not necessarily coincide with air voids in terms of the slab cored from three orthogonal directions. For the Z direction, specimens with lower air voids tend to show lower permanent deformation resistance. In contrast,

for Y and X directions, the specimens with lower air voids tend to have higher permanent deformation resistance. Therefore, the permanent deformation results may not correspond to the air voids of specimens with respect to the slab specimens in this study.

Table 4.15: Differences of axial strain in each cored position (Z-direction)

Parameter	Slab Compaction *D* = 100 mm specimens (Z direction)			
Position	A	B	C	D
Air voids (%)	3.3	3.0	2.3	2.0
Final Axial Strain (%)	1.22	1.37	1.76	1.75
Strain Rate (%/cycle)	7.59E-05	9.42E-05	1.37E-04	1.44E-04

* 3 specimens were tested in each position.

Table 4.16: Differences of axial strain in each cored part (Y-direction)

Parameter	Slab Compaction *D* = 100 mm specimens (Y direction)		
Position	Front	Middle	Back
Air voids (%)	3.0	2.7	2.9
Final Axial Strain (%)	1.11	1.05	0.96
Strain Rate (%/cycle)	1.14E-04	9.07E-05	7.26E-05

* 4 specimens were tested in each position.

Table 4.17: Differences of axial strain in each cored part (X direction)

Parameter	Slab Compaction *D* = 100 mm specimens (X direction)		
Position	Left	Middle	Right
Air voids (%)	3.1	2.9	2.9
Final Axial Strain (%)	1.21	1.23	1.01
Strain Rate (%/cycle)	9.89E-05	1.06E-04	8.14E-05

* 4 specimens were tested in each position.

Table 4.18: Relationship of axial strain between cored directions and positions

Direction	Parameter	Position			
		A	B	C	D
Z*1	Air voids (%)	3.3	3.0	2.3	2.0
	Final Axial Strain (%)	1.22	1.37	1.76	1.75
	Strain Rate (%/cycle)	7.59E-05	9.42E-05	1.37E-04	1.44E-04
Y*2	Air voids (%)	3.1	3.0	2.9	2.9
	Final Axial Strain (%)	1.08	1.15	0.89	1.04
	Strain Rate (%/cycle)	1.18E-04	1.10E-04	6.29E-05	8.24E-05
X*2	Air voids (%)	2.8	2.7	3.5	3.2
	Final Axial Strain (%)	1.10	1.02	1.33	1.00
	Strain Rate (%/cycle)	9.10E-05	7.65E-05	1.07E-04	8.63E-05

*1: 3 specimens were tested in each position.

*2: 2 specimens were summarized in each position.

4.7 RELATIONSHIP BETWEEN ELASTIC STIFFNESS AND AXIAL STRAIN

In order to understand the property of specimen orientation, the relationship between elastic stiffness modulus and axial strain is examined in this section. Although elastic stiffness and axial strain in each direction were compared in the previous sections, these two results were not compared with each other. By comparing mechanical properties in each direction, some significant features would appear. The aim of this section is to show the trend in each direction and to specify the differences in specimen orientation in terms of elastic stiffness.

As stated above, the ITSM test and RLA test were conducted to look at the mechanical behaviour of each specimen. The results are summarized in Table 4.19. The mean elastic stiffnesses for Z, Y and X directions were 6577 MPa, 5868 MPa and 4945 MPa, respectively. On the other hand, mean axial strain for Z, Y and X directions were 1.52%, 1.04% and 1.15%, respectively. Figure 4.17 shows the relationship between the two parameters. The vertical axis represents axial strain, whereas the horizontal axis indicates elastic stiffness.

Usually, axial strain would decrease steadily as elastic stiffness increased. For X and Y directions, that trend can be seen in Figure 4.17, although this line is relatively flat. The value of axial strain decreased slightly from 1.15% to 1.04% with an increase of elastic stiffness from 4945 MPa to 5868 MPa.

However, for the Z-direction specimens, the result did not follow this trend. Mean axial strain was 1.52% in the Z-direction, despite the fact that the mean elastic stiffness showed 6577 MPa as described in previous sections.

As the value of elastic stiffness was relatively high compared with other directions, it was expected that the mean axial strain would give a lower value than X-direction specimen which showed 1.04% axial strain (see Table 4.13). However, axial strain for the Z-direction showed 1.52% which is significantly higher value than other two directions. Therefore, it is obvious that the mechanical properties of the slab in orthogonal directions are different. As the RLA test was carried out at 50°C (i.e. the binder was soft), it is assumed that these differences were attributed to the internal structure of aggregate.

As a result, there were clear differences between these three directions. Specimens cored from the X and Y directions showed similar trends, as these two strains were almost the same.

In addition to this, these specimens were cored out from longitudinal and transverse directions. Therefore, it appears that specimens cored out from longitudinal and transverse directions have similarity in terms of mechanical properties such as stiffness and axial strain.

On the other hand, specimens cored out from Z-direction indicated notably higher strain, despite the fact that the specimens also showed the highest stiffness value of

any direction. Therefore, it is assumed that these differences were attributed to aggregate structure. To look at the structure in more detail, image analysis was conducted after ITSM testing. The results and discussion for the image analysis are described in Chapters 6 and 7.

Table.4.19: Relationship between stiffness and axial strain in slab specimens

	Slab *D* = 100 mm specimens		
Cored Directions	Z direction (Top)	Y direction (Roller)	X direction (Side)
Average Air Voids (%)	2.6	2.9	3.0
Average Stiffness (MPa)	6577	5868	4945
Average Axial Strain (%)	1.52	1.04	1.15

* 12 specimens were tested in each direction.

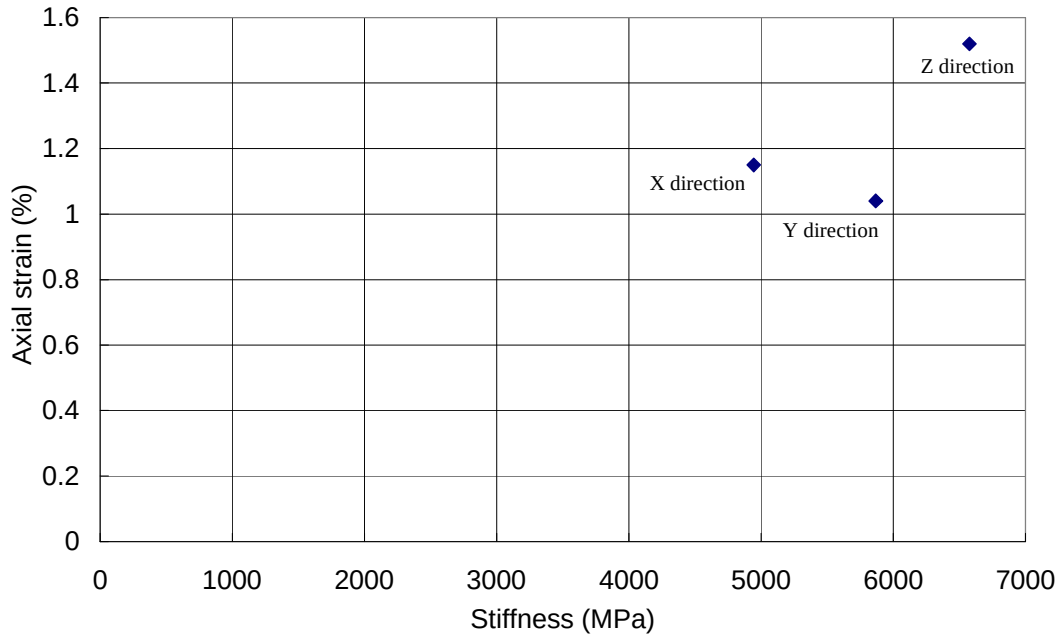

Figure 4.17: Relationship between stiffness and axial strain

4.8 CONCLUSIONS

With respect to mechanical properties, influence of specimen geometry size and direction were examined in this chapter. Through mechanical testing, some significant features for mould and slab type specimens were found.

In terms of mould type specimens, stiffnesses for 150 mm specimens were higher than for 100 mm specimens which were cored out from 150 mm specimens. This fact was confirmed in almost all specimens. This might be the effect of mould confinement. Also, with respect to compaction type, vibratory compacted specimens showed much higher stiffness than gyratory compacted specimens. This trend was consistent even in 100 mm specimens. Therefore, it is said that vibratory compaction tends to create specimens with higher stiffness.

From the perspective of slab compaction, specimens taken from three orthogonal coring directions (i.e. Z, Y and X directions) were also examined in this study. As a result, these three types of specimen showed anisotropy in terms of mechanical properties such as stiffness and axial strain. This phenomenon is examined and discussed using image analysis technique in Chapters 6 and 7.

CHAPTER 5

Image Analysis Methodology

5.1 INTRODUCTION

Using a digital camera, it is possible to photograph the aggregate matrix in a cross section of an asphalt mixture sample. The 2-D image can then be used through image analysis techniques to quantify the internal structure or matrix of the asphalt mixture. In this study, image analysis was used to quantify the aggregate matrix and understand the relationship between aggregate orientation and mechanical properties of asphalt mixtures. The aim of this chapter is to describe the calculation procedure of the image analysis used in this study.

5.2 IMAGE ANALYSIS PROCEDURE

In order to evaluate differences in the internal structure of specimens, image analysis has been used in this study. As stated in Chapter 2, image analysis has the ability to quantify the internal structure of asphalt mixture specimens. By quantifying the internal structure of each specimen, the differences of compaction method, influence of specimen size and specimen orientation can be understood.

This section describes the usage and procedures for image analysis. These procedures are shown in Figure 5.1.

Image analysis was conducted by using a digital camera and computer software to analyze the aggregate matrix. Picture 5.1 and Figure 5.2 show the image analysis equipment and a schematic representation of the procedure, respectively. The surface of a specimen is captured using a digital camera called QImageing Evolution MP12 bit. After photographing the surface of the specimen, the picture was analyzed using Image pro-plus analysis software to quantify the data from each surface. By following the sequences, image analysis was carried out in this study.

The procedure for image analysis was divided into three phases. Firstly, the specimen was placed into the equipment to photograph the surface. In the case of 150 mm diameter specimens, the height between camera and surface of specimen was fixed 56.5 cm, whereas for 100 mm diameter specimen, that distance was set to 43.5 cm. After setting the camera, the image was photographed using a digital camera. The colour of image was monochrome.

Secondly, the image was calibrated using image pro-plus software. As the software does not recognize specimen diameter, it is necessary to quantify the specimen diameter from the picture. Therefore, calibration work was required. After that, a process called ‘thresholding’ was conducted to distinguish grey and white particles. These were recognized by a grey scale (8bit) value between 0 and 255. As a result

of this, aggregate and bitumen were distinguished in the image, and then information for aggregate matrix was quantified in each particle.

Finally, each dataset was summarized using an excel spread sheet which analyzes measured data; then particle angle (ε), regional segregation and peripheral segregation were calculated. The calculation procedure is described in more detail in the following sections.

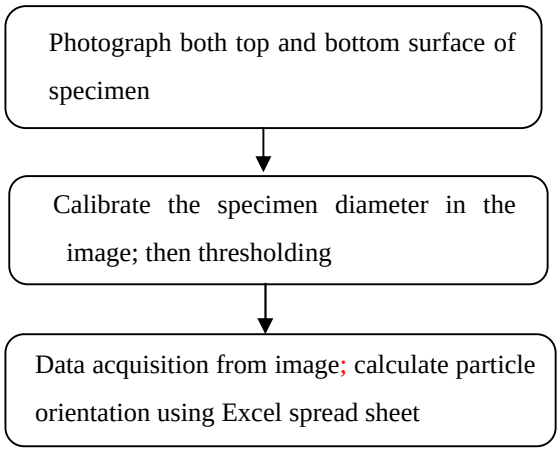

Figure 5.1: Sequences of image analysis

Picture 5.1: Image analysis equipment

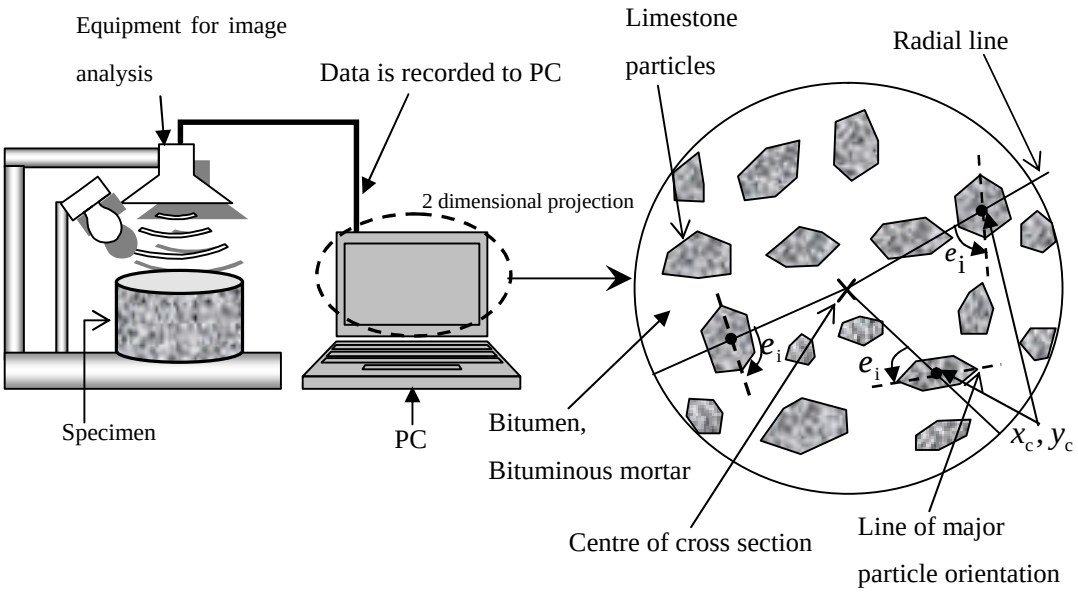

Figure 5.2: Schematic representation for image analysis equipment

5.3 CALCULATION PROCESS

An excel spread sheet was used to determine individual particle orientation. The calculation procedure is described as follows:

Firstly, parameters which are related to the calculation of particle orientation were measured using the digital camera. After 'thresholding', some parameters which are needed for the calculation were determined. These parameters are shown below:

- Area of particle,
- Centre of mass (X,Y),
- Angle (Cartesian coordinate),
- Perimeter,
- Size (Length), Size (Width).

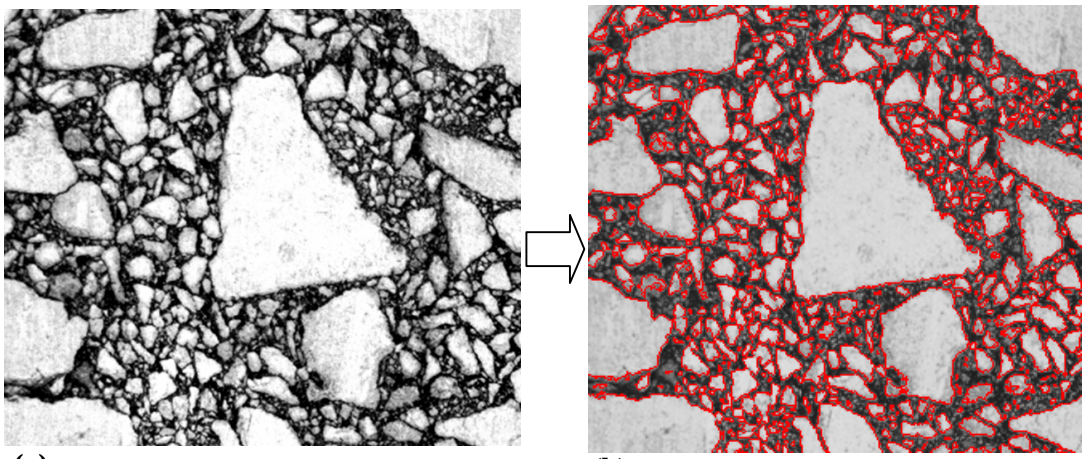

(a) **(b)**

Figure 5.3: Thresholding work (a) Before thresholding (b) After thresholding

After pasting these parameters into the excel spread sheet, other parameters which are related to the angle of orientation were determined. These parameters are indicated below:

- Ratio of particle length and width (for elongated particle),
- Angle plus 180°,
- Adjusted centre X, Y,
- Radial angle,
- Angle (for 360°).

By determining each parameter, the angle of orientation was calculated. One part of the excel spread sheet for the calculation of orientation is shown in Figure 5.4.

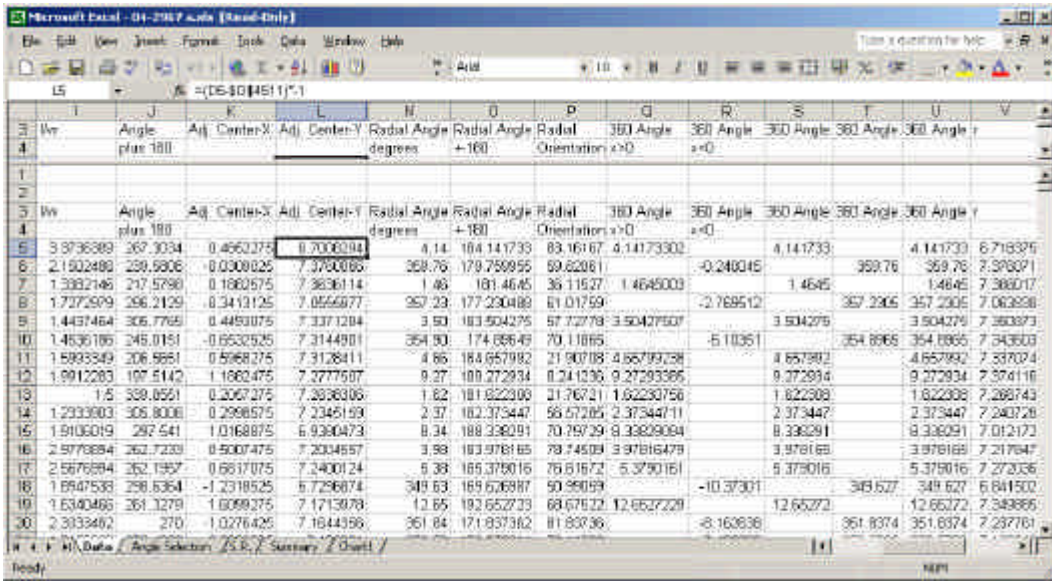

Figure 5.4: Excel spread sheet for the calculation of orientation

Using these parameters, particle orientation e was calculated. The angle of orientation is defined as the minor angle between the line of major particle orientation and a radial line. A schematic representation of the concept is shown in Figure 5.5.

The angle of orientation e varies from 0° to 90°. If e = 90° then particles are aligned circumferentially. If e = 0° then particles are aligned radially. If average e = 45°, this means aggregate aligned randomly. The schematic representation of the concept is depicted in Figure 5.6.

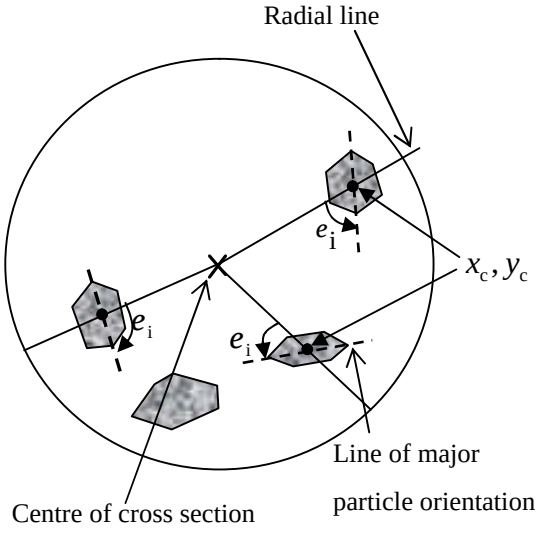

Figure 5.5: Definition of particle orientation (after Hunter et al. 2004)

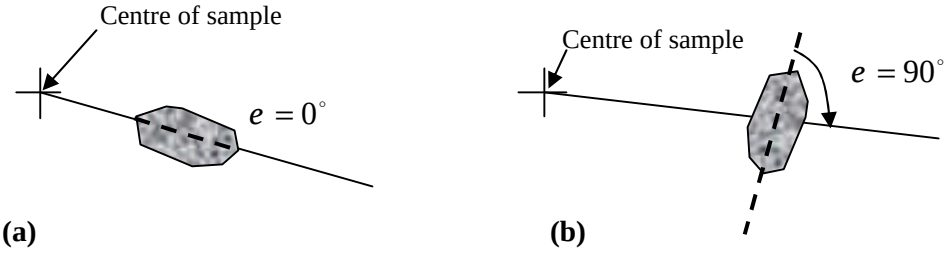

Figure 5.6: Angle of orientation (a) $e = 0^\circ$ **(b)** $e = 90^\circ$

5.4 CALIBRATION FOR DATA ACQUISTION

In order to carry out image analysis appropriately, it is necessary to calibrate the size of specimen because image analysis software recognizes the particle information after the thresholding process. Moreover, the information on the aggregate particles is used for other calculations such as particle orientation and segregation. If the calibration is not conducted appropriately, it would lead to wrong calculation and interpretation of aggregate particle information. Therefore, it is necessary to calibrate carefully the cross section of each specimen. This process is mainly divided into five steps. The sequence is as follows:

Step1; Set specimen and choose unit (cm is chosen in this study)

Step2; Calibrate diameter of specimen (refer measured data)

Step3; Confirm diameter in order to avoid mis-calibration

Step4; Select the range of measurement using a circle

Step5; Count particles using a thresholding function

By doing the above mentioned processes, aggregate particles are counted. In addition to this, individual information on each particle which is needed for the calculation is acquired.

As mentioned in the previous section, the cross section of the specimen is recognized as monochrome on the image analysis software, when the surface of the specimen is photographed. The range of grey scale is between 128 and 255 in this

study. According to Hunter et al. (2004), image analysis is highly effective, when the objects in the specimen have distinct colour. In addition, black and white contrast (i.e. bitumen and aggregate particle) is important to recognize the objects successfully. This process is shown in Figures 5.7 to 5.12.

From the image, bitumen mastic and aggregate are clearly recognized through the thresholding process. By using the data taken through this process, image analysis was carried out to find out the differences in compaction methods.

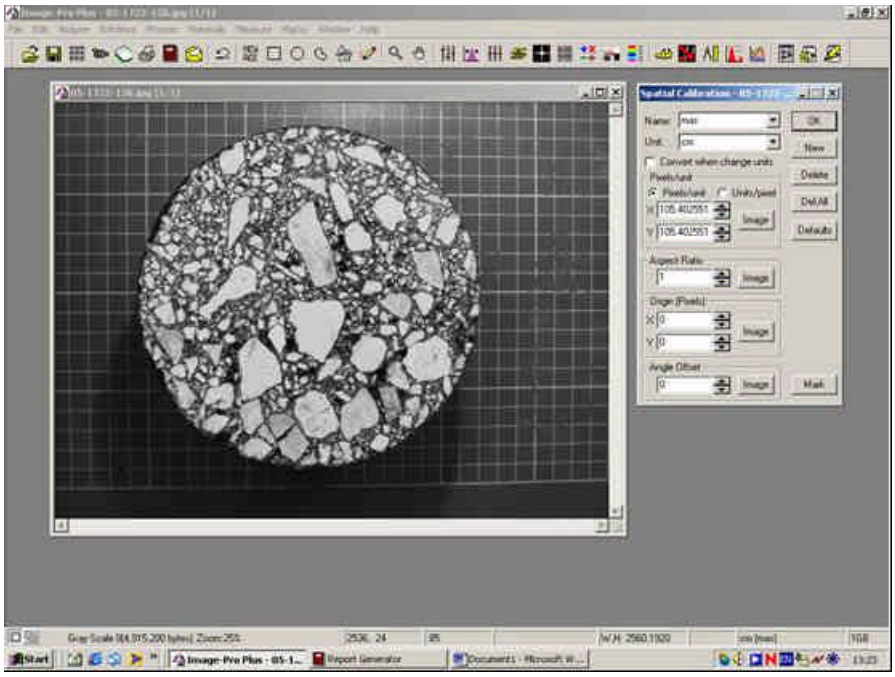

Figure 5.7: Photograph of specimen surface

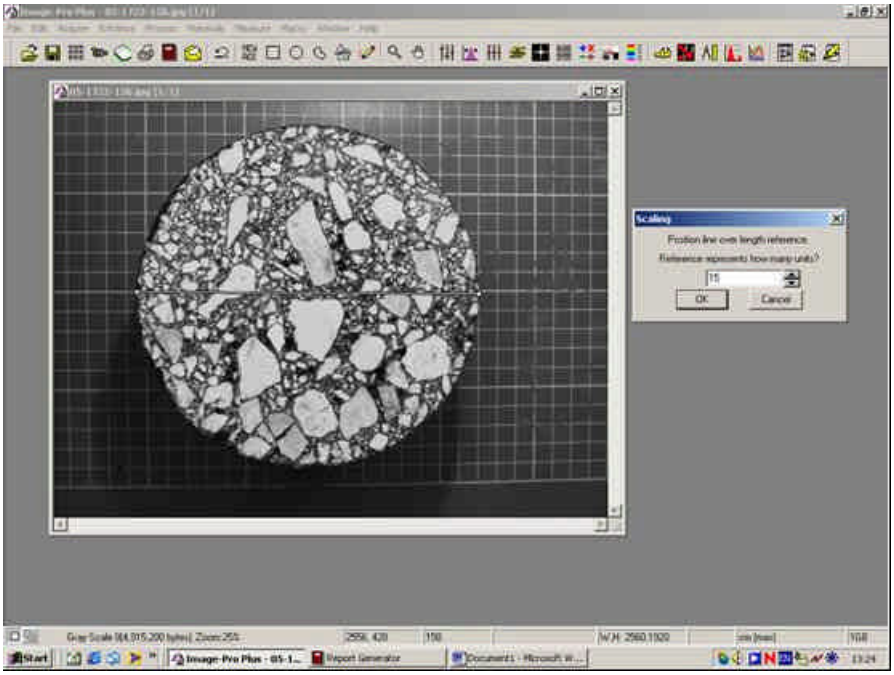

Figure 5.8: Calibration of specimen diameter

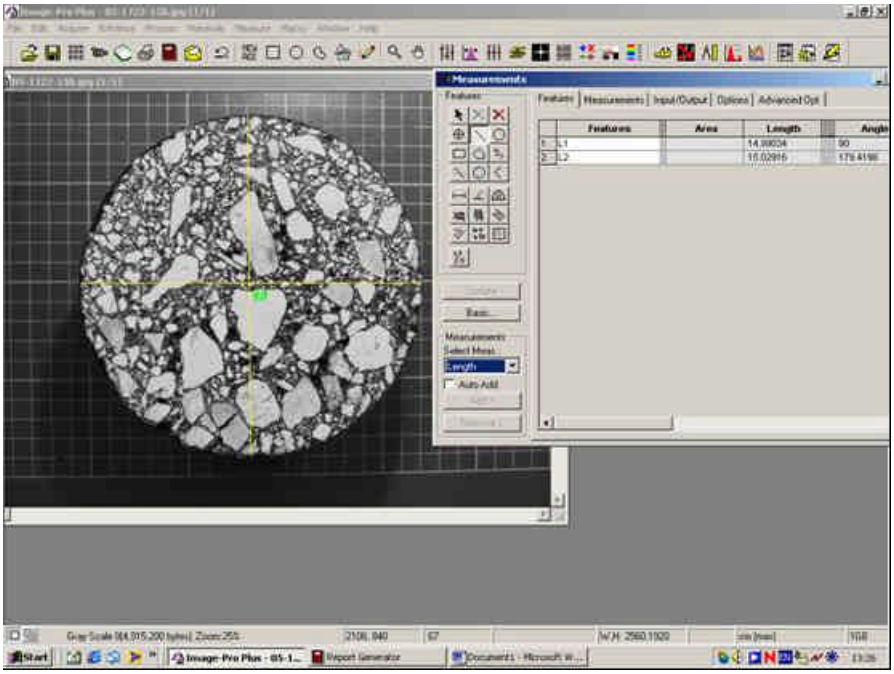

Figure 5.9: Confirmation of diameter

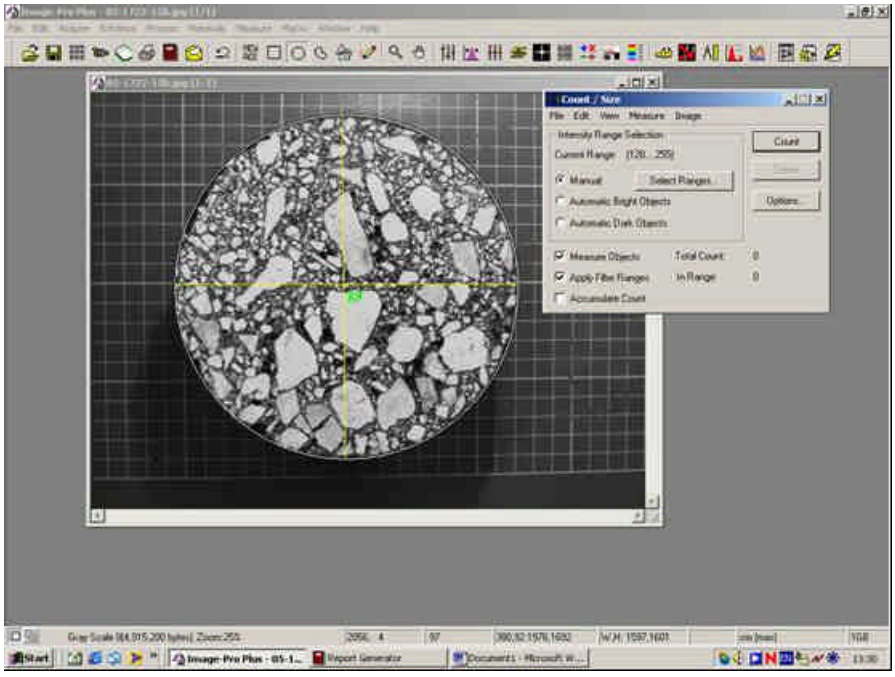

Figure 5.10: Selection of range

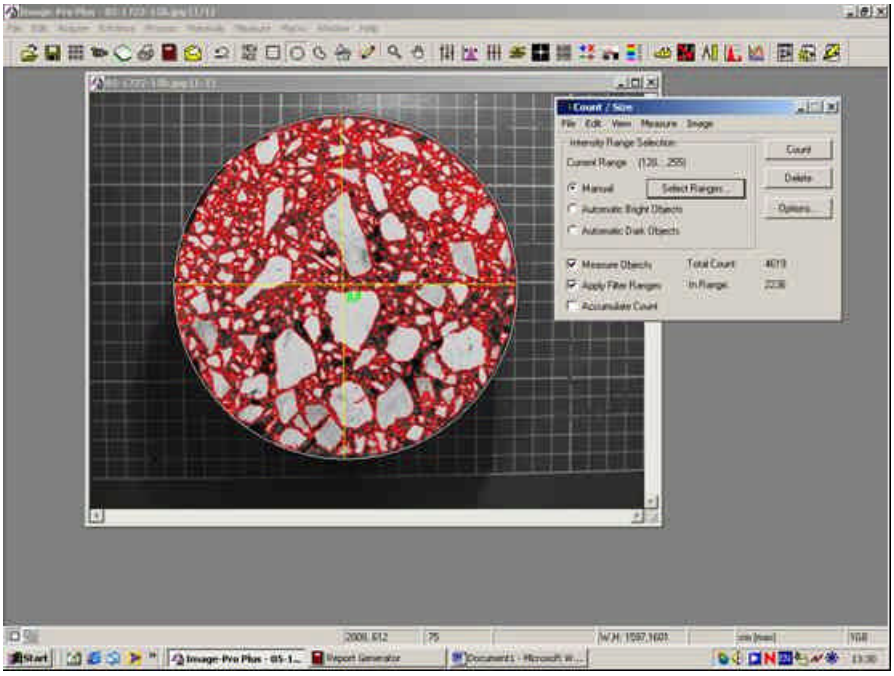

Figure 5.11: Thresholding

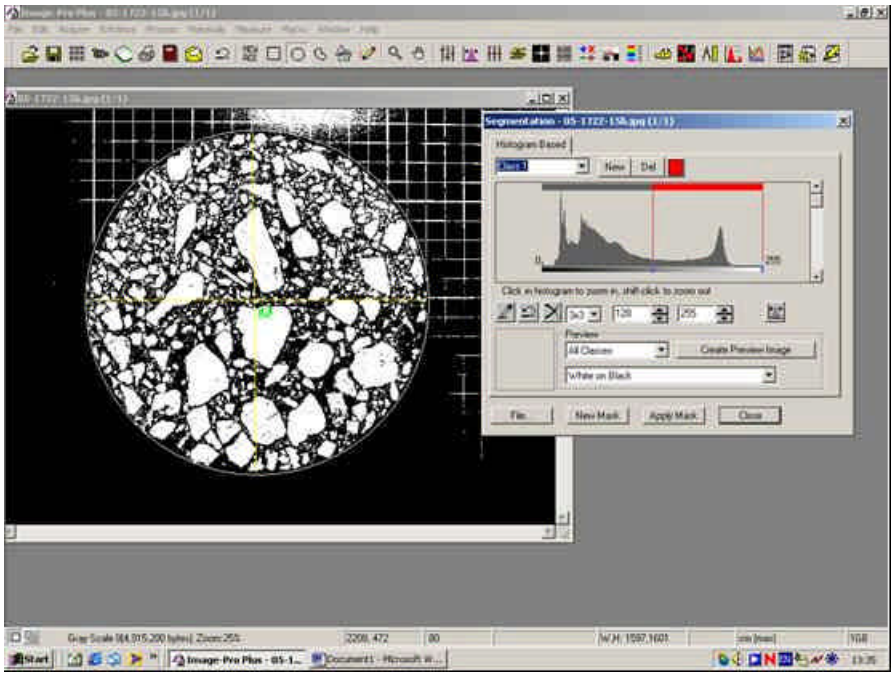

Figure 5.12: Recognition of aggregate and bitumen

5.5 CALCULATION PROCESS FOR IMAGE ANALYSIS

5.5.1 Coordinates of Particles

When the thresholding process is carried out, the information on particles such as area, length, width, perimeter and centre (x,y coordinates) are acquired**.** After that, image analysis is conducted to determine the particle orientation using the information. Before determining particle orientation, each particle is plotted on the image based on the information. The artificial plot of aggregate particles is shown in Figure 5.13. However, downward is positive with respect to the Y-axis in this plot. In order to determine particle orientation mathematically, it would be necessary to change this coordinate to Cartesian coordinates. Therefore, all particles are adjusted to Cartesian coordinates by calculating the centre point of the specimen. That coordinates are depicted in Figure 5.14.

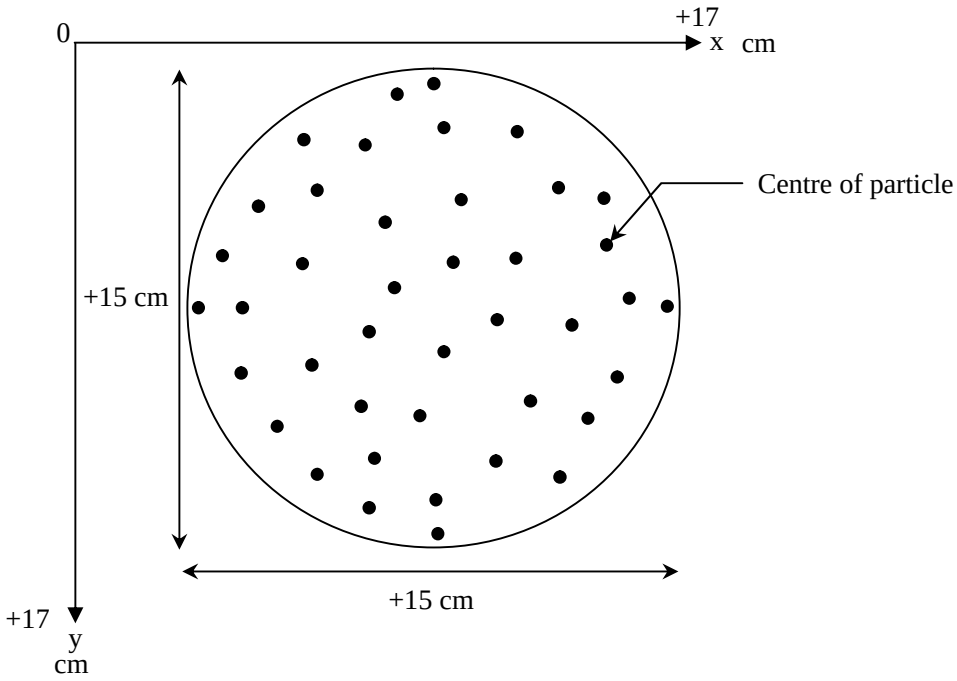

Figure 5.13: Artificial x,y coordinates

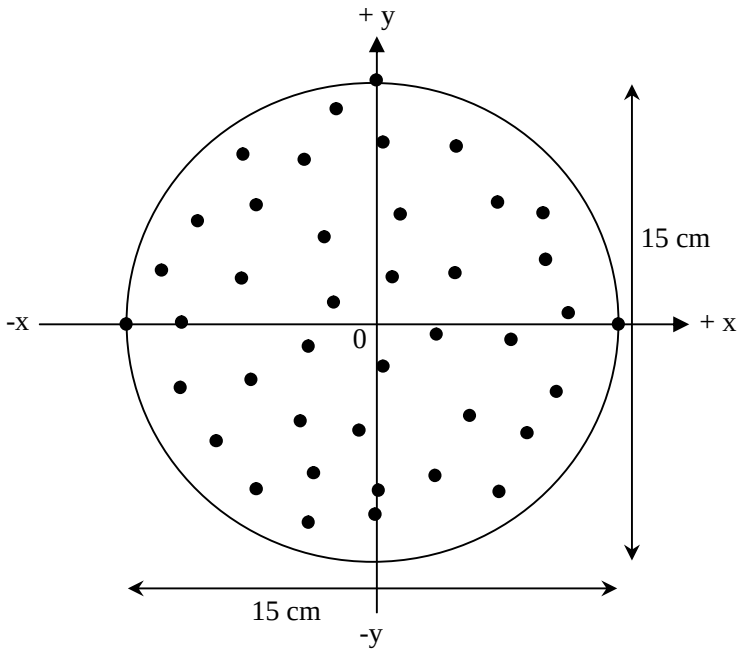

Figure 5.14: Adjusted x,y coordinates

5.5.2 Calculation for Radial Orientation

Radial orientation of each particle is calculated by using the coordinates of particle centres. The equation for the determination of particle orientation is as follows;

$$q = \tan^{-1} \frac{(y-0)}{(x-0)} \tag{5.1}$$

By using this equation, each radial orientation was calculated. The schematic of this calculation is illustrated in Figure 5.15.

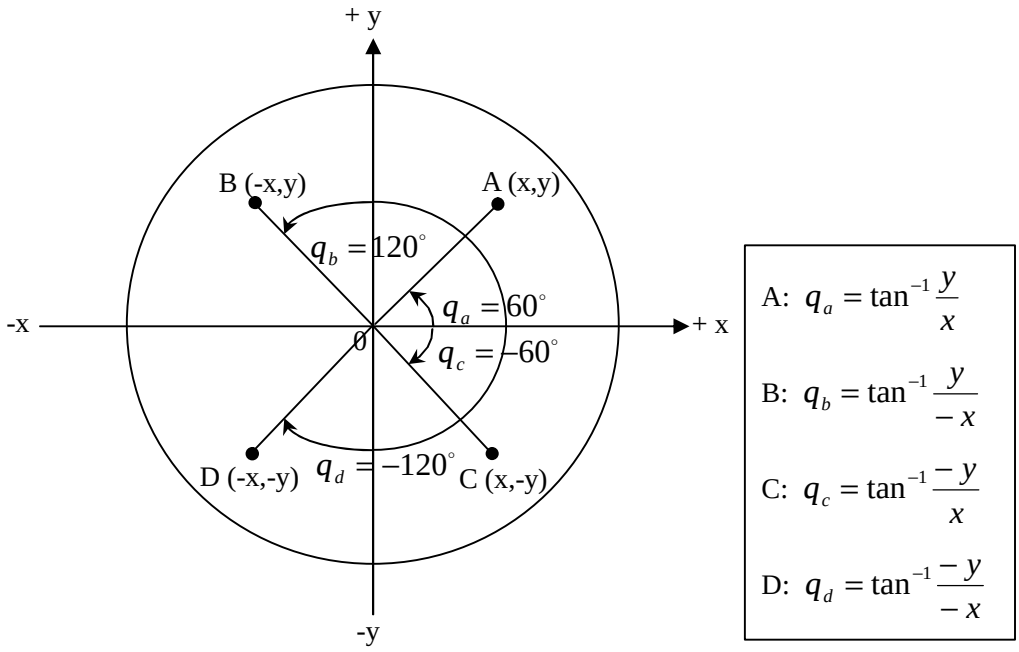

Figure 5.15: Determination of angle from coordinates

In the next step, radial angle q is determined from the radial orientation. In this case, the calculation for each particle is dependant on the coordinates where particles are located. For example, if a particle is located at A in Figure 5.15, the radial orientation is less than 90°. In such a case, it is necessary to calculate 90°-q as the radial angle. Other points (i.e. B, C and D) are also examined using the same method as for point A. The components of the calculation process are depicted with the logic used for the analysis in Figures 5.16 to 5.19.

After that, radial angle degree which added 180° in each particle was derived from previous information. In this case, if the degree of particle radial angle is less than 180°, then 150° is added to its radial angle which is determined before. Similarly, if the radial angle degree of particle is more than 180°, then it is needed to subtract 180° from its radial angle degree. By conducting this process, the value for radial angle degree +/- 180° is determined in each particle.

In the next step, radial orientation is determined from the information provided before. For instance, if particle #1554 in sample 05-1930-15b is calculated, four types of calculation are carried out using the provided information. The detail of this calculation is depicted in Figures 5.18 to 5.19. In order to calculate the four types of radial orientation provided, four parameters (i.e. particle angle, angle +180°, radial angle$q$ and radial orientation e and radius) are required.

By putting these parameters into the equation shown in Figure 5.19, four possibilities for the determination of radial orientation are examined. According to the definition of radial orientation (Hunter et al. 2004), it is required to take the lowest angle from the four possible answers. Therefore, the radial orientation of particle #1554 is determined as e =13°.

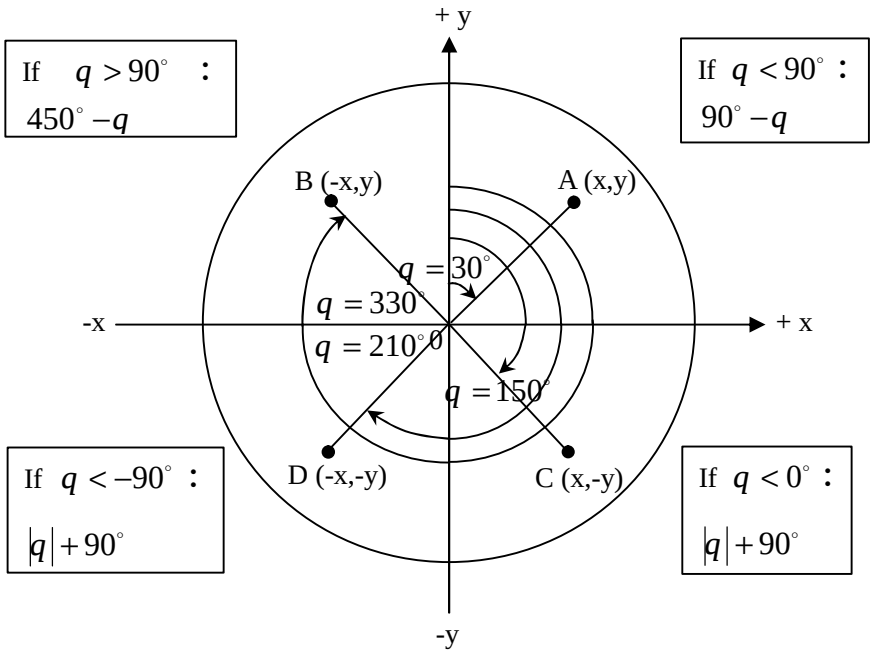

Figure 5.16: Radial angle degree

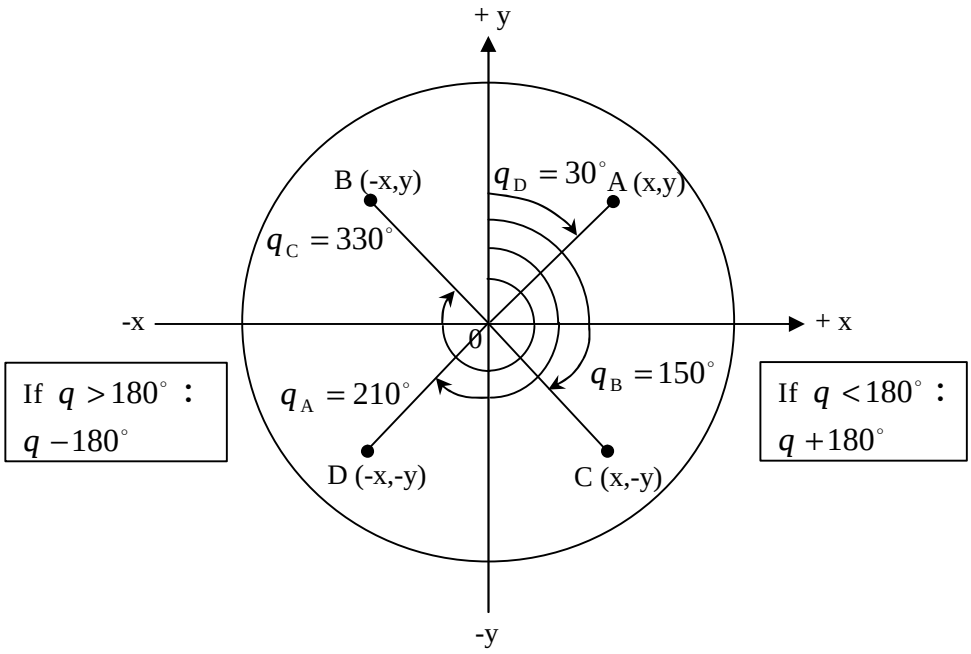

Figure 5.17: Radial angle degree +/- 180°

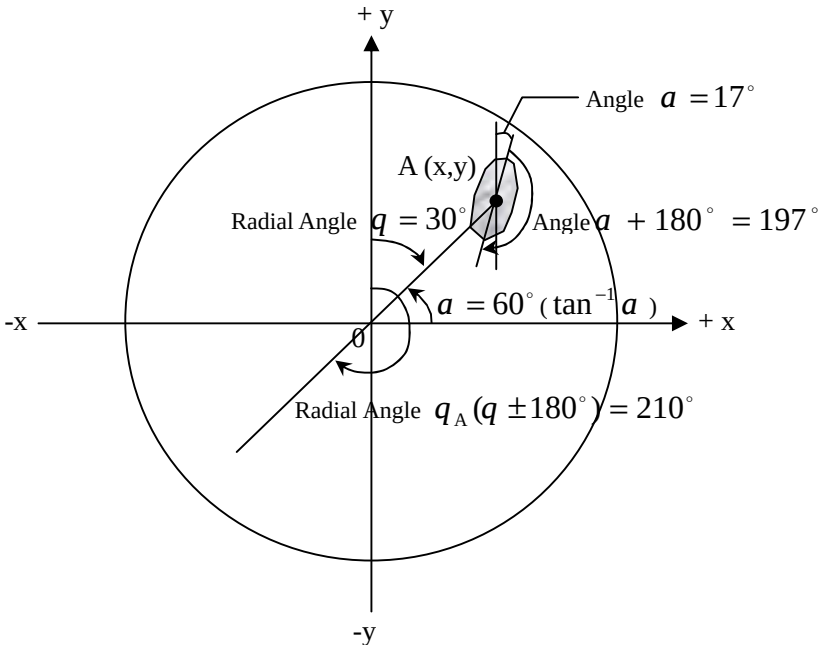

Figure 5.18: Selection of minor angle (coordinate)

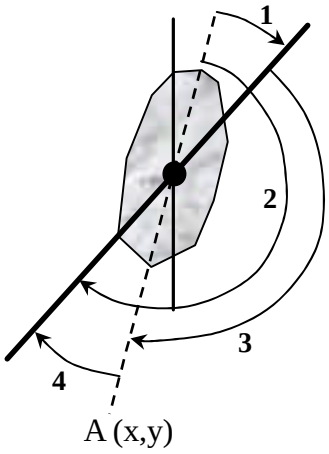

1: Angle a – Radial angle q

$\left|17^\circ - 30^\circ\right| = 13^\circ$

2: Angle a – Radial angle $q_A (q \pm 180^\circ) = 210^\circ$

$\left|17^\circ - 210^\circ\right| = 193^\circ$

3: (Angle $a + 180^\circ$) — Radial angle q

$\left|197^\circ - 30^\circ\right| = 167^\circ$

4: (Angle $a + 180^\circ$) — Radial angle $q_A (q \pm 180^\circ) = 210^\circ$

$\left|197^\circ - 210^\circ\right| = 13^\circ$

Choose minor angle from **1** to **4**

Radial Orientation: $e = 13^\circ$

Figure 5.19: Selection of minor angle (calculation)

5.5.3 360° orientation and Radial for Particles

In order to determine the location of particles in the coordinates, it would be necessary to find the 360° orientation of each particle. In this case, 360° orientation q is determined from

$$q = \tan^{-1} \frac{x}{y} \tag{5.2}$$

After determining q for each particle, these are translated to 360° angle degrees in accordance with each condition which is dependant on the location of particles. The detailed condition is schematized in Figure 5.20. As shown in Figure 5.20, the

condition is different in each location. For example, for particle A, 360° angle degree is the same as orientation, whereas for particle B, its angle in this coordinate system is determined by subtracting its orientation from 360°. Therefore, it is said that the coordinate for the determination of particle angle is different in each location.

Through the above mentioned process, the 360° angle for each particle was determined in the calculation of image analysis as shown in Figure 5.21.

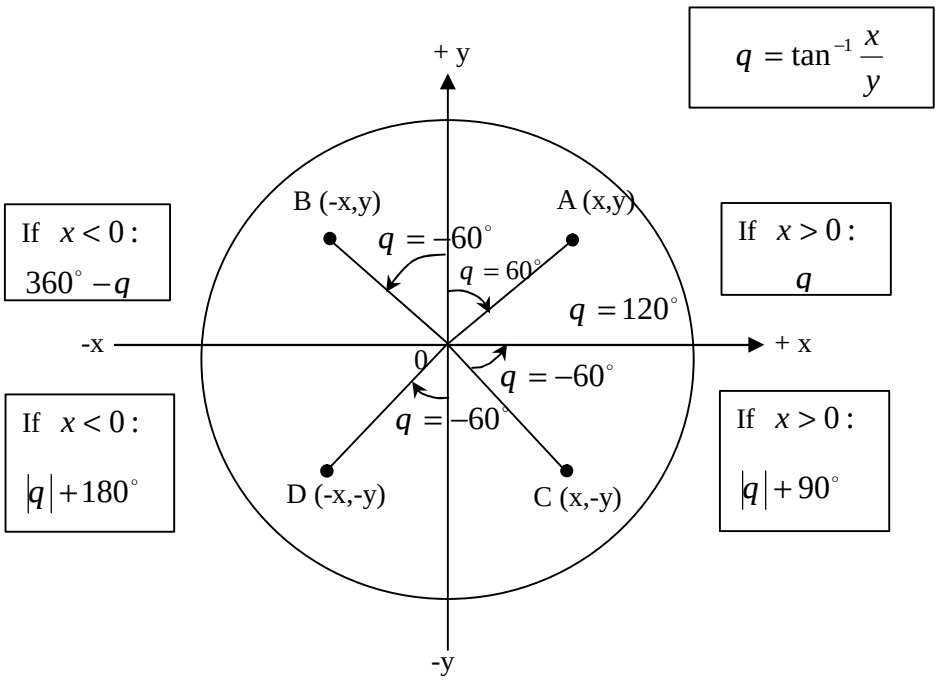

Figure 5.20: Calculation for 360° angle degrees

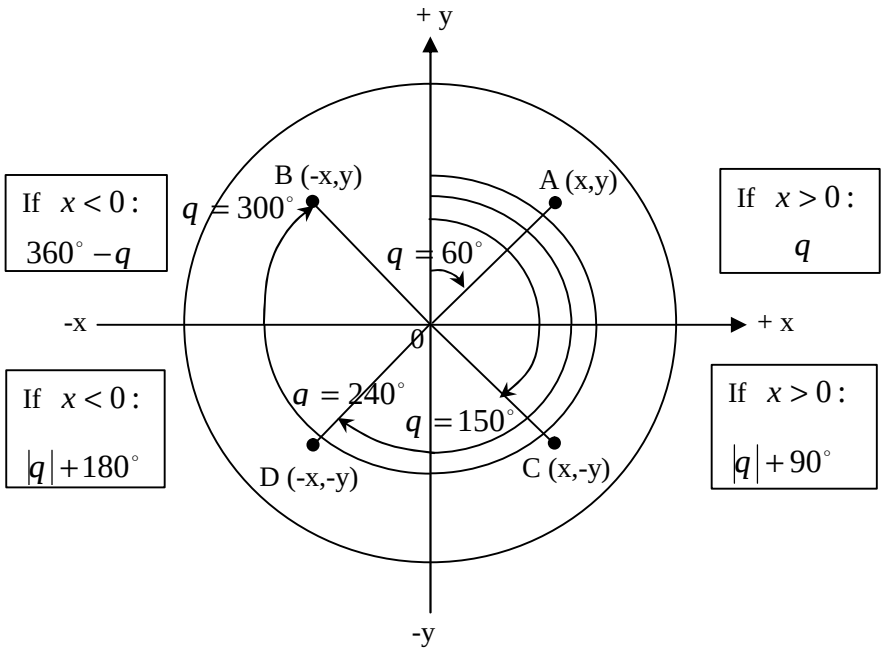

Figure 5.21: 360° angle degrees

5.5.4 Distance from Origin to Centre of Particle

Using the data taken from the image analysis software, it is possible to calculate the distance *r* from the origin point to the centre of each particle. Therefore, the coordinate of each particle was determined since the centre point of each particle was already acquired through the thresolding process. The components of this calculation and the equation used for this process are shown in Figures 5.22 to 5.23.

In addition, combining 360° angle degrees and the distance *r*, the exact location of each particle was represented in the excel spreadsheet. The state of particle distribution is shown in Figure 5.23.

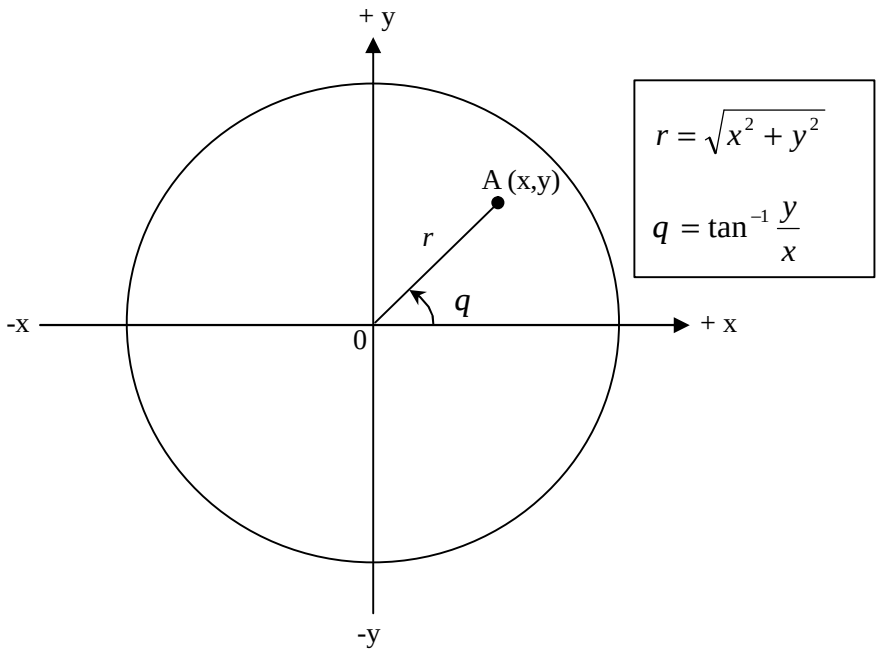

Figure 5.22: Calculation for length to particle

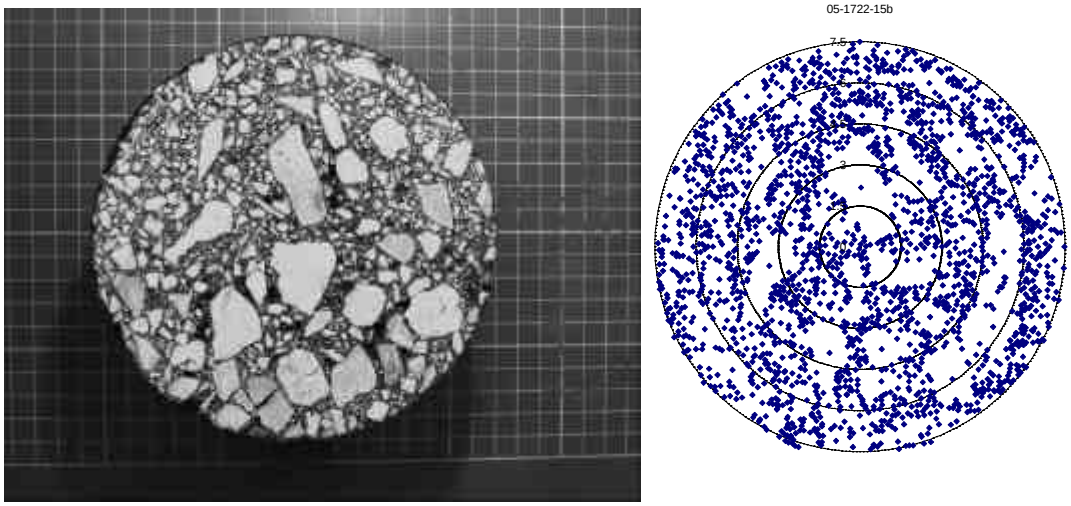

(a) **(b)**

Figure 5.23: Image and Coordinate of surface (a) Photo of specimen (b) Position of particles

5.6 ANGLE SELECTION

In the “Angle selection” process, particles are divided into each VSA range. This is because particle orientation (radial orientation) is represented by each particle size (VSA). Therefore, it is necessary to calculate particle orientation in each VSA range. In this study, the ranges are presented from 0 to 11 cm^2 in VSA (see Figure 5.24). In addition, these ranges are divided into 29 sections (i.e. 0-0.005, 0.005-0.01, 0.01-0.02……10.5-11 cm^2). After that, the radial orientation of each particle is multiplied by its area. Then each area and the multiplied value are summed up in each VSA range. An example from an actual excel spread sheet is shown in Figure 5.24; and the detail of an angle selection sheet is shown in Figure 5.25.

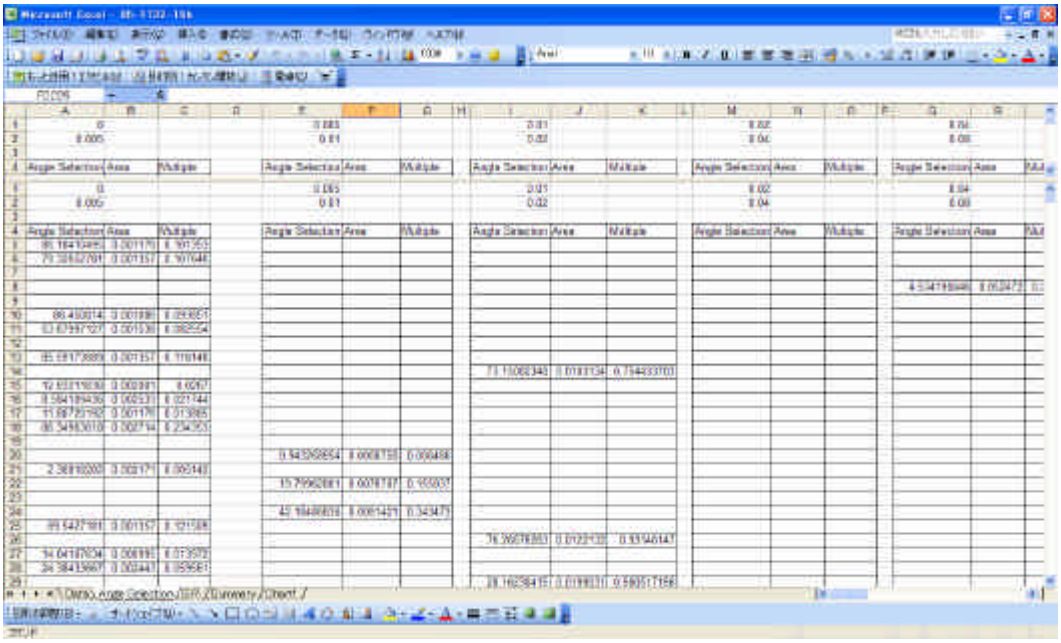

Figure 5.24: Angle selection sheet (Excel spreadsheet)

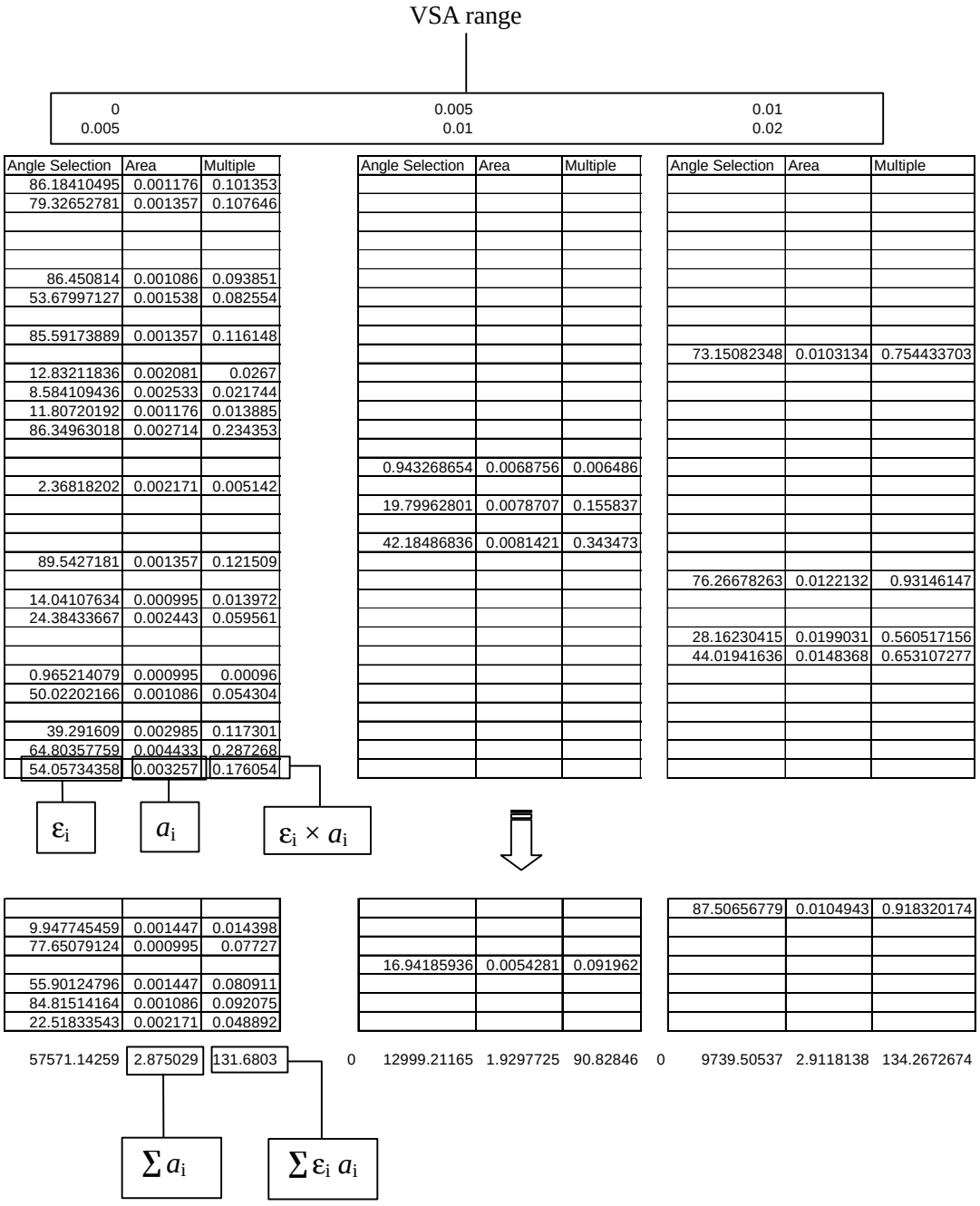

Figure 5.25: Detail of Angle Selection sheet

5.7 SEGREGATION RATIO (S.R.)

Segregation ratio is an important factor to evaluate the differences in compaction methods. In order to assess the segregation of each specimen, the cross section of specimens is divided into 72 sectors. This means that the cross section is spitted into 5° segments. In this study, aggregate segregation is evaluated by summing up each 18 adjacent segments. By doing that, the area of aggregate in a quarter of cross section is calculated. The quarter of cross section is examined by shifting around the cross section by 5°. Then maximum quarter of 72 sections is selected in order to calculate segregation ratio. An example from an actual excel spread sheet is shown in Figure 5.26; and the detail of an angle selection sheet is shown in Figure 5.27. The explanation for this process is described in more detail in Chapter7.

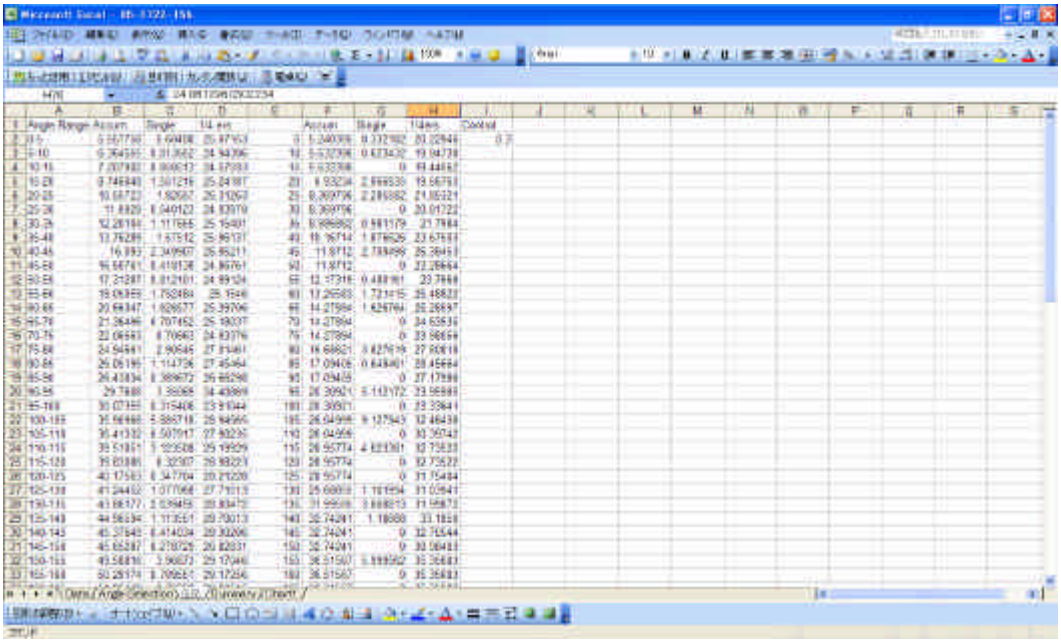

Figure 5.26: S.R sheet (Excel spreadsheet)

Angle Range	Accum.	Single	1/4 ers
0-5	5.557758	5.60498	25.07153
5-10	6.364555	0.813652	24.94306
10-15	7.207902	0.850513	24.57593
15-20	8.746048	1.551216	25.24187
20-25	10.55723	1.82657	26.31263
25-30	11.0928	0.540123	24.93978
30-35	12.20104	1.117655	25.15401
35-40	13.76289	1.57512	25.96137
40-45	16.093	2.349907	26.95211
45-50	16.50761	0.418138	24.86761
50-55	17.31287	0.812101	24.99124
55-60	19.05059	1.752484	26.1546
60-65	20.66347	1.626577	25.39706
65-70	21.36496	0.707452	25.18037
70-75	22.06563	0.70663	24.83376
75-80	24.94661	2.90545	27.01461
80-85	26.05195	1.114736	27.45464
85-90	26.43834	0.389672	26.66298
90-95	29.7608	3.35069	24.40869
95-100	30.07355	0.315406	23.91044
100-105	35.90968	5.885718	28.94565
105-110	36.41332	0.507917	27.90235
110-115	39.51051	3.123508	29.19929
115-120	39.83086	0.32307	28.98223
120-125	40.17563	0.347704	28.21228
125-130	41.24452	1.077968	27.71513
130-135	43.86177	2.639495	28.00472
135-140	44.96594	1.113551	28.70013
140-145	45.37649	0.414034	28.30206
145-150	45.65287	0.278729	26.82831
150-155	49.58816	3.96873	29.17046
155-160	50.29174	0.709551	29.17256
160-165	51.05448	0.76922	29.23515
165-170	51.66288	0.613569	26.94327
170-175	53.19595	1.546106	27.37464
175-180	54.25824	1.071306	28.05627
180-185	54.6677	0.412939	25.11852
185-190	56.12542	1.470106	26.27322
190-195	57.26903	1.15333	21.54083
195-200	58.90633	1.651212	22.68413
200-205	59.11061	0.206013	19.76663
205-210	60.40711	1.307521	20.75108
210-215	60.60777	0.202363	20.60574
215-220	65.60354	5.038215	24.56599
220-225	67.11789	1.52722	23.45372
225-230	67.50844	0.39387	22.73404
230-235	68.869	1.372116	23.69212
235-240	70.5044	1.649295	25.06268
240-245	70.77942	0.27736	21.37131
245-250	71.59735	0.824875	21.48664
250-255	73.69016	2.110591	22.82801
255-260	74.37383	0.689478	22.90392
260-265	75.63975	1.276682	22.63449
265-270	76.25855	0.624061	22.18725
270-275	79.85495	3.626954	25.40126
275-280	80.78913	0.942115	24.87327
280-285	81.99652	1.217652	24.93759
285-290	82.87434	0.885275	24.17166
290-295	83.62378	0.755808	24.72145
295-300	85.52063	1.912971	25.3269
300-305	86.41645	0.90343	26.02797
305-310	87.17774	0.76776	21.75751
310-315	88.52545	1.359161	21.58945
315-320	91.007	2.502638	23.69822
320-325	91.68968	0.688475	23.01458
325-330	92.27383	0.589118	21.9544
330-335	94.63787	2.384121	24.06116
335-340	95.55422	0.924141	24.16043
340-345	96.59859	1.053242	23.10308
345-350	97.31709	0.724604	23.13821
350-355	97.9861	0.674698	22.53622
355-360	99.15749	1.181339	23.0935
			29.23515
			22.82801
			23.10308
			24.83376
sum		100	100

A quarter of cross section

Quarter with maximum aggregate density

Quarter with minimum aggregate density

Figure 5.27: Detail of S.R sheet

5.8 REPRESENTATION OF PARTICLE ORIENTATION (Summary sheet)

Particle orientation is represented in each VSA range. In this process, the data taken from "Angle selection" is used to calculate particle orientation as shown in Figure 5.28. Hunter et al (2004) defined particle orientation to be represented by average (weighted) circumferential particle orientation. The equation for calculating aggregate orientation is shown below;

$$e_w = \frac{\sum_{i=1}^{i=n} e_i a_i}{\sum_{i=1}^{i=n} a_i} \qquad (5.3)$$

where ε_w is the weighted circumferential orientation, ε_i is radial orientation of an individual particle , a_i is its area.

In the "Angle selection" process, summed up particle orientation (i.e. $\sum \varepsilon_i \ a_i$), which is the sum of individual particle orientations multiplied by this areas, is defined for each VSA. By using this, the weighted particle orientation was calculated in accordance with Equation 5.3 in each VSA range. A calculation sheet is shown in Figure 5.29.

Since particle orientation (weighted particle orientation) is calculated for each VSA, the result is plotted as shown in Figure 5.30. Although these plots show considerable scatter, the particle orientation of each specimen is represented by a best fit straight line fixed at 45° as y intercept. By looking at the results for each specimen, the trends for different compaction methods were examined in this study. The whole process of the image analysis calculation is presented in Figure 5.31.

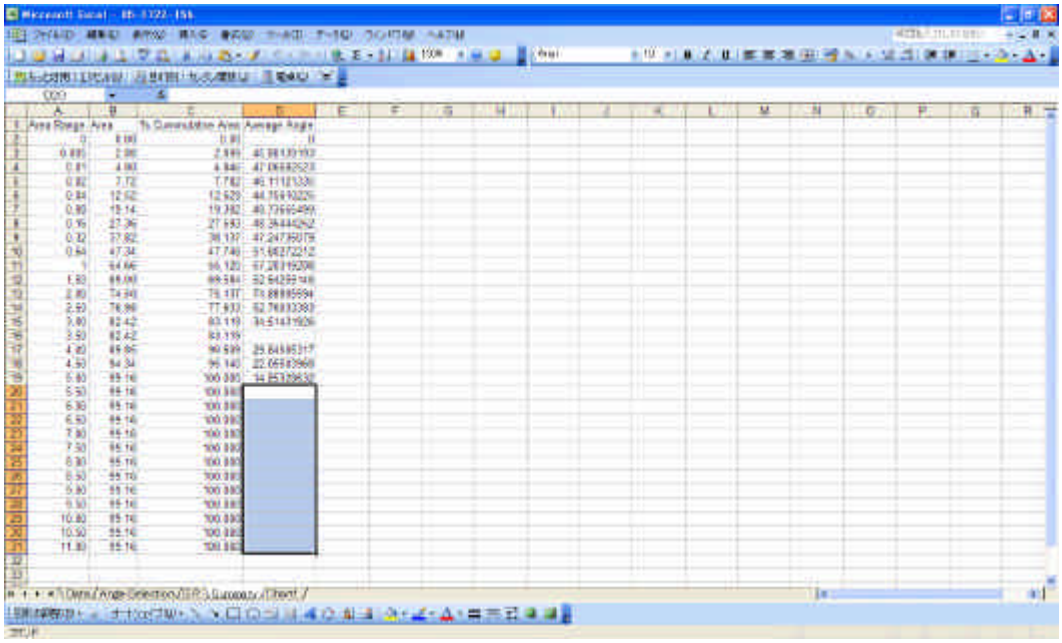

Figure 5.28: Summary sheet (Excel spreadsheet)

Area Range	Area	% Cummulative Area	Average Angle
0	0.00	0.00	0
0.005	2.88	2.899	45.80139193
0.01	4.80	4.846	47.06692523
0.02	7.72	7.782	46.11121335
0.04	12.52	12.629	44.75610225
0.08	19.14	19.302	49.73655499
0.16	27.36	27.593	48.35444252
0.32	37.82	38.137	47.24735079
0.64	47.34	47.746	51.80272212
1	54.66	55.120	57.20319208
1.50	69.00	69.584	52.64259146
2.00	74.50	75.137	74.88805594
2.50	76.98	77.633	52.76033383
3.00	82.42	83.119	34.51431926
3.50	82.42	83.119	
4.00	89.85	90.609	29.84505317
4.50	94.34	95.140	22.05503968
5.00	99.16	100.000	14.85328632
5.50	99.16	100.000	
6.00	99.16	100.000	
6.50	99.16	100.000	
7.00	99.16	100.000	
7.50	99.16	100.000	
8.00	99.16	100.000	
8.50	99.16	100.000	
9.00	99.16	100.000	
9.50	99.16	100.000	
10.00	99.16	100.000	
10.50	99.16	100.000	
11.00	99.16	100.000	

$\varepsilon_w = \sum \varepsilon_i \, a_i / \sum a_i$
(from “Angle Selection”)

Figure 5.29: Calculation of summary sheet

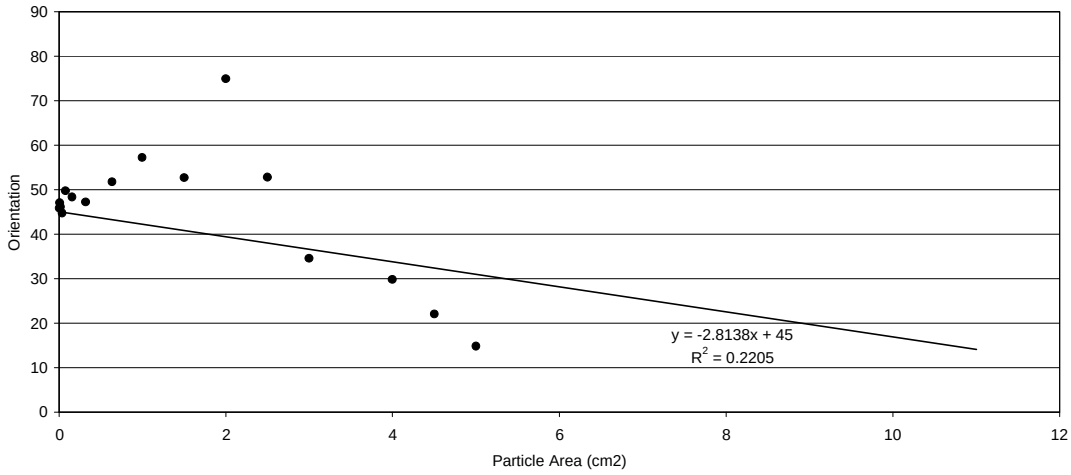

Figure 5.30: Particle orientation vs VSA plot

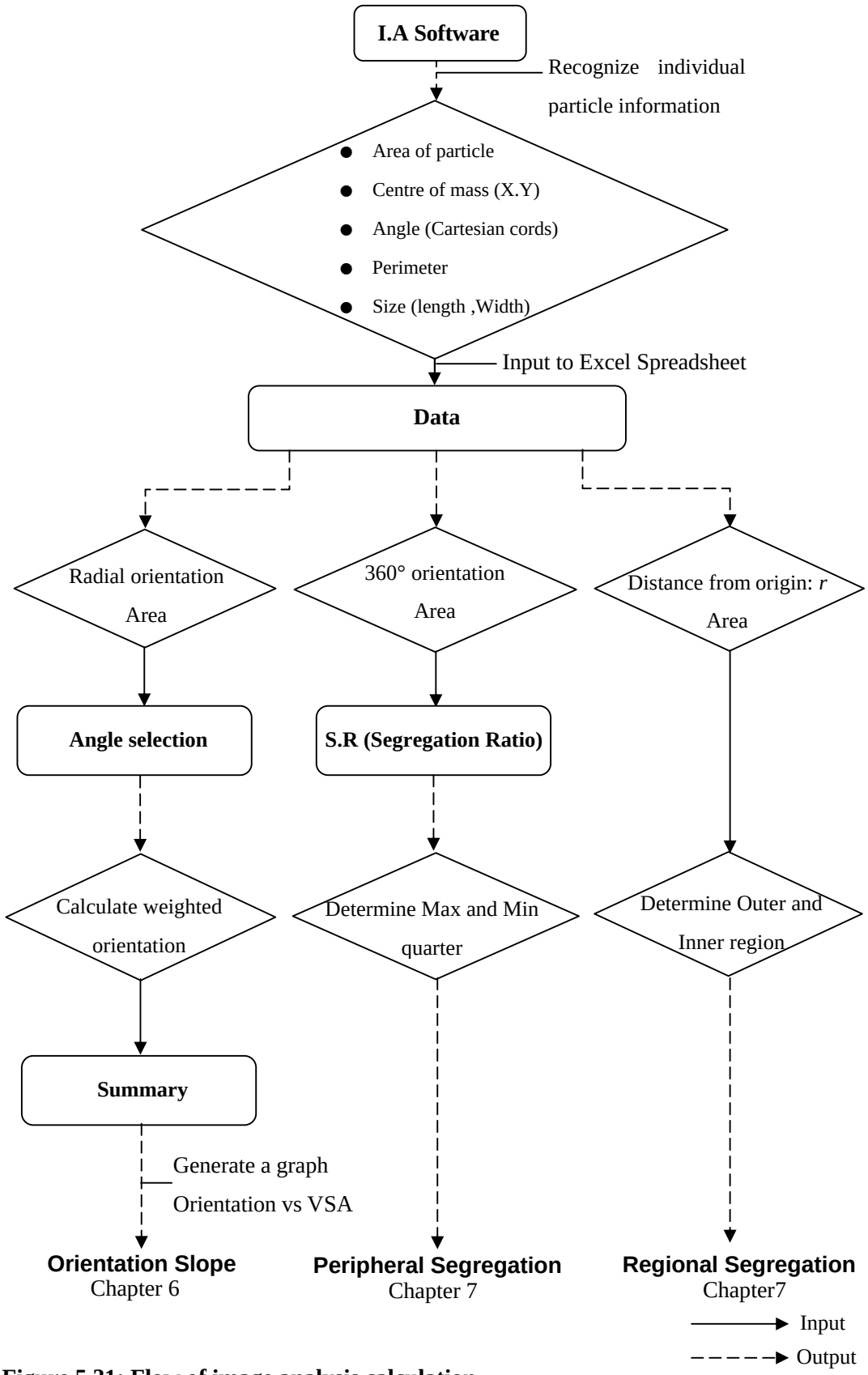

Figure 5.31: Flow of image analysis calculation

5.9 CONCLUSIONS

In conclusion, the procedure for image analysis and the calculation for the determination of particle orientation were described in this chapter. Hunter et al. (2004) came up with a process to calculate the particle orientation utilizing the information taken from image analysis software. In addition, this calculation system enables other useful information such as peripheral and regional segregations to be determined. These are very useful parameters to determine the differences between compaction methods. By using the image analysis equipment and calculation system, detailed information which is related to the properties from and compaction method is provided. These calculations and their results are discussed in Chapters 6 and 7.

CHAPTER 6

Particle Orientation

6.1 INTRODUCTION

As described in Chapter 5, image analysis software identifies some significant features for asphalt mixture particles such as area, centre (X-Y coordinate), angle, perimeter and the size (length, wide) of particles. Utilizing the information, the aggregate orientations for the asphalt mixture specimens are calculated to look at the differences between compaction methods.

The aim of this chapter is to analyse the differences in particle orientation in each combination of compaction and specimen size.

6.2 PARTICLE ORIENTATION IN EACH TYPE OF SPECIMEN

6.2.1 Gyratory and Vibratory Compacted Specimens

All particles

The particle orientation for the gyratory and vibratory compacted specimens was examined through the image analysis before conducting mechanical tests. The images of top and bottom surfaces were photographed for both 150 mm and 100

mm diameter specimens. Then, the aggregate particles were analysed following the procedure described in Chapter 5.

Table 6.1 shows the results for both the gyratory and vibratory compacted specimens, looking at all particles. In general, these two types of specimen showed aggregate orientation more than 0 (°/cm^2) in both the 150 mm and 100 mm diameter specimens (see Figures 6.1 and 6.2).

In theory, laboratory compacted specimens should have the same particle orientation as in the field which has random particle orientation. However, Paterson et al. (1973) indicated that aggregate particles tend to be moved into generally parallel directions perpendicular to imposed stress during compaction. Therefore, it seems that both the gyratory and vibratory compaction produce specimens with a higher degree of circumferential orientation (i.e. VSA>45 (°/cm^2)) rather than manufacturing the specimens with random orientation due to the effect of mould confinement and compaction mode. This trend was also observed in the research conducted by Hunter et al. (2004) and Airey et al. (2006).

However, despite the fact that both the 100 mm diameter gyratory and vibratory compacted specimens eliminated the effect of mould boundary by coring from the 150 mm diameter specimens, there was still a degree of circumferential orientation in the 100 mm diameter specimens. Hunter et al. (2004) suggested that slab compacted specimens have a lower degree of circumferential orientation than gyratory and vibratory compacted specimens as the cores taken from a large slab

do not experience mould confinement. However, they also observed that the cores taken from the large slab have bisected aggregate particles due to the coring process; this results in the production of erroneous elongated particles which were recognised as circumferentially oriented particles in the image (see Figure 6.3).

In order to overcome the assumed error, the images of the 150mm diameter specimens were re-analyzed by using computer software. The 100 mm diameter specimens were trimmed artificially by scanning the radius of 50 mm from the data of the 150 mm diameter specimens as depicted in Figure 6.4.

As shown in Table 6.1, the computer trimmed 100 mm diameter specimens indicated a large reduction in the aggregate orientation slope on both the gyratory and vibratory compactions (see Figures 6.5 and 6.6). In other words, more random particle orientations were confirmed within the range of 100 mm diameter in both the 150 mm diameter gyratory and vibratory compacted specimens.

Table 6.1: Aggregate orientation slopes for all particles

Surface	Aggregate Orientation (°/cm^2)					
	Gyratory Compaction			Vibratory Compaction		
	150 mm	100 mm	100 mm(C)	150 mm	100 mm	100 mm(C)
S2 (Top)	1.59	2.79	-0.05	2.09	1.77	0.54
S3 (Bottom)	1.58	1.10	-0.96	1.23	2.23	0.04
Average	1.56	1.53	0.17	1.98	2.26	0.39

* Calculation was conducted using protocol #3.

* (C) stands for Computer trimmed 100mm diameter specimen.

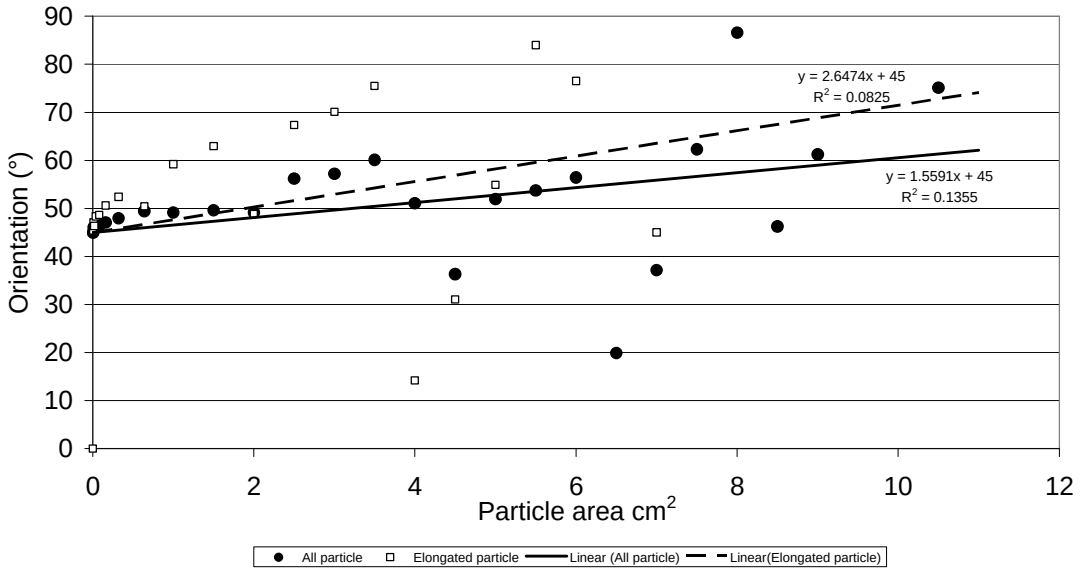

Figure 6.1: Plot of all average particle orientation versus particle area for gyratory compacted specimen (*D* = 150 mm)

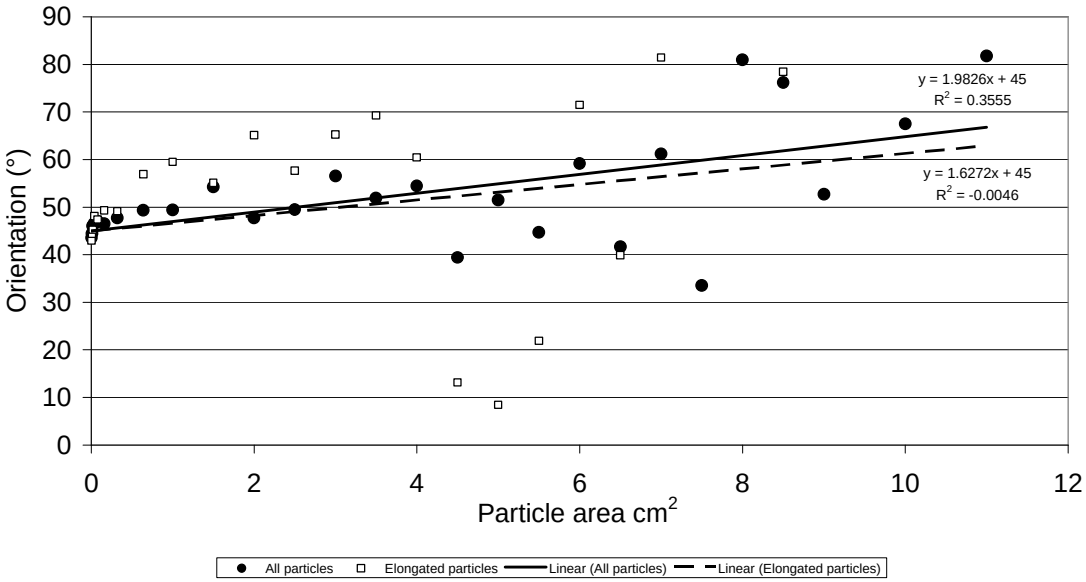

Figure 6.2: Plot of all average particle orientation versus particle area for vibratory compacted specimen (*D* = 150 mm)

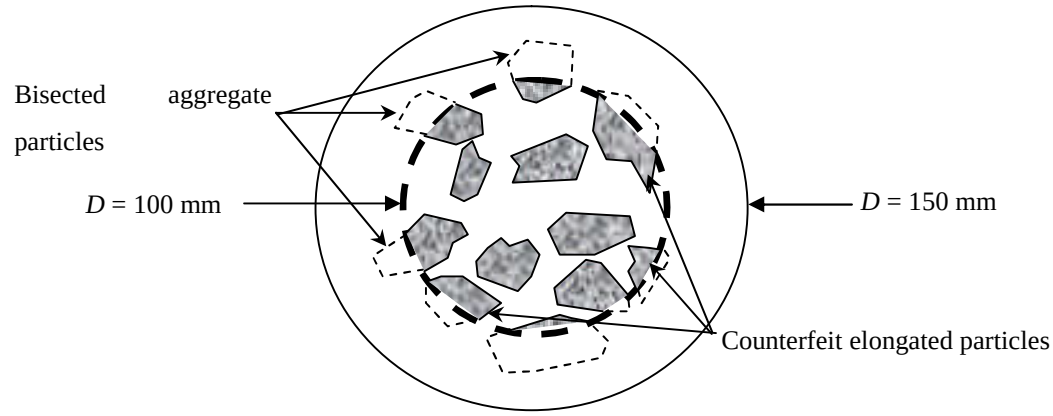

Figure 6.3: Schematic representation of bisected aggregate particles

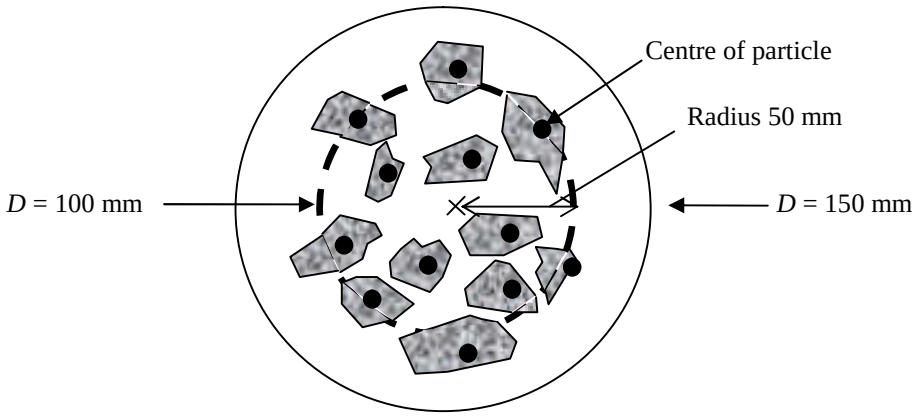

Figure 6.4: Schematic representation of scanning for radius 50 mm to determine correct aggregate orientation with 100 mm diameter specimen

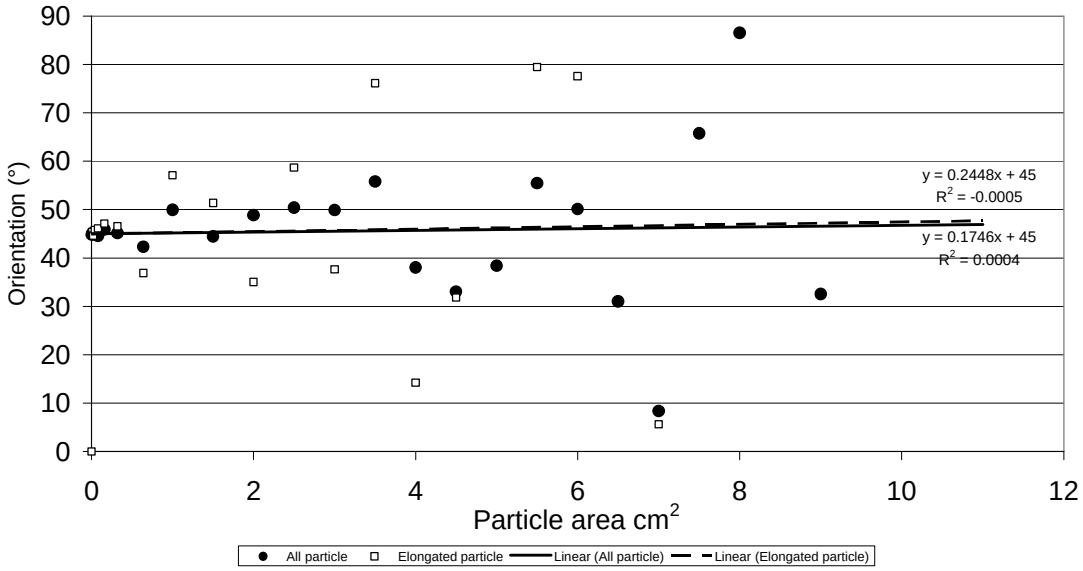

Figure 6.5: Plot for average particle orientation versus particle area for gyratory compacted specimen (Computer trimmed *D* = 100 mm)

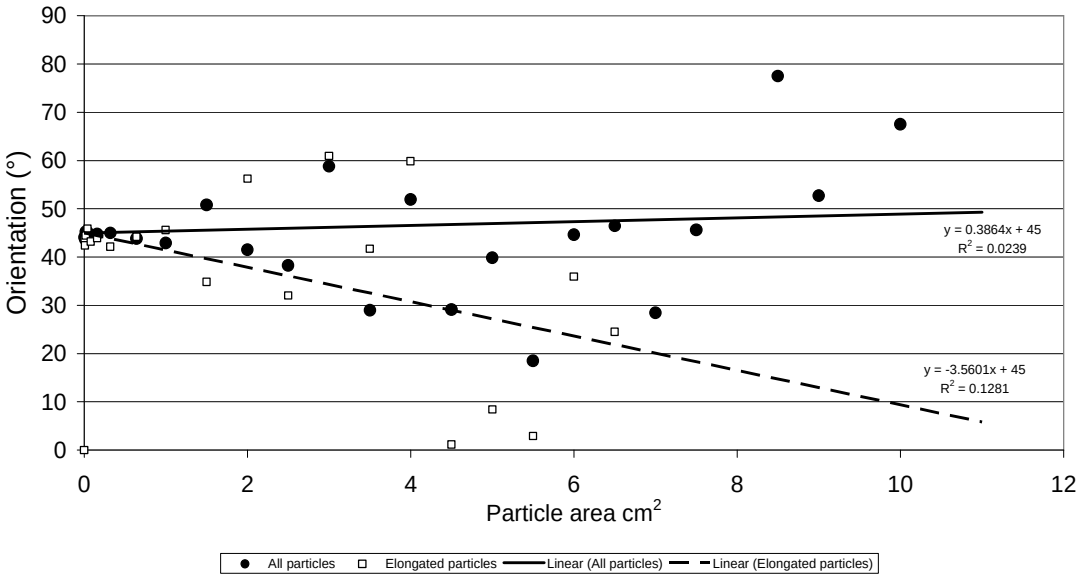

Figure 6.6: Plot for average particle orientation versus particle area for vibratory compacted specimen (Computer trimmed *D* = 100 mm)

Elongated particles

Aggregate particles were analysed looking at the elongated particles. In this case, the aggregate particles, whose elongation ratio are greater than 2:1 (length: width), were chosen using the computer software. The results are shown in Table 6.2.

In general, both the gyratory and vibratory compacted specimens showed a large degree of circumferential orientation in the 150 mm and 100 mm diameter specimens. In particular, the gyratory compacted 150 mm diameter specimens showed significant increase in aggregate orientation, compared the results considering all particles. This trend was also confirmed in Hunter et al (2004). Therefore, it seems that the elongated particles tend to be affected by gyratory motion so that the circumferential particle orientation occurs. This assumption is schematized in Figure 6.7. This may lead to an increase in aggregate orientation in elongated particles. In addition, comparing the 150 mm diameter specimens with the 100 mm diameter specimens, the 100 mm diameter specimens had an increased circumferential orientation in both the gyratory and vibratory compaction. This phenomenon may occur due to the production of bisected elongated particles caused by the coring process as suggested previously.

As previously, the images of 150 mm diameter specimens were re-analyzed by trimming to a radius of 50 mm using the computer software. As shown in Table 6.2, the computer trimmed 100 mm diameter gyratory specimens indicated significant reduction in average aggregate orientation. This trend was also observed, when considering all particles. Therefore, the aggregate particles located in the inner

region of 150 mm diameter specimens (i.e. inside a radius of 50 mm) may not be affected significantly by gyratory motion during compaction. This assumption is depicted in Figure 6.8 and Picture 6.1. In contrast, for the computer trimmed vibratory compacted specimen, the results showed a downward slope rather than a flat slope as shown in Figure 6.6. The reason why this phenomenon occurred is not understood. Therefore, this should be investigated in more detail in the future research.

Table 6.2: Elongated particles

Surface	Aggregate Orientation (°/cm^2)					
	Gyratory Compaction			Vibratory Compaction		
	150mm	100mm	100mm(C)	150mm	100mm	100mm(C)
S2 (Top)	5.76	4.75	1.70	3.02	3.38	-1.93
S3 (Bottom)	0.41	4.82	-0.46	1.13	4.79	-3.69
Average	2.65	5.06	0.24	1.63	3.90	-3.56

* Calculation was conducted using protocol #3 – See Section 6.3

* (C) stands for Computer trimmed 100 mm diameter specimen.

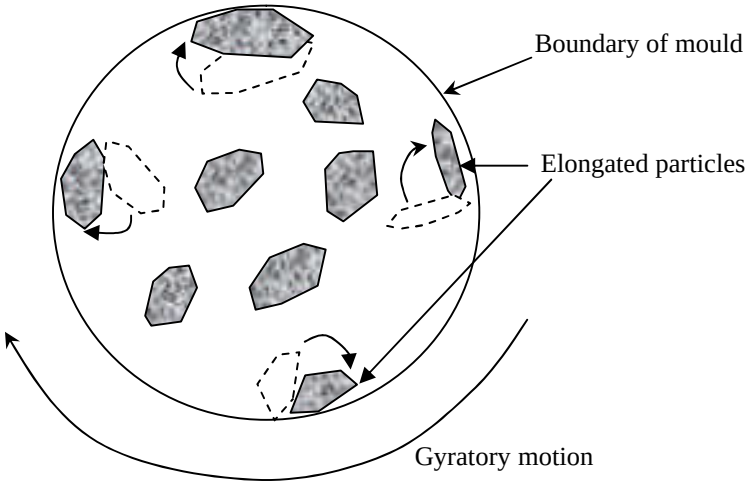

Figure 6.7: Schematic representation of reorientation for elongated particle during gyratory compaction

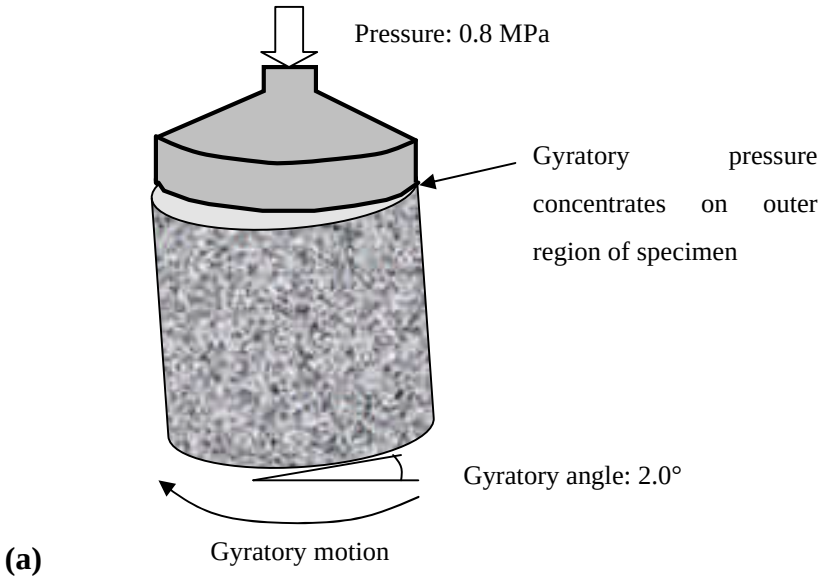

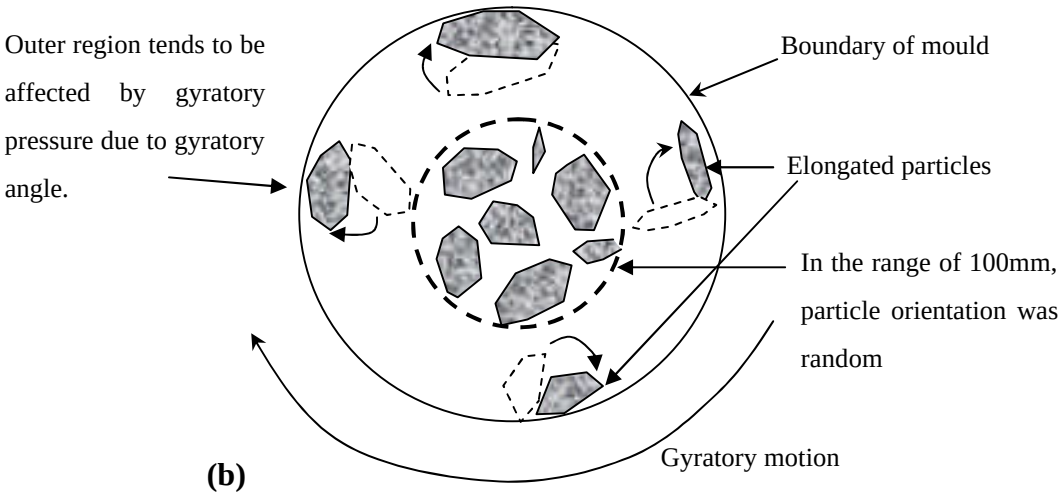

Figure 6.8: Schematic representations of differences of particle orientation (a) Effect of gyration (b) Differences of outer and inner region in terms of particle orientation

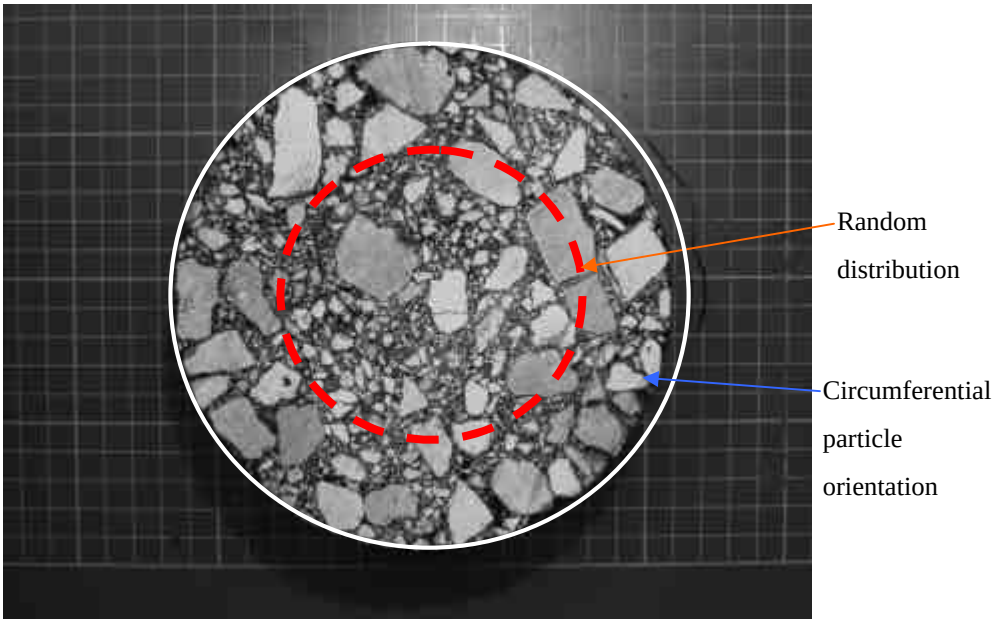

Picture 6.1: Schematic representation of scanning for radius 50 mm to determine correct aggregate orientation with 100 mm diameter specimen

6.2.2 Slab Specimen in Three Orthogonal Directions

As described in Chapter 3, 100 mm diameter cores were taken in the three orthogonal directions (i.e. Z, Y and X directions) from slabs with dimensions of 300 mm by 300 mm by 100 mm in height. Then, the specimens were photographed; and the aggregate orientation was analyzed in each direction. The results are shown in Table 6.3.

The results indicate significant variation in the slope of aggregate orientation, despite the fact that the specimens are cored from slabs which consist of the same aggregate gradation. In addition, the aggregate orientations looking at the three directions show extremely high values. Therefore, it is assumed that the higher aggregate orientation is caused by the bisected aggregate particles, as observed in mould-based 100 mm diameter cores.

This trend is also confirmed for elongated particles. As shown in Table 6.4, the elongated aggregate orientations show differences in each direction. Moreover, the aggregate orientations are higher than when considering all particles. This phenomenon was also observed in gyratory and vibratory compacted specimens. Therefore, the effect of coring appears to be more pronounced for elongated particles, as the particles for 100 mm diameter specimens show higher angle after coring from the 150 mm diameter specimens.

Table 6.3: Slope of aggregate orientation in slab specimens (All particles)

Direction & Surface	Slab Compaction	Aggregate Orientation (°/cm^2)	
	100 mm (Z)	100 mm (Y)	100 mm (X)
S2 (Top)	3.53	4.31	4.37
S3 (Bottom)	3.74	3.64	4.84
Average	3.72	4.08	4.69

* Calculation was conducted using protocol #3.

Table 6.4: Slope of aggregate orientation in slab specimens (Elongated particles)

Direction & Surface	Slab Compaction	Aggregate Orientation (°/cm^2)	
	100 mm (Z)	100 mm (Y)	100 mm (X)
S2 (Top)	7.30	4.51	5.54
S3 (Bottom)	4.74	5.76	5.38
Average	5.89	4.33	5.16

* Calculation was conducted using protocol #3.

6.3 CALCULATION METHODS FOR PARTICLE ORIENTATION SLOPE

The results of the image analysis were discussed in the previous section. However, the comparisons between Hunter et al. (2004) and this research were different in terms of the calculation of the averaged slope of particle orientation. Therefore, it is necessary to examine all the possibilities for the determination of averaged slopes. In this section, four possible approaches for the determination of averaged slopes were analyzed using both all and elongated particles. These approaches are explained separately as follows.

6.3.1 Protocol #1

Average of individual slopes for different surfaces, each determined from averaged orientation angle versus particle area from 30 images per surface

Hunter et al. (2004) determined the averaged slope from 30 specimens in each compaction method. According to their paper, firstly, they manufactured 30 asphalt specimens for each compaction combination, and then produced 4 cut surfaces from one specimen (see Figure 6.9).

Secondly, 2-D images of each cut surface were captured using a digital camera (120 images per compaction combination). After that, the aggregate slopes were calculated from individual aggregate orientation angle (ε_i) in each surface and an average (weighted) aggregate orientation angle (ε_w) for each particle area range was determined.

Thirdly, the combined aggregate orientation angle (ε_{combw}) for each particle area range (average of 30 images) was determined in each of four surfaces (S1 to S4). Then, the combined aggregate orientation angle (ε_{combw}) versus particle area (Visible Surface Area (VSA)) was plotted to determine aggregate orientation slope (°/cm^2) (best fit straight line with intercept 45° through average ε versus VSA plot) for each surface.

Finally, the averaged slope was determined from the average slopes of 4 surfaces. In other words, averaged slope was calculated from simple averaging of slopes for S1, S2, S3 and S4 in order to determine the averaged slope for each compaction combination.

6.3.2 Protocol #2

Average of 24 individual slopes from 24 images

In this study, 24 individual slopes were calculated from 24 images (i.e. top and bottom surface per one specimen). Therefore, it is possible to average 24 slopes per a compaction combination in order to determine averaged slope. In protocol #2, that trial was examined to look at differences of particle orientation in each compaction combination. The procedure for protocol #2 is as follows.

Firstly, 12 asphalt mixture specimens per compaction combination were prepared and specimens were trimmed to produce 2 cut faces (surfaces) per specimen. In this trial, the top and bottom surfaces are equivalent to S2 and S3 surfaces in protocol #1.

Secondly, a 2-D image of each cut surface (24 images per compaction method combination) was photographed and then, the aggregate orientation angle (ε_i) for each individual aggregate particle was calculated in each image.

Thirdly, an averaged (weighted) aggregate orientation angle (ε_w) for each particle area range was calculated. After that, the combined aggregate orientation angle (ε_{combw}) versus particle area (visible surface area (VSA)) was plotted to determine aggregate orientation slope (°/cm^2) (best fit straight line with intercept 45° through average ε versus VSA plot) for each surface.

Finally, the slopes for the 24 individual images were averaged to determine the average slope for the compaction combination. In this case, 18 compaction combinations were analyzed in total.

6.3.3 Protocol #3

One slope determined from averaged orientation angle versus particles area from 24 images

This is the protocol which was used in the previous section. The slope for each compaction combination was calculated from the combined aggregate orientation angle (ε_{combw}) as all of top and bottom surfaces per compaction combination were averaged at once. In this case, all the average (weighted) aggregate orientation angles (ε_w) for top and bottom (S2 and S3) surfaces were calculated on an Excel spreadsheet and then the combined aggregate orientation angle (ε_{combw}) was determined. A brief explanation for this protocol is described below.

Firstly, 12 asphalt mixture specimens per compaction combination were prepared and specimens were trimmed to produce 2 cut faces (surfaces) per specimen. In this trial, top and bottom surfaces are equivalent to S2 and S3 surfaces in protocol #1.

Secondly, a 2-D image of each cut surface (24 images per compaction method combination) was photographed and then, the aggregate orientation angle (ε_i) for each individual aggregate particle was calculated in each image.

Thirdly, an averaged (weighted) aggregate orientation angle (ε_w) for each particle area range was calculated and then the combined aggregate orientation angle (ε_{combw}) for each particle range (average of 24 images) was determined.

Finally, the combined aggregate orientation angle (ε_{combw}) versus particle area (Visible Surface Area (VSA)) was plotted to determine aggregate orientation slope ($°/cm^2$) (best fit straight line with intercept 45° through average ε versus VSA plot) for each surface.

6.3.4 Protocol #4

Average of 2 individual slopes for top and bottom surfaces determined from averaged orientation angle versus particle area from 12 images per surface

This protocol was applied to top and bottom (S2 and S3) surfaces to determine the average slope for the compaction combination. Although the calculation procedure was almost same as in protocol #3, this protocol calculated the slope for top and bottom surfaces separately and then determined the slope in each compaction

combination by averaging the mean slopes for top and bottom surfaces. The calculation sequence for this protocol is as follows.

Firstly, 12 asphalt mixture specimens per compaction combination were prepared and specimens were trimmed to produce 2 cut faces (surfaces) per specimen. In this trial, top and bottom surfaces are equivalent to S2 and S3 surfaces in protocol #1.

Secondly, a 2-D image of each cut surface (24 images per compaction method combination) was photographed and then, the aggregate orientation angle (ε_i) for each individual aggregate particle was calculated in each image.
Thirdly, an averaged (weighted) aggregate orientation angle (ε_w) for each particle area range was calculated and then the combined aggregate orientation angle (ε_{combw}) for each particle range (average of 12 images) was determined for each of the two surfaces (S2 and S3).

Finally, the combined aggregate orientation angle (ε_{combw}) versus particle area (Visible Surface Area (VSA)) was plotted to determine aggregate orientation slope (°/cm^2) (best fit straight line with intercept 45° through average e versus VSA plot) for each surface and the slopes for S2 and S3 (top and bottom) surfaces were averaged to determine the average slope for the compaction combination.

To understand the differences of each protocol more clearly, the procedure for each protocol is schematized in Figure 6.9; the flow of each protocol is shown in Figure 6.10.

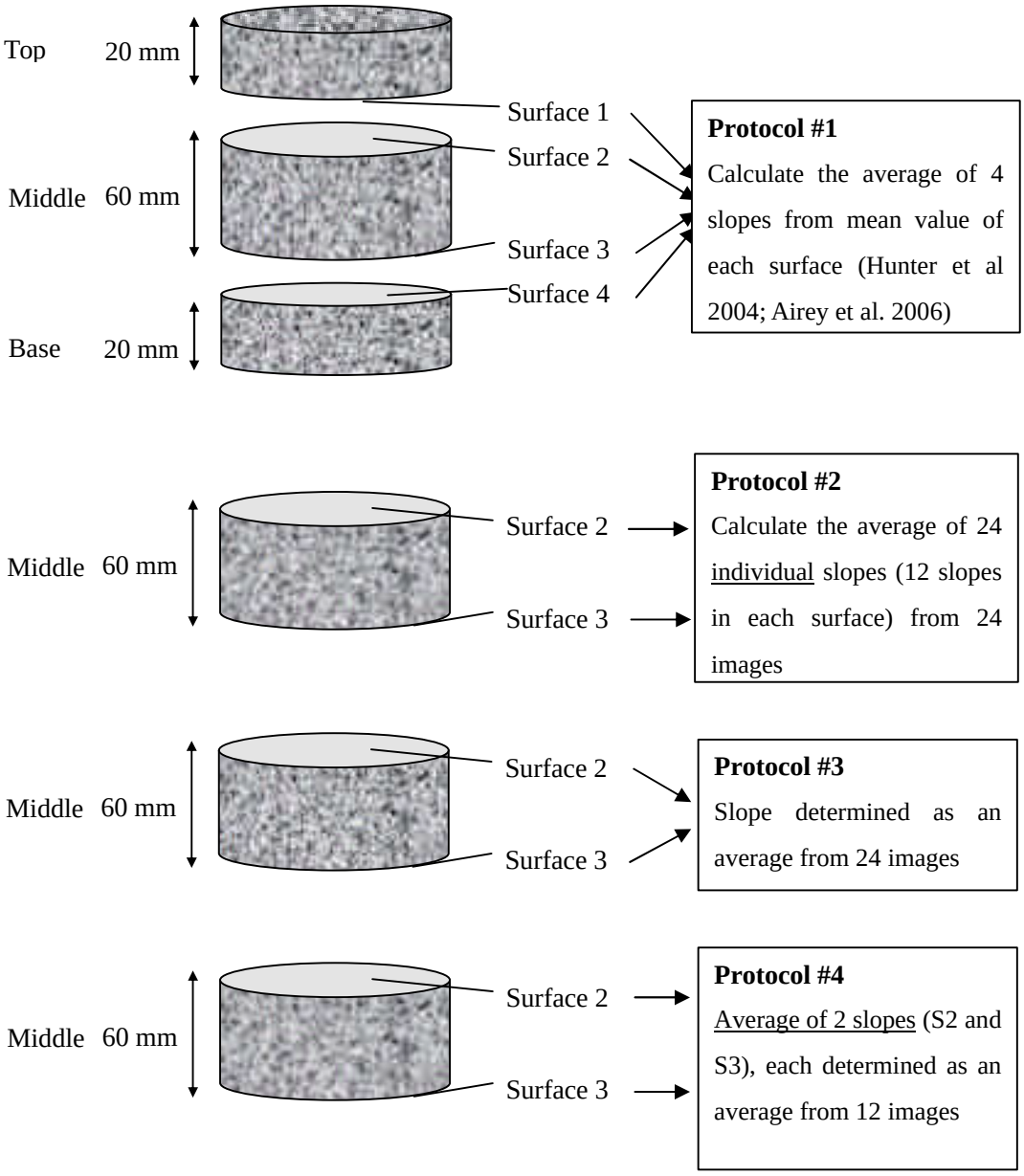

Figure 6.9: Schematic of four types of calculation protocol for the determination of particle orientation

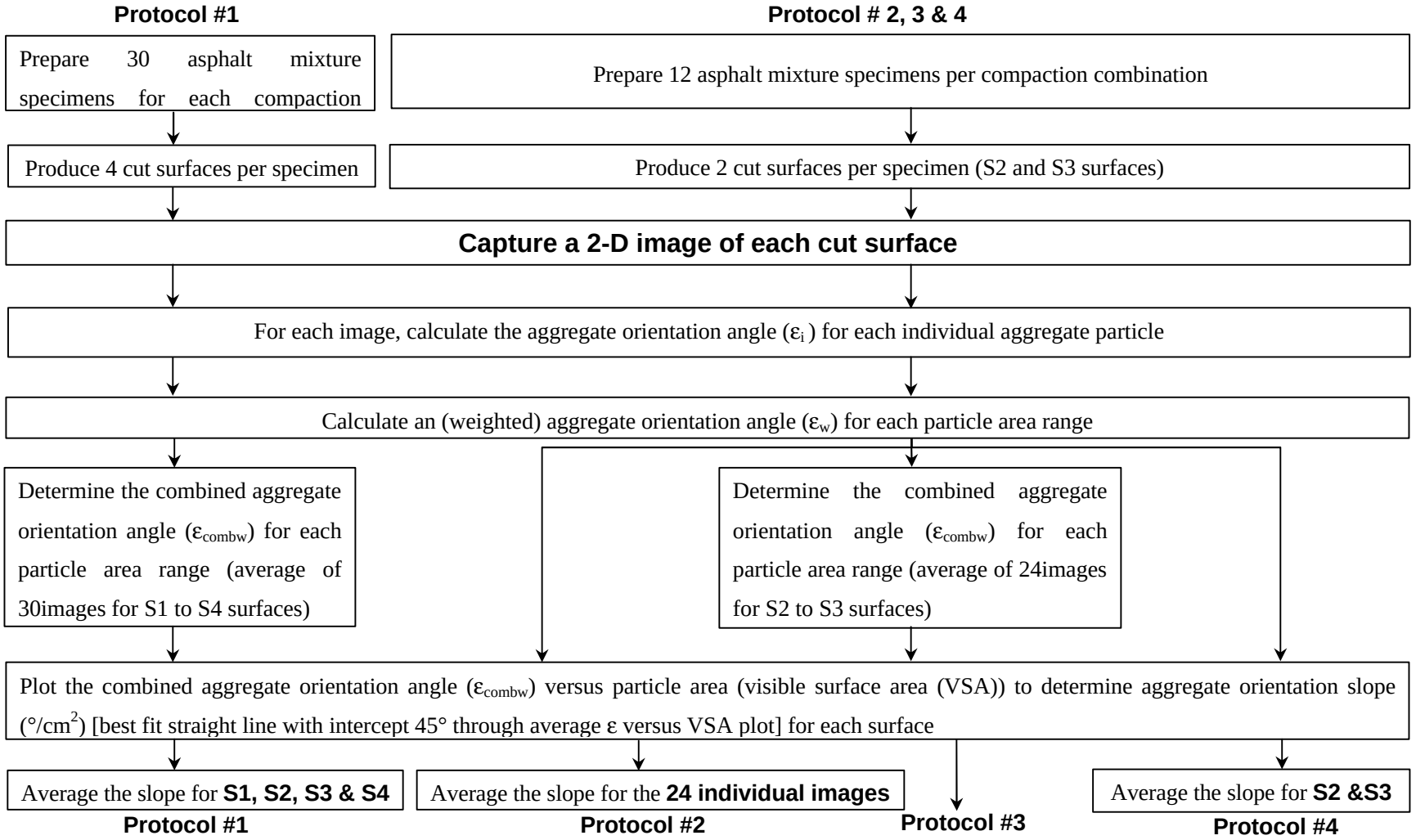

Figure 6.10: Flow of each protocol

6.3.5 Discussion for Each Protocol Result

The slopes of aggregate orientation for the three compaction methods were examined using the four protocols described in the previous section. In order to look at the effect of compaction combinations (i.e. compaction method, specimen size, analysis method, coring orientation and particle geometry), the slopes of aggregate orientation were analyzed for all particles and for elongated particles (2:1 ratio length to breath).

All particles (Gyratory and Vibratory compacted specimens)

Table 6.5 shows the result of average slopes for all particles using the four protocols. There are some similarities in the trend of the aggregate orientation slope between the gyratory and vibratory compacted specimens.

Comparing the 150 mm diameter specimens with cored 100 mm diameter specimens, it is confirmed that the cored 100 mm specimens tend to have a greater slope than that of the 150 mm diameter specimens in protocols #2, #3 and #4. However, considering the process of producing the 100 mm diameter cores from the 150 mm diameter specimens, artificial circumferential oriented particles may give a greater influence on the slope of aggregate orientation due to the smaller cross-sectional area. This is examined in more detail in the following sections.

In contrast to an increase of the slope in the 100 mm diameter cores, the computer trimmed 100 mm diameter specimens for both the gyratory and vibratory compacted specimens show a significant reduction in the aggregate orientation

slope in protocols #2, #3 and #4. Based on the data, the value of ε was calculated to compare the results of each protocol with respect to actual aggregate particles. The results are presented in Tables 6.6 to 6.7.

For 8 cm^2 VSA, the slopes of aggregate orientation for the computer trimmed specimens are close to 45°, compared to a greater orientation in the 100 mm diameter cores. Similarly, the same trend is observed even for smaller VSA (i.e. 2 cm^2). Therefore, it is evident that aggregate particles placed within the radius of 50 mm in the 150 mm diameter specimens have a random particle orientation.

All particles (Slab compacted specimens)

Table 6.5 also shows the average slopes for all particles in slab cores. Lees et al. (1969) stated that a specimen compacted by laboratory roller compactor achieves the same particle orientation as in the field. Airey et al. (2006) also suggested that both field and laboratory slab 'roller' compacted specimens (150 mm diameter) have random particle distribution which is recognized as 0 (°/cm^2) in the slope of aggregate orientation in this study.

However, the 100 mm diameter cores from the slabs are significantly different in terms of aggregate orientation compared to the 150 mm diameter cores with random particle distribution. Although both methods have involved the coring process, which may produce artificial circumferential orientation of particles, the 150 mm diameter specimens have a flat slope in aggregate orientation. Therefore, as shown in the 100 mm diameter cores for the gyratory and vibratory specimens,

the 100 mm diameter slab cores may also suffer from the effect of artificial circumferential particle orientation.

However, it should be noted that there is considerable variability in the three orthogonal directions with regard to the aggregate orientation slope. This trend is observed in the three protocols. The influence of the three orthogonal directions on the internal aggregate structure is discussed further in the following sections.

Table 6.5: Average slopes for all particles (28 mm DBM)

Compaction combinations	Particle orientation slope (°/cm^2)			
	Protocol #1	Protocol #2	Protocol #3	Protocol #4
Gyratory 150 mm	1.56	0.94	1.56	1.59
Gyratory 100 mm		2.66	1.53	1.95
Gyratory comp. 100 mm		-0.26	0.17	-0.51
Vibratory 150 mm	2.45	1.70	1.98	1.66
Vibratory 100 mm		2.33	2.26	2.00
Vibratory comp. 100 mm		-0.30	0.39	0.29
Slab Z 150 mm	0.73			
Slab Z 100 mm		3.51	3.72	3.64
Slab Y 100 mm		3.36	4.08	3.98
Slab X 100 mm		4.27	4.69	4.61

* Comp.: Computer trimmed

Table 6.6: Average orientation angles (e) at 8 cm^2 VSA for all particles (28 mm DBM)

Compaction combinations	Particle orientation angle (°)			
	Protocol #1	Protocol #2	Protocol #3	Protocol #4
Gyratory 150 mm	57	53	57	58
Gyratory 100 mm		66	57	61
Gyratory comp. 100 mm		43	46	41
Vibratory 150 mm	65	59	61	58
Vibratory 100 mm		64	63	61
Vibratory comp. 100 mm		43	48	47
Slab Z 150 mm	51			
Slab Z 100 mm		73	75	74
Slab Y 100 mm		72	78	77
Slab X 100 mm		79	83	82

* Comp.: Computer trimmed

Table 6.7: Average orientation angles (e) at 2 cm^2 VSA for all particles (28 mm DBM)

Compaction combinations	Particle orientation angle (°)			
	Protocol #1	Protocol #2	Protocol #3	Protocol #4
Gyratory 150 mm	48	47	48	48
Gyratory 100 mm		50	48	49
Gyratory comp. 100 mm		44	45	44
Vibratory 150 mm	50	48	49	48
Vibratory 100 mm		50	50	49
Vibratory comp. 100 mm		44	46	46
Slab Z 150 mm	47			
Slab Z 100 mm		52	52	52
Slab Y 100 mm		52	53	53
Slab X 100 mm		54	54	54

* Comp.: Computer trimmed

Elongated particles (Gyratory and Vibratory compacted specimens)

Table 6.8 shows the average slopes for elongated particles calculated with the four protocols. Also, the value of ε was calculated to compare the results of each protocol with respect to actual aggregate particles. The results are presented in Table 6.9. As would be expected, greater aggregate orientation slopes than when considering all particles are confirmed in both the 150 mm diameter specimens and 100 mm diameter cores. Both the gyratory and vibratory 100 mm diameter cores indicate a dramatic increase in the slope of aggregate orientation, compared to the 150 mm diameter specimens. This may be caused by the coring process, as described in previous sections.

However, despite the fact that there is general increase in the slopes of aggregate orientation for the 150 mm and 100 mm diameter specimens, the computer trimmed 100 mm diameter specimens tend to show a flat slope, especially in the gyratory compacted specimens. This trend was also observed, when considering all particles. Although the computer trimmed vibratory compacted 100 mm diameter specimens show a different trend in protocols #3 and #4, this fact may strongly support aggregate particles placed within the radius of 50 mm in the 150 mm diameter specimens having a random particle orientation, even in elongated particles.

Elongated particles (Slab specimens)

As shown in Tables 6.8 and 6.9, the slopes for elongated particles for slab specimens indicate greater slopes than those for all particles. Therefore, similar

trends to the gyratory and vibratory 100 mm diameter cores are confirmed for the elongated particles of the slab specimens. In addition, it is confirmed that there are also considerable differences in the three orthogonal directions.

Table 6.8: Average slopes for elongated particles (28 mm DBM)

Compaction combinations	Particle orientation slope (°/cm^2)			
	Protocol #1	Protocol #2	Protocol #3	Protocol #4
Gyratory 150 mm	4.92	6.40	2.65	3.09
Gyratory 100 mm		12.68	5.06	4.79
Gyratory comp. 100 mm		-0.15	0.24	0.62
Vibratory 150 mm	3.58	9.71	1.63	2.08
Vibratory 100 mm		11.20	3.90	4.09
Vibratory comp. 100 mm		-0.21	-3.56	-2.81
Slab Z 150 mm	1.48			
Slab Z 100 mm		9.76	5.89	6.02
Slab Y 100 mm		6.57	4.33	5.14
Slab X 100 mm		7.03	5.16	5.46

* Comp.: Computer trimmed

Table 6.9: Average orientation angles (e) at 2 cm^2 VSA for elongated particles (28 mm DBM)

Compaction combinations	Average particle orientation angle at 2 cm^2 (°)			
	Protocol #1	Protocol #2	Protocol #3	Protocol #4
Gyratory 150 mm	55	58	50	51
Gyratory 100 mm		70	55	55
Gyratory comp. 100 mm		45	45	46
Vibratory 150 mm	52	64	48	49
Vibratory 100 mm		67	53	53
Vibratory comp. 100 mm		45	37	39
Slab Z 150 mm	48			
Slab Z 100 mm		65	57	57
Slab Y 100 mm		58	54	55
Slab X 100 mm		59	55	56

* Comp.: Computer trimmed

6.3.6 Discussion for Aggregate Particle Orientation

Through the image analysis, the differences of compaction mode were examined by aggregate orientation slope. As mentioned in Chapter 5, this was conducted for the purpose of comparing each compaction method. However, some properties regarding the aggregate orientation slope were found through this analysis.

The unit of °/cm^2 indicated whether laboratory compacted specimens have circumferential orientation. From the image analysis results, it was found that mould based specimens such as the gyratory and vibratory compacted specimens have circumferential particle orientation since these specimens showed greater values than that of the slab specimens. Therefore, it can be said that the unit of °/cm^2 may be used as a parameter for whether specimens are influenced by the effect of mould confinement.

Moreover, Hunter et al (2004) suggested that the slope of particle orientation versus particle area in units of °/cm^2 represents visually that the degree of circumferential orientation increases with particle area. This trend was also seen in this study as bigger particles tend to show grater aggregate orientation; the mould based 150 mm diameter specimens showed greater slope than that of the cored 100 mm diameter specimens. Therefore, the slope for aggregate orientation might be useful to investigate how the specimens are influenced by mould. However, for the cored 100 mm diameter specimens, the bisected aggregate particles strongly influence on the aggregate orientation slope, especially in larger particles; further research would be necessary for the slope of the cored 100 mm specimens.

6.4 DIFFERENCES OF SURFACE IN IMAGE ANALYSIS

Gyratory and Vibratory specimens (All particles)

The slope of aggregate orientation was separately calculated for the S2 (top) and S3 (bottom) surfaces of the specimens. Tables 6.10 and 6.11 show the average slope of aggregate orientation looking at all particles. Also, the values of ε for the S2 and S3 surfaces are shown in Tables 6.12 and 6.13.

Although protocol #1 shows significant differences in the slope in each surface, protocols #2 and #3 do not indicate any remarkable trend in each surface. However, a general increase in the slope is seen on both surfaces of the 100 mm cores in the gyratory and vibratory specimens. In addition, it is found that the slopes of aggregate orientation for the computer trimmed 100 mm specimens are close to 0 ($°/cm^2$) on both surfaces. These trends are also observed in the average slopes.

Slab specimens (All particles)

Tables 6.10 to 6.13 include the data from slab cores. The 100 mm cores from the slab are very different in terms of aggregate orientation compared to the 150 mm diameter cores from slabs. As suggested in the previous sections, this may be due to the artificial circumferential orientation of particles, which were produced in coring process.

However, significant variation is seen in the slopes of aggregate orientation on both surfaces. This is analysed and discussed further in the following sections.

Table 6.10: Average S2 slopes for all particles (28 mm DBM)

Compaction Combinations	Particle orientation slope (°/cm^2)		
	Protocol #1	Protocol #2	Protocol #3
Gyratory 150 mm	2.62	0.58	1.59
Gyratory 100 mm		1.72	2.79
Gyratory comp. 100 mm		-0.87	-0.05
Vibratory 150 mm	3.44	1.93	2.09
Vibratory 100 mm		2.98	1.77
Vibratory comp. 100 mm		0.14	0.54
Slab Z 150 mm	0.63		
Slab Z 100 mm		3.97	3.53
Slab Y 100 mm		3.68	4.31
Slab X 100 mm		4.35	4.37

* Comp.: Computer trimmed

Table 6.11: Average S3 slopes for all particles (28 mm DBM)

Compaction Combinations	Particle orientation slope (°/cm^2)		
	Protocol #1	Protocol #2	Protocol #3
Gyratory 150 mm	0.38	1.31	1.58
Gyratory 100 mm		3.59	1.10
Gyratory comp. 100 mm		0.35	-0.96
Vibratory 150 mm	2.44	1.46	1.23
Vibratory 100 mm		1.67	2.23
Vibratory comp. 100 mm		-0.74	0.04
Slab Z 150 mm	0.37		
Slab Z 100 mm		3.05	3.74
Slab Y 100 mm		3.04	3.64
Slab X 100 mm		4.19	4.84

* Comp.: Computer trimmed

Table 6.12: Average orientation angles (e) for S2 at 8 cm^2 VSA for all particles (28 mm DBM)

Compaction Combinations	Particle orientation angle (°)		
	Protocol #1	Protocol #2	Protocol #3
Gyratory 150 mm	66	50	58
Gyratory 100 mm		59	67
Gyratory comp. 100 mm		38	45
Vibratory 150 mm	73	60	62
Vibratory 100 mm		69	59
Vibratory comp. 100 mm		46	49
Slab Z 150 mm	50		
Slab Z 100 mm		77	73
Slab Y 100 mm		74	79
Slab X 100 mm		80	80

* Comp.: Computer trimmed

Table 6.13: Average orientation angles (e) for S3 at 8 cm^2 VSA for all particles (28 mm DBM)

Compaction Combinations	Particle orientation angle (°)		
	Protocol #1	Protocol #2	Protocol #3
Gyratory 150 mm	48	55	58
Gyratory 100 mm		74	54
Gyratory comp. 100 mm		48	37
Vibratory 150 mm	65	57	55
Vibratory 100 mm		58	63
Vibratory comp. 100 mm		39	45
Slab Z 150 mm	48		
Slab Z 100 mm		69	75
Slab Y 100 mm		69	74
Slab X 100 mm		79	84

* Comp.: Computer trimmed

Gyratory and Vibratory compacted specimens (Elongated particles)

Tables 6.14 and 6.15 indicate the average slopes of aggregate orientation for elongated particles, looking at S2 and S3 surfaces. Also, the values of ε for S2 and S3 surfaces are presented in Tables 6.16 and 6.17.

As would be expected, there is a general increase in average slopes for elongated particles on both S2 (top) and S3 (bottom) surfaces, compared to slopes for all particles. Also, increases in the slope from the 150 mm diameter specimens to the 100 mm diameter cores are seen on both surfaces. In addition, a significant reduction in the slope is also confirmed in the computer trimmed 100 mm diameter specimens. However, no significant trend is shown between S2 and S3 surfaces in protocols #2 and #3.

Slab specimens (Elongated particles)

Tables 6.14 to 6.17 include the data from slab cores. The 100 mm diameter cores taken from the slabs are very different in terms of aggregate orientation compared to the 150 mm diameter cores from slabs. As suggested in the previous sections, this may be due to the artificial circumferential orientation of particles, which were produced in coring process.

However, the general pattern is similar to that for all particles as significant variation in the slope of aggregate orientation is seen on both surfaces. Therefore, these variations should be examined and discussed together with the mechanical testing results. The results are discussed in Chapter 7.

Table 6.14: Average S2 slopes for elongated particles (28 mm DBM)

Compaction Combinations	Particle orientation slope (°/cm^2)		
	Protocol #1	Protocol #2	Protocol #3
Gyratory 150 mm	4.27	7.70	5.76
Gyratory 100 mm		14.55	4.75
Gyratory comp. 100 mm		2.54	1.70
Vibratory 150 mm	1.91	10.07	3.02
Vibratory 100 mm		7.93	3.38
Vibratory comp. 100 mm		-0.63	-1.93
Slab Z 150 mm	3.44		
Slab Z 100 mm		11.24	7.30
Slab Y 100 mm		4.93	4.51
Slab X 100 mm		4.76	5.54

* Comp.: Computer trimmed

Table 6.15: Average S3 slopes for elongated particles (28 mm DBM)

Compaction Combinations	Particle orientation slope (°/cm^2)		
	Protocol #1	Protocol #2	Protocol #3
Gyratory 150 mm	4.07	5.11	0.41
Gyratory 100 mm		10.80	4.82
Gyratory comp. 100 mm		-2.84	-0.46
Vibratory 150 mm	4.38	9.35	1.13
Vibratory 100 mm		14.48	4.79
Vibratory comp. 100 mm		0.21	-3.69
Slab Z 150 mm	0.37		
Slab Z 100 mm		8.29	4.74
Slab Y 100 mm		8.21	5.76
Slab X 100 mm		9.30	5.38

* Comp.: Computer trimmed

Table 6.16: Average orientation angles (e) for S2 at 2 cm^2 VSA for elongated particles (28 mm DBM)

Compaction Combinations	Particle orientation angle (°)		
	Protocol #1	Protocol #2	Protocol #3
Gyratory 150 mm	54	60	57
Gyratory 100 mm		74	55
Gyratory comp. 100 mm		50	48
Vibratory 150 mm	49	65	51
Vibratory 100 mm		61	52
Vibratory comp. 100 mm		44	41
Slab Z 150 mm	52		
Slab Z 100 mm		67	60
Slab Y 100 mm		55	54
Slab X 100 mm		55	56

* Comp.: Computer trimmed

Table 6.17: Average orientation angles (e) for S3 at 2 cm^2 VSA for elongated particles (28 mm DBM)

Compaction Combinations	Particle orientation angle (°)		
	Protocol #1	Protocol #2	Protocol #3
Gyratory 150 mm	53	55	46
Gyratory 100 mm		67	55
Gyratory comp. 100 mm		39	44
Vibratory 150 mm	54	64	47
Vibratory 100 mm		74	55
Vibratory comp. 100 mm		45	38
Slab Z 150 mm	46		
Slab Z 100 mm		62	54
Slab Y 100 mm		61	57
Slab X 100 mm		64	56

* Comp.: Computer trimmed

6.5 THE EFFECT OF DIFFERENT DEGREES OF ELONGATION

Gyratory and Vibratory compacted specimens

The image analysis data obtained in this study identified the degree of elongation in each particle. Using the data, the effect of different degrees of elongation was examined for each compaction method and specimen size. The aggregate orientation slope (°/cm^2) has all been calculated using protocol #2. The results are shown in Table 6.18. Also, a lower VSA of 1cm^2 is used to represent the ε angles. The results are presented in Table 6.19. Overall, there is a general trend of a showing steep slope as the degree of elongation increases.

For the 150 mm diameter specimens, both gyratory and vibratory compacted specimens showed a general increase in the slope of aggregate orientation. The gyratory compacted specimens indicate a steady increase in the slopes of all and 2:1 elongated particles. However, the slope increases up dramatically for elongations of 3:1 and 4:1. A similar trend is observed in the vibratory compacted specimens.

However, for the 100 mm diameter cores, the results show clearly an increase or a reduction in the slope for the gyratory and the vibratory compactions. Therefore, it would be expected that the results are greatly influenced by the particles at the circumference, which were created due to the coring process.

In order to look at the change in the slope of 100 mm diameter cores in more detail,

the data of the computer trimmed specimens were analyzed. From the result shown in Table 6.17, it was found that particles with elongations of 3:1 and 4:1 show considerably higher values in the slopes of aggregate orientation in both the gyratory and vibratory specimens, despite seeing flat slope in all and 2:1 elongated particles. However, looking at the data of the 150 mm and computer trimmed 100 mm diameter specimens in both the gyratory and vibratory compaction, the specimens show similar values in the elongations of 3:1 and 4:1. Therefore, it appears that the 3:1 and 4:1 elongated particles are located at the inner region of the 150 mm diameter specimens, whilst 2:1 elongated particles are in the outer region of the 150 mm diameter specimens, where is nearby the mould boundary. This point is discussed further in the next sections.

Slab specimens

The slopes of aggregate orientation of slabs shown in Table 6.18 indicate significantly higher values in each direction with increase in elongation ratio. Also, a lower VSA of 1.0 cm^2 is indicated to represent the ε angles in Table 6.19. However, once again, it could be expected that the cored 100 mm diameter specimens are greatly affected by bisected circumferential particles due to the smaller cross-sectional area than that of the 150 mm diameter specimens. Therefore, it seems that the aggregate orientation slopes are influenced by the circumferential particles; this may result in extremely greater slopes in the three orthogonal directions.

Table 6.18: Average slopes for all particles and elongated particles (28 mm DBM)

Compaction combinations	Particle orientation slope (°/cm^2)			
	All particles	2:1 elongated	3:1 elongated	4:1 elongated
Gyratory 150 mm	0.94	6.4	25	195
Gyratory 100 mm	2.66	12.7	82	-21
Gyratory comp. 100 mm	-0.26	-0.15	25	197
Vibratory 150 mm	1.70	9.7	32	76
Vibratory 100 mm	2.33	11.2	68	104
Vibratory comp. 100 mm	-0.30	-0.21	32	76
Slab Z 100 mm	3.51	9.8	67	311
Slab Y 100 mm	3.36	6.6	17	411
Slab X 100 mm	4.27	7.0	62	-294

Comp.: Computer trimmed

Table 6.19: Average orientation angles (e) at 1 cm^2 VSA (28 mm DBM)

Compaction combinations	Particle orientation angle at 1 cm^2 VSA (°)			
	All particles	2:1 elongated	3:1 elongated	4:1 elongated
Gyratory 150 mm	46	51	70	-
Gyratory 100 mm	48	58	-	24
Gyratory comp. 100 mm	45	45	70	-
Vibratory 150 mm	47	55	77	-
Vibratory 100 mm	47	56	-	-
Vibratory comp. 100 mm	45	45	77	-
Slab Z 100 mm	49	55	-	-
Slab Y 100 mm	48	52	62	-
Slab X 100 mm	49	52	-	-

* Comp.: Computer trimmed

6.6 PERCENTAGE OF AREA FOR ELONGATED PARTICLES

Gyratory and Vibratory specimens

As discussed in the previous sections, the effect of different elongations was examined looking at the aggregate particle orientation. Aho et al. (2001) studied the effect of flat and elongated aggregate on both field and laboratory compaction of asphalt mixtures; they concluded that increasing the rate of elongated particles will lead to an increase in the amount of aggregate breakage; this phenomenon is more pronounced in gyratory compacted specimens, when compared to the filed compaction. Therefore, in order to look at whether the different elongation ratio influences compaction properties, the percentage of area for elongated particles was also analysed in each compaction combination. The results are shown in Tables 6.20 to 6.25.

The data is obtained for all particles and three elongation ratios of 2:1, 3:1 and 4:1. As would be expected, the percentage area (i.e. area, percent of total area and percent of all particles) decreases with increase in elongation ratio. Also, it is confirmed that few particles have extremely large elongation.

As the asphalt mixture design is kept constant, the percentage of 2:1 elongated particles can be assumed to be constant at a value of approx. 20% of all the aggregates. The percentages for the 3:1 and 4:1 elongated particles are approx. 2.8% and 0.9%, respectively. The above mentioned data is based on the mould confined 150 mm diameter gyratory and vibratory compacted specimens.

As shown in Tables 6.22 and 6.23, the process of producing the 100 mm cores from the 150 mm mould confined specimens resulted in an increase in the percent of 2:1 elongated particles from approximately 20% to about 24% of the total aggregate particles. In contrast, the percent for the computer trimmed 100 mm diameter specimens are approximately 19% in both the gyratory and vibratory specimens. These facts may strongly support the increase in elongated particles being produced due to the coring (cutting) process as discussed in the previous sections.

Considering the above mentioned facts, the cored 100 mm specimens appear to have had higher aggregate orientation slopes due to the increase in the percentage of the 2:1 elongated particles. In addition, looking at the 3:1 and 4:1 elongated particles, the area of aggregate for the computer trimmed 100 mm specimens is the same as that of 150 mm diameter specimens. Also, the computer trimmed specimens show a significant increase in the percentage of all particles, compared to the 150 mm diameter specimens. Instead, a dramatic reduction in area is observed in 2:1 elongated particles for the computer trimmed specimens.

Therefore, it seems that the inner region of 150 mm mould confined specimens has smaller particles with bigger ratios of elongation, although the outer region contains bigger particles with smaller ratios of elongation. This point is discussed further in the next Chapter.

Slab specimens

Tables 6.26 to 6.28 offer the percent of area for elongated particles of the 100 mm

slab specimens. As shown in mould based specimens, an increase in the percentage of 2:1 elongated particles is also seen for the 100 mm diameter cores taken from the slabs.

However, it should be noted that the percentage of elongated particles is not constant in the different orientations. These figures show considerable variation in the three orthogonal coring directions. Also, comparing the 150 mm diameter specimens to the computer trimmed 100 mm diameter specimens, the percentage of total area for the 2:1 elongated particles in the three directions is considerably higher, especially in Y and X directions. In addition, the percent of total area is significantly higher than those of other compactions.

Therefore, it can be assumed that the higher percent of elongated particle was caused by the coring process so that the aggregate orientation slopes of slab specimens were influenced significantly by the erroneous elongated particles. As a result, it could be expected that extremely higher slopes are seen in the three directions. The pictures of aggregate particles in the three orthogonal directions are represented in Figure 6.11.

Table 6.20: Percentage of area for elongated particles for 150 mm gyratory specimens

Parameter	All particles	2:1 elongation	3:1 elongation	4:1 elongation
Area (cm^2)	101.1	20.1	2.4	0.6
% of total area	57.2	11.4	1.3	0.3
% of all particles		19.8	2.3	0.6

Table 6.21: Percentage of area for elongated particles for 150 mm vibratory specimens

Parameter	All particles	2:1 elongation	3:1 elongation	4:1 elongation
Area (cm^2)	101.5	22.1	3.3	1.1
% of total area	57.4	12.5	1.9	0.6
% of all particles		21.8	3.3	1.1

Table 6.22: Percentage of area for elongated particles for 100 mm gyratory specimens

Parameter	All particles	2:1 elongation	3:1 elongation	4:1 elongation
Area (cm^2)	41.5	10.1	1.7	0.4
% of total area	55.0	13.4	2.2	0.5
% of all particles		24.3	4.1	1.0

Table 6.23: Percentage of area for elongated particles for 100 mm vibratory specimens

Parameter	All particles	2:1 elongation	3:1 elongation	4:1 elongation
Area (cm^2)	41.3	9.7	1.1	0.4
% of total area	54.8	12.9	1.5	0.6
% of all particles		23.5	2.8	1.0

Table 6.24: Percentage of area for elongated particles for computer trimmed 100 mm gyratory specimens

Parameter	All particles	2:1 elongation	3:1 elongation	4:1 elongation
Area (cm^2)	45.2	8.9	2.4	0.6
% of total area	57.6	11.3	3.0	0.8
% of all particles		19.7	5.3	1.4

Table 6.25: Percentage of area for elongated particles for computer trimmed 100 mm vibratory specimens

Parameter	All particles	2:1 elongation	3:1 elongation	4:1 elongation
Area (cm^2)	42.5	7.9	3.3	1.1
% of total area	54.2	10.0	4.2	1.4
% of all particles		18.5	7.7	2.6

Table 6.26: Percentage of area for elongated particles for 100 mm slab Z specimens

Parameter	All particles	2:1 elongation	3:1 elongation	4:1 elongation
Area (cm^2)	45.0	9.9	1.0	0.3
% of total area	59.7	13.2	1.4	0.4
% of all particles		22.1	2.3	0.7

Table 6.27: Percentage of area for elongated particles for 100 mm slab Y specimens

Parameter	All particles	2:1 elongation	3:1 elongation	4:1 elongation
Area (cm^2)	47.0	12.0	1.1	0.6
% of total area	62.4	15.8	1.4	0.8
% of all particles		25.3	2.3	1.3

Table 6.28: Percentage of area for elongated particles for 100 mm slab X specimens

Parameter	All particles	2:1 elongation	3:1 elongation	4:1 elongation
Area (cm^2)	45.2	12.6	1.5	0.2
% of total area	60.0	16.7	2.0	0.2
% of all particles		27.8	3.3	0.4

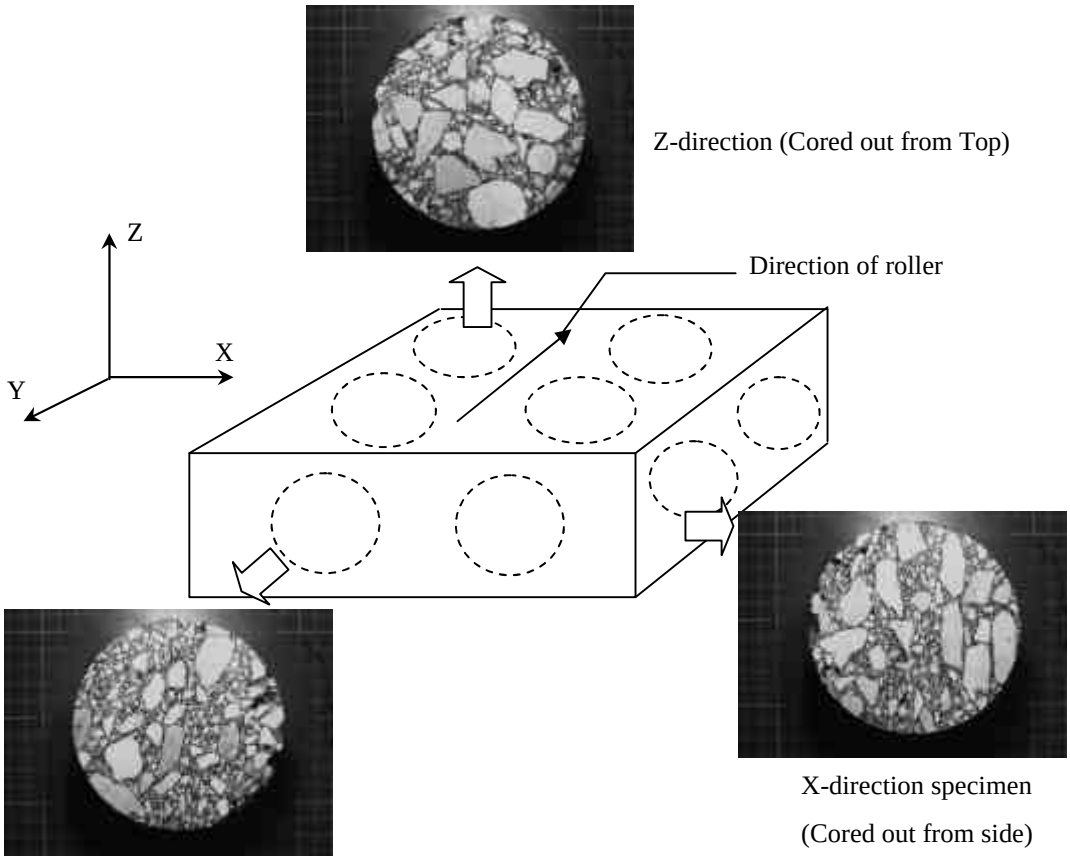

Figure 6.11: Differences of particle distribution in each direction

6.7 CHANGES IN PARTICLE ORIENTATION BY CORING

As described in the previous sections, it was assumed that the particle orientation has been changed from the mould confined 150 mm diameter specimens to the cored 100 mm diameter specimens due to the coring process. To examine the effects, the change in the particle orientation was investigated using both the image analysis software and calculation results. The results are shown in Table 6.29. Also, the pictures of the specimens and aggregates are depicted in Figures 6.12 to 6.13.

Particles *P*1 to *P*5 are located nearby the mould boundary, where cutting will be applied to the 150 mm diameter specimens, while particles *P*6 to *P*10 are placed within the 100 mm diameter. By calculating the particle orientations before and after coring, the changes in aggregate orientation were analysed.

As would be expected, the ε angles for particles *P*1 to *P*5 increase from the mould confined 150 mm diameter specimen to the cored 100 mm diameter specimen, whilst the particles *P*6 to *P*10 indicate almost the same ε angle before and after coring.

Therefore, it is immediately evident that the changes in ε angle occurred due to the coring process; as a result, the slopes of aggregate orientation for the cored 100 mm specimens are considerably greater than those of 150 mm diameter specimens. Also, it can be said that the image analysis methodology used in this study is verified since the particles *P*6 to *P*10 did not show a dramatic change in the ε angle.

Table 6.29: Changes in particle orientation

Aggregate I.D.	Particle (Radial) Orientation ε (°)		
	D = 150 mm	*D* = 100 mm	Location
*P*1	69.5	86.2	Edge
*P*2	3.32	84.5	Edge
*P*3	40.1	53.4	Edge
*P*4	52.6	69.8	Edge
*P*5	26.7	70.4	Edge
*P*6	61.0	60.3	Within *D* = 100 mm
*P*7	61.9	61.2	Within *D* = 100 mm
*P*8	18.0	15.2	Within *D* = 100 mm
*P*9	59.6	58.2	Within *D* = 100 mm
*P*10	80.4	82.1	Within *D* = 100 mm

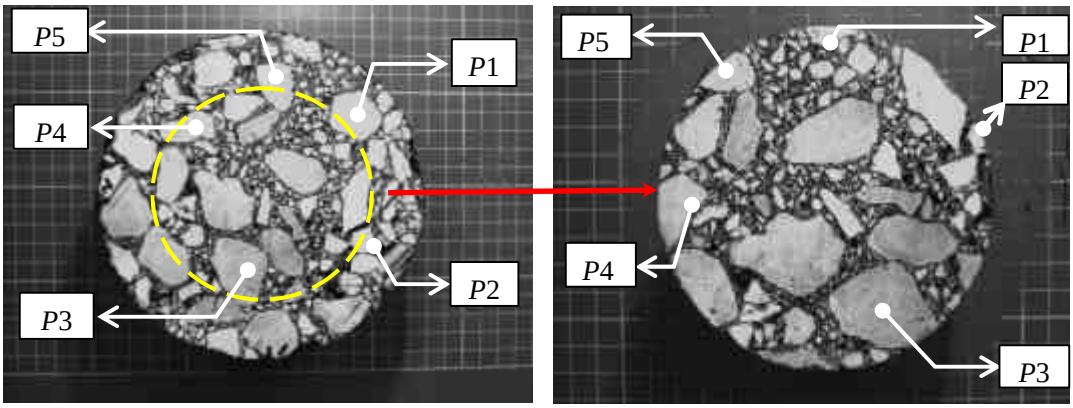

(a)

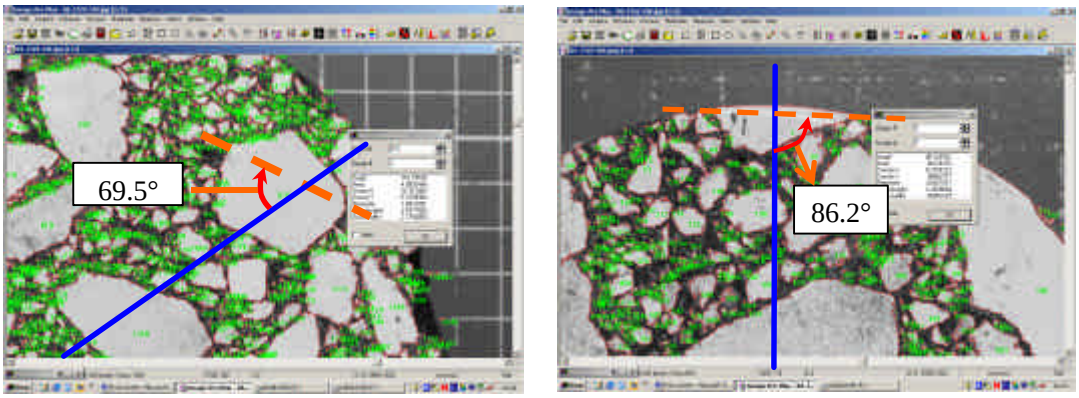

(b)

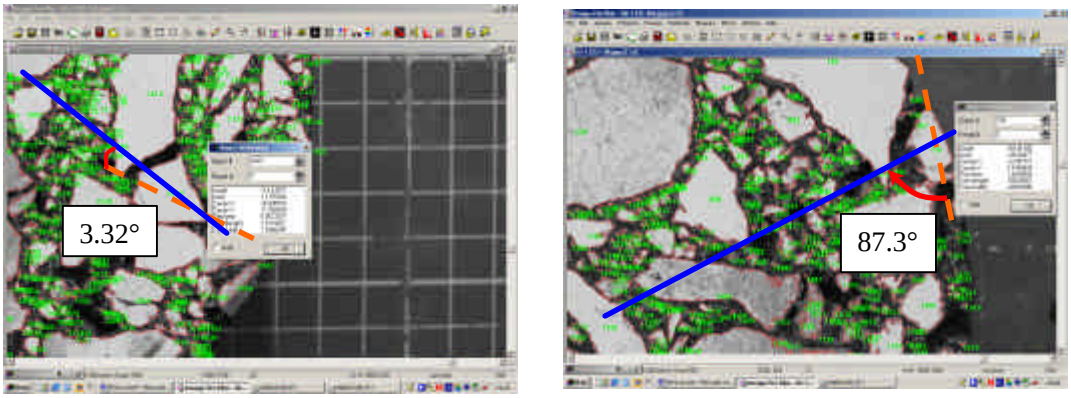

(c)

Figure 6.12: Particle angle change due to coring process left side: before coring, Right side: after coring (a) Original photo with particle location, (b) *P*1, (c) *P*2

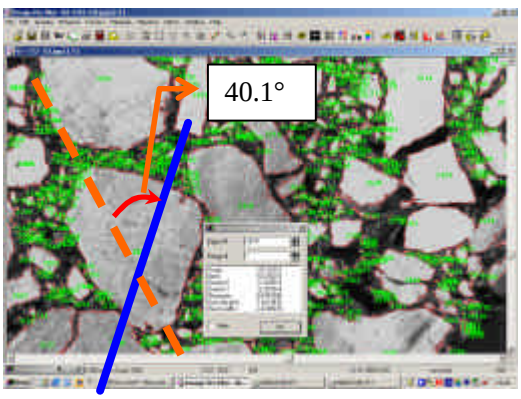

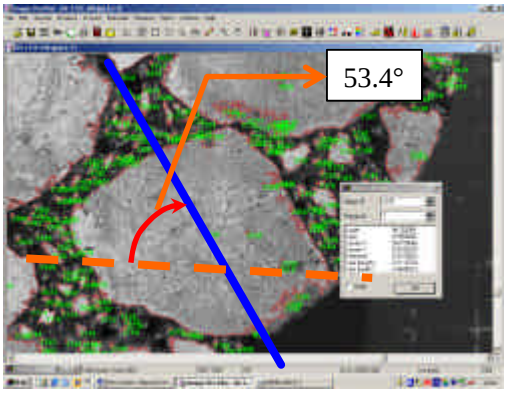

(d)

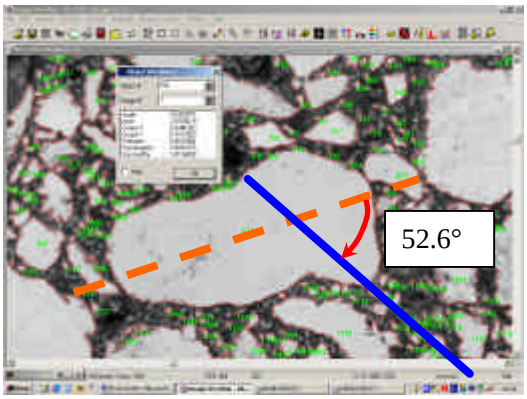

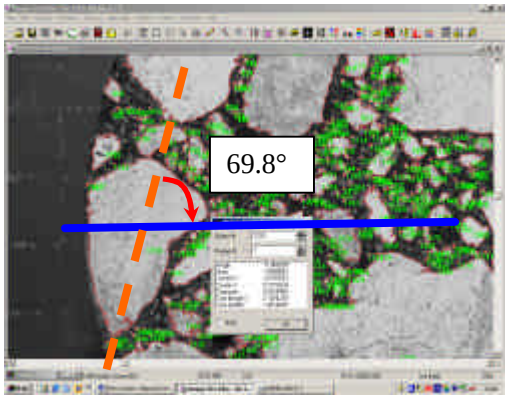

(e)

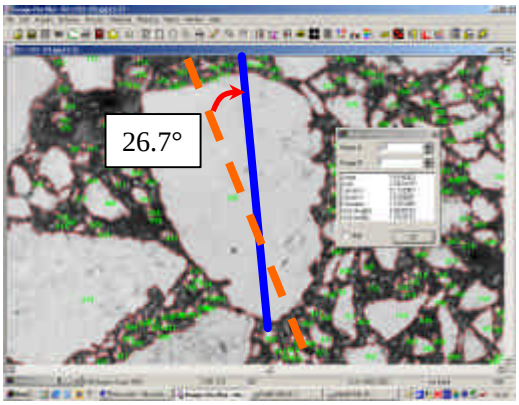

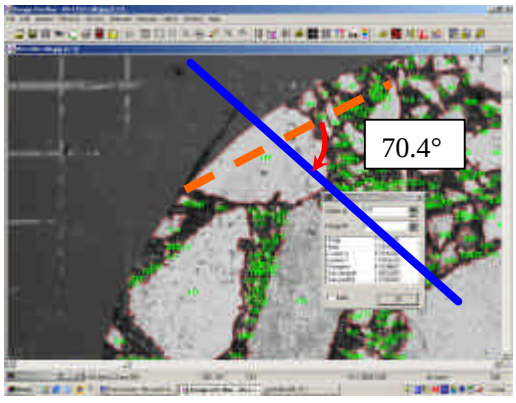

(f)

Figure 6.12: Continued (d) *P*3, (e) *P*4, (f) *P*5

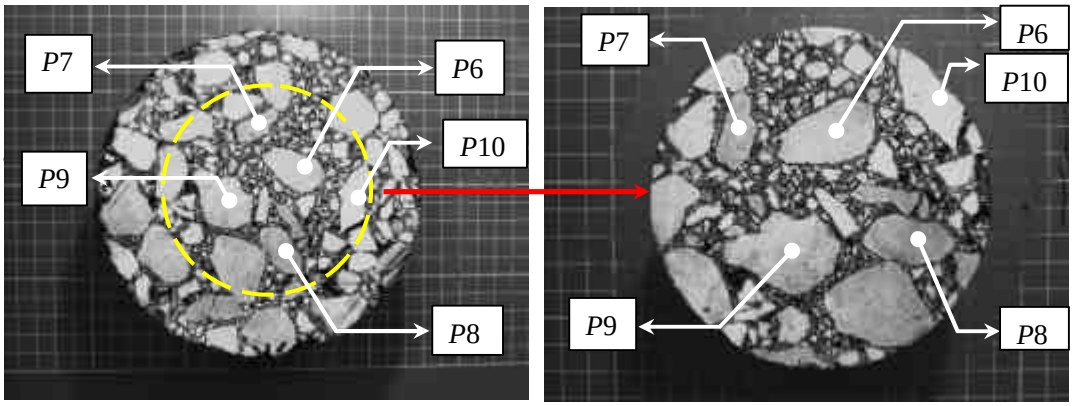

(a)

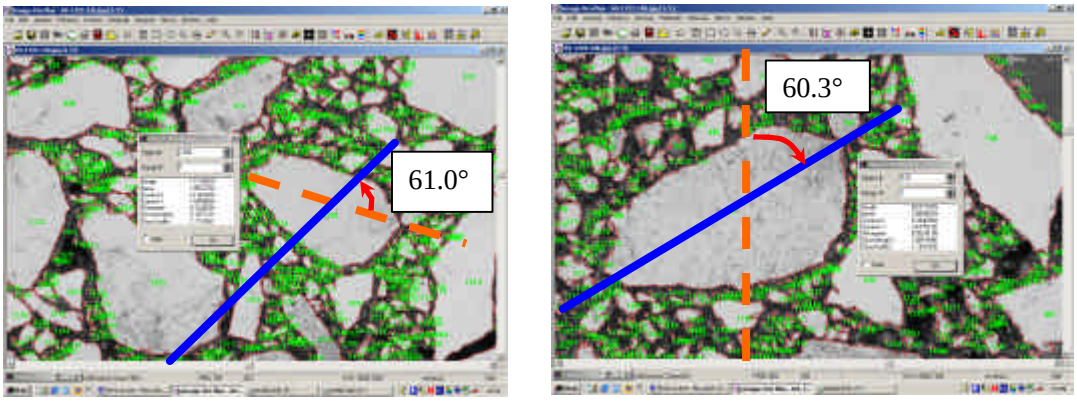

(b)

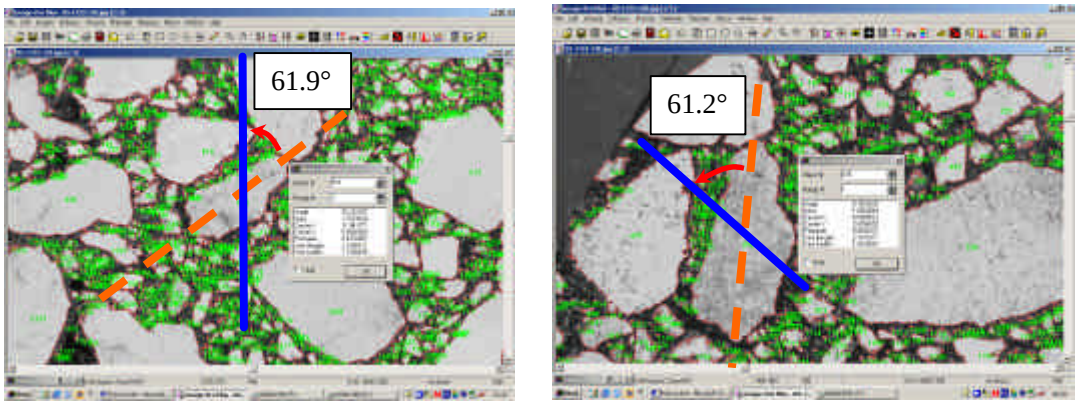

(c)

Figure 6.13: Particle angle within *D*=100 mm left side: before coring, Right side: after coring (a) Original photo with particle location, (b) *P*6, (c) *P*7

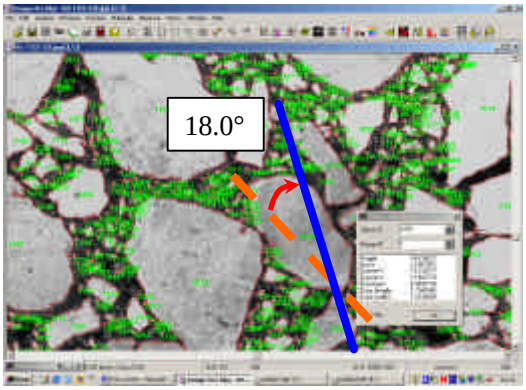

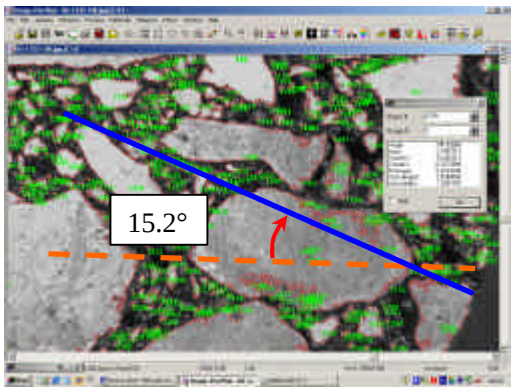

(d)

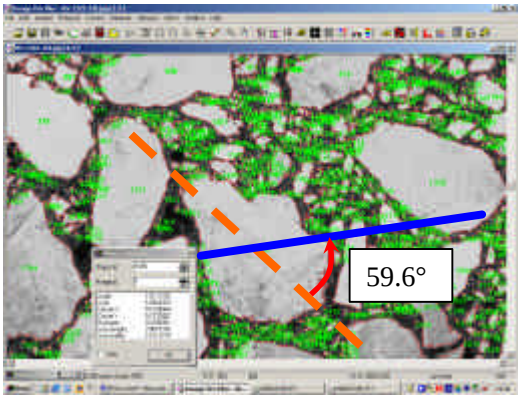

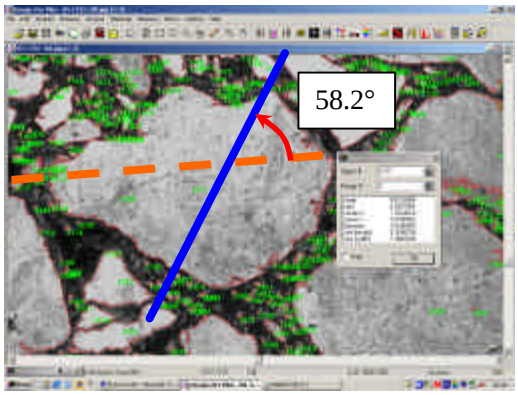

(e)

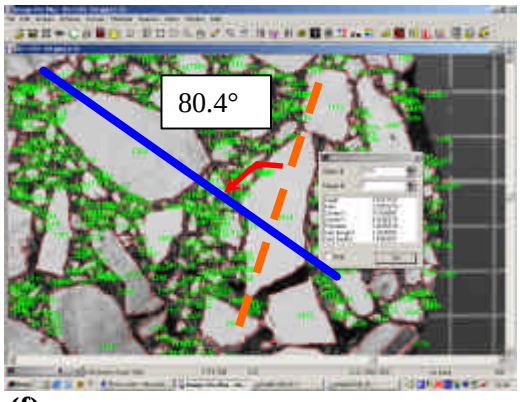

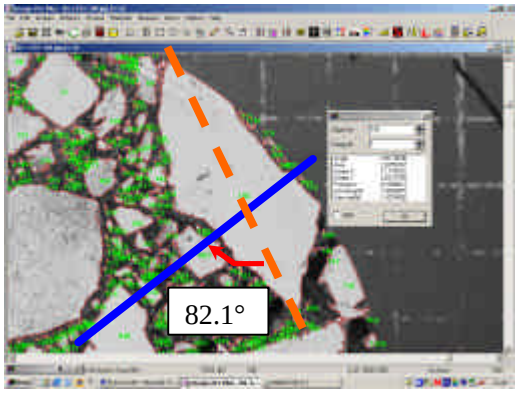

(f)

Figure 6.13: Continued (d) *P*8, (e) *P*9, (f) *P*10

6.8 EFFECT OF LARGE PARTICLES ON THE AGGREGATE ORIENTATION SLOPE

Particle orientations focused on the largest 20 particles were investigated to look at how the larger particles influence the results of average particle orientation for all particles. To examine the effect, protocol #2 was used. The result is presented in Table 6.30.

The result indicates how much the area of the largest 20 particles contribute to the slope of aggregate orientation. Both the gyratory and vibratory compacted specimens have the same trend in the slope of particle orientation. For the 150 mm diameter specimens, the slopes for all particles and for the largest 20 particles are almost identical in both the gyratory and vibratory specimens. Similarly, for the cored 100 mm and computer trimmed 100 mm diameter specimens, almost the same slopes are observed in both the gyratory and vibratory specimens.

As a result, it seems that the slope of aggregate orientation is influenced by larger particles as the slopes for all particles and the largest 20 particles showed a good agreement. In other words, the slopes of particle orientation may be governed by the larger particles, especially the largest 20 particles.

Table 6.30: Particle orientation slope for largest 20 particles

Gyratory (°/cm^2)	150 mm	100 mm	100 mm (C)
All particles	0.94	2.66	-0.26
Largest 20 particles	0.84	2.65	-0.04

Vibratory (°/cm^2)	150 mm	100 mm	100 mm (C)
All particles	1.70	2.33	-0.30
Largest 20 particles	1.65	2.32	-0.30

* (C) stands for Computer trimmed 100 mm diameter specimen.

6.9 PARTICLE ORIENTATION AND MECHANICAL PROPERTIES

The particle orientations in each compaction combination were examined in the previous sections. Based on the results, the relation between particle orientation and mechanical properties is discussed in this section.

From the results obtained from mould based compaction such as gyratory and vibratory, it was found that the mould based compaction methods tend to produce the specimens with circumferential orientation due to the effect of mould confinement. In addition, the image analysis results revealed that the particle orientation of the inner part in the 150 mm diameter specimens have random particle orientation. Based on the finding from Hunter et al. (2004), it seems that the specimens with the random particle orientation tend to be less stiff than the specimens with circumferential orientation. In other words, mould based compaction may produce artificially stiffer specimens. This is discussed further in Chapter 7.

In terms of the slab specimens, no clear trend in particle orientation related to the mechanical properties was shown. However, looking at the results obtained from Section 6.6 (see Tables 6.26 to 6.28), 2:1 elongation showed considerable variation in the three orthogonal directions. Vavarik et al. (1999) recommended a lower percentage of elongated particles as the particles may influence the mechanical performance of asphalt mixtures. Therefore, the variation may be related to the stiffness and permanent deformation results of the slab specimens.

6.10 CONCLUSIONS

The results presented in this Chapter have provided detailed evidence of the aggregate orientation for the three compaction methods. The trends of aggregate orientation slope looking at both the compaction combinations and specimen size are summarized below.

In terms of the 150 mm diameter specimens, the particle orientation for the vibratory compacted specimens has a greater slope than that of the gyratory compacted specimens. This trend is seen in the four protocols. In addition, the slope of elongated particles tends to show a greater slope than that of all particles.

For the 100 mm diameter specimens, particle orientation for both the gyratory and vibratory compacted specimens shows higher orientation slope than that of the 150 mm diameter specimens.

In contrast, for the computer trimmed 100 mm diameter specimens, the particle orientation for both the gyratory and vibratory compacted specimen is a random since the slope for all particles showed approximately 0 (°/cm^2).

With regard to the slab specimens, the 100 mm diameter cores from the slabs are very different in terms of aggregate orientation compared to the 150 mm diameter cores from slab. Also, despite the fact that both methods have involved coring, a greater slope in the aggregate orientation was seen for the 100 mm cores. As shown in the 100 mm diameter gyratory and vibratory cores, the increased circumferential orientation of 100 mm diameter cores may simply be due to the smaller cross-sectional area of the 100 mm diameter cores, compared to the 150 mm diameter cores.

Looking at the largest 20 particles of mould based specimens (i.e. gyratory and vibratory compacted specimens), it was found that the slopes obtained from only the largest 20 particles are almost identical to the slopes obtained from all particles (i.e. approx. 2000 particles).

In terms of an increase in particle orientation slope from 150 mm to 100 mm diameter specimens, it was found that this was caused by the coring process of specimens as the edge five particles indicated the changes in particle orientation, whilst the inner five particles showed almost the same orientation within the radius of 50 mm in the 150 mm diameter specimens, when the 100 mm diameter specimens were cored out from the 150 mm diameter specimens.

CHAPTER 7

Aggregate Distribution and Segregation

7.1 INTRODUCTION

Aggregate distribution is one of the main factors governing the mechanical properties of asphalt mixture since the asphalt mixture consists of three components: air, binder and aggregate. In particular, the volume of aggregate is much larger than the other two the components. In addition, it is generally said that the mechanical properties of asphalt mixture depends on the aggregate distribution as well as bitumen properties. Therefore, it is crucial to understand how aggregate particles are distributed in the mixture.

The aim of this chapter is to examine the aggregate distribution in the mixture and to discuss the relationship between particle distribution and the mechanical properties of asphalt mixtures. This chapter is mainly divided into two parts. In the first part, the number of aggregate particles is counted and compared in each compaction combination. In the second part, the differences in aggregate segregation looking at the three compaction methods are discussed.

7.2 NUMBER OF PARTICLES AND AREA AT S2 AND S3 SURFACES

In order to evaluate the differences in compaction methods, aggregate distribution is divided into two factors: the number of particles and particle area. These were taken through the data acquisition of the image, when the specimens were photographed for the image analysis. By utilizing the data, the number of particles and its area were examined in each compaction method. Moreover, the differences in particle distribution were investigated in each VSA range. The aim of this section is to understand the differences in laboratory compaction methods by looking at the number of particles and the area.

7.2.1 Number of Particles and Area

To investigate the state of particle distribution, the number of particles and its area were examined using the data from the image analysis. The results for gyratory and vibratory compacted specimens are shown in Tables 7.1 to 7.2.

In terms of the number of particles (see Table 7.1), the gyratory compacted specimens indicate more particles than the vibratory compacted specimens. Also, looking at S2 and S3 surfaces, the S3 surface has relatively more particles than S2 surface on both the gyratory and vibratory compacted specimens. The results may indicate that there are more particles at S3 than at S2, due to the compaction process and gravity as suggested in Chapter 3.

However, these differences decreased steadily from the 150 mm specimens to the computer trimmed 100 mm specimens. In addition, the ratio between S2 and S3

surfaces indicated a steady increase from the 150 mm to 100 mm diameter specimens. Consequently, the S2/S3 ratio showed approximately 1.00 for the computer trimmed 100 mm diameter specimens in both the gyratory and vibratory compaction. Therefore, it seems that the number of particles between S2 and S3 surfaces is almost identical at the inner region of specimens.

With respect to the particle area (see Table 7.2), the results indicate that both the S2 and S3 surfaces have almost the same area in the gyratory and vibratory specimens. Moreover, the average area at the S2 and S3 surfaces shows a similar number in both the gyratory and vibratory compacted specimens. Therefore, no clear differences in particle area are shown between the gyratory and vibratory compactions.

Overall, comparing each compaction method, the gyratory compacted specimens may include more particles than the vibratory compacted specimens, despite the fact that the area of both specimens was almost identical. This result might explain the assumption that the vibratory compacted specimens contain larger particles than the gyratory specimens as stated in Chapter 3. However, the reason for this has not been understood clearly from 2-D analysis. Further research would be necessary for this result.

Table 7.1: Number of particles for gyratory and vibratory specimens

Surface	Number of particles					
	Gyratory			Vibratory		
	150 mm	100 mm	C.100 mm	150 mm	100 mm	C.100 mm
Top	2108	1649	874	1685	1399	786
Bottom	2305	1694	864	1918	1394	744
Ratio T/B	0.91	0.97	1.01	0.88	1.00	1.06
Average T&B	2207	1672	869	1801	1396	765

Table 7.2: Particle area for gyratory and vibratory specimens

Surface	Particle area (cm^2)					
	Gyratory			Vibratory		
	150 mm	100 mm	C.100 mm	150 mm	100 mm	C.100 mm
Top	103	43	47	103	43	42
Bottom	99	40	44	100	40	43
Ratio T/B	1.04	1.08	1.06	1.03	1.07	0.98
Average T&B	101	41	45	101	41	43

* C stands for Computer trimmed 100 mm specimen.

7.2.2 Particle Distribution in VSA range

0.08 cm^2- 11 cm^2 in VSA

In order to evaluate the particle distribution more correctly, the number of particles between the gyratory and vibratory compacted specimens for different visible particle cross sectional area (VSA) bands (ranges) was examined. In particular, larger particles, which are greater than 0.08 cm^2 in VSA, were examined to look at the differences in compaction characteristics. The results are presented in Figures 7.1 to 7.9. In general, the number of particles for the gyratory compacted specimens tends to show more particles at smaller ranges, while the number of particles for the vibratory compacted specimens is likely to indicate many particles

at larger ranges in VSA.

For the 150 mm diameter specimens, the number of particles for the gyratory and vibratory compacted specimens shows almost the same value from 0.08 cm^2 to 5.0 cm^2 in VSA, although theses numbers decreased as VSA ranges increased (see Figure 7.1). The same trend was confirmed from 5.0 cm^2 to 11.0 cm^2 in VSA ranges. However, it seems that the vibratory compacted specimens have larger aggregate particles than the gyratory compacted specimens at the S2 and S3 surfaces.

This trend is more pronounced in the 100 mm diameter specimens. As shown in Figure 7.2, the number of particles for the vibratory compacted specimens shows more particles than that of the gyratory compacted specimens in VSA ranges. In particular, the vibratory compacted specimens tend to show more particles than the gyratory compacted specimens at VSA ranges from 5.0 cm^2 to 11.0 cm^2. A similar trend is also observed in the computer trimmed specimens as shown in Figure 7.3. In addition, the particle distributions for both the gyratory and vibratory specimens were analysed looking at both the S2 (Top) and S3 (Bottom) surfaces. The results are presented in Figures 7.4 to 7.9.

Considering these data, the observed information may have a significant influence on the mechanical properties of the compacted specimens. Based on the above data, it is assumed that the vibratory compaction manufactures stiffer specimens than the gyratory compaction due to the larger aggregates inside the specimen as stated in Chapter 3 and Section 7.2.1. This is discussed further in the following sections.

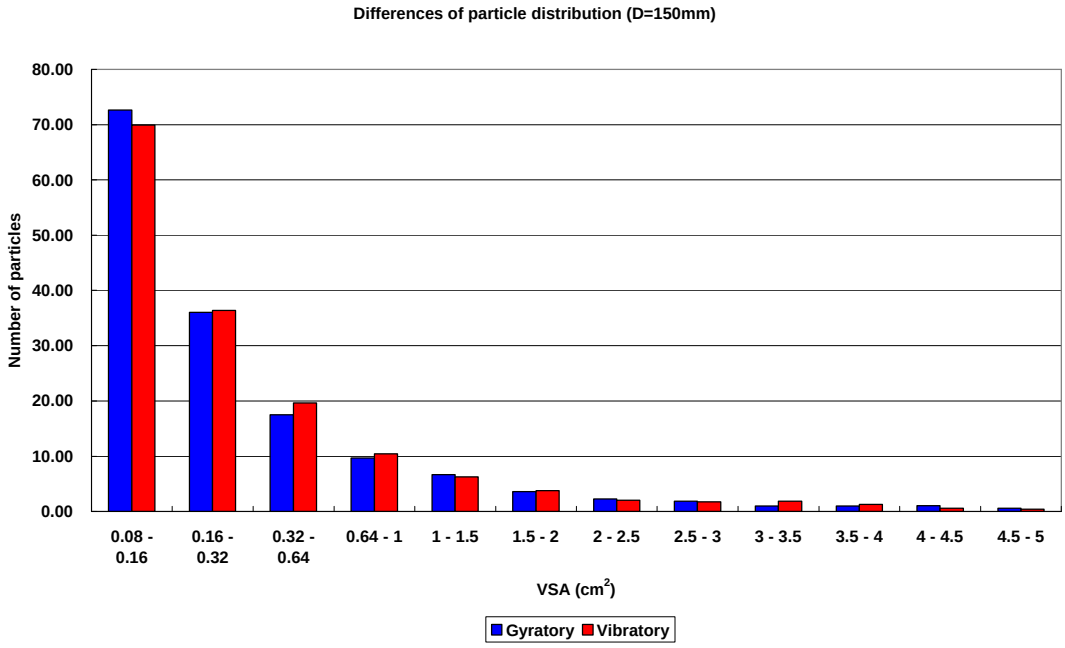

(a)

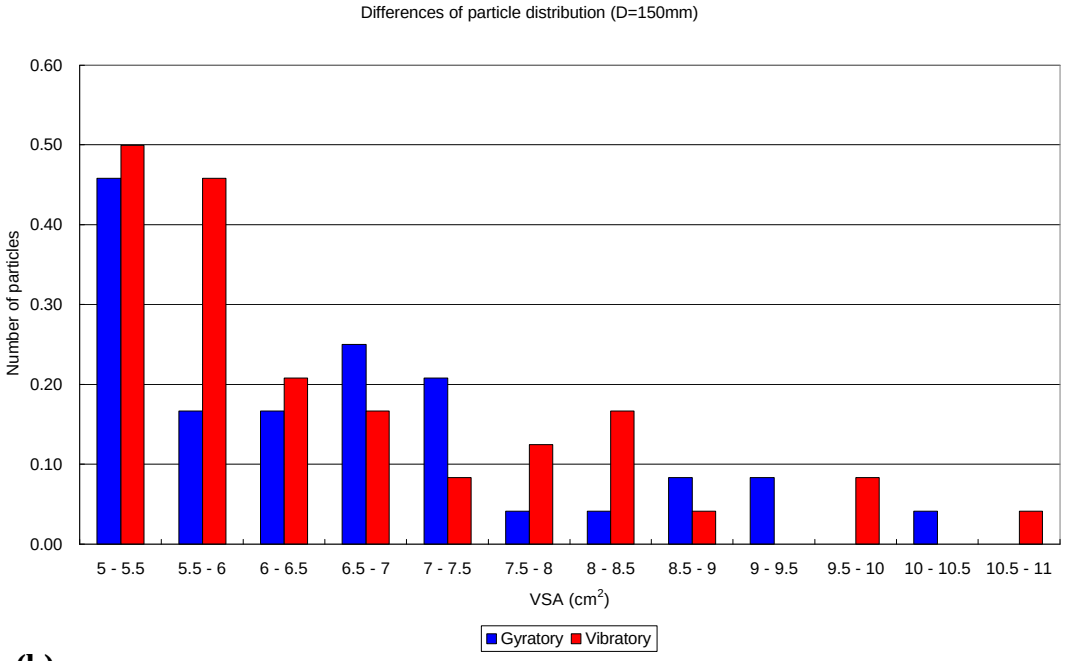

(b)

Figure7.1: Differences of particle distribution Gyratory vs Vibratory *D* = 150 mm specimens (a) 0.08-5.0 cm^2 in VSA (b) 5.0-11 cm^2 in VSA

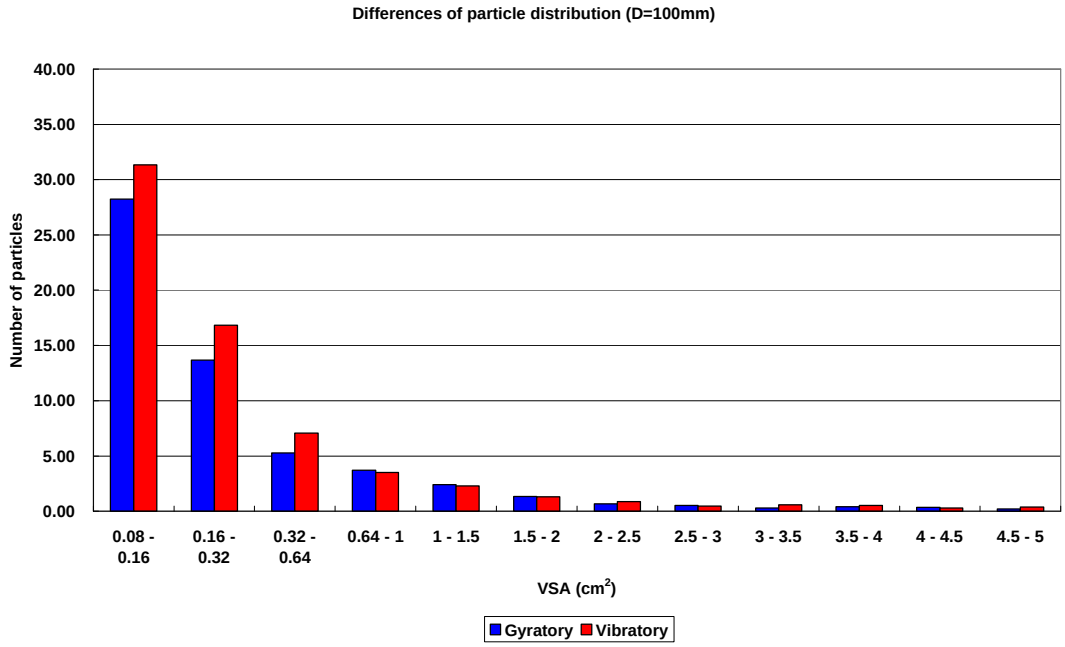

(a)

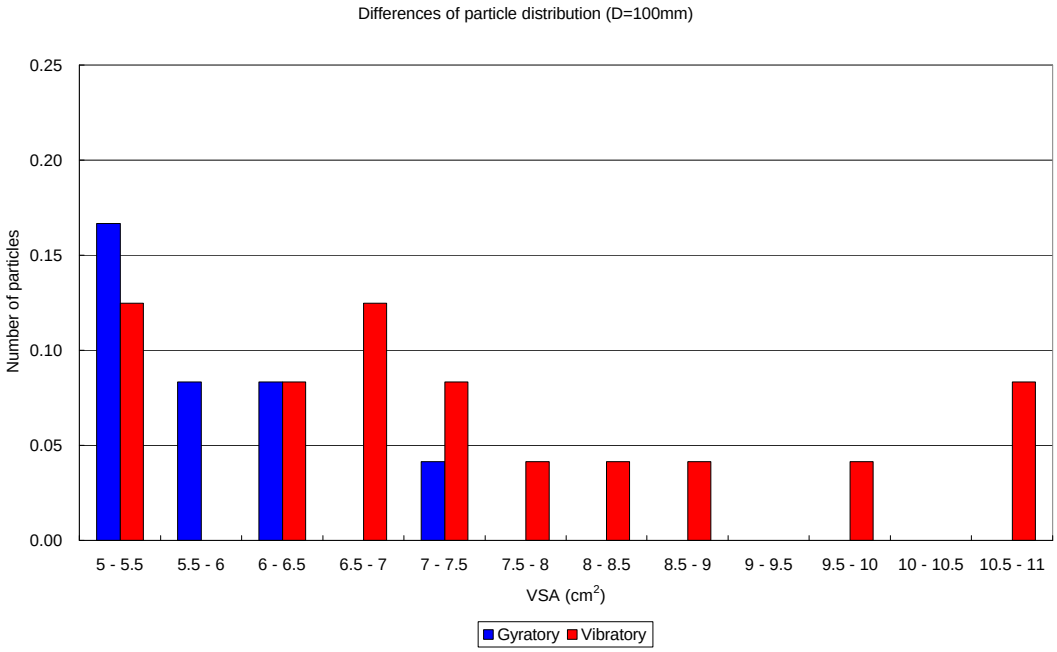

(b)

Figure7.2: Differences of particle distribution Gyratory vs Vibratory *D* = 100 mm specimens (a) 0.08-5.0 cm^2 in VSA (b) 5.0-11 cm^2 in VSA

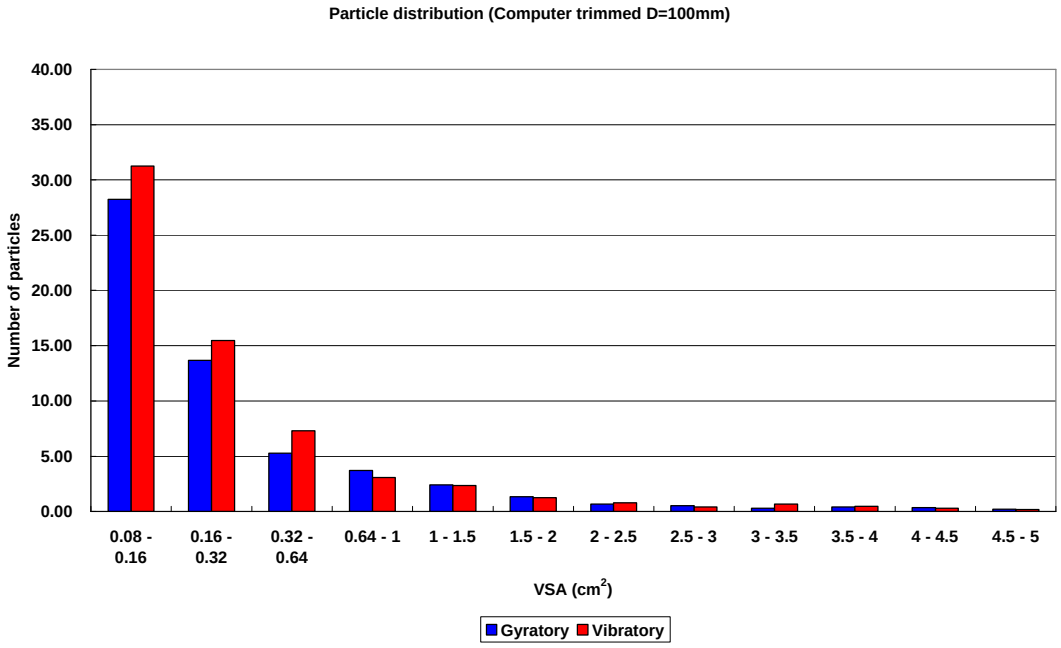

(a)

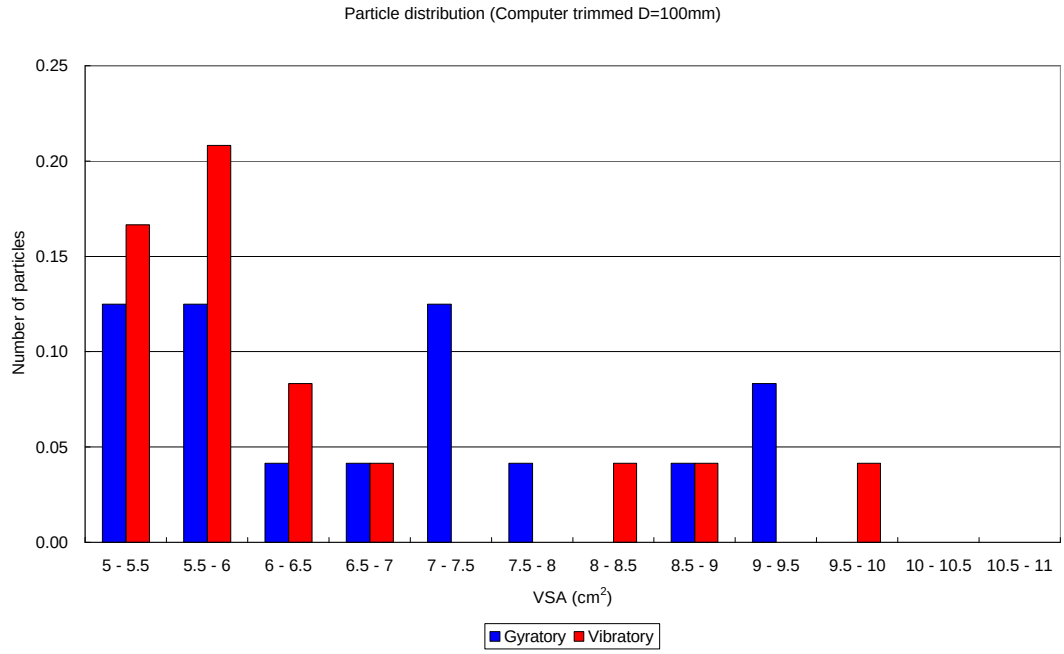

(b)

Figure7.3: Differences of particle distribution Gyratory vs Vibratory Computer trimmed *D* = 100 mm specimens (a) 0.08-5.0 cm^2 in VSA (b) 5.0-11 cm^2 in VSA

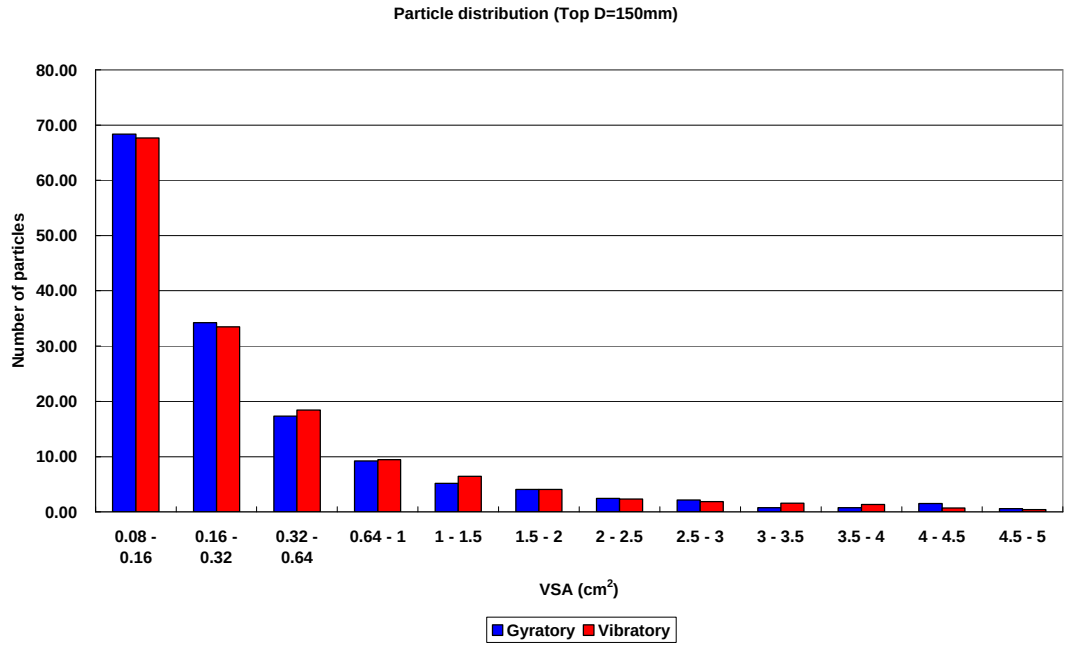

(a)

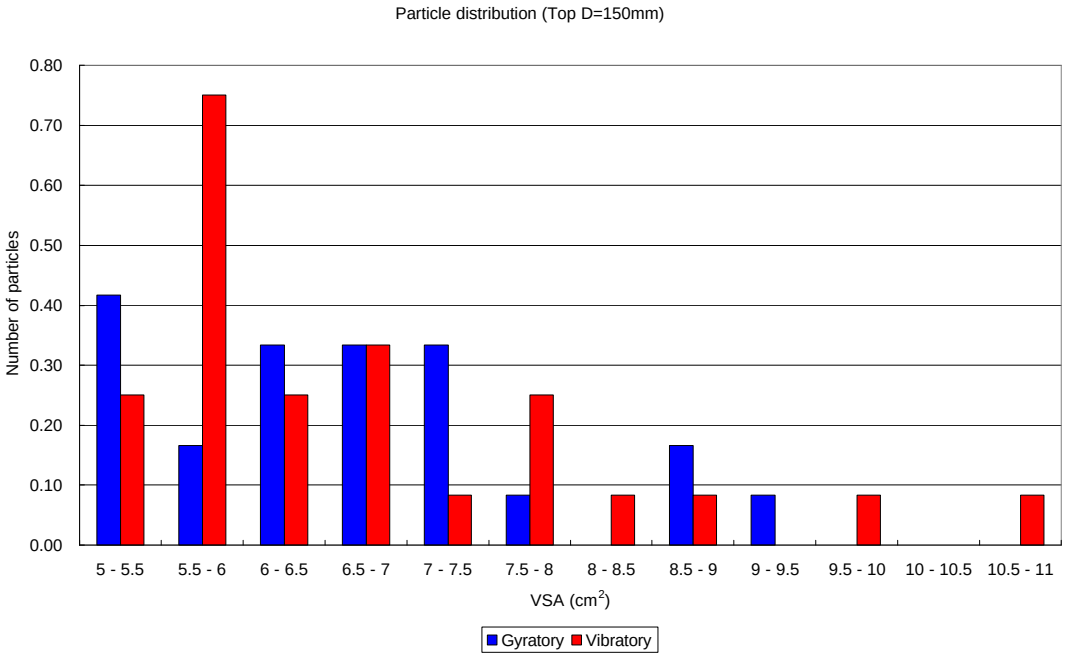

(b)

Figure7.4: Differences of particle distribution, Gyratory vs Vibratory S2 (Top) surface *D* = 150 mm specimens (a) 0.08-5.0 cm^2 in VSA (b) 5.0-11 cm^2 in VSA

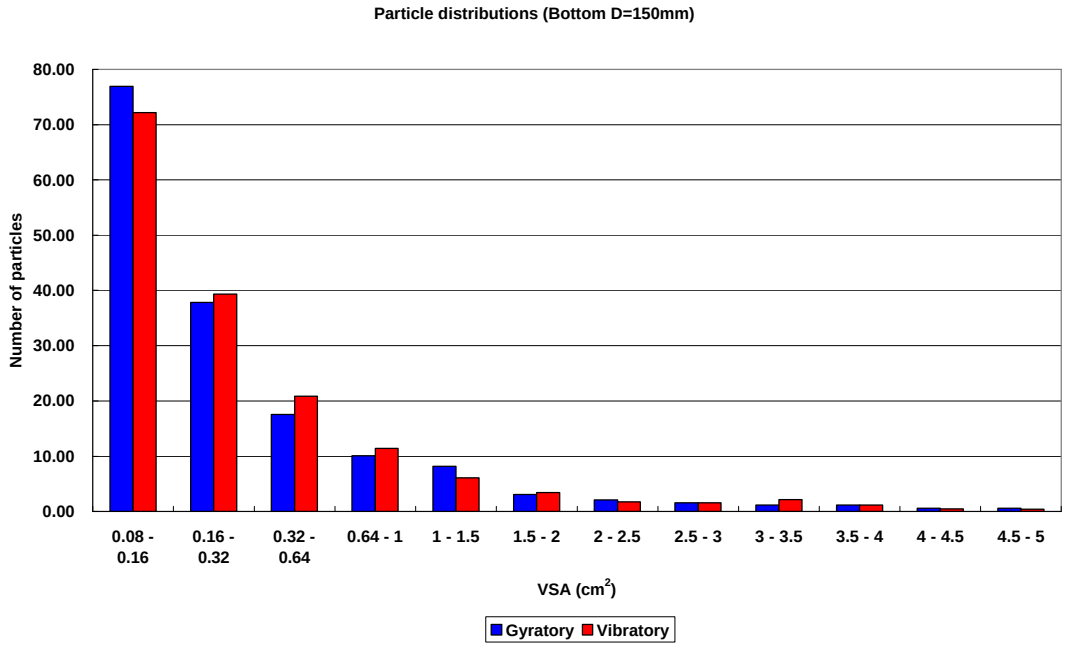

(a)

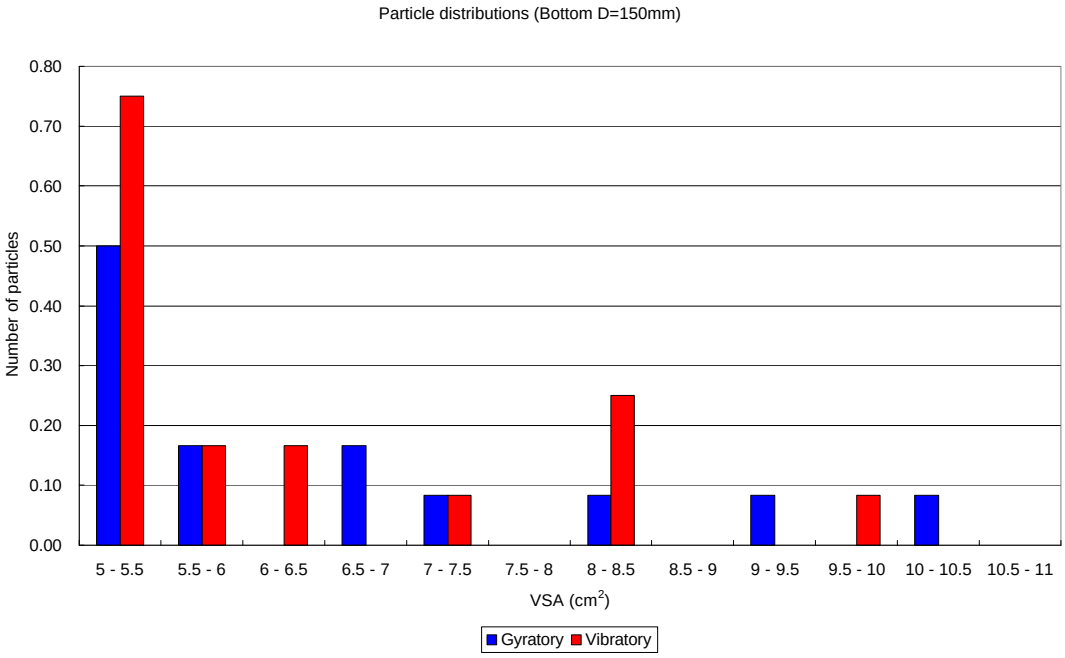

(b)

Figure7.5: Differences of particle distribution, Gyratory vs Vibratory S3 (Bottom) surface *D* = 150 mm specimens (a) 0.08-5.0 cm^2 in VSA (b) 5.0-11 cm^2 in VSA

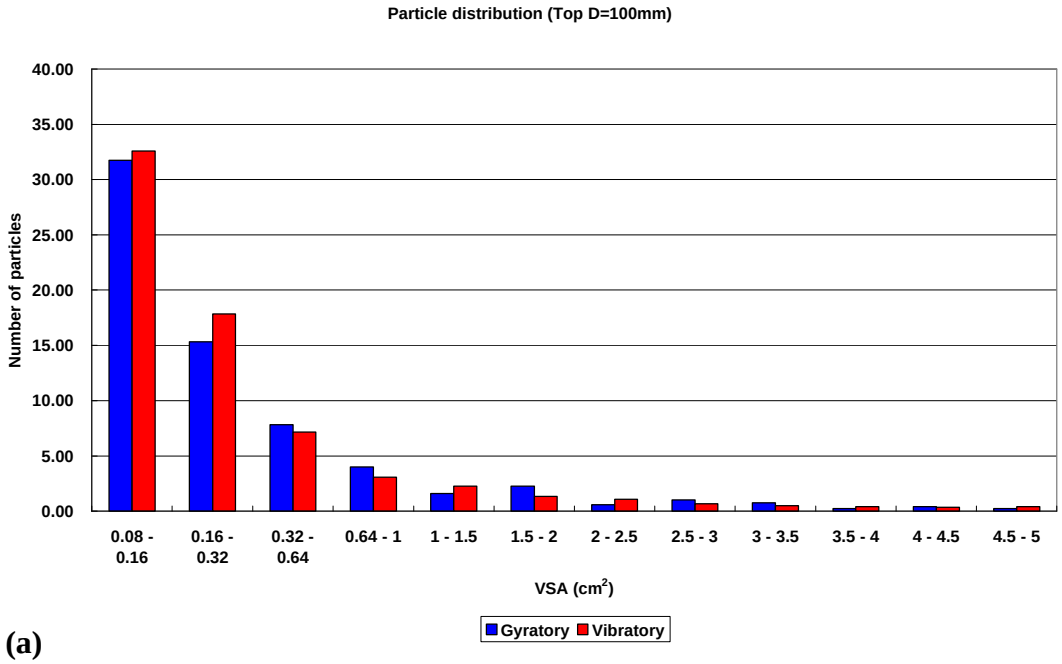

(a)

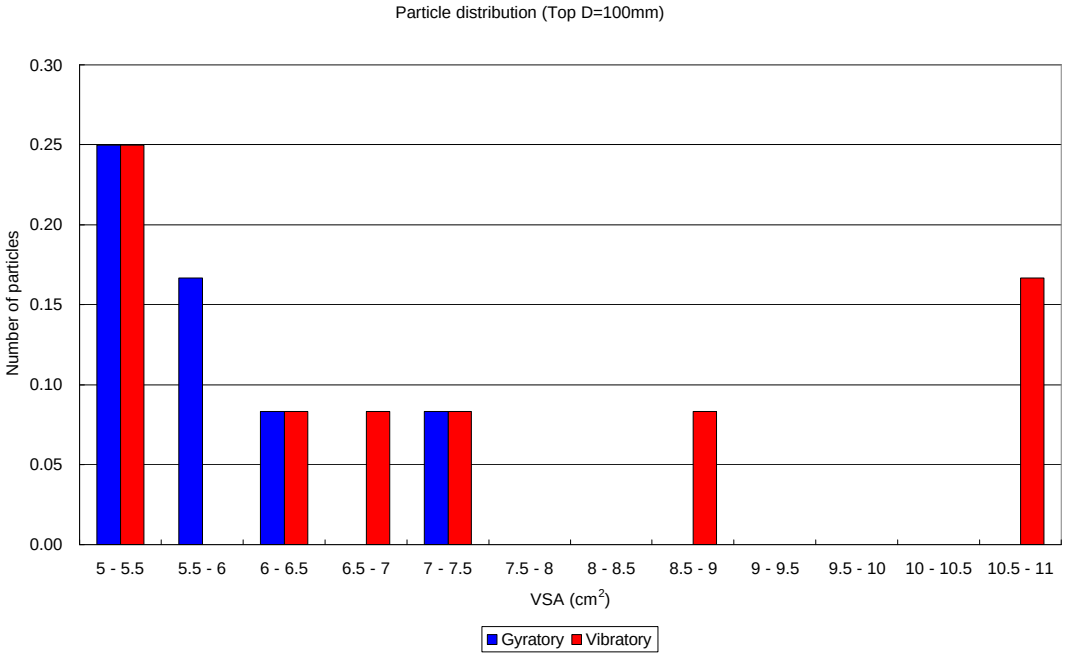

(b)

Figure7.6: Differences of particle distribution, Gyratory vs Vibratory S2 (Top) surface *D* = 100 mm specimens (a) 0.08-5.0 cm^2 in VSA (b) 5.0-11 cm^2 in VSA

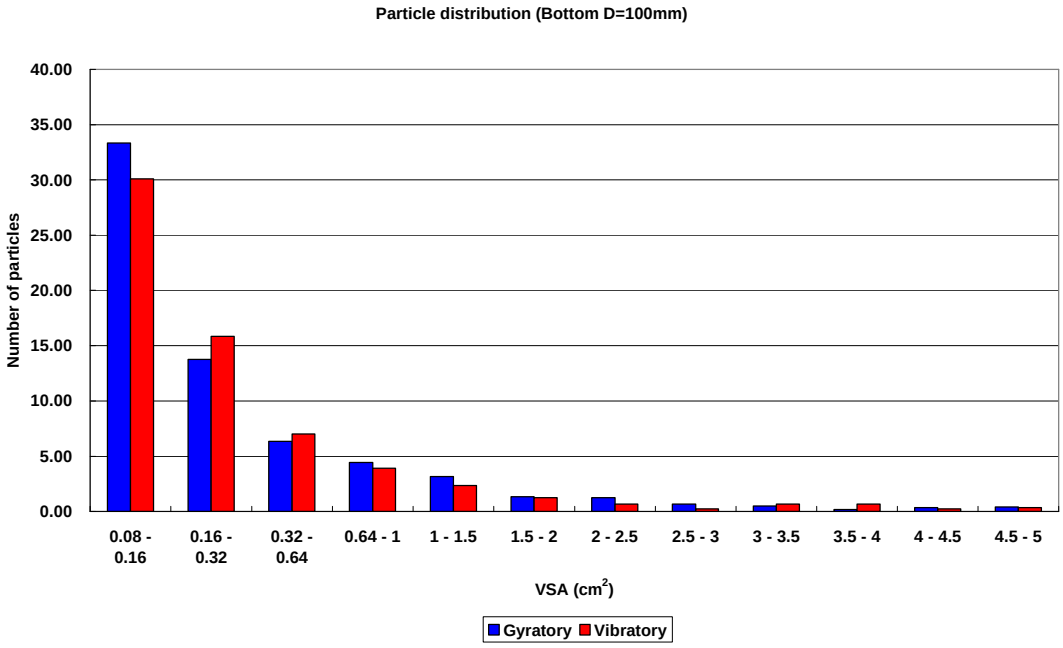

(a)

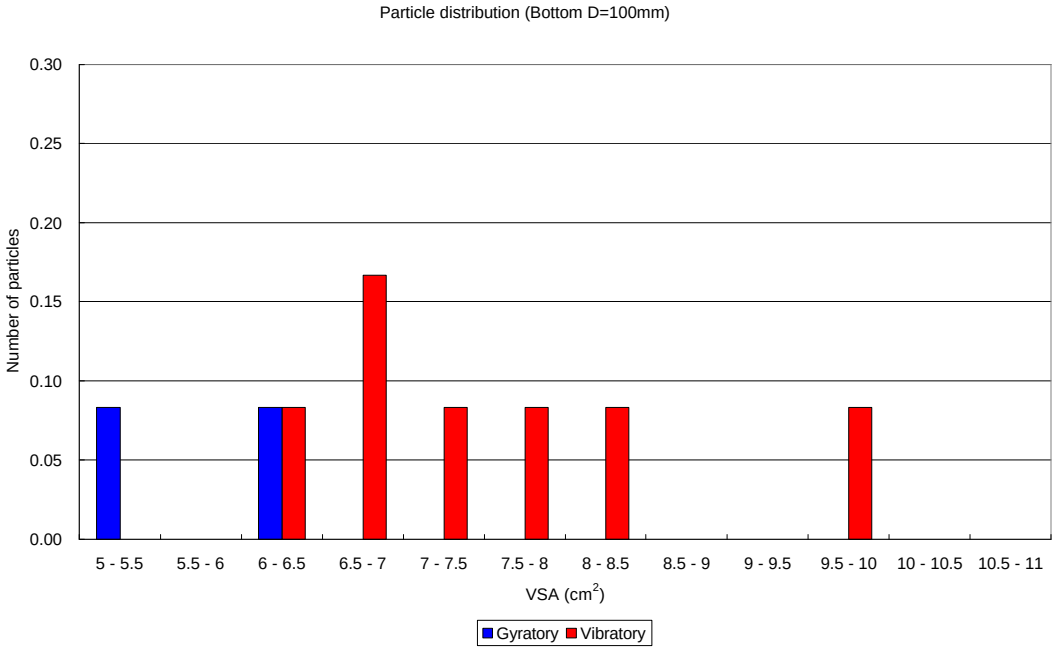

(b)

Figure7.7: Differences of particle distribution, Gyratory vs Vibratory S3 (Bottom) surface *D* = 100 mm specimens (a) 0.08-5.0 cm^2 in VSA (b) 5.0-11 cm^2 in VSA

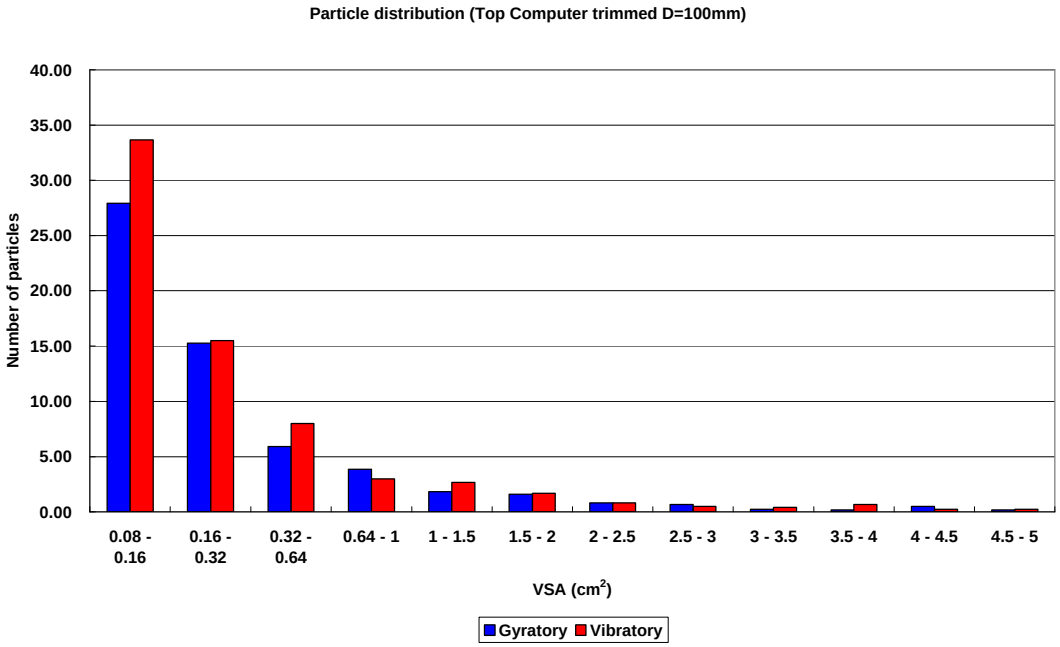

(a)

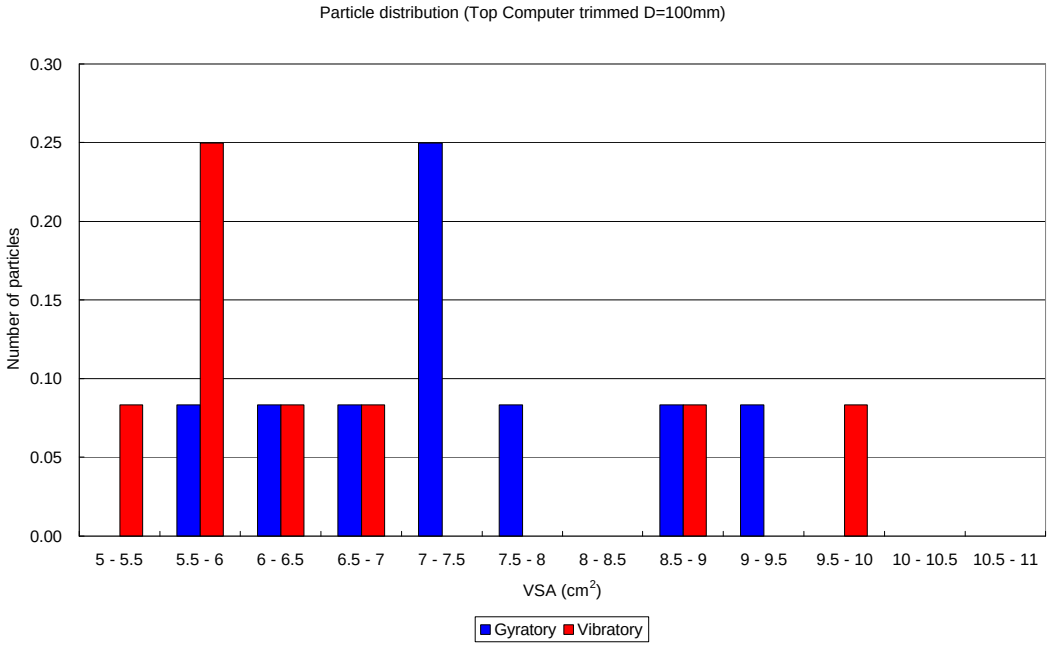

(b)

Figure7.8: Differences of particle distribution, Gyratory vs Vibratory S2 (Top) surface computer trimmed *D* = 100 mm specimens (a) 0.08-5.0 cm^2 in VSA (b) 5.0-11 cm^2 in VSA

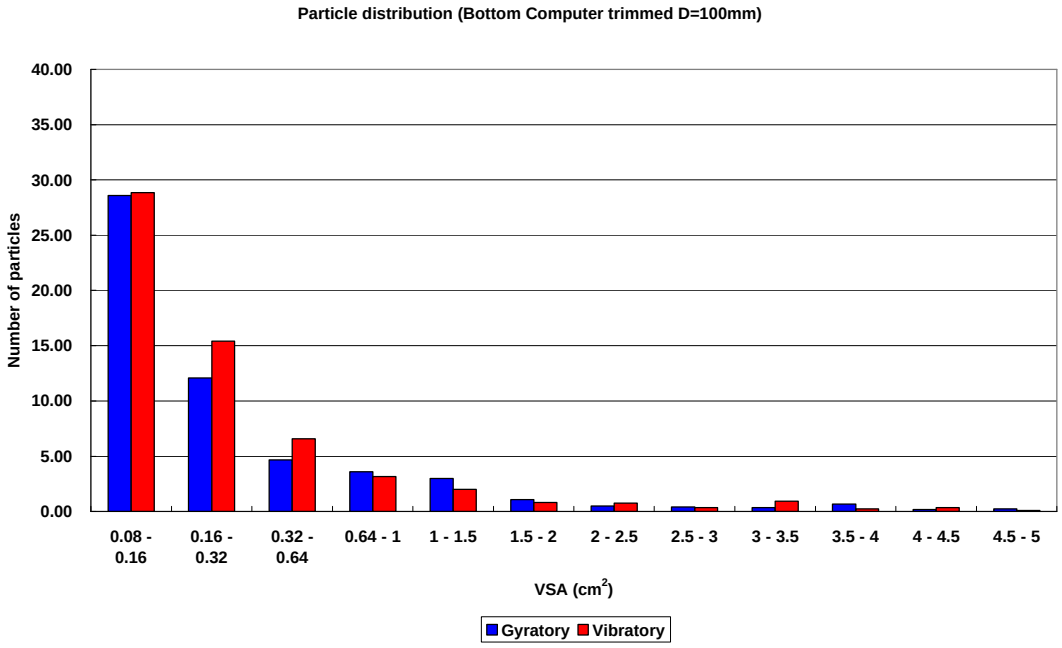

(a)

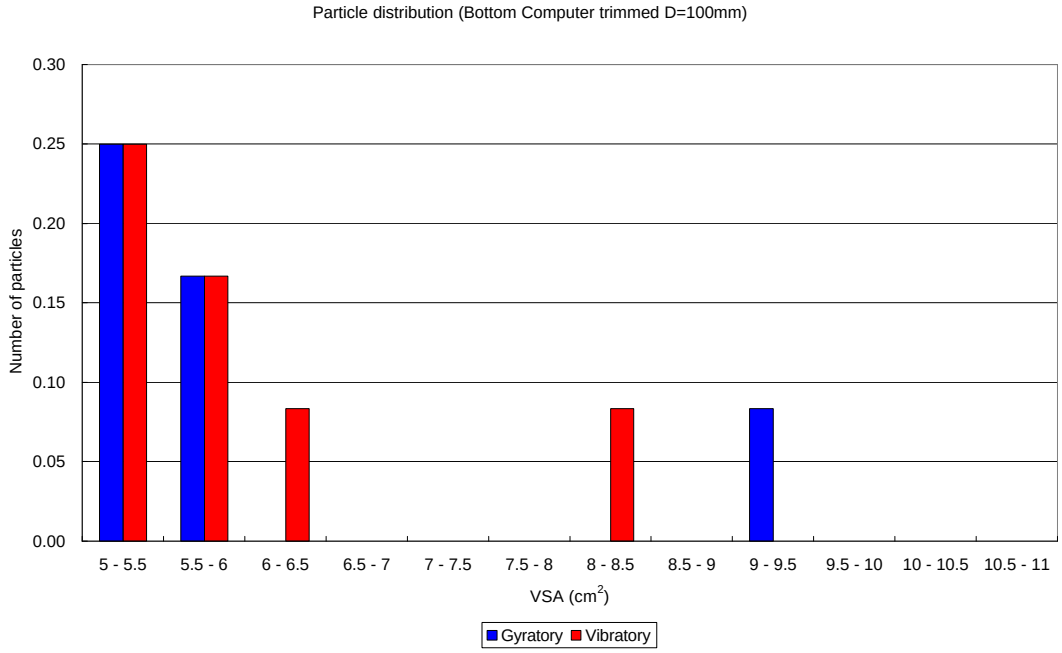

(b)

Figure7.9: Differences of particle distribution, gyratory vs vibratory S3 (Bottom) surface computer trimmed *D* = 100 mm specimens (a) 0.08-5.0 cm^2 in VSA (b) 5.0-11 cm^2 in VSA

7.3 PERCENTAGE OF AGGREGATES

Image analysis software identifies some useful information such as aggregate particle area and size. Utilizing the data, the area of bitumen mastic and the particle size are also determined, based on the components of the asphalt mixture. This section analyzes the three components of a specimen: area, discrete particles and bitumen mastic.

7.3.1 Percentage of Particles and Mastic

Gyratory and Vibratory specimens

The percentage for particle areas of specimens was calculated from the data taken through the image analysis. The results are shown in Tables 7.3 to 7.4.

The results indicate that the 100 mm diameter specimens have less particle area percentage than the 150 mm diameter specimens. This trend was also observed in the previous section. However, it should be noted that the percentage area of particles to total area is not the same between the 150 mm and 100 mm diameter specimens, although the same particle distribution was expected. If the distribution is uniform across the horizontal section, the same percentage area of particles should be observed in both the 150 mm and 100 mm diameter specimens.

This fact may strongly support the assumption that the larger particles migrate towards the outer edge of the specimens during compaction. The inner section of 150mm specimens (i.e. 100 mm diameter cores), therefore, contains less aggregate

particles relative to mastic and air than the outer section. Moreover, it is also interesting to note that the rate of mastic for the cored 100 mm diameter specimens is more than that of the 150 mm diameter specimens. This trend is observed in both the gyratory and vibratory compacted specimens. Therefore, it is assumed that there is a greater amount of bitumen in the central region of specimens, while larger aggregates move towards the mould boundary during the compaction process. This may result in the manufacture of weaker 100 mm diameter specimens, when it is cored from the 150 mm diameter specimen. In other words, for the 150 mm diameter specimen, lesser aggregate matrix in the centre may produce the 100 mm core with lower stiffness since the cored specimen is dominated by bitumen mastic rather than aggregates. This is discussed further in Section 7.7.

Slab specimens

In terms of slab specimens, the results show a difference in particle area among Z, Y and X directions. In addition, the specimens indicate relatively smaller particle area compared to the 100 mm diameter gyratory and vibratory specimens. The reason for showing the different particle area is not clearly understood. However, these differences may explain the mechanical properties of slab compacted specimens.

7.3.2 Discrete Particles, Mastic and Size of Particle as a Part of Mastic

In the previous section, the area of discrete aggregate was identified in each specimen. The information enables to calculate the particle size in the bitumen mastic from the components of the asphalt mixture (see Figure 7.10). The formula

which calculates the size of bitumen mastic, and the procedure are as follows:

$$V_b = \frac{\left(\frac{M_B}{G_b}\right) \times (100 - V_V)}{\left(\frac{M_B}{G_b}\right) + \left(\frac{M_A}{G_a}\right)} \tag{7.1}$$

where V_b is volume of bitumen (%), V_v is volume of air void (%), M_b is mass of bitumen (%), G_b is specific gravity of bitumen, M_a is mass of aggregate (%) and G_a is specific gravity of aggregate.

Firstly, the percentage of aggregate particles which occupies the total cross sectional area of 176 cm^2, is determined from the data of image analysis. Secondly, the volume of bitumen is calculated from the components of the asphalt mixture. In this case, the mass of bitumen is 4.0%, the specific gravity of bitumen is assumed as 1.02, and the specific gravity of aggregate is 2.66. The volume of bitumen V_b (%) and the volume of aggregate V_a (%) for the mixture are calculated using air void contents of specimens.

Utilizing the percentage area of the aggregate (discrete aggregate) and assuming the same volume for percent of air, the effective area (volume) (%) of mastic for each compaction combination was determined. After determining the percentage of bitumen mastic, the size of particles, which form the bitumen mastic, was derived from the grading curve of the aggregate as shown in Figure 7.13. The results of the calculation for different compaction combinations are also shown in Tables 7.3 and 7.4. Also, the results are presented in Figures 7.11 to 7.14.

The results show that both the gyratory and vibratory specimens have the same particle size within the bitumen mastic. However, comparing the 150 mm diameter specimens with the 100 mm diameter specimens for the gyratory and vibratory specimens, the size of particles shows slight differences, despite the fact that the specimens consist of the same components.

For the 150 mm diameter specimens, the particle size is approximately 2.2 mm, whilst the value for the 100 mm diameter specimens is approximately 2.8 mm. The reason why this phenomenon occurs is not understood. However, it seems that these differences are caused by the height set for the digital camera, when the specimens were photographed for the image analysis.

In addition, the particle size for the slab specimens is slightly lower than for the gyratory and vibratory specimens, despite the fact that the three types of compaction combination are the same aggregate and bitumen composition. This may be a difference between mould-based and slab type compaction. Moreover, the particle size for the slab specimens shows slight differences in each direction. This fact may be one of factors to explain the differences in the mechanical properties of the slab specimens. Further research, therefore, would be necessary to understand this property in more detail.

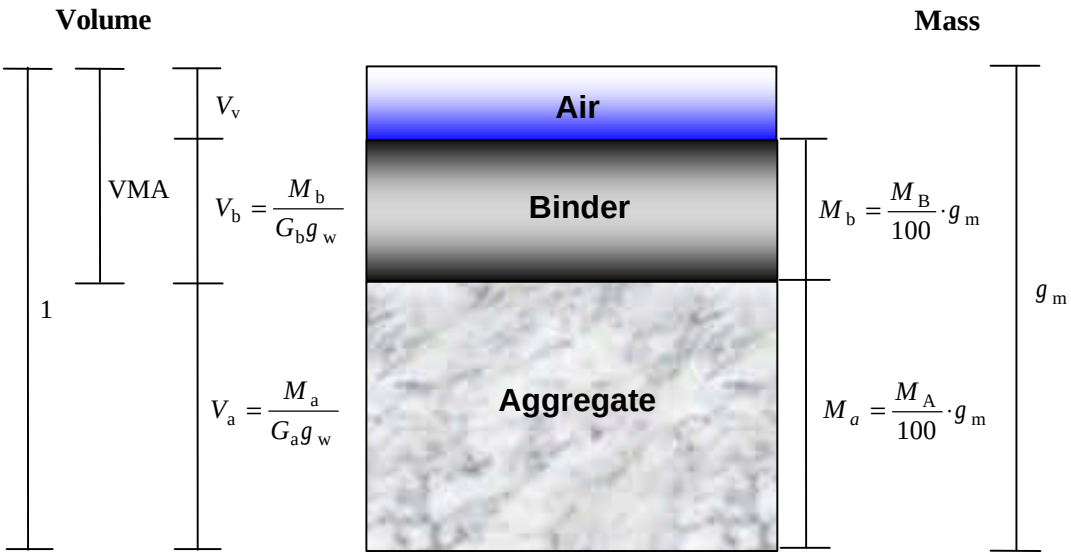

Figure 7.10: Component of asphalt mixture

Table 7.3: Determination of bitumen mastic (*D* = 150 mm specimens)

	Component			Mixture (Image)		Assumed bitumen mastic		
D=150mm	Air void (%)	V_b (%)	V_a (%)	Discrete aggregate (%)	Mastic (%)	Bitumen mastic (%)	Passing (%)	Particle size (mm)
Gyratory	2.8	9.53	87.72	57.24	40.01	30.48	34.74	2.29
Vibratory	3.1	9.49	87.37	57.43	39.43	29.94	34.27	2.20

Table 7.4: Determination of bitumen mastic (*D* = 100 mm specimens)

	Component			Mixture (Image)		Assumed bitumen mastic		
D=100mm	Air void (%)	V_b (%)	V_a (%)	Discrete aggregate (%)	Mastic (%)	Bitumen mastic (%)	Passing (%)	Particle size (mm)
Gyratory	2.48	9.56	87.96	55.00	42.51	32.96	37.44	2.81
Vibratory	2.68	9.54	87.79	54.76	42.56	33.02	37.61	2.81
Slab – Z	2.64	9.54	87.78	59.72	37.64	28.10	32.00	1.90
Slab – Y	2.85	9.52	80.55	62.36	34.79	25.27	28.83	1.44
Slab – X	2.96	9.51	87.53	59.97	37.07	27.56	31.49	1.80

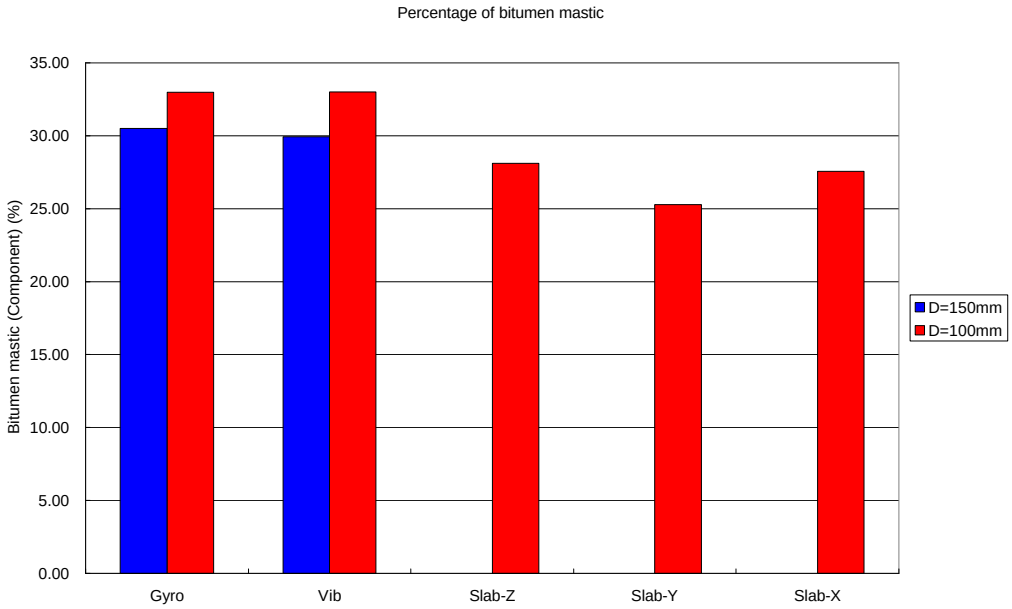

Figure 7.11: Percentage of bitumen mastic

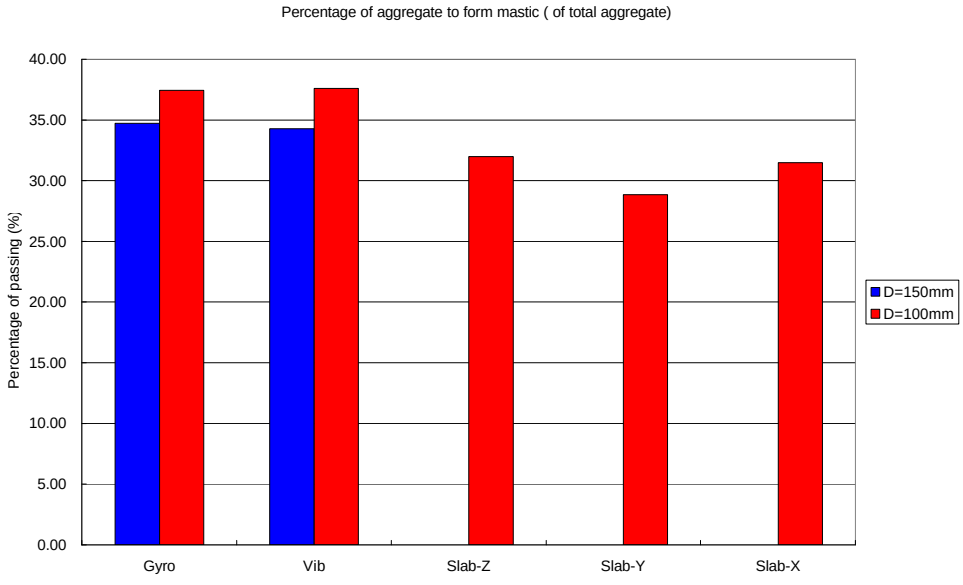

Figure 7.12: Percentage of aggregate to form bitumen mastic

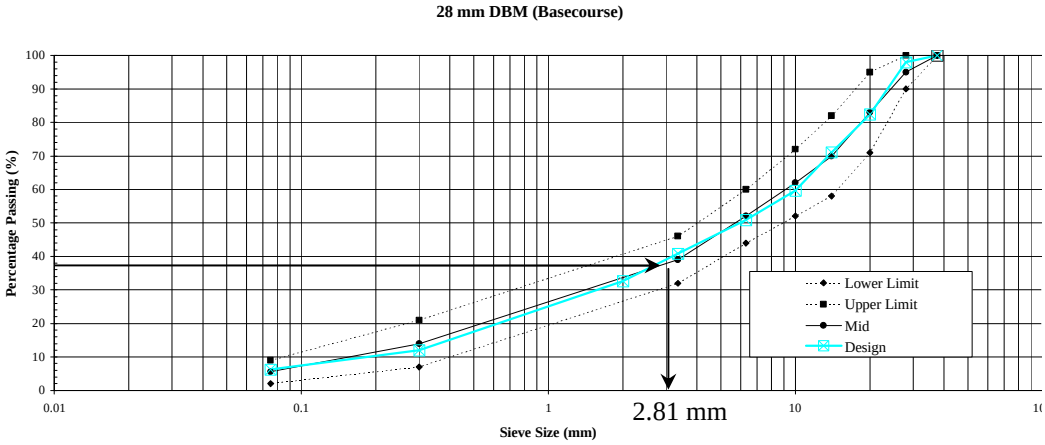

Figure 7.13: Determination of size of bitumen mastic from grading curve (e.g. gyratory specimen)

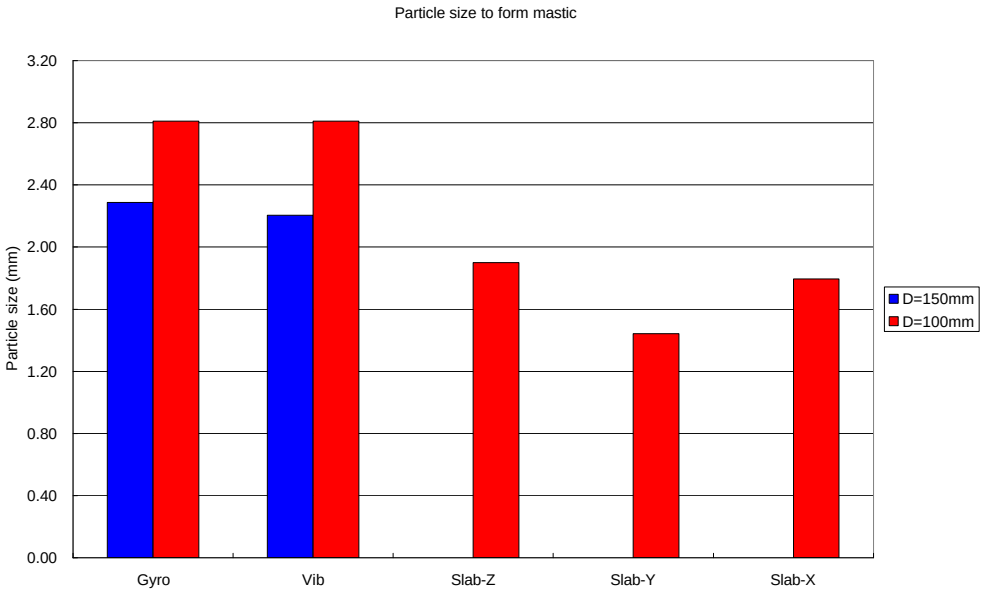

Figure 7.14: Particle size to form mastic

7.3.3 Smallest 20 Particles

Utilizing the information taken from image analysis, the smallest 20 particles were analyzed to look at how the properties of smaller particles are different in each compaction method. These results are shown in Tables 7.5 to 7.7. In general, there is no significant difference between compaction combinations, although the size of smaller particles for the 150 mm and 100 mm diameter specimens is different.

In terms of average size, the 150 mm diameter specimens show approximately 0.36 mm and 0.21 mm as particle length and width, respectively. On the other hand, for the 100 mm diameter specimens, the length and width are approximately 0.21 mm and 0.13 mm, respectively.

With respect to the range for maximum particle size, the 150 mm diameter specimens showed almost the same maximum and minimum size in both the gyratory and vibratory specimens, whilst the 100 mm diameter specimens indicated slightly lower size than that of the 150 mm specimens (see Table 7.6). This trend is observed in average size range for the smallest 20 particles (see Table 7.7). Therefore, it seems that the particle size for both the 150 mm and 100 mm diameter specimens is slightly different, although these specimens have the same aggregate composition and materials. The trends are presented in Figures 7.16 and 17.

As a result, it is thought that these differences are caused by the difference in the height of digital camera. When the surfaces of specimen were photographed, the distance between the camera and specimen surface is different between the 150 mm

and 100 mm diameter specimens. As the 100 mm diameter specimen is smaller than the 150 mm diameter specimen, it is needed to move the camera close to the specimen surface to capture the image clearly. The camera height for the 150 mm and 100 mm diameter specimens were 56.4 cm and 43.5 cm, respectively. Consequently, the minimum particle size would be different, if the height of camera changed from the 150 mm to 100 mm diameter specimens.

From the perspective of particle area, some strange phenomena were confirmed in all specimens. For example, according to Figure 7.15, the area of the smallest particles was 0.09186 cm^2. The particle length and width are 0.34 mm and 0.21 mm, respectively. In theory, the particle area can be less than 0.0714 mm^2, if particle is assumed to be rectangular. However, the recognized particle area is more than the theoretical area. This phenomenon is confirmed in all specimens.

It is, therefore, thought that the determination of the particle area through the thresholding process is different from this assumption (i.e. rectangular assumption). As a result, it is assumed that the area of particles may be calculated from pixel size.

However, Stakston et al. (2002) suggested that fine aggregate angularity affects the mechanical properties of asphalt mixtures, especially in shearing resistance. This research looked at only smaller particle size (i.e. length and width). Therefore, the relationship between the fine particles size and mechanical properties would also be needed to be verified in further research.

Table 7.5: Average size for smallest 20 particles (Unit: mm)

Diameter	Compaction	Size (length)	Size (width)
D=150mm	Gyro	0.36	0.21
	Vibratory	0.35	0.21
D=100mm	Gyro	0.22	0.13
	Vibratory	0.22	0.13
	Slab Z	0.21	0.13
	Slab Y	0.21	0.13
	Slab X	0.21	0.13
Computer trimmed D=100	Gyro	0.37	0.20
	Vibratory	0.35	0.21

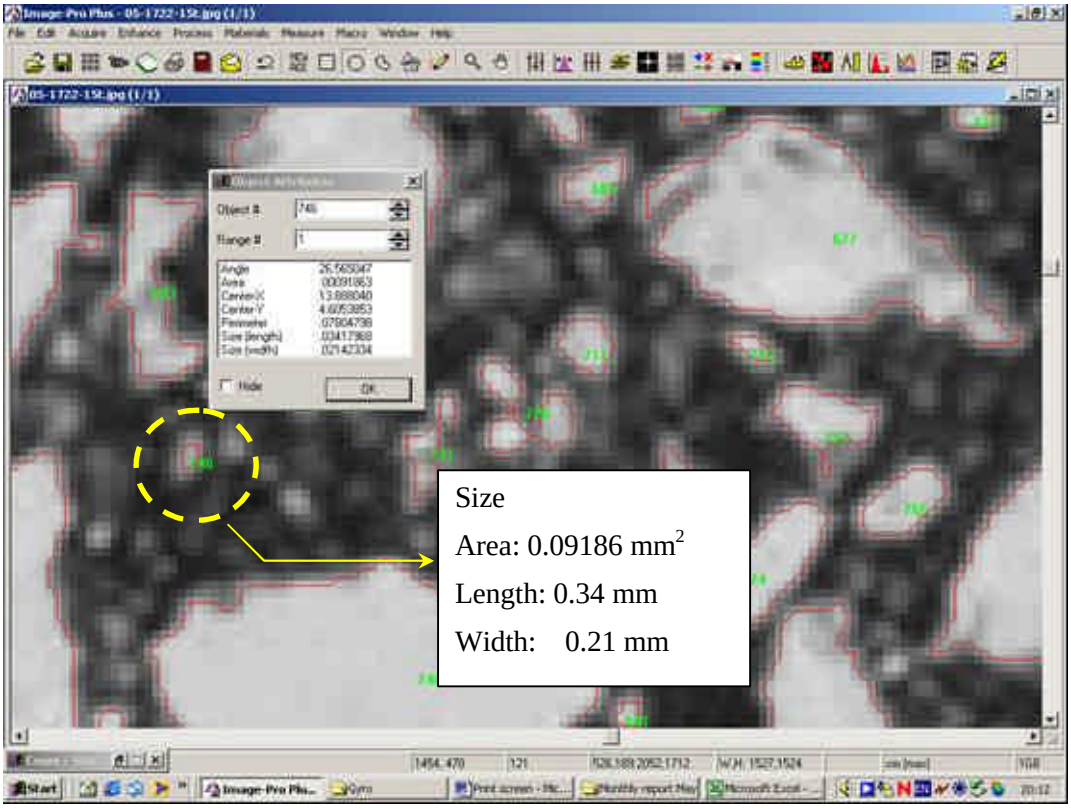

Figure 7.15: Smallest particle on the image

Table 7.6: Size range for smallest 20 particles (Unit: mm)

Compaction type	Max/Min	Size (length)	Size (width)
Gyro D=150	Max	0.62	0.29
	Min	0.27	0.09
Vib D=150	Max	0.62	0.38
	Min	0.27	0.10
Gyro D=100	Max	0.38	0.19
	Min	0.16	0.06
Vib D=100	Max	0.43	0.19
	Min	0.17	0.06
Slab Z	Max	0.41	0.18
	Min	0.17	0.06
Slab Y	Max	0.36	0.18
	Min	0.17	0.06
Slab X	Max	0.48	0.19
	Min	0.17	0.06
C.Gyro D=100	Max	0.69	0.29
	Min	0.27	0.09
C.Vib D=100	Max	0.60	0.30
	Min	0.27	0.10

* C stands for Computer trimmed 100mm specimen

Table 7.7: Average size range for smallest 20particles (Unit: mm)

Compaction type	Max/Min	Size (length)	Size (width)
Gyro D=150	Max	0.50	0.27
	Min	0.28	0.13
Vib D=150	Max	0.49	0.27
	Min	0.28	0.14
Gyro D=100	Max	0.31	0.17
	Min	0.18	0.08
Vib D=100	Max	0.32	0.16
	Min	0.18	0.08
Slab Z	Max	0.30	0.16
	Min	0.17	0.09
Slab Y	Max	0.29	0.16
	Min	0.17	0.09
Slab X	Max	0.30	0.16
	Min	0.17	0.09
C.Gyro D=100	Max	0.52	0.26
	Min	0.29	0.13
C.Vib D=100	Max	0.48	0.27
	Min	0.28	0.13

* C stands for Computer trimmed 100 mm specimen

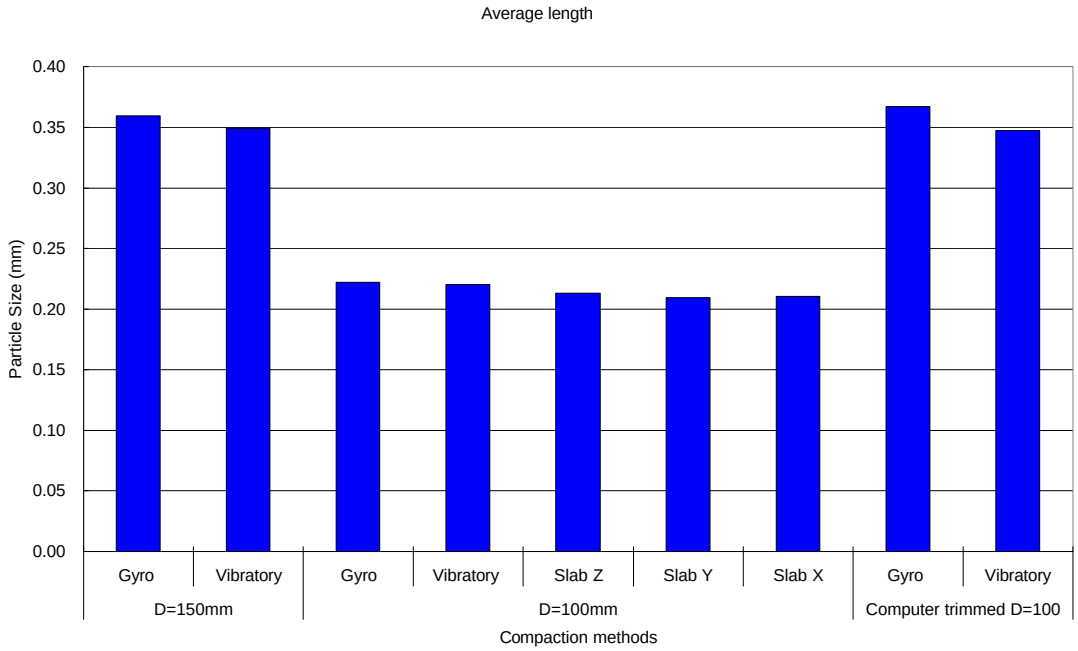

Figure 7.16: Average length for smallest 20 particles in each compaction combination

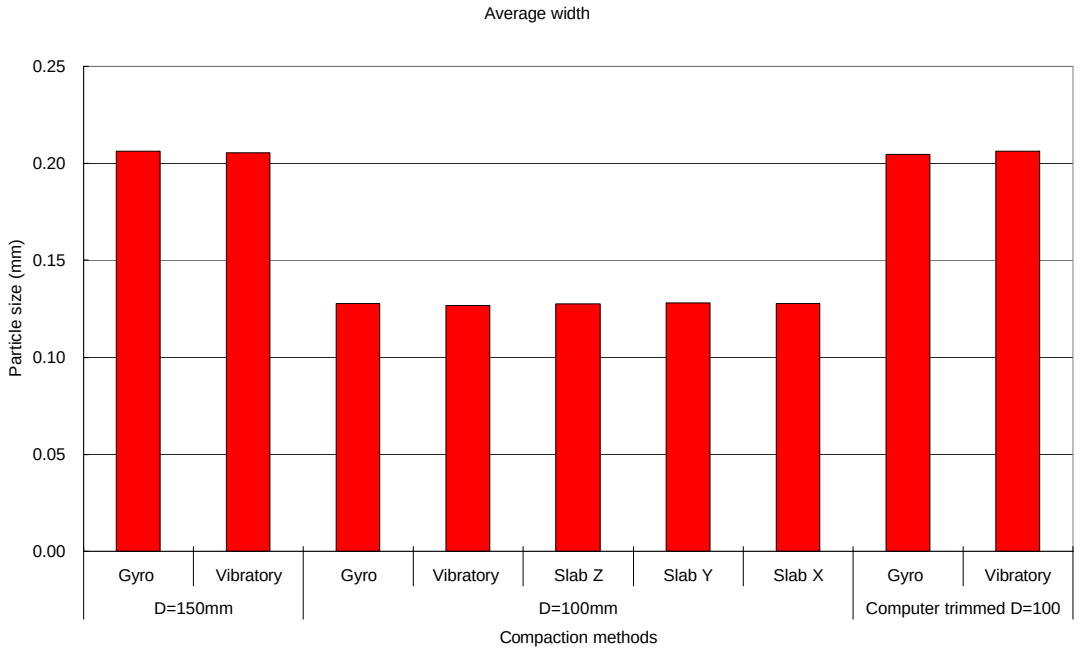

Figure 7.17: Average width for smallest 20 particles in each compaction combination

7.4 EFFECT OF TRIMMING

The number of particles and the area changes, when 100 mm diameter cores are taken from 150 mm diameter specimens. However, as mentioned in Section 7.2, the number of particles and area for the cored 100 mm and computer trimmed 100 mm diameter specimens are different, despite the fact that these two types of specimen have almost the same cross section area. In order to confirm these differences, a detailed investigation was carried out using the information taken from image analysis calculation. The results are presented in Tables 7.8 to 7.10. Also, plots for the centre of aggregate particles in each specimen type are shown in Figure 7.18.

In general, it is understood that there are significant differences in the particle number and area among each specimen size. This phenomenon is confirmed in each compaction combination as well. However, despite the fact that both the 100 mm and computer trimmed 100mm diameter specimens have almost the same cross section area, there are significant differences between two types of specimen. It is, therefore, thought that this is caused by coring, when the 100 mm diameter cores were taken from the 150 mm diameter specimens.

Comparing the cored 100 mm diameter specimens with the computer trimmed 100 mm diameter specimens, the particle area results for the computer trimmed specimens may depend on the centre of each particle as described in Section 6.2. If particles are scanned within the radius of 50 mm, then the image analysis software recognizes the whole particle area which including that in the outer region.

Therefore, the presented data strongly supports the evidence that total area in computer trimmed specimens is likely to be bigger than that of the cored 100 mm diameter specimens, even though the number of particles for the computer trimmed specimens is less than that of the cored 100 mm diameter specimens.

Table 7.8: Particle information for gyratory compacted specimens

Gyro.	150 mm			100 mm			Computer trimmed 100 mm		
	Number of particles	Area (cm^2)	Area (%)	Number of particles	Area (cm^2)	Area (%)	Number of particles	Area (cm^2)	Area (%)
Ave.	2206.5	101.1	57.2	1671.7	41.5	55.0	868.9	45.2	57.6
StDv	369.6	6.7	3.8	302.4	3.7	4.9	75.5	6.9	8.7

Table 7.9: Particle information for vibratory compacted specimens

Vib.	150 mm			100 mm			Computer trimmed 100 mm		
	Number of particles	Area (cm^2)	Area (%)	Number of particles	Area (cm^2)	Area (%)	Number of particles	Area (cm^2)	Area (%)
Ave.	1801.4	101.5	57.4	1396.1	41.3	54.8	764.8	42.5	54.2
StDv	248.4	5.9	3.4	221.8	3.1	4.1	120.7	3.7	4.7

Table 7.10: Particle information for slab compacted specimens

Slab	Z-direction			Y-direction			X-direction		
	Number of particles	Area (cm^2)	Area (%)	Number of particles	Area (cm^2)	Area (%)	Number of particles	Area (cm^2)	Area (%)
Ave.	1889.5	45.0	59.7	1709.7	47.0	62.4	1970.6	45.2	60.0
StDv	403.5	3.6	4.8	219.2	1.6	2.1	191.8	2.5	3.3

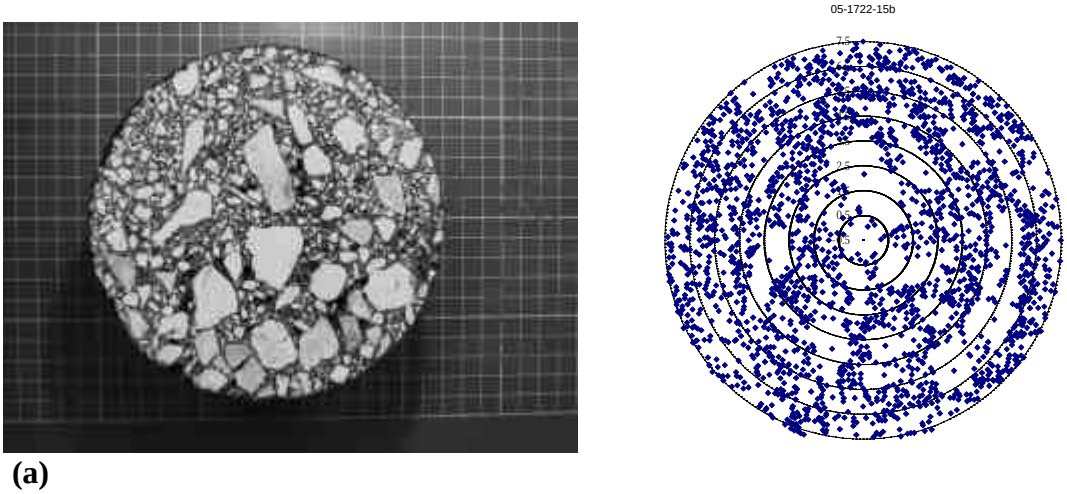

(a)

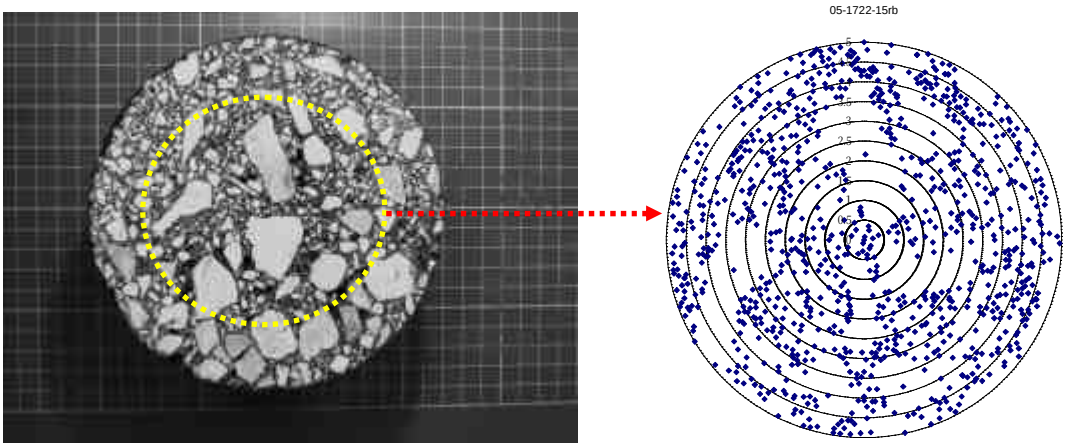

(b)

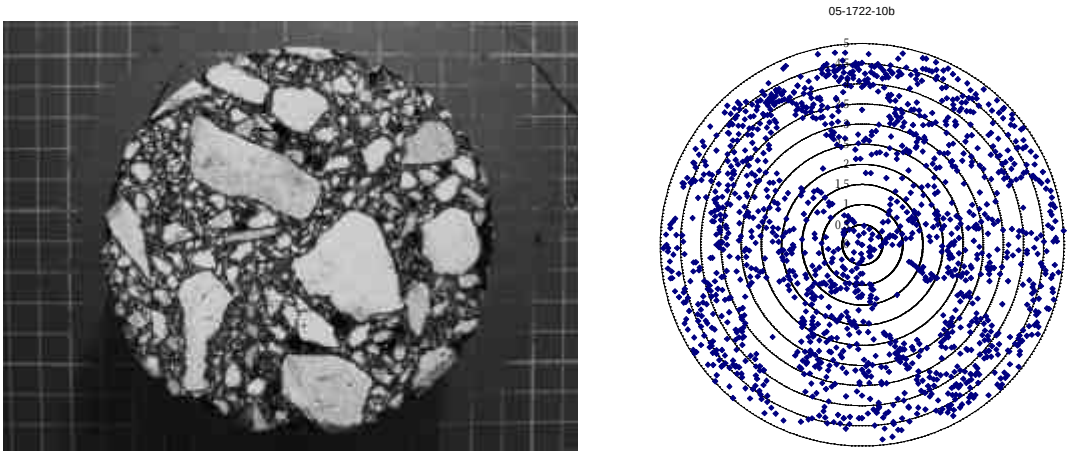

(c)

Figure7.18: Differences of data acquisition in each specimen size left: photo of specimen right: recognized particles (a) *D* = 150 mm specimen (b) computer trimmed *D* = 100 mm specimen (c) *D* = 100 mm (cored out) specimen

7.5 AGGREGATE SEGREGATION

Aggregate segregation is another parameter to evaluate the internal structure of the asphalt mixtures. In theory, specimens manufactured in the laboratory should have uniform aggregate distribution across the entire volume. In practice, however, it is difficult to achieve this due to the compaction dynamics which may lead to aggregate segregation (Airey et al. 2006). In general, segregation is a problem which results in poor performance of the surface layer (Brock, 1986; Cross et al. 1993; Khedaywi et al. 1996; Williams et al. 1996; Stroup-Gardiner et al. 2000). In addition, Kandhal et al. (1993) and Brown et al. (1989) suggested that base course asphalt mixtures with larger aggregates tend to segregate. Therefore, aggregate segregation should be analysed to understand the differences between compaction methods and the influences on the mechanical properties in asphalt mixtures.

This study examined the segregation phenomena from two perspectives: peripheral segregation and regional segregation.

7.5.1 Peripheral Segregation

Peripheral segregation was determined by splitting into sectors of 5 degrees. The whole cross section, therefore, comprises 72 sectors (Hunter et al. 2004; Airey et al. 2006). By moving around the cross section in 5 degree steps, the area of aggregate which comprises the 72 different sections can be determined. This process is depicted in Figure 7.19, where each sector is represented as α. This process enables the quarters with maximum aggregate density to be located as well as the aggregate

densities in the remaining three quarters. In other words, after determining maximum aggregate density which is identified as the 1st quarter, the other remaining quarters are also determined by shifting around the cross section by 90 degrees from the 1st quarter. In this study, peripheral segregation ratio is defined as

Peripheral segregation ratio=Max. aggregate quarter / Min. aggregate quarter.

Tables 7.11 to 7.14 show the calculation results looking at all particles for the 150 mm and 100 mm diameter specimens. However, no significant differences were observed between the gyratory and vibratory compaction. Hunter et al. (2004) also showed almost the same value as this study with respect to the 150 mm diameter specimens (see Table 7.12).

In their study, the particles which were greater than 1.0 cm^2 in VSA were also considered to look in more detail at segregation. In addition, they suggested that approximately 50% of the aggregate particle area on the cross section would consist of particles with a VSA greater than 1.0 cm^2. However, as the results taken from this study did not indicate this fact in all surfaces, the particles which comprise 50% of the particle area are directly scanned from the raw data; the peripheral segregation focused on larger aggregates (i.e. more than approximately 1.0 cm^2 in VSA).

Table 7.11 indicates the peripheral segregation (>50% in VSA) of the 150 mm diameter specimens. In general, larger aggregates show a greater segregation than

all aggregates in both the gyratory and vibratory specimens. Since Hunter et al. (2004) also showed a similar trend as shown in Table 7.12, it appears that the segregation states between the two studies are almost identical as the two studies used the same aggregate and grading.

Tables 7.13 to 7.14 also contain the peripheral segregation ratio of the 100 mm specimens for larger aggregates. The results show a significant variation in the peripheral segregation among the three compaction methods. For mould based specimens, the vibratory compacted specimens showed a greater segregation than the gyratory compacted specimens. For the slab specimens, the results indicate that the segregation ratios for the three orthogonal directions are different, despite the fact that the cores were taken from the slabs with the same aggregate composition.

Therefore, these differences may influence the mechanical properties of the three orthogonal slab specimens. This is discussed further in Section 7.7.

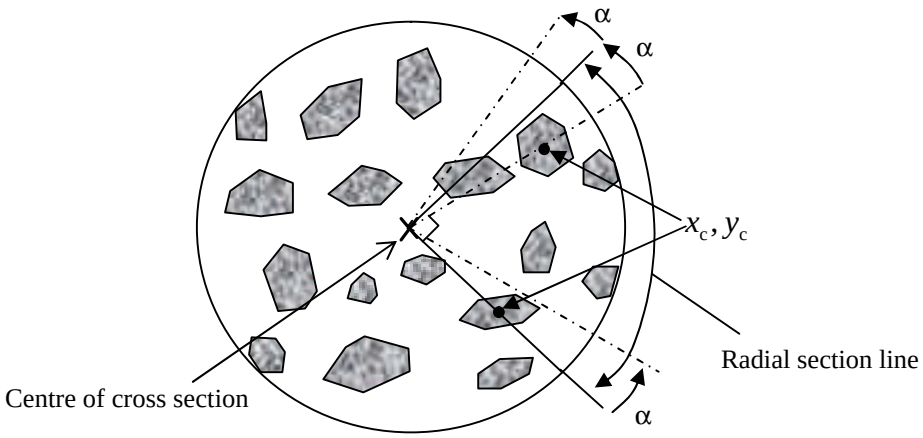

Figure 7.19: Schematic representation of peripheral segregation

Table.7.11: Peripheral segregation in each compaction method (*D* = 150 mm)

	All particles		>50% of area	
Segregation	Gyratory	Vibratory	Gyratory	Vibratory
Max.	31.68	32.79	42.84	42.97
Min.	20.42	19.20	12.03	11.87
Ratio	**1.55**	**1.70**	**3.56**	**3.62**

Table 7.12: Peripheral segregation in each compaction method (*D* = 150 mm) (Hunter et al. 2004)

	All particles			>50% of area		
Segregation	Gyratory	Vibratory	Slab	Gyratory	Vibratory	Slab
Max.	30.66	30.80	29.97	40.87	40.26	38.00
Min.	20.95	21.02	21.30	11.73	12.40	15.30
Ratio	**1.46**	**1.46**	**1.40**	**3.48**	**3.25**	**2.48**

Table 7.13: Peripheral segregation (*D* = 100 mm, all particles)

Segregation	Gyratory	Vibratory	Slab (Z-direction)	Slab (Y-direction)	Slab (X-direction)
Max.	34.94	37.39	37.02	37.65	36.82
Min.	17.37	17.30	16.45	17.06	17.28
Ratio	**2.01**	**2.16**	**2.25**	**2.21**	**2.13**

Table 7.14: Peripheral segregation (*D* = 100 mm, >50% of particle area)

Segregation	Gyratory	Vibratory	Slab (Z-direction)	Slab (Y-direction)	Slab (X-direction)
Max.	47.37	52.73	51.85	54.74	54.39
Min.	7.71	6.32	7.00	5.96	8.07
Ratio	**6.14**	**8.35**	**7.41**	**9.18**	**6.74**

7.5.2 Particle Area greater than 0.5 cm^2, 1.0 cm^2 and 1.5 cm^2 in VSA

The peripheral segregation for all particles and particles which occupy 50% of the total particle area were examined in the previous section. However, it is also useful to note what percentage of area the particles make up in each VSA range. In order to investigate this effect, the aggregate particles greater than 0.5 cm^2, 1.0 cm^2 and 1.5 cm^2 in VSA, were examined in each specimen size.

Gyratory and Vibratory compacted specimens

Tables 7.15 to 7.17 show the aggregate particle areas looking at different VSA. The results indicate that the vibratory compacted specimens tend to show greater segregation than the gyratory compacted specimens in each VSA. Also, the results verify the assumption that particles greater than 1.0 cm^2 in VSA comprise approximately 50% of the all particles on the cross section, as the data is about 50% of 150 mm diameter specimens. However, the area of 100 mm diameter specimens indicates less than 50%.

With respect to specimen size, the results indicate significant reduction in the area greater than 0.5 cm^2, 1.0 cm^2 and 1.5 cm^2 in VSA, when the specimens are cored from the 150 mm diameter specimens. Comparing the 150 mm specimens with the 100 mm diameter cores, the percentage of area for the 100 mm diameter specimens is smaller than that of the 150 mm diameter specimens in both the gyratory and vibratory compaction. This trend is seen in the computer trimmed 100 mm diameter specimens.

However, it should be noted that the computer trimmed specimens have smaller aggregate area than that of the 150 mm diameter specimens, despite the fact that the computer specimens are trimmed from the 150 mm diameter specimens. Therefore, this fact supports the view that larger aggregates migrate toward the mould boundary during compaction so that the percentage of area for the computer trimmed 100 mm diameter specimens tends to show a smaller value than the 150 mm specimens.

Slab specimens

The same procedure as for the gyratory and vibratory specimens was conducted for the slab specimens. The results are described in Table 7.18.

The results show significant variation in the percentage of VSA for the three orthogonal coring directions. However, it may be interesting to note that the slab X specimens show an extremely low value in the percent of aggregate area, compared to the slab Z and Y specimens. Therefore, this may be related to the mechanical properties of the slab specimens.

Table 7.15: Percentage of particles at different VSA (*D* = 150 mm specimens)

Compaction	Gyratory			Vibratory		
Size of particle	0.5 cm^2	1.0 cm^2	1.5 cm^2	0.5 cm^2	1.0 cm^2	1.5 cm^2
Area (%)	59.2	48.9	40.3	62.6	50.6	43.1

Table 7.16: Percentage of particles at different VSA (*D* = 100 mm specimens)

Compaction	Gyratory			Vibratory		
Size of particle	0.5 cm^2	1.0 cm^2	1.5 cm^2	0.5 cm^2	1.0 cm^2	1.5 cm^2
Area (%)	55.9	45.2	37.8	57.7	47.9	41.1

Table 7.17: Percentage of particles at different VSA (Computer trimmed *D* = 100 mm)

Compaction	Gyratory			Vibratory		
Size of particle	0.5 cm^2	1.0 cm^2	1.5 cm^2	0.5 cm^2	1.0 cm^2	1.5 cm^2
Area (%)	58.6	46.4	40.8	58.6	49.1	41.7

Table 7.18: Percentage of particles at different VSA (Slab specimens *D* = 100 mm)

Compaction	Z-direction			Y-direction			X-direction		
Particle Size	0.5cm^2	1.0cm^2	1.5cm^2	0.5cm^2	1.0cm^2	1.5cm^2	0.5cm^2	1.0cm^2	1.5cm^2
Area (%)	56.0	47.6	39.6	59.1	47.3	39.1	51.9	40.5	33.9

7.5.3 Peripheral Segregation with Particle Areas greater than 0.5 cm^2, 1.0 cm^2 and 1.5 cm^2

Based on the data taken from particle area, the peripheral segregation with particle areas greater than 0.5 cm^2, 1.0 cm^2 and 1.5 cm^2 were analysed.

Gyratory and Vibratory compacted specimens

Tables 7.19 to 7.21 present the peripheral segregation for the gyratory and vibratory specimens looking at particles greater than 0.5 cm^2, 1.0 cm^2 and 1.5 cm^2 in VSA. The results show a general increase in the peripheral segregation as the VSA value increases.

For the 150 mm diameter specimens, both the gyratory and vibratory specimens indicate a similar value for peripheral segregation (see Table 7.19). This trend is seen in all particles as described in the previous section. In addition, the particles greater than 1.0 cm^2 in VSA also show similar value to approximately 50% of the all particles on cross section.

However, the 100 mm diameter cores show greater segregation than the 150 mm diameter specimens as presented in Table 7.20. In addition, the vibratory specimens tend to indicate a greater segregation than the gyratory specimens. Furthermore, the particles greater than 1.5 cm^2 in VSA show considerably greater segregation than the others, although this may be due to statistical variation. The same trend is observed in the computer trimmed 100 mm diameter specimens as shown in Table 7.21.

Considering the above mentioned facts, it appears that the 100 mm diameter cores taken from the 150 mm diameter specimens have greater segregation, especially in particles greater than 1.5 cm^2 in VSA.

Slab specimens

Table 7.22 shows the peripheral segregation at different VSA for the orthogonal directions. The results show that there are significant variations in the three orthogonal directions. In particular, as shown in percentage of particle area, the slab X specimens also show much greater segregation than the slab Z and Y specimens.

Despite the fact that specimens were cored from the same slab, the ratio of peripheral segregation for the three directions is different. Therefore, the differences in the peripheral segregation appear to have had negligible influence on the mechanical properties of slab specimens. This is discussed further in the Section 7.7.

Table 7.19: Peripheral segregation ratio at different VSA (*D* = 150 mm specimens)

	Gyratory			Vibratory		
Size >VSA	0.5 cm^2	1.0 cm^2	1.5 cm^2	0.5 cm^2	1.0 cm^2	1.5 cm^2
Max.	39.3	43.3	47.4	38.8	42.1	44.2
Min.	15.4	12.7	10.9	15.5	12.1	10.6
Ratio	**2.55**	**3.40**	**4.36**	**2.51**	**3.47**	**4.16**

Table 7.20: Peripheral segregation ratio at different VSA (*D* = 100 mm specimens)

	Gyratory			Vibratory		
Size >VSA	0.5 cm^2	1.0 cm^2	1.5 cm^2	0.5 cm^2	1.0 cm^2	1.5 cm^2
Max.	45.6	51.6	55.1	48.6	55.1	61.7
Min.	10.2	5.88	4.10	9.45	5.54	2.67
Ratio	**4.45**	**8.77**	**13.4**	**5.15**	**9.94**	**23.1**

Table 7.21: Peripheral segregation ratio at different VSA (Computer trimmed *D* = 100 mm specimens)

	Gyratory			Vibratory		
Size>VSA	0.5 cm^2	1.0 cm^2	1.5 cm^2	0.5 cm^2	1.0 cm^2	1.5 cm^2
Max.	45.6	50.4	55.1	47.6	53.3	57.5
Min.	9.98	6.26	3.36	7.84	5.36	2.83
Ratio	**4.57**	**8.05**	**16.4**	**6.07**	**9.94**	**20.3**

Table 7.22: Peripheral segregation ratio at different VSA (Slab specimens *D*=100 mm)

	Z-direction			Y-direction			X-direction		
Size>VSA	0.5cm^2	1.0cm^2	1.5cm^2	0.5cm^2	1.0cm^2	1.5cm^2	0.5cm^2	1.0cm^2	1.5cm^2
Max.	48.0	53.6	62.0	48.9	55.8	60.7	52.3	61.1	68.3
Min.	8.87	6.61	3.02	8.64	5.64	2.38	8.19	4.56	1.72
Ratio	**5.41**	**8.11**	**20.5**	**5.66**	**9.90**	**25.6**	**6.39**	**13.4**	**39.8**

7.5.4 Peripheral Segregation by Number of Aggregate Particles

The peripheral segregation looking at aggregate particle numbers was also examined following the same procedure as for aggregate area. The particle segregation by numbers is also determined from the ratio (maximum divided by minimum quarter). The states of the segregation for the 150 mm diameter gyratory and vibratory specimens are represented in Figures 7.20 to 21.

Table 7.23 shows the peripheral segregation for the gyratory and vibratory specimens. These two compaction methods yield extremely similar results, in terms of particle numbers. Although the peripheral segregation looking at area did not indicate considerable results in all particles, no clear trend in the peripheral segregation by particle numbers is also shown between compaction combinations.

Table 7.24 presents the peripheral segregation for the slab specimens looking at the three orthogonal directions. The results reveal that the slab Z specimens have greater segregation than other two specimens (i.e. slab Y and X specimens), with respect to particle numbers.

However, it should be noted that the slab specimens indicate differences in peripheral segregation by number, despite the fact that the segregation with aggregate area showed no trend among the three directions. Therefore, further investigation may be necessary to look at whether the differences have effect on the mechanical properties of slab specimens.

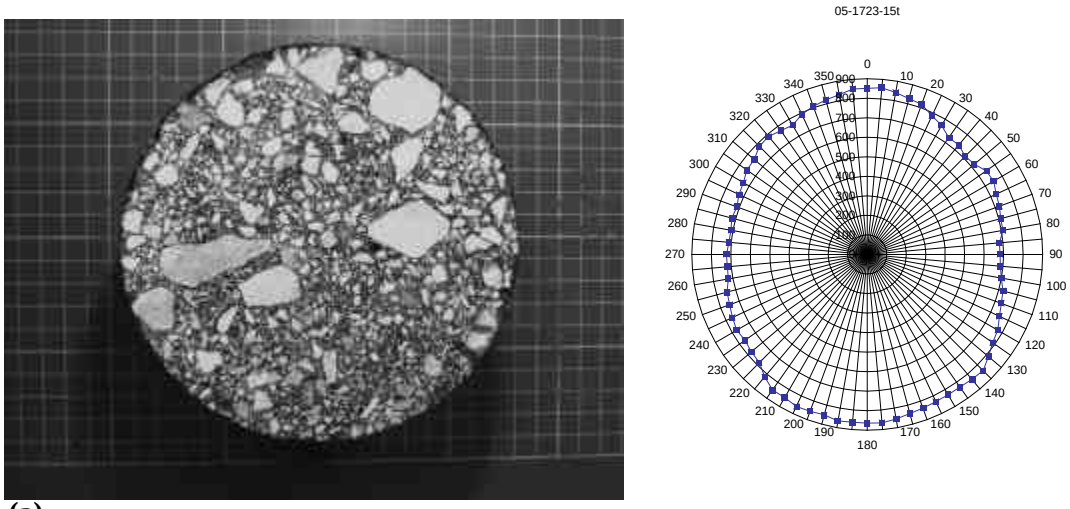

(a)

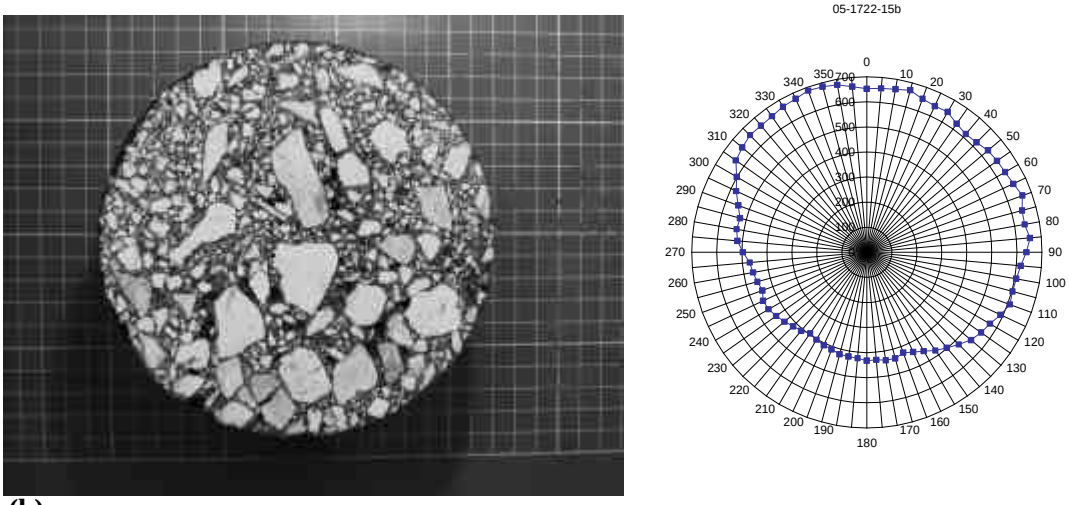

(b)

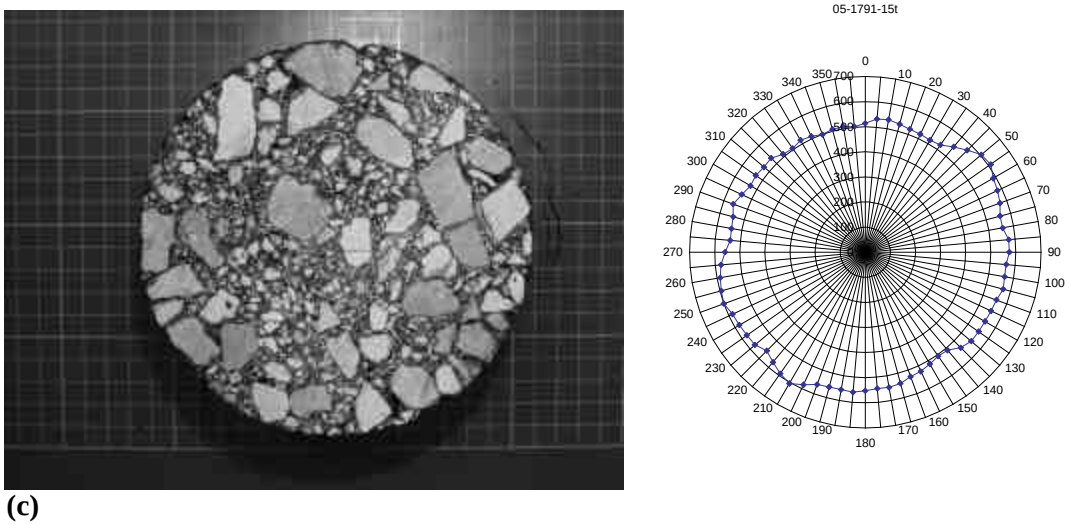

(c)

Figure 7.20: Particle number distribution for gyratory compacted specimen, left side: photo of specimen, right side: particle distribution (a) Uniform distribution (b) Non-uniform distribution (c) Circumferential distribution

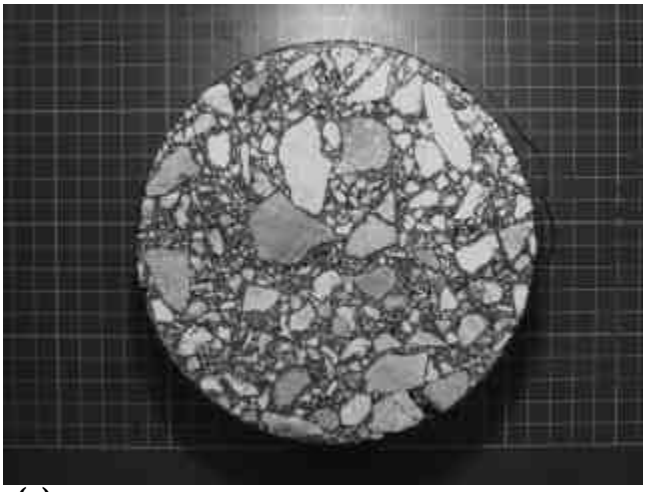

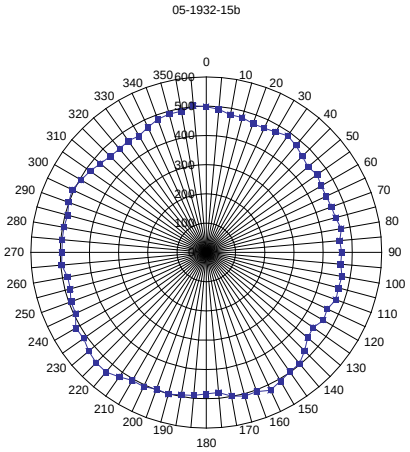

(a)

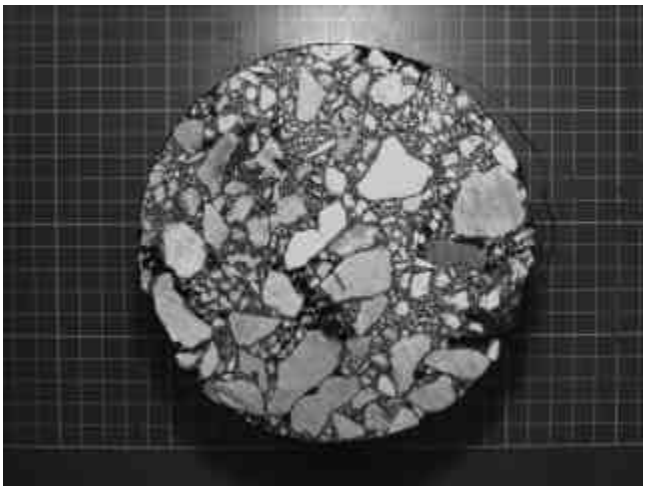

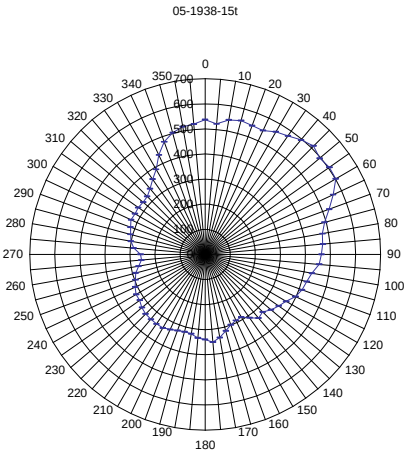

(b)

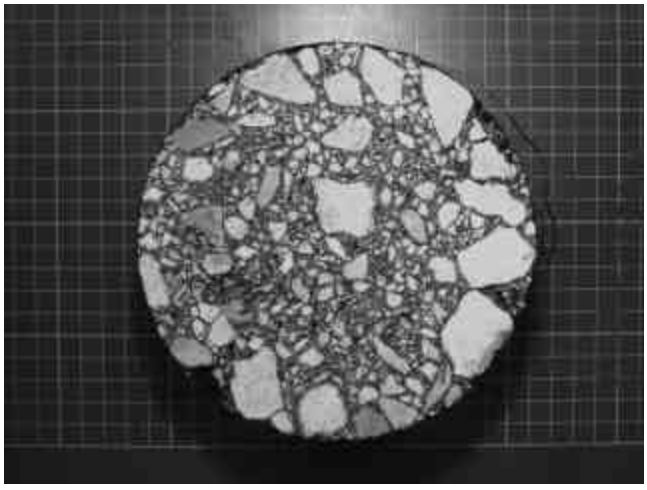

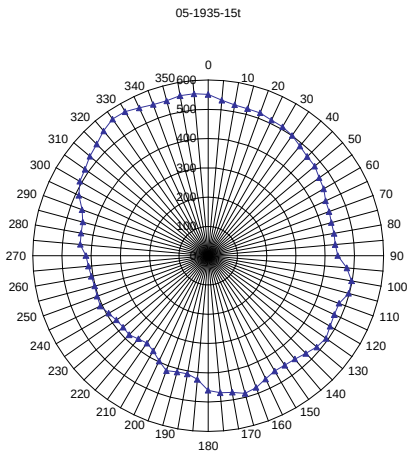

(c)

Figure 7.21: Particle number distribution for vibratory compacted specimen, left side: photo of specimen, right side: particle distribution (a) Uniform distribution (b) Non-uniform distribution (c) Circumferential distribution

Table 7.23: Peripheral segregation by number of aggregates (Gyratory and Vibratory specimens)

	Gyratory			Vibratory		
Segregation	150 mm	100 mm	C.100 mm	150 mm	100 mm	C.100 mm
Max.	678	539	346	551	439	256
Min.	453	375	196	375	284	167
Ratio	**1.57**	**1.59**	**1.76**	**1.47**	**1.55**	**1.53**

* (C) stands for Computer trimmed 100 mm diameter specimen.

Table 7.24: Peripheral segregation by number of aggregates (Slab specimens)

Segregation	Slab (Z-direction)	Slab (Y-direction)	Slab (X-direction)
Max.	660	549	611
Min.	376	350	393
Ratio	**1.76**	**1.57**	**1.56**

7.6 REGIONAL SEGREGATION

Hunter et al. (2004) and Airey et al. (2006) looked at the regional segregation by splitting the cross section of cores into inner and outer regions of equal area; and the average VSA in the respective region was calculated. The schematic for regional segregation is shown in Figure 7.22. In this study, regional segregation is defined as

Regional Segregation Ratio = Outer region / Inner region (in average VSA).

This study also follows the same procedure as the previous two studies to calculate the regional segregation. The analysis was conducted for all particles and particles greater than certain sizes in VSA (i.e. 0.5 cm^2, 1.0 cm^2 and 1.5 cm^2).

7.6.1 All particles

The results presented in Table 7.25 show that a relatively large difference in average VSA exists in both the 150 mm diameter gyratory and vibratory specimens, in terms of all particles. This trend was also observed in Hunter et al. (2004) and Airey et al. (2006) as shown in Table 7.26. Therefore, it seems that the phenomenon is caused by the gyratory and vibratory action in which larger particles migrate towards the boundary of the mould. Tashman et al. (2001) also confirmed the behaviour.

For the 100 mm diameter specimens, however, the results shown in Table 7.27

indicate a different trend from the results of 150 mm diameter specimens. The regional segregations for gyratory and vibratory specimens are almost identical, although the specimens show differences in the values of outer and inner regions. Also, comparing the results shown in Table 7.26, the gyratory and vibratory 100 mm diameter specimens appear to have similar value to slab specimens and site. Therefore, it seems that the centre part of the mould based specimens (i.e. gyratory and vibratory specimens) may have a near uniform particle distribution which is similar to slab specimens and site.

With regard to slab specimens, Table 7.28 shows a significant variation in the regional segregation ratio. The slab Z specimens present a slightly higher concentration in the inner region, while the slab X specimens show a clustering in the outer region; and the slab Y specimens indicate a relatively uniform particle distribution.

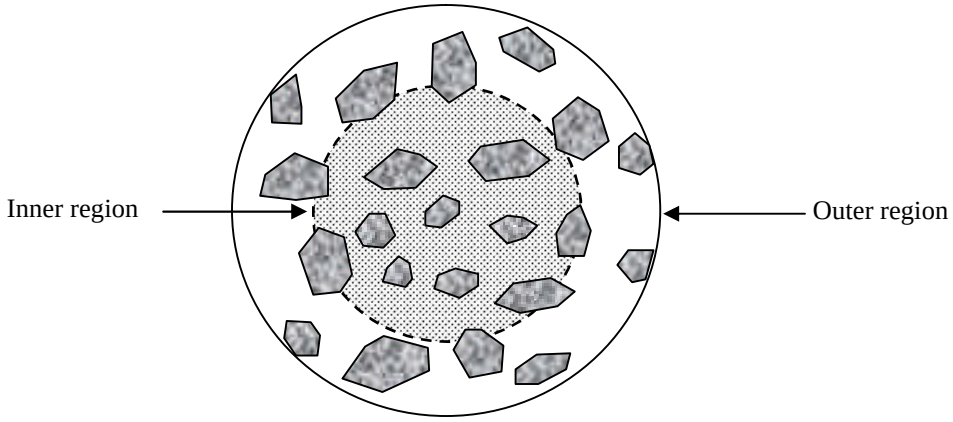

Regional Segregation Ratio = Outer (average VSA) / Inner (average VSA)

Figure 7.22: Schematic representation of regional segregation

Table 7.25: Regional segregation (*D* = 150 mm specimens)

	Gyratory	Vibratory
Outer region	0.051	0.064
Inner region	0.045	0.053
Ratio	1.13	1.21

Table 7.26: Regional segregation (*D* = 150 mm specimens) (Airey et al. 2006)

	Gyratory	Vibratory	Slab	Site
Outer region	0.044	0.051	0.038	0.035
Inner region	0.036	0.037	0.036	0.039
Ratio	1.22	1.39	1.06	0.90

Table 7.27: Regional segregation (*D* = 100 mm specimens)

	Cored *D* = 100 mm		Computer trimmed *D* = 100 mm	
	Gyratory	Vibratory	Gyratory	Vibratory
Outer region	0.025	0.030	0.051	0.051
Inner region	0.027	0.032	0.042	0.060
Ratio	0.93	0.94	1.19	0.85

Table 7.28: Regional segregation (Slab specimens *D* = 100 mm)

	Slab (Z-direction)	Slab (Y-direction)	Slab (X-direction)
Outer region	0.024	0.028	0.026
Inner region	0.026	0.029	0.021
Ratio	0.92	0.97	1.24

7.6.2 Particles greater than 0.5 cm^2, 1.0 cm^2 and 1.5 cm^2 in VSA

The regional segregation ratio obtained from the 150 mm diameter specimens suggest a view that larger aggregates may migrate to the boundary of the sample during the compaction process, especially in vibratory compaction. In order to confirm the effect, the particles greater than 0.5 cm^2, 1.0 cm^2 and 1.5 cm^2 in VSA were examined.

Gyratory and Vibratory compacted specimens

Tables 7.29 to 7.31 provide the regional segregation ratio for the gyratory and vibratory specimens. For the vibratory specimens, the result shown in Table 7.29 indicates a general trend of a slight increasing in the ratio of regional segregation in the 150 mm diameter specimens, although the ratio is less than 1.0. The same trend is confirmed in the cored and computer trimmed 100 mm diameter specimens (see Table 7.30 and 7.31). Therefore, the fact seen in the vibratory compaction may strongly support the assumption that larger particles move toward outer region during the compaction process.

In contrast, for the gyratory specimens, the result offered in Table 7.29 shows a different trend from the vibratory compaction. The regional segregation ratio of 150 mm diameter specimens remains constant, despite increasing in particle size from 0.5 cm^2 to 1.5 cm^2 in VSA. In addition, the data shown in Tables 7.30 and 7.31 indicate that larger particles in the cored and computer trimmed 100 mm diameter specimens tend to migrate to the inner region of the specimens. It seems, therefore, that all the larger particles do not necessarily move to the outer region, in

the case of the gyratory compaction.

Slab specimens

Table 7.32 shows the regional segregation ratio at certain particle sizes for slab specimens. The results present a significant variation in the three orthogonal coring directions, although the specimens taken from the three directions indicate a general increase in the ratio from 0.5 cm^2 to 1.5 cm^2 in VSA.

For the slab Z specimens, the result shows that a slightly higher concentration of aggregates is seen in the inner region for particles greater than 0.5 cm^2 in VSA; near uniform particle distribution is seen for 1.5 cm^2 in VSA. However, for the slab Y and X specimens, significantly higher concentration is observed in the outer region, especially for the slab X specimens.

Therefore, it could be argued that although the specimens were cored from the slabs with the same aggregate composition, the three types of specimens indicate differences in the regional segregation ratio. In addition, the specimens show slight differences in the regional segregation ratio for different VSA. Therefore, this fact may explain the differences in the mechanical properties of the slab specimens such as stiffness and strain as discussed in Chapter 4.

Table 7.29: Regional segregation at different VSA (*D* = 150 mm specimens)

	Gyratory			Vibratory		
Size (>VSA)	0.5 cm^2	1.0 cm^2	1.5 cm^2	0.5 cm^2	1.0 cm^2	1.5 cm^2
Outer region	1.67	2.38	3.02	1.64	2.51	3.14
Inner region	1.85	2.64	3.33	1.87	2.69	3.26
Ratio	**0.90**	**0.90**	**0.91**	**0.88**	**0.93**	**0.96**

Table 7.30: Regional segregation at different VSA (*D* = 100 mm specimens)

	Gyratory			Vibratory		
Size (>VSA)	0.5 cm^2	1.0 cm^2	1.5 cm^2	0.5 cm^2	1.0 cm^2	1.5 cm^2
Outer region	2.01	2.32	2.67	1.77	2.61	3.36
Inner region	2.14	2.48	3.19	2.11	2.99	3.81
Ratio	**0.94**	**0.94**	**0.84**	**0.84**	**0.87**	**0.88**

Table 7.31: Regional segregation at different VSA (Computer trimmed *D* = 100 mm specimens)

	Gyratory			Vibratory		
Size (>VSA)	0.5 cm^2	1.0 cm^2	1.5 cm^2	0.5 cm^2	1.0 cm^2	1.5 cm^2
Outer region	1.99	2.71	3.39	1.55	2.29	2.86
Inner region	1.68	2.50	3.28	2.11	3.03	3.58
Ratio	**1.19**	**1.08**	**1.03**	**0.73**	**0.76**	**0.80**

Table 7.32: Regional segregation at different VSA (Slab specimens *D* = 100 mm)

	Z-direction			Y-direction			X-direction		
Size (>VSA)	0.5cm^2	1.0cm^2	1.5cm^2	0.5cm^2	1.0cm^2	1.5cm^2	0.5cm^2	1.0cm^2	1.5cm^2
Outer region	1.76	2.48	3.38	1.81	2.88	3.57	1.78	2.95	3.75
Inner region	2.04	2.66	3.29	1.68	2.39	2.95	1.48	2.22	2.88
Ratio	**0.86**	**0.93**	**1.03**	**1.08**	**1.20**	**1.21**	**1.21**	**1.33**	**1.30**

7.7 PARTICLE DISTRIBUTION, SEGREGATION AND MECHANICAL PROPERTIES

Particle distribution and segregation were examined in each compaction method in the previous sections. Comparing these results with mechanical testing results, some of the mechanical properties of laboratory compacted specimens could be explained as follows.

Looking at differences in particle numbers, the gyratory compacted specimens have more particles than the vibratory compacted specimens. This trend was consistent in both the 150 mm and 100 mm diameter specimens. Considering the stiffness results, it is assumed that the vibratory compaction may produce stiffer specimens than the gyratory compaction as the vibratory specimens tend to contain larger particles.

Also, comparing the ratio of area in both the gyratory and vibratory specimens, the ratio of aggregate area to total area in the 100 mm diameter specimens is smaller than that of the 150 mm specimens. In addition, it was observed that the rate of larger particles for the 150 mm specimens is higher than that of the 100 mm diameter specimens. Furthermore, the image analysis results showed that the 100 mm diameter specimens contain more bitumen mastic than the 150 mm diameter specimens. Therefore, it is assumed that the outer part of the 150 mm diameter specimens contain larger particles, while the inner region has more bitumen with smaller aggregates. This may explain the reduction in stiffness from the 150 mm to

100 mm diameter specimens.

Considering the above mentioned assumptions, it would be necessary to consider both total particle and elongated particle distribution to discuss the mechanical properties of laboratory compacted specimens in more detail (see Figure 7.23). Also, as shown in Figure 7.24, the investigation looking at the particle distribution in each 5 degrees may be required to examine the mechanical properties.

Moreover, based on the mechanical testing and image analysis results, the existence of an arching effect in mould based specimens is assumed as shown in Figure 7.25. Nevitt (1957) suggested that the resistance of asphalt mixture is attributed to internal arch resistance described as interlock; frictional resistance; viscous or flow resistance and inertia effects. This may be related to the mechanical testing results of both the gyratory and vibratory specimens as the 100 mm diameter specimens showed significant reduction in stiffness compared to the 150 mm diameter specimens.

However, the above assumptions can only be described as a hypothesis. No evidence yet exists for the results.

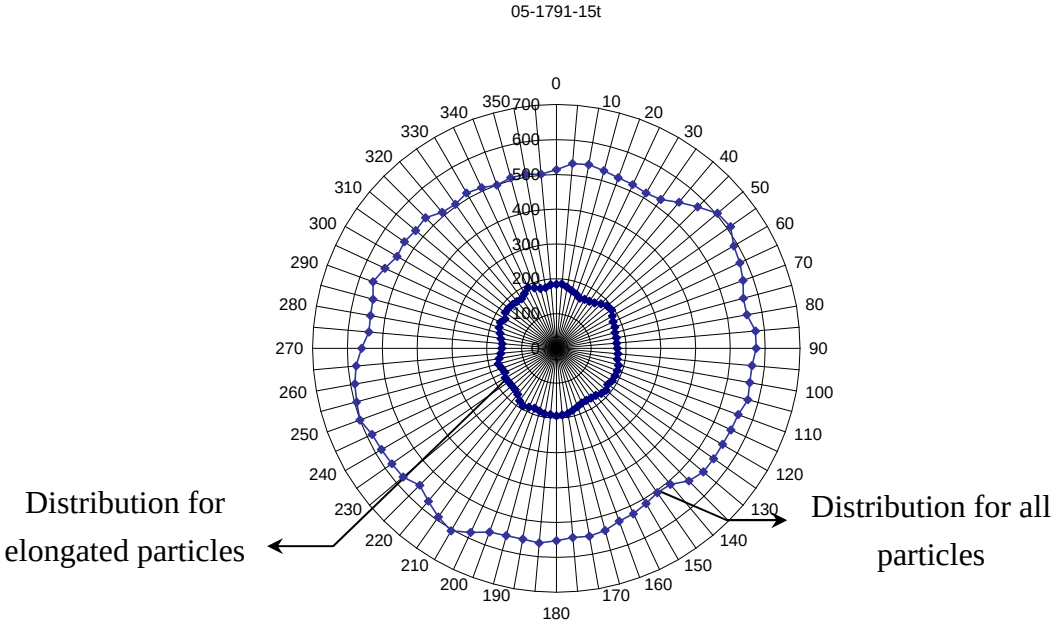

Figure 7.23: Particle distribution for all particles and elongated particles

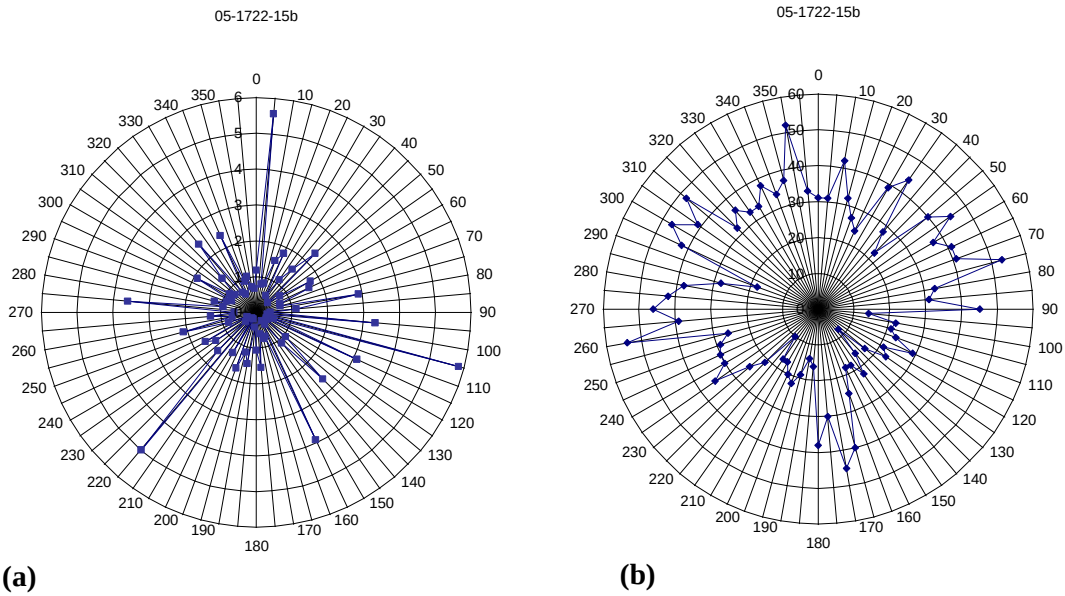

Figure 7.24: Particle distribution in each 5° segment: (a) Area distribution (b) Particle number distribution

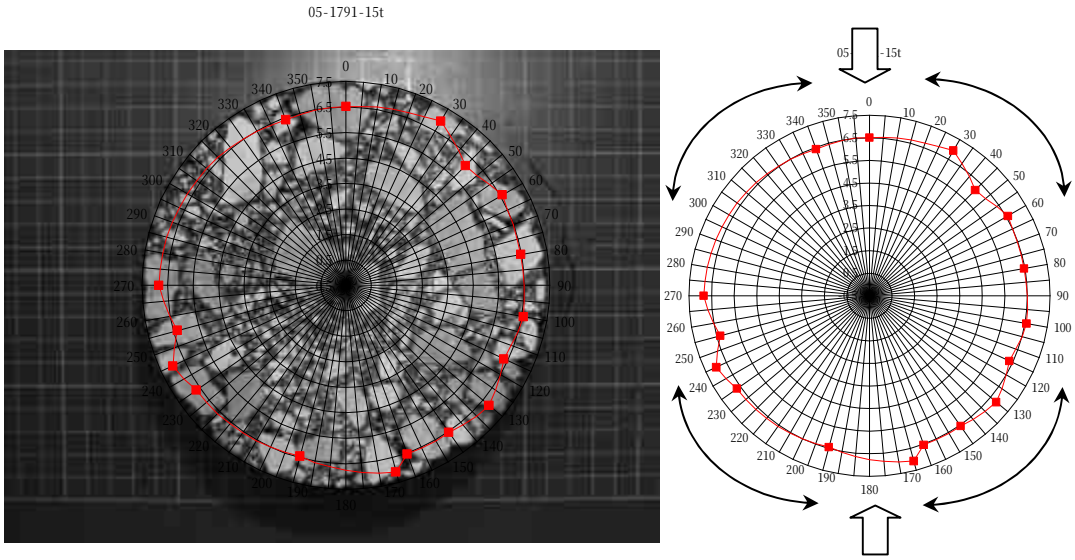

Figure 7.25: Representation of arching effect caused by mould confinement

7.8 CONCLUSIONS

The detailed information on the aggregate distribution and segregation were presented and analysed in this Chapter. The results provided in each section can be summarized as follows:

In terms of number of particles, the gyratory compacted specimens have more particles than the vibratory compacted specimens, despite the fact that these two types of specimen have almost the same particle area.

With respect to the percentage of particle area, the vibratory compacted specimens have a higher ratio of particle area than that of the gyratory compacted specimens.

Looking at the particle area for the mould based specimens, the ratio of aggregate area for the 150 mm diameter specimens was higher than that of the 100 mm specimens. In contrast, the ratio of bitumen mastic for the 100 mm diameter specimens (i.e. within the radius of 50 mm in 150 mm diameter specimen) was higher than that of the 150 mm diameter specimens.

With respect to the peripheral segregation, the vibratory compacted specimens tend to show a higher rate of segregation than the gyratory compacted specimens. This trend is consistent, even when the size of aggregate was changed (i.e. 0.5 cm^2, 1.0 cm^2 and 1.5 cm^2 in VSA), although it appears that this is due to statistical variation.

However, from the perspective of segregation by the number of particles, the gyratory compacted specimens showed a higher degree of peripheral segregation than the vibratory compacted specimens.

With regard to the regional segregation, the vibratory compacted specimens tend to show larger particle area in the outer region. This trend is more pronounced as particle size is becomes bigger. On the other hand, the gyratory compacted specimens are likely to show relatively uniform particle distribution.

In terms of the slab specimens, an anisotropy for particle distribution was confirmed as the ratio of peripheral and regional segregation in the three orthogonal directions (i.e. Z, Y and X directions) indicated significant differences. This might be related to the mechanical properties of the slab specimens.

CHAPTER 8

Conclusions and Further Research

8.1 INTRODUCTION

Provisional conclusions have been described through this thesis. This chapter provides only conclusions combining the mechanical testing and image analysis results; these conclusions are followed by further research that could be related to this study.

8.2 INFLUENCE OF SPECIMEN SIZE

The mechanical testing and image analysis results obtained from this study reveal that mould confinement found in mould based compaction methods such as gyratory and vibratory has the effect of producing aggregate reorientation at the outer edge of the compacted specimen. The circumferential particle alignment caused by the effect may influence two perspectives of mould based specimens. Firstly, the outer region of the 150 mm diameter mould based specimens differs considerably from the inner region (i.e. the radius of 50 mm in the 150 mm diameter specimens) in terms of internal structure. Gyratory and vibratory

compaction tends to produce asphalt mixture specimens which have circumferential particle orientation at the outer edge of mould, while the inner region of the specimens contains particles with random orientation. Secondly, the circumferential particle orientation may contribute to the higher stiffness.

In terms of segregation in the mould based specimens, the image analysis results may support the fact that larger particles tend to move towards the outer edge of compacted specimen. The 150 mm diameter gyratory and vibratory compacted specimens showed a relatively higher regional segregation ratio. In addition, looking at the ratio of aggregate area, the ratio of the 100 mm diameter specimens is smaller than that of 150 mm diameter specimens. This may indicate that the inner region of mould based specimens contains smaller aggregates with much bitumen, while the outer region of the specimen is occupied by larger aggregates with circumferential orientation. The cored 100 mm diameter specimen, therefore, has lower stiffness than the 150 mm diameter specimen.

Looking at the differences between gyratory and vibratory specimens, the vibratory specimens have less aggregate particles than the gyratory specimen, despite the fact that both specimens have the same aggregate composition. In other words, the vibratory compacted specimens seem to contain larger aggregate particles than the gyratory compacted specimens due to the differences in compaction mode. This fact may explain the result that the vibratory specimen is stiffer than the gyratory and slab specimens. However, as mentioned in Chapter 7, clear evidence has not appeared from 2-D analysis. Further investigation would be necessary.

8.3 INFLUENCE OF SPECIMEN ORIENTATION

Specimen orientation has also been shown to be extremely influential on the mechanical properties of asphalt mixture specimens. Stiffness and permanent deformation results from cores taken horizontally, transversely and aligned with the direction of compaction from a ‘roller’ compacted asphalt mixture slab show considerable variation.

The results obtained from regional segregation may explain the variation in stiffness. Larger segregation is seen in specimens cored from X and Y directions, whereas relatively uniform particle distribution is confirmed in the specimens cored from Z-direction. This trend is consistent with the stiffness results of those specimens. The observed trend shows that slab Z specimens have higher stiffness than slab X and Y specimens. Therefore, the results of segregation ratio may provide an explanation for the variation of stiffness in the three orthogonal directions. However, the variation of permanent deformation is still not understood. Further research is required to understand the results.

8.4 FURTHER RESEARCH

Some significant features related to aggregate particle orientation and segregation were found through this research. Some of the results might be related to mechanical properties of asphalt mixtures, whilst others are not explained. In this research, it was found that image analysis is a powerful tool to understand the

mechanical properties of asphalt mixtures as well as differences in compaction modes. However, the image analysis deals with only S2 and S3 surfaces of the specimens throughout this research. Therefore, in order to understand the behaviour of asphalt mixtures more correctly, it is required to analyze whole specimens using 3-D analysis rather than 2-D analysis.

To analyze asphalt mixtures with 3-D, the research using X-ray computed tomography has been increasing. X-ray CT enables the internal structure of porous media to be analyzed (Shashidar et al. 1999; Romero et al. 2001; Papagiannakis et al. 2002; Watson et al. 2004; Michell et al. 2005). Therefore, it is expected to combine X-ray CT and the calculation process used in this research.

However, before using this system, it is required to correct the error of image analysis. Some papers suggest that image analysis software identifies particles which are adjacent to each other, as a single particle. This phenomenon is confirmed in this study as well. Therefore, it would be necessary to fix this problem. Some researchers have already solved this problem by creating a system called ‘edge detection algorithm’.

If X-ray CT analysis and the calculation process used in this research are combined, it would be possible to analyse the whole structure of an asphalt mixture. This would lead to the understanding of anisotropy in the slab specimens. Therefore, further research using X-ray CT would be needed to understand the behaviour of asphalt mixtures.

References

Aho, B. D., Vavrik W.R. and Carpenter, S.H. 2001 Effect of Flat Elongated Coarse Aggregate on Field Compaction of Hot-Mix Asphalt. *Transportation Research Record 1761*, Transportation Research Board, Washington,D.C., pp.26-31.

Airey, G.D., Hunter, A.E., Collop,A.C.& Zoorob,S.E. 2006 Comparison of Field and Laboratory Compacted Asphalt Mixtures. *Proceedings of the 10th International Conference on Asphalt Pavements*, Quebec City.

Alexander, M. and Mindess, S. 2005 *Aggregates in Concrete*. London, Taylor & Francis.

BS EN 12697-6 2003 *Bituminous mixtures, test method for hot mix asphalt, Determination of bulk density of bituminous specimens*

BS EN 12697-31 2004 *Bituminous mixtures, test methods for hot mix asphalt, specimen preparation by gyratory compactor*

BS EN 12697-32 2003 *Bituminous mixtures, test methods for hot mix asphalt, laboratory compaction of bituminous mixtures by vibratory compactor*

BS EN 12697-33 2003 *Bituminous mixtures, test methods for hot mix asphalt, specimen prepared by roller compactor*.

BS EN 12697-35 2004 *Bituminous mixtures, test methods for hot mix asphalt. Laboratory mixing.*

British Standards Institution 1993 Draft for Development 213. *Determination of indirect tensile stiffness modulus of bituminous mixtures*, London.

British Standards Institution 1996 Draft for Development 226. *Method for determining the resistance to permanent deformation of bituminous mixtures subject to unconfined dynamic loading*, London.

British Standards Institution 2001 4987 Coated macadam (asphalt concrete) for roads and other paved areas. *Part1: Specification for constituent materials and for mixtures*.

Brock, J.D. 1986 Segregation of Asphaltic Mixtures. *Proceedings, Association of Asphalt Paving Technologists*, Vol. 55, pp.269-276.

Brown, E.R., Collins, R. and Brownfield, J.R. 1989 Investigation of Segregation of Asphalt Mixtures in the State of Georgea. *Transportation Research Record 1217*, Transportation Research Board, Washington,D.C., pp.1-8.

Brown, E.R., Hanson, D.I. and Mallick, R.B. 1996 Evaluation of Superpave Gyratory Compaction of Hot-Mix Asphalt. *Transportation Research Record 1543*, Transportation Research Board, Washington,D.C., pp.145-150.

Brown, S.F. and Cooper, K.E. 1980 A Fundamental Study of the Stress-Strain Characteristics of a Bituminous Materials. *Proceedings of the Association of Asphalt Paving Technologists*, Vol. 49, pp. 476-496.

Brown, S.F. and Gibb, J. M. 1999 Effect of Compaction Method on Mechanical Properties of Asphalt Mixture. *7th Conference on Asphalt Pavement for South Africa*, Victoria Falls, Zimbabwe.

Brown, S.F., Preston, J.N. and Cooper, K.E. 1991 Application of New Concepts in Asphalt Design. *Journal of the Association of Asphalt Paving Technologists*, Vol. 60, pp.264-286.

Buchanan, M. S. and Brown, E.R. 2001 Effect of Superpave Gyratory Compactor Type on Compacted Hot-Mix Asphalt Density. *Transportation Research Record 1761*, Transportation Research Board, Washington,D.C., pp.50-60.

Butcher, M. 1997 *Determining Gyratory Compaction Characteristics using the Servopac Gyratory Compactor*. Department of Transport, South Australia.

Button, J.W., Little, D.N, Jagadam, V. and Pendleton, O. J. 1992 Correlation of Selected Laboratory Compaction Methods with Field Compaction. *Transportation Research Record 1454*, Transportation Research Board, Washington,D.C.

Cooper, K. E. and Brown, S.F. 1989 Development of a Simple Apparatus for the Measurement of the Mechanical Properties of Asphalt Mixes. *Proceedings of Eurobitume Symposium*, Madrid, pp.494-498.

Cooper, K.E., Brown, S.F. and Pooley, G.R. 1985 The design of Aggregate Gradings for Asphalt Basecourses. *Journal of the Association of Asphalt Paving Technologists*, pp.324-391.

Cooper, K.E., Brown, S.F., Preston, J.N. and Akeroyd, F.M.L. 1991 Development of a Practical Method for Design of Hot-Mix Asphalt. *Transportation Research Record 1317*, Transportation Research Board, Washington,D.C.,pp.42-51.

Consuegra, A., Little, D.N., Quintas, H.V. and Burati, J. 1989 Comparative Evaluation of Laboratory Compaction Devices Based on Their Ability to Produce Mixtures with Engineering Properties Similar to those Produced in the Field. *Transportation Research Record 1228*, Transportation Research Board, Washington,D.C., pp.80-87.

Cross, S.A. and Brown, E.R. 1993 Effect of Segregation on Performance of Hot-Mix Asphalt. *Transportation Research Record 1417*, Transportation Research Board, Washington,D.C., pp.117-126.

Epps, J. 1969 *Influence of Mixture Variables on the Flexural and Tensile Properties of Asphalt Concrete.* Institute of Transportation and Traffic Engineering, University of California, Berkeley.

Eta, K.E. 1991 *Moisture susceptibility of bituminous road base and base course mixture*. MSc. Dissertation, the University of Nottingham

Fletcher, T., Chandan, C., Masad, E. and Sivakumar, K. 2003 Aggregate Imaging System for Characterizing the Shape of Fine and Coarse Aggregates. *Transportation Research Record 1832*, Transportation Research Board, Washington,D.C.,pp.67-76.

Gibb, J.M. 1996 *Evaluation of resistance to permanent deformation in the design of bituminous paving mixture*. PhD Thesis, the University of Nottingham.

Hopman, P.C., Vallering, C.P. and Van der Heide, J.P.J. 1992 Mixes and Five Design Procedure: search for a performance related mix design procedure. *Journal of the Association of Asphalt Paving Technologists*, Vol.61, pp.188-216.

Harman, T., Bukowski, J.R., Moutier, F., Huber, G.. and McGennis, R. 2002 History and Future Challenges of Gyratory Compaction: 1939 to 2001. *Transportation Research Record 1789*, Bituminous Pavement Mixtures 2002, Transportation Research Board, Washington,D.C., pp.200-207.

Hartman, A.M., Gilchrist, M.D. and Walsh, G. 2001 Effect of Mixture Compaction on Indirect Tensile Stiffness and Fatigue. ASCE, *Journal of Transportation Engineering*, pp.370-378.

Harvey, J., Eriksen, K., Sousa, J. and Monismith, C. L. 1994 Effects of Laboratory Specimen Preparation on Aggregate-Asphalt Structure, Air-Void Content Measurement, and Repetitive Simple Shear Test Results. *Transportation Research Record 1454*, Transportation Research Board, Washington,D.C., pp.113-122.

Harvey, J., Monismith, C. L. 1994 Effect of Laboratory Asphalt Concrete Specimen Preparation Variables on Fatigue and Permanent Deformation Test Results Using Strategic Highway Research Program A-003A Proposed Testing Equipment. *Transportation Research Record 1417*, Transportation Research Board, Washington,D.C., pp.38-48.

Harvey, J., Monismith, C. L. and Sousa, J.B. 1994 An Investigation of Field-And Laboratory–Compacted Asphalt-Rubber, SMA, Recycled and Conventional Asphalt-Concrete Mixes Using SHRP Project A-003A Equipment. *Journal of the Association of Asphalt Paving Technologists*, pp. 512-559.

Harvey, J., Sousa, J.B., Deacon, J. A. and Monismith, C. L. 1991 Effects of Sample Preparation and Air-Void Measurement on Asphalt Concrete Properties. *Transportation Research Record 1317*, Transportation Research Board, Washington,D.C., pp. 61- 67.

Harvey, J.and Tsai, B. 1996 Effects of Asphalt Content and Air Void Content on Mix Fatigue and Stiffness. *Transportation Research Record 1543*, Transportation Research Board, Washington,D.C.,pp.38-45.

Highways Agency 1998 Manual of Contract Documents for Highway Works. Specification for Highway Works. Vol.1.

Hunter, A. E., Airey, G..D. and Collop, A.C. 2004 Aggregate Orientation and Segregation in Laboratory Compacted Asphalt Sample. *83rd Annual Meeting*, Washington, D.C., Transportation Research Board.

Kandhal, P.S. and Cross, S.A. 1993 Effect of Aggregate Gradation on Measured Asphalt Content. *Transportation Research Record 1417*, Transportation Research Board, Washington,D.C., pp.21-28.

Khedaywi, T.S. and White, T.D., 1996 Effect of Segregation on Fatigue Performance of Asphalt Paving Mixtures. *Transportation Research Record 1543*, Transportation Research Board, Washington,D.C., pp.63-70.

Lai, J.S. and Shami, H. 1995 Development of Rolling Compaction Machine for Preparation of Asphalt Beam Samples. *Transportation Research Record 1492*, Transportation Research Board, Washington,D.C., pp.18-25.

Lees, G. and Salehi, M. 1969 Orientation of Particle with Special Reference to Bituminous Paving Materials. *Highways Research Record No.273*, Highway Research Board, Washington,D.C., pp.63-75.

McRae, J.L. 1957 Compaction of Bituminous Concrete. *Journal of the Association of Asphalt Paving Technologists*, Vol. 26, pp.206-213.

Masad, E., Muhunthan, B., Shashidhar, N. and Harman, T. 1999 Quantifying Laboratory Compaction Effects on the Internal Structure of Asphalt Concrete. *Transportation Research Record* No.1681, Transportation Research Board, Washington,D.C., pp.179-185.

Masad, E. and Button, J. 2004 Implication of Experimental Measurement and Analyses of the Internal Structure of HMA. *83rd Annual Meeting*, Washington, D.C., Transportation Research Board.

Michell, J.K. and Soga, K. 2005 *Fundamentals of soil behaviour* (Third edition). New jersey, John Wiley.

Nevitt, H.G. 1957 Compaction Fundamentals. *Journal of the Association of Asphalt Paving Technologists*, Vol. 26, pp.201-206.

Nevitt, H.G. 1959 Some Sources of Stability Measurement Variations. *Journal of the Association of Asphalt Paving Technologists*, Vol. 28, pp.16-30.

Nukunya, B., Roque, R., Tia, M., and Mehta, Y. A. 2002 Effect of Aggregate Structure on Rutting Potential of Dense-Graded Asphalt Mixtures. *Transportation Research Record 1789*, Transportation Research Board, Washington, D.C., pp136-145.

Nunn, M.E. 1996 The characterisation of bituminous macadams by indirect tensile stiffness modulus. *Transportation Research Laboratory Report 160*, Berkshire.

Papagiannakis, A.T., Abbas, A. and Masad, M. 2002 Micromechanical Analysis of Viscoelastic Properties of Asphalt Concretes. *Transportation Research Record 1789,* Transportation Research Board, Washington,D.C., pp.113-120.

Paterson, W. D.O. 1974 Consideration of Particle Orientation in the Compaction of Asphalt Concrete. *Transportation Research Record No. 515*, Transportation Research Board, Washington,D.C., pp.151-156.

Read, J. and Whiteoak, D. (ed) 2003 *The Shell Bitumen Handbook* (Fifth edition). London: Thomas Telford

Renken, P. 2000 Influence of specimen preparation onto the mechanical behaviour of asphalt mixtures. *Proceedings of the 2nd Eurasphalt & Eurobitume Congress*, Barcelona , pp. 729-735.

Romero, P and Masad, E. 2001 Relationship between the Representative Volume Element and Mechanical Properties of Asphalt Concrete. ASCE, *Journal of Materials in Civil Engineering*, 13, pp.77-84.

Scholz, T.V., Allen, W.L., Terrel, R.L. and Hicks, R.G.. 1993 Preparation of Asphalt Concrete Test Specimen Using Rolling Wheel Compaction. *Transportation Research Record 1417,* Transportation Research Board, Washington,D.C.,pp.150-157.

Seo, Y., Kim, R., Witczak, M.W. and Bonaquist, R. 2002 Application of Digital Imaging Correlation Method to Mechanical Testing of Asphalt-Aggregate Mixtures. *Transportation Research Record 1789*, Transpiration Research Board, Washington,D.C., pp.162-172.

Shashidar, N. 1999. X-Ray Tomograpy of Asphalt Concrete. *Transportation Research Board 1681*, Transportation Research Board, Washington,D.C., pp.186-192.

Sousa, J. B., Deacon, J. A., and Monismith, C. L. 1991 Effect of Laboratory Compaction Method on Permanent Deformation Characteristics of Asphalt-Aggregate Mixtures. *Journal of the Association of Asphalt Paving Technologists*, pp.533-585.

Stakston, A.D., Hussain, U. B. and Bushek, J. J. 2002 Effect of Fine Aggregate Angularity on Compaction and Shearing Resistance of Asphalt Mixtures. *Transportation Research Record 1789*, Transportation Research Board, Washington,D.C., pp.14-24.

Strop-Gardiner,M. and Brown, E.R. 2000 *Segregation in Hot-Mix Asphalt Pavements*. National Cooperative Highway Research Program, Transportation Research Board, Washington,D.C.

Tashman, L., Masad, E., Peterson, B, and Slaeh, H. 2001 Internal Structure Analysis of Asphalt Mixes to Improve the Simulation of Superpave Gyratory Compaction to Field Conditions. *Journal of the Association of Asphalt Paving Technologists*, pp.605-645.

The Asphalt Institute 2007 *The Asphalt Handbook MS-4*. 7th edition.

Tashman, L., Masad, E., D'Angelo, J., Bukowski, J. & Harman, T. 2002 X-Ray Tomography to Characterize Air Void Distribution in Superpave Gyratory Compacted Specimens. *The International Journal of Pavement Engineering*, 3(1): pp.19–28.

Vallerga, B. 1951 Recent Laboratory Compaction Studies of Bituminous Paving Mixtures. *Proceedings of the Association of Asphalt Paving Technologists*, Vol.20, 117-153.

Vavrik, W.R., Fries, R.J. and Carpenter, S.H. 1999 Effect of Flat and Elongated Coarse Aggregate on Characteristics of Gyratory Compacted Samples. *Transportation Research Record 1681*, Transportation Research Board, Washington,D.C., pp.28-36.

Von Quintas, H.L., Scherocman, J.A., Hughes, C.S. and Kennedy, T.W. 1991 *Asphalt-Aggregate Mixture Analysis System, AAMAS*. National Cooperative Highway Research Program Report 338, Transportation Research Board, Washington, D.C.

Watson, D., Masad, E., Moore, K. A, and Cooley, A. 2004 Verification of VCA testing to Determine Stone on Stone Contact of HMA Mixture. *83rd Annual Meeting*, Washington, D.C., Transportation Research Board.

Williams, R.C., Duncan, G. Jr. and White, T.D. 1996 Hot-Mix Asphalt Segregation: Measurement and Effects. *Transportation Research Record 1543*, Transportation Research Board, Washington,D.C., pp.97-105.

Yue, Q.Z., Bekking, W. & Morin, I. 1995 Application of Digital Image Processing to Quantitative Study of Asphalt Concrete Microstructure. *Transportation Research Record 1492*, Transportation Research Board, Washington, D.C., pp.53-60.

APPENDIX-A

Experiment data
(Batching details)
(Gyratory compacted specimen with150 mm, 100 mm diameter)
(Vibratory compacted specimen with 150 mm, 100 mm diameter)
(Roller compacted specimen with 150 mm, 100 mm diameter)

Batching Details

Grading Curve

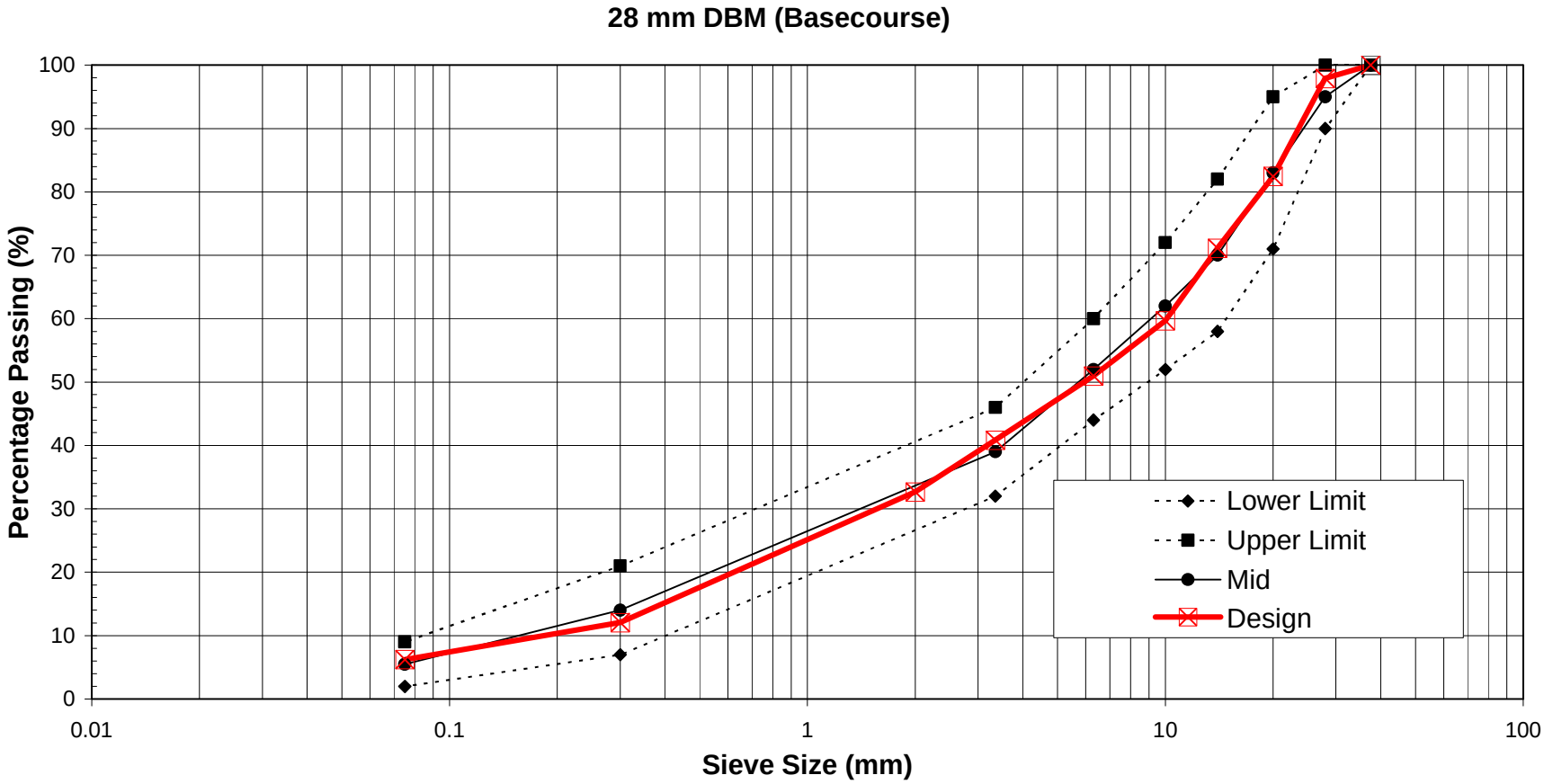

Baching for Grading: 28 mm Size Dense Roadbase 28mm DBM BS 4987 Part1

Material	Percentage	37.5 mm	28 mm	20 mm	14 mm	10 mm	6.3 mm	3.35 mm	2mm	0.3 mm	0.075 mm
40mm	0	100	100	0	0	0	0	0	0	0	0
28mm	19	100	89	14	6	2	2	2	2	0	0
20mm	11	100	100	88.9	9.6	2.8	2.8	2	2	2	1.5
14mm	11	100	100	100	90.3	8.7	2.7	2.2	2.2	2.2	1.5
10mm	11	100	100	100	99.9	91.1	24.3	3.7	2.6	2.6	2
6mm	10	100	100	100	100	100	93	18	8	1	1
Dust	38	100	100	100	100	100	100	99.4	80.9	29.5	14.7
Sand	0	100	100	100	100	100	100	100	100	66.24	1.92
Filler	0	100	100	100	100	100	100	99.81	99.81	99.2	95.93
Total	100										
Combined Grading		100.0	97.9	82.4	71.1	59.7	51.0	40.8	32.7	12.1	6.2

Gyratory Compacted Specimens

Diameter	***D* = 150 mm**					***D* = 100 mm**		
Height	Before trimming *h* = 100 mm		After trimming *h* = 60 mm			After trimming *h* = 60 mm		
Parameters.	Density (kg/m^3)	Air Voids (%)	Density (kg/m^3)	Air Voids (%)	Stiffness (MPa)	Density (kg/m^3)	Air Voids (%)	Stiffness (MPa)
05-1722	2381.2	4.8	2410.9	3.6	6505	2405.1	3.8	6540
05-1723	2413.6	3.5	2437.2	2.5	7148	2443.5	2.3	6449
05-1724	2408.7	3.7	2428.4	2.9	6700	2426.8	2.9	5987
05-1725	2364.9	5.4	2380.9	4.8	5563	2373.8	5.0	5151
05-1791	2409.2	3.5	2446.2	2.2	7814	2464.1	1.4	7150
05-1792	2407.3	3.7	2437.0	2.5	6766	2435.1	2.6	6358
05-1793	2426.9	2.9	2456.0	1.8	6780	2466.5	1.3	6159
05-1794	2404.4	3.8	2437.5	2.5	7472	2456.5	1.7	6892
05-1795	2399.0	4.0	2438.3	2.5	6308	2445.5	2.2	5530
05-1796	2410.2	3.6	2437.3	2.5	6951	2435.8	2.6	6946
05-1797	2400.4	4.0	2432.8	2.7	6614	2447.3	2.1	5845
05-1798	2410.5	3.6	2437.4	2.5	6809	2451.7	1.9	6639
Average	2403.025	3.88	2431.7	2.75	6785.83	2437.6	2.48	6303.8
StDv	16.05	0.65	19.13	0.77	566.23	26.18	1.05	597.43

Vibratory Compacted Specimens

Diameter	***D* = 150 mm**					***D* = 100 mm**		
Height	Before trimming *h* = 100 mm		After trimming *h* = 60 mm			After trimming *h* = 60 mm		
Parameters.	Density (kg/m^3)	Air Voids (%)	Density (kg/m^3)	Air Voids (%)	Stiffness (MPa)	Density (kg/m^3)	Air Voids (%)	Stiffness (MPa)
05-1930	2373.0	5.1	2361.5	5.5	7535	2383.8	4.6	8227.0
05-1931	2440.1	2.4	2440.2	2.4	7851	2447.3	2.1	7418.0
05-1932	2448.3	2.1	2454.3	1.8	8183	2471.2	1.2	7899.0
05-1933	2443.3	2.3	2450.6	2.0	7753	2446.6	2.1	7225.0
05-1934	2445.3	2.2	2449.4	2.0	8129	2460.0	1.6	8127.0
05-1935	2432.6	2.7	2438.2	2.5	9338	2449.8	2.0	8278.0
05-1936	2427.7	2.9	2429.4	2.8	7106	2430.2	2.8	6620.0
05-1937	2433.2	2.7	2431.3	2.7	8105	2438.7	2.5	7491.0
05-1938	2408.6	3.7	2406.3	3.7	7532	2422.6	3.1	6268.0
05-1939	2402.6	3.9	2390.5	4.4	8702	2408.3	3.7	7655.0
05-1940	2407.3	3.7	2401.3	3.9	7343	2413.1	3.5	7071.0
05-1941	2403.9	3.8	2401.1	4.0	8927	2426.8	2.9	6939.0
Average	2422.2	3.13	2421.2	3.14	8042.0	2433.2	2.68	7434.8
StDv	22.9	0.9	28.8	1.1	669.6	24.3	1.0	641.9

Slab specimens Z direction

Diameter	***D* = 100 mm**				
Height	After trimming *h* = 60 mm				
Parameters.	Density (kg/m^3)	Air Voids (%)	Stiffness (MPa)	Axial Strain (%)	e* (%/Cycles)
05-2103-A	2420.8	3.2	5852.0	1.3546	8.68E-05
05-2104-B	2431.5	2.7	6987.0	1.7034	1.40E-04
05-2105-C	2441.4	2.3	6475.0	1.7993	1.57E-04
05-2106-D	2454.6	1.8	7548.0	2.5582	2.41E-04
05-2107-A	2406.3	3.7	4948.0	1.2894	7.87E-05
05-2108-B	2413.8	3.4	5886.0	1.2209	7.39E-05
05-2109-C	2429.9	2.8	6552.0	1.8712	1.38E-04
05-2110-D	2441.7	2.3	7334.0	1.2677	9.10E-05
05-2111-A	2428.5	2.9	6534.0	1.0187	6.21E-05
05-2112-B	2426.4	2.9	6166.0	1.1935	6.85E-05
05-2113-C	2454.9	1.8	6927.0	1.6092	1.17E-04
05-2114-D	2452.8	1.9	7713.0	1.4117	1.01E-04
Average	2433.55	2.64	6576.8	1.52	1.13E-04
StDv	15.9	0.6	794.0	0.42	5.06E-05

Slab specimens Y direction

Diameter	***D* = 100 mm**				
Height	After trimming *h* = 60 mm				
Parameters.	Density (kg/m^3)	Air Voids (%)	Stiffness (MPa)	Axial Strain (%)	ε* (%/Cycles)
05-2083-A (top)	2417.3	3.3	5773.0	0.8621	9.06E-05
05-2084-A (mid)	2423.1	3.1	5498.0	1.0623	9.44E-05
05-2085-A (bot)	2438.9	2.4	5822.0	0.9747	7.13E-05
05-2086-B (top)	2427.1	2.9	6859.0	0.9029	6.40E-05
05-2087-B (mid)	2423.2	3.1	5355.0	1.0864	9.15E-05
05-2088-B (bot)	2431.1	2.8	5212.0	1.2057	1.12E-04
05-2089-A (top)	2428.9	2.8	5871.0	1.2982	1.45E-04
05-2090-A (mid)	2441.2	2.4	5785.0	0.9967	8.82E-05
05-2091-A (bot)	2414.7	3.4	5523.0	0.8080	5.44E-05
05-2092-B (top)	2424.6	3.0	6198.0	1.3896	1.56E-04
05-2093-B (mid)	2449.2	2.0	6096.0	1.0644	8.84E-05
05-2094-B (bot)	2424.0	3.0	6429.0	0.8711	5.31E-05
Average	2428.6	2.85	5868.4	1.04	9.24E-05
StDv	10.1	0.4	469.5	0.18	3.22E-05

Slab specimens X direction

Diameter	***D* = 100 mm**				
Height	After trimming *h* = 60 mm				
Parameters.	Density (kg/m^3)	Air Voids (%)	Stiffness (MPa)	Axial Strain (%)	ε* (%/Cycles)
05-2115-A (left)	2434.5	2.6	4955.0	1.1141	8.93E-05
05-2116-A (mid)	2438.6	2.5	4347.0	1.3794	1.18E-04
05-2117-A (right)	2422.0	3.1	4978.0	0.9971	8.16E-05
05-2118-B (left)	2430.5	2.8	5258.0	1.1435	9.56E-05
05-2119-B (mid)	2434.7	2.6	4617.0	1.0608	9.42E-05
05-2120-B (right)	2411.8	3.5	5131.0	0.9704	8.94E-05
05-2121-A (left)	2427.7	2.9	5150.0	1.0821	9.26E-05
05-2122-A (mid)	2435.9	2.6	4860.0	1.1255	9.38E-05
05-2123-A (right)	2445.0	2.2	5324.0	1.0431	7.14E-05
05-2124-B (left)	2398.1	4.1	5372.0	1.5150	1.18E-04
05-2125-B (mid)	2407.6	3.7	4692.0	1.3605	1.18E-04
05-2126-B (right)	2426.7	2.9	4651.0	1.0282	8.32E-05
Average	2426.1	2.96	4944.6	1.15	9.54E-05
StDv	13.9	0.6	319.7	0.17	1.51E-05

APPENDIX-B

Image analysis summary
Figures of averaged particle orientation for gyratory, vibratory and slab compacted specimens
(150mm, 100 mm and computer trimmed 100mm diameter specimens)

Gyratory compacted specimens (*D* = 150 mm)

All average

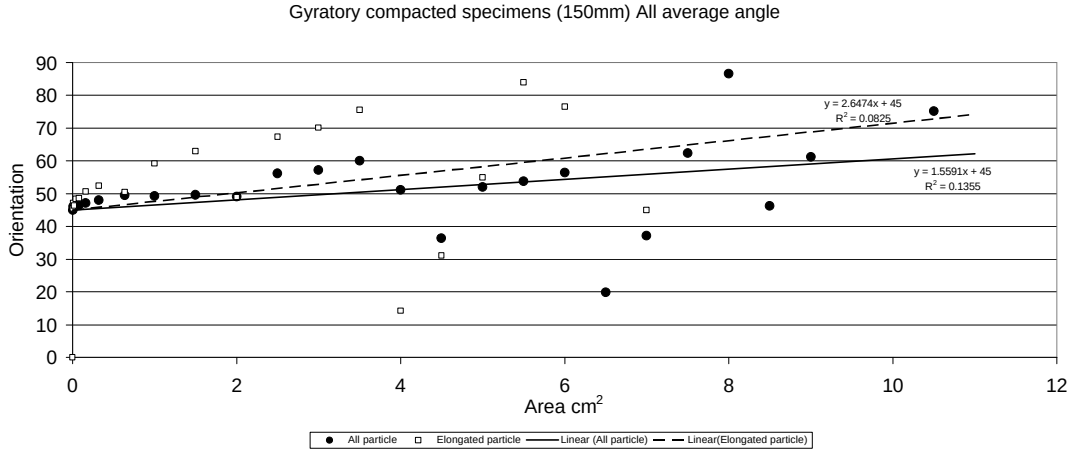

Top average

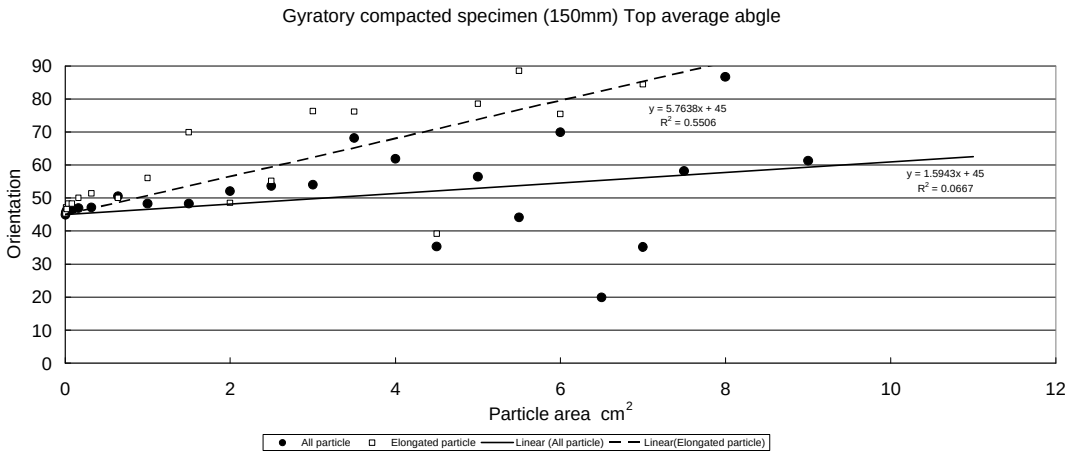

Bottom average

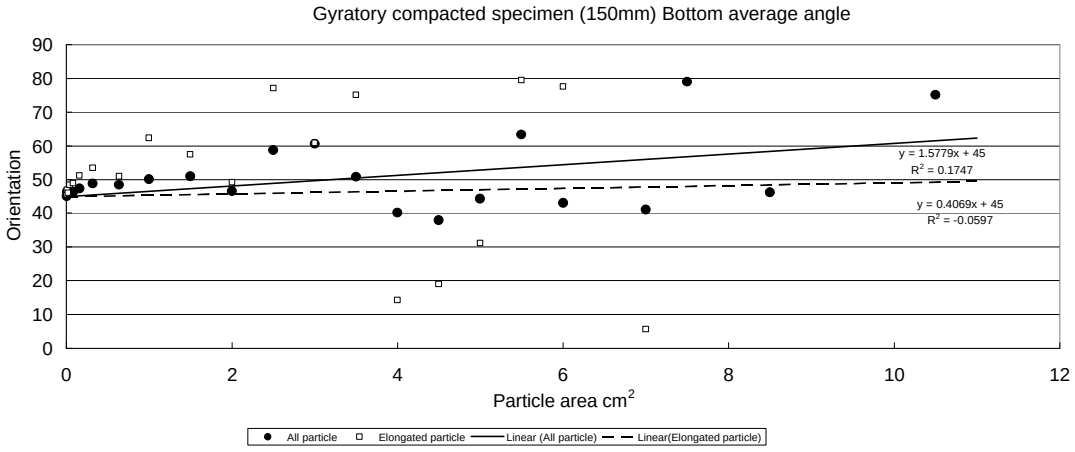

Gyratory compacted specimens (*D* = 100 mm)

All average

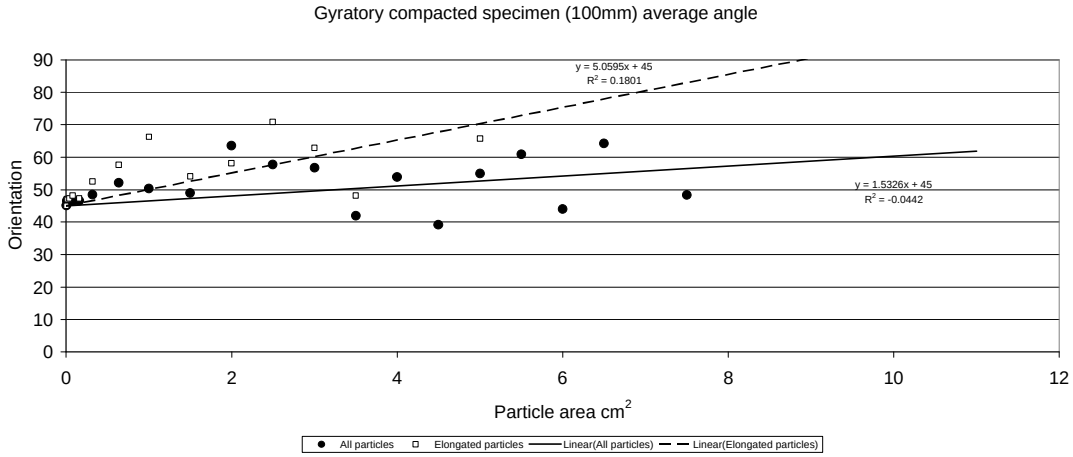

Top average

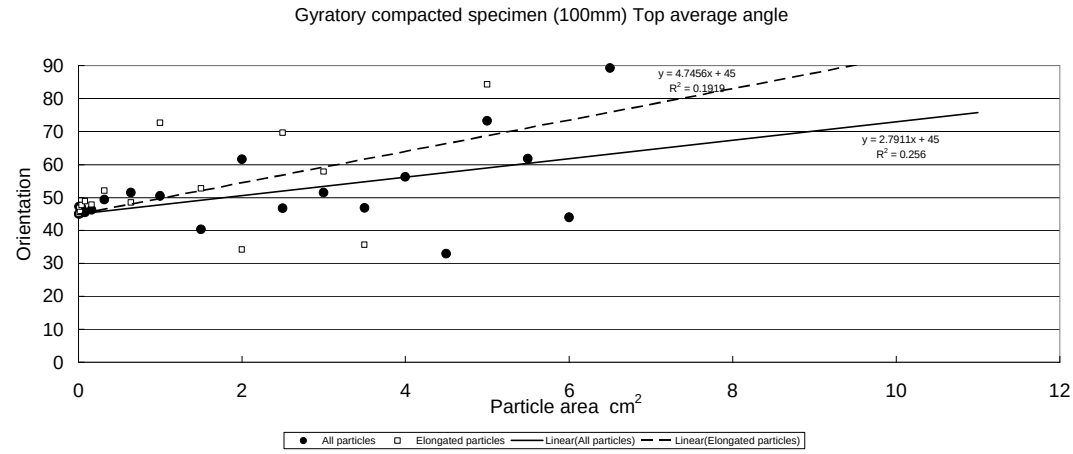

Bottom average

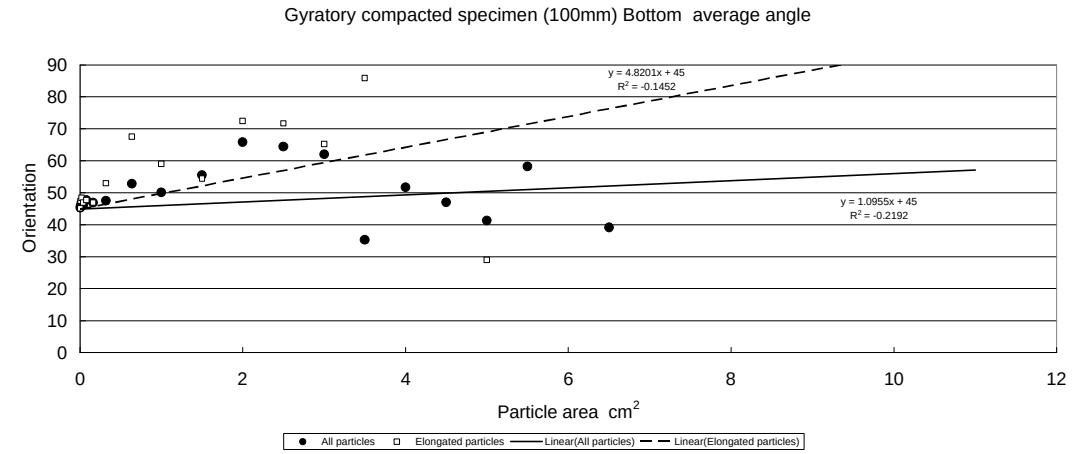

Gyratory compacted specimens (Computer trimmed *D* = 100 mm)

All average

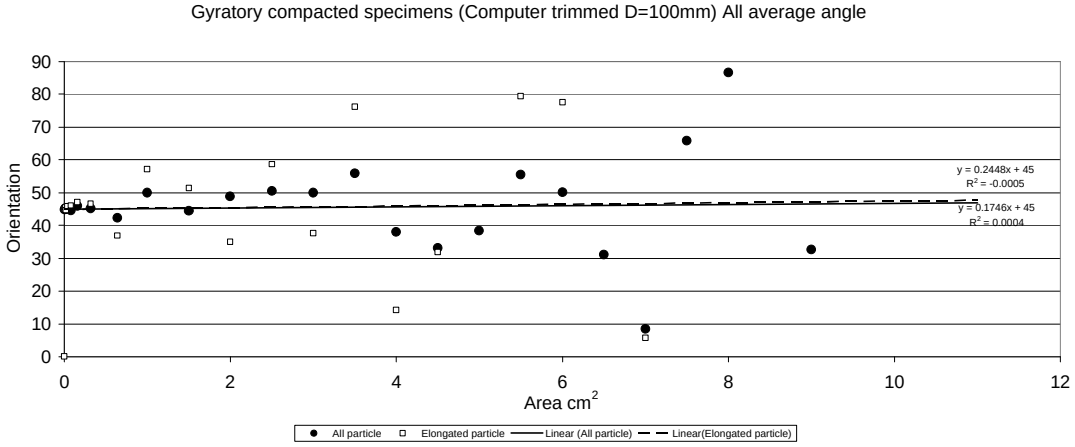

Top average

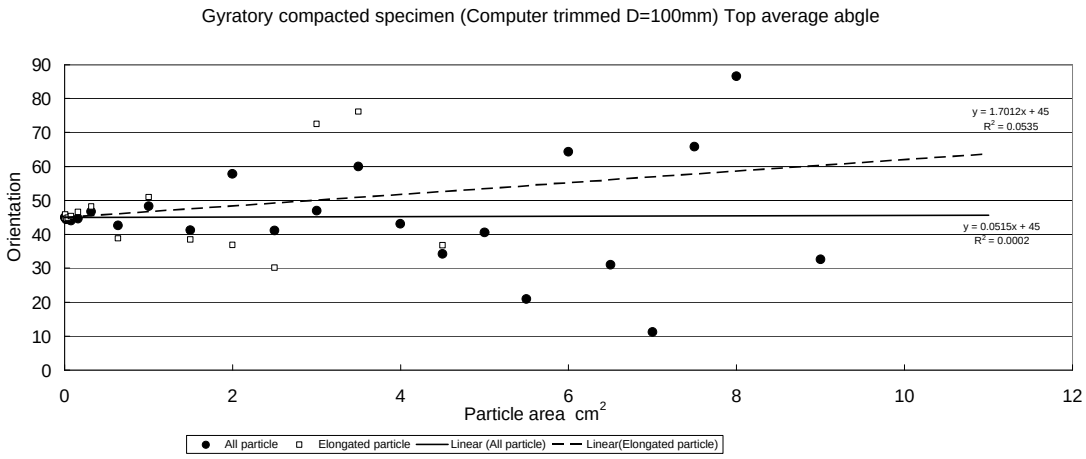

Bottom average

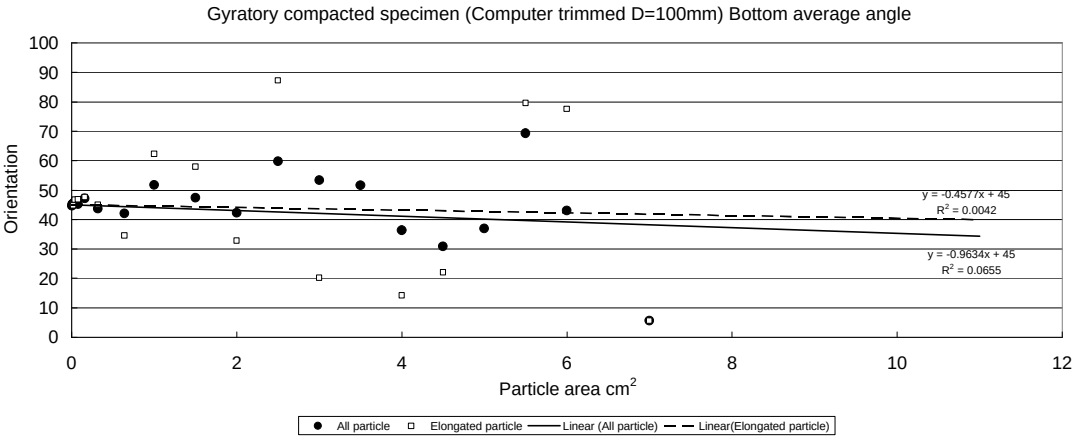

Vibratory compacted specimens (*D* = 150 mm)

All average

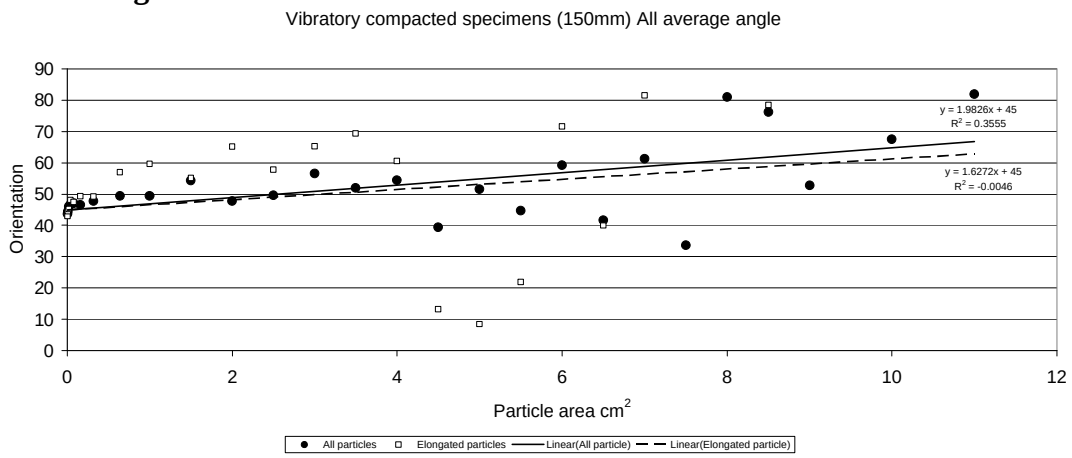

Top average

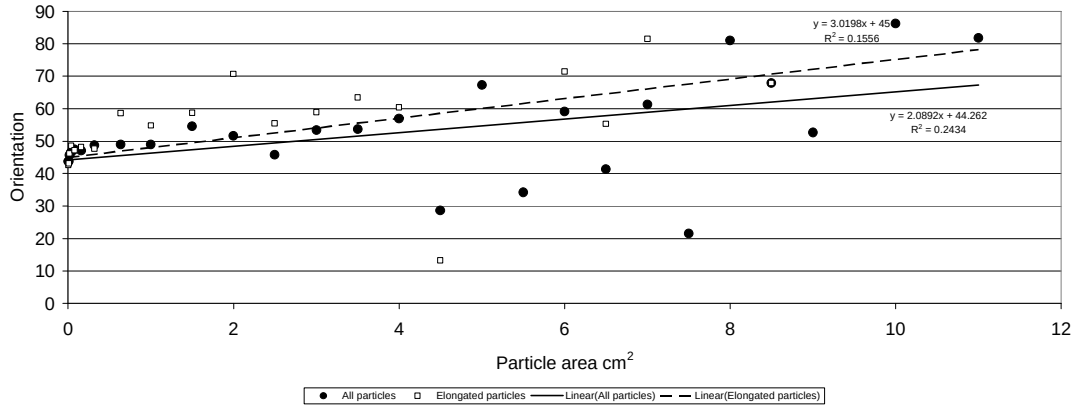

Bottom average

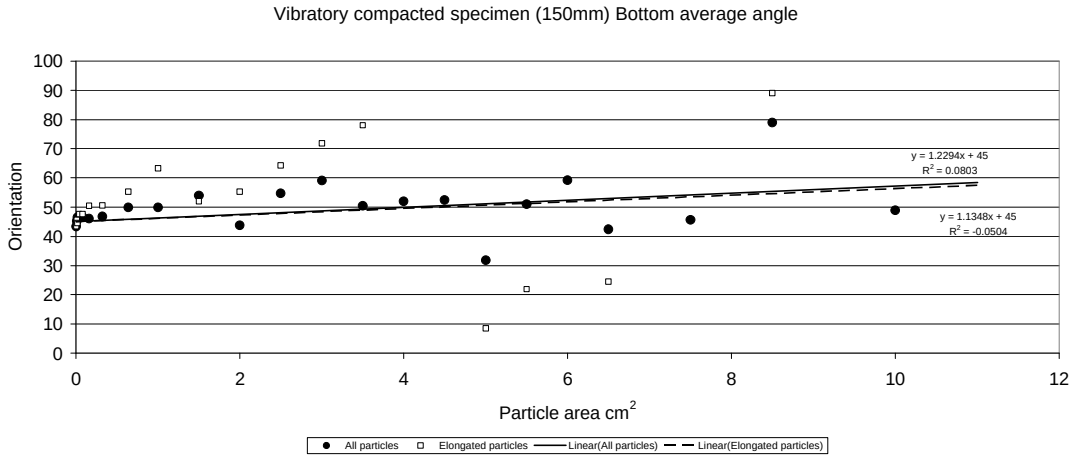

Vibratory compacted specimens (*D* = 100 mm)

All average

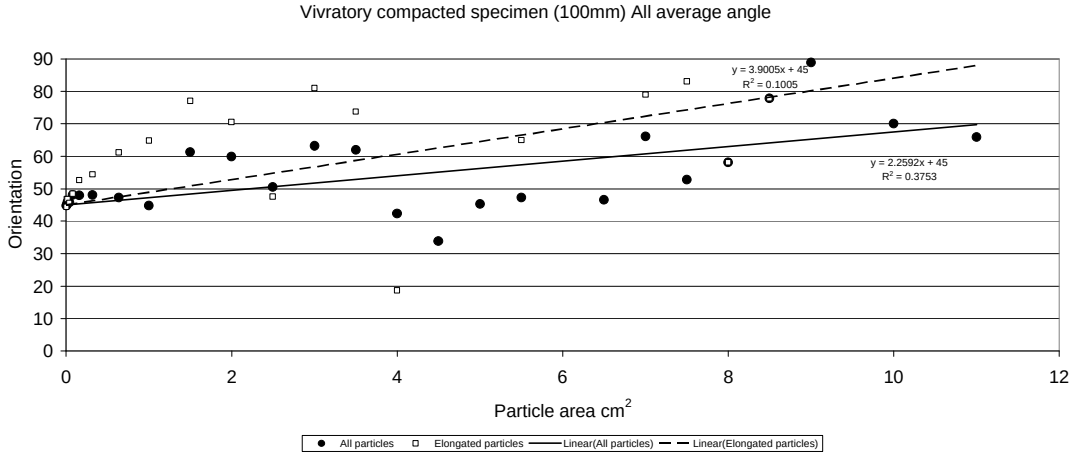

Top average

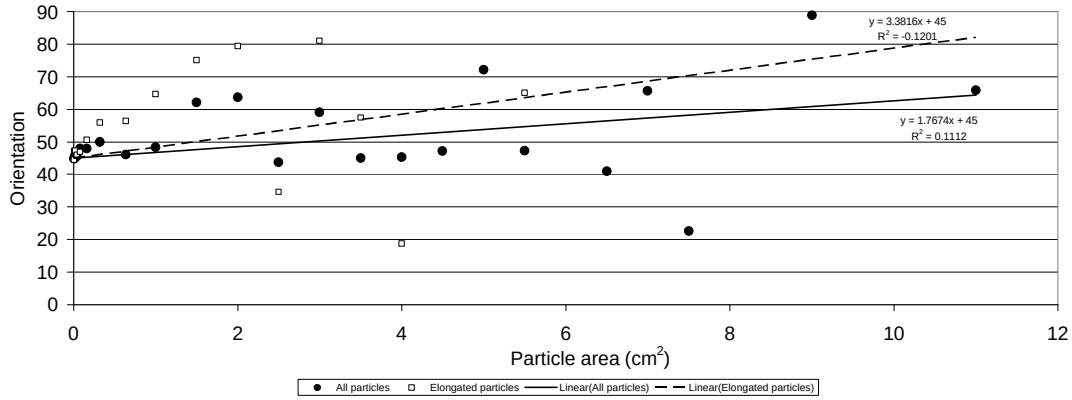

Bottom average

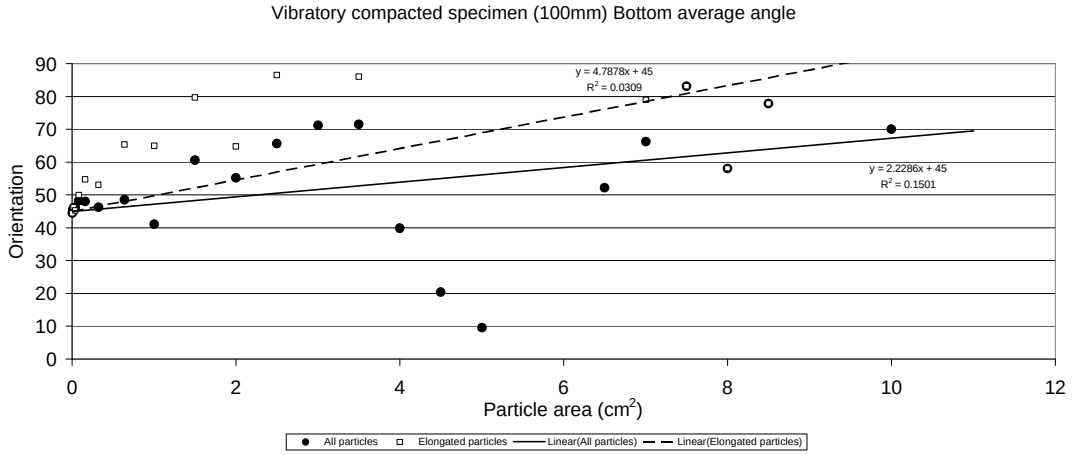

Vibratory compacted specimens (Computer trimmed *D* = 100 mm)

All average

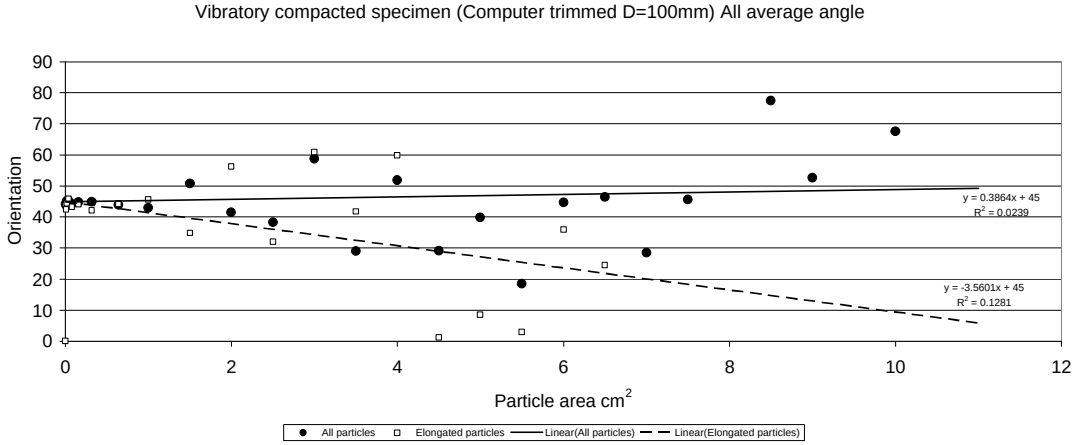

Top average

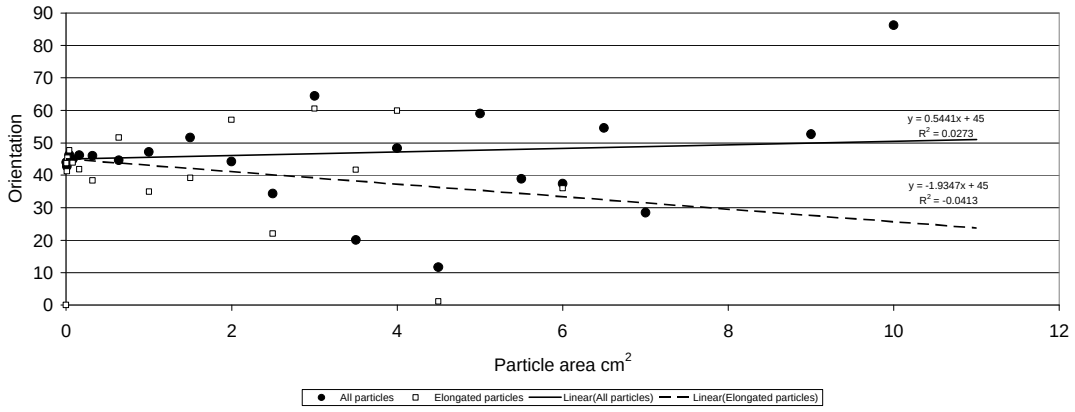

Bottom average

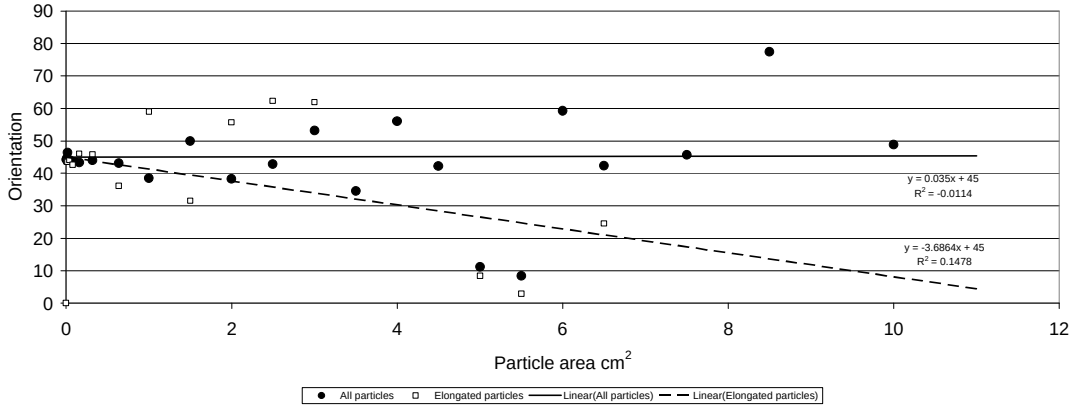

Slab compacted specimens (Z-direction *D* = 100 mm)

All average

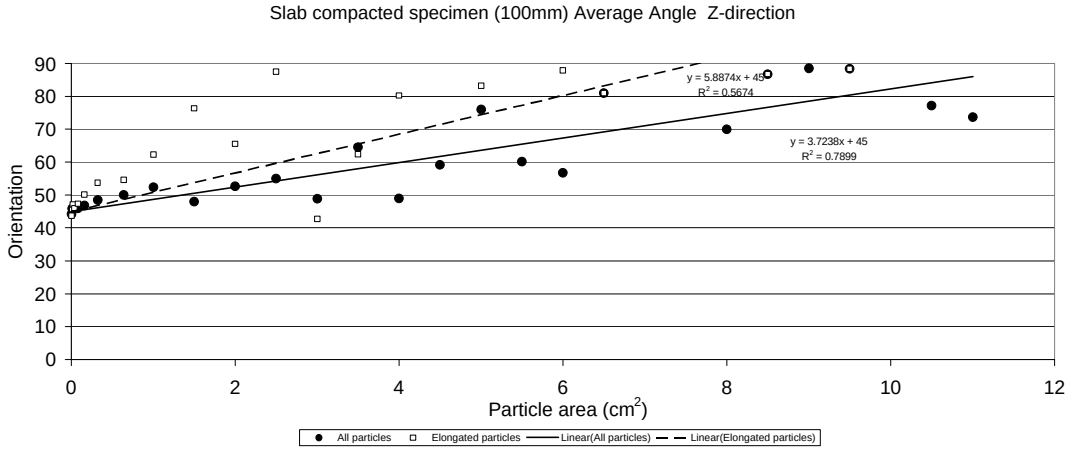

Top average

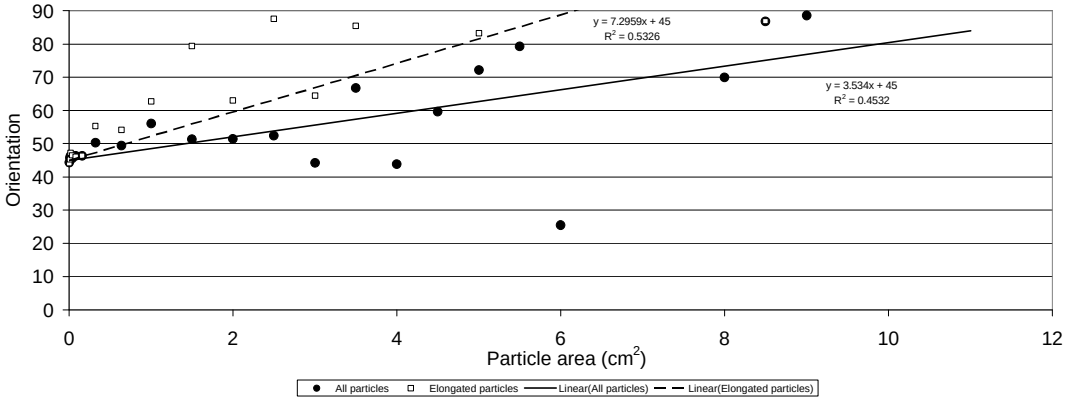

Bottom average

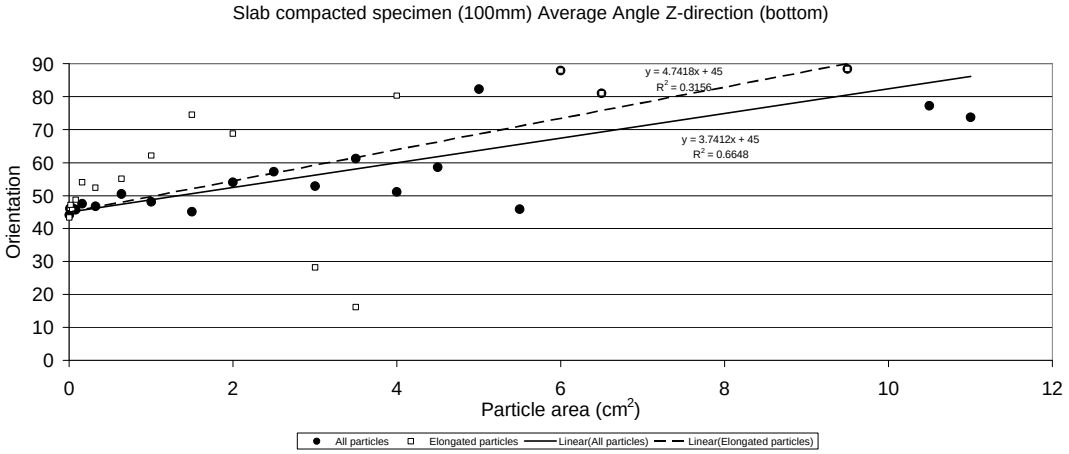

Slab compacted specimens (Y-direction *D* = 100 mm)

All average

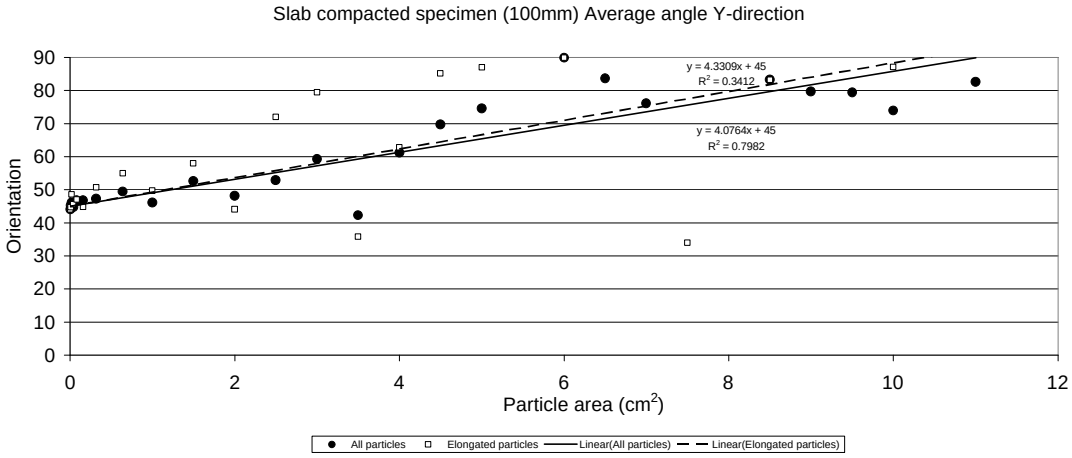

Top average

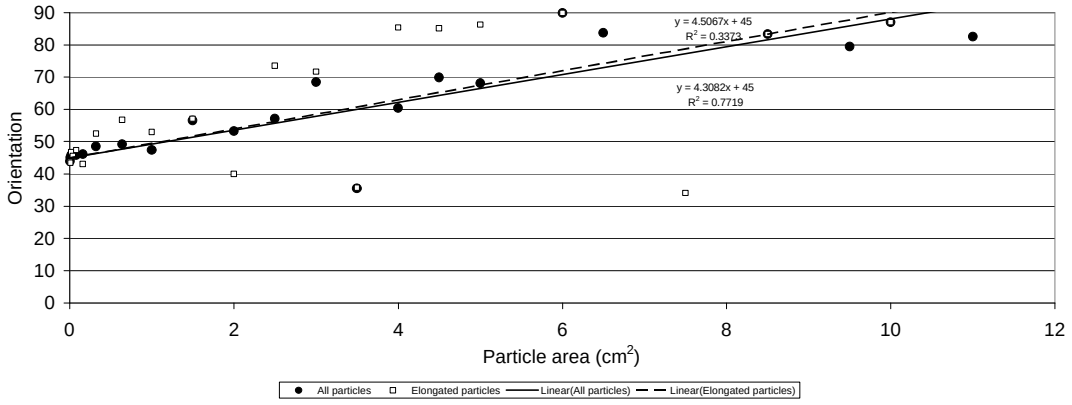

Bottom average

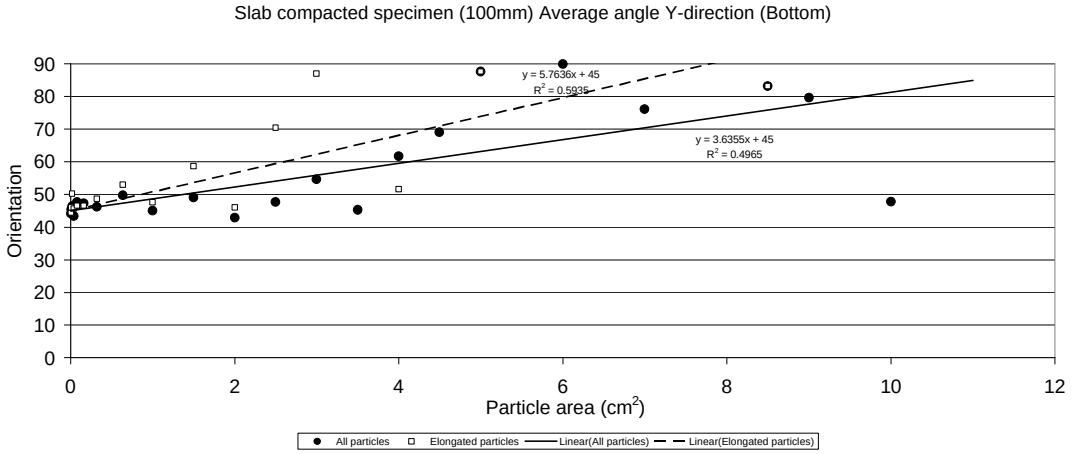

Slab compacted specimens (X-direction *D* = 100 mm)

All average

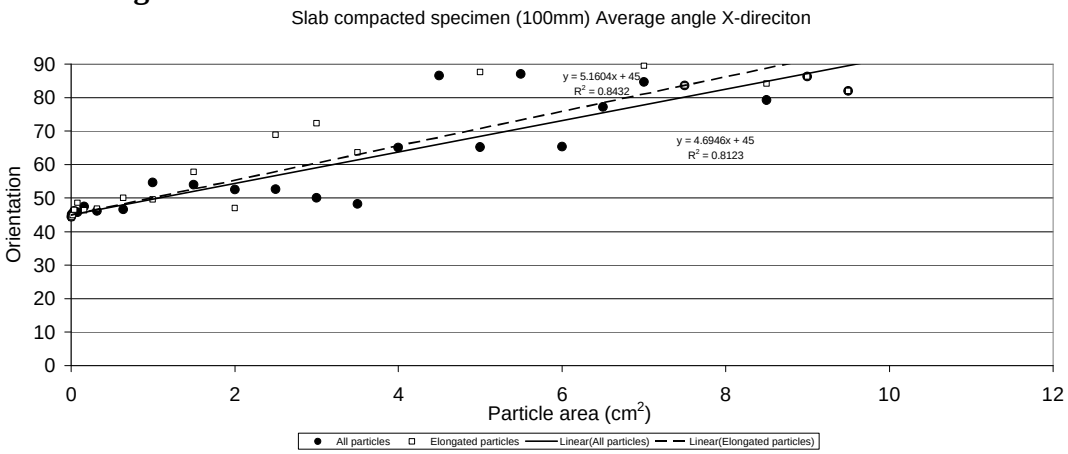

Top average

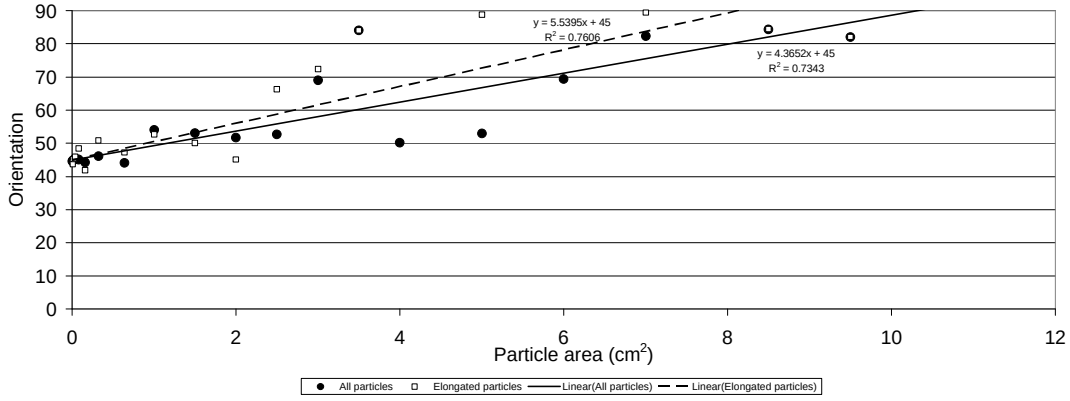

Bottom average

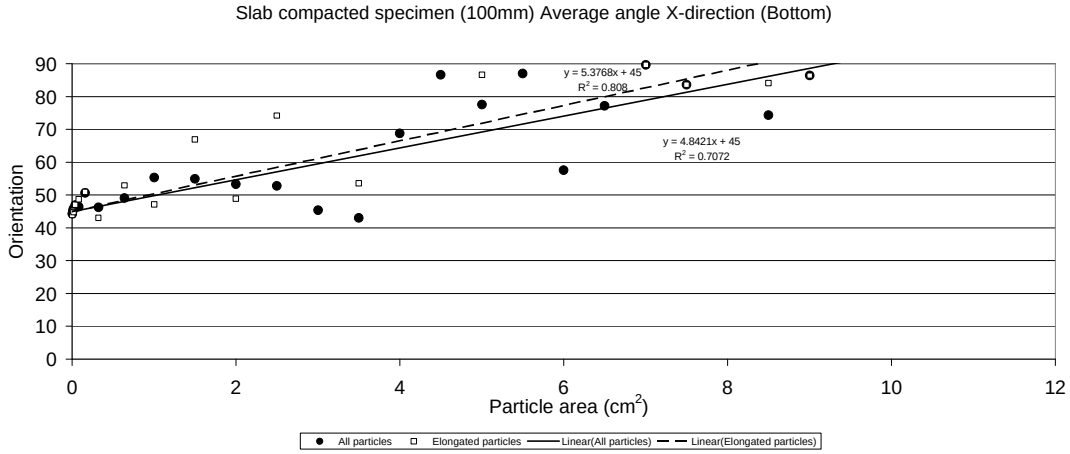

APPENDIX-C

Details of ITSM test results
Gyratory, vibratory and slab compacted specimens
(150 mm and 100 mm diameter specimens)

ITSM test results for gyratory compacted specimens (*D* = 150 mm)

Sample I.D	Initial Test		Repeated Test		Mid Point
05-1722-15	1st	2nd	1st	2nd	
Stiffness (MPa)	6573	6437			
Differences (%)	2.1				
Mean (MPa)	6505				

Sample I.D	Initial Test		Repeated Test		Mid Point
05-1723-15	1st	2nd	1st	2nd	
Stiffness (MPa)	7235	7060			
Differences (%)	2.4				
Mean (MPa)	7148				

Sample I.D	Initial Test		Repeated Test		Mid Point
05-1724-15	1st	2nd	1st	2nd	
Stiffness (MPa)	6857	6543			
Differences (%)	4.6				
Mean (MPa)	6700				

Sample I.D	Initial Test		Repeated Test		Mid Point
05-1725-15	1st	2nd	1st	2nd	
Stiffness (MPa)	6194	4376	5702	5423	
Differences (%)	29.4		4.9		
Mean (MPa)	5285		5563		

Sample I.D	Initial Test		Repeated Test		Mid Point
05-1791-15	1st	2nd	1st	2nd	
Stiffness (MPa)	7873	7754			
Differences (%)	1.5				
Mean (MPa)	7813.5				

Sample I.D	Initial Test		Repeated Test		Mid Point
05-1792-15	1st	2nd	1st	2nd	
Stiffness (MPa)	7056	6476			
Differences (%)	8.2				
Mean (MPa)	6766				

Sample I.D	Initial Test		Repeated Test		Mid Point
05-1793-15	1st	2nd	1st	2nd	
Stiffness (MPa)	6908	6651			
Differences (%)	3.7				
Mean (MPa)	6780				

Sample I.D	Initial Test		Repeated Test		Mid Point
05-1794-15	1st	2nd	1st	2nd	
Stiffness (MPa)	7424	7520			
Differences (%)	-1.3				
Mean (MPa)	7472				

Sample I.D	Initial Test		Repeated Test		Mid Point
05-1795-15	1st	2nd	1st	2nd	
Stiffness (MPa)	6316	6299			
Differences (%)	0.3				
Mean (MPa)	6308				

Sample I.D	Initial Test		Repeated Test		Mid Point
05-1796-15	1st	2nd	1st	2nd	
Stiffness (MPa)	7044	6858			
Differences (%)	2.6				
Mean (MPa)	6951				

Sample I.D	Initial Test		Repeated Test		Mid Point
05-1797-15	1st	2nd	1st	2nd	
Stiffness (MPa)	6812	6416			
Differences (%)	5.8				
Mean (MPa)	6614				

Sample I.D	Initial Test		Repeated Test		Mid Point
05-1798-15	1st	2nd	1st	2nd	
Stiffness (MPa)	7604	6691	7150	6468	
Differences (%)	12		9.5		
Mean (MPa)	7147.5		6809		

ITSM test results for gyratory compacted specimens (*D* = 100 mm)

Sample I.D	Initial Test		Repeated Test		Mid Point
05-1722-10	1st	2nd	1st	2nd	
Stiffness (MPa)	6417	6662			
Differences (%)	-3.8				
Mean (MPa)	6540				

Sample I.D	Initial Test		Repeated Test		Mid Point
05-1723-10	1st	2nd	1st	2nd	
Stiffness (MPa)	6471	6427			
Differences (%)	0.7				
Mean (MPa)	6449				

Sample I.D	Initial Test		Repeated Test		Mid Point
05-1724-10	1st	2nd	1st	2nd	
Stiffness (MPa)	6085	5888			
Differences (%)	3.2				
Mean (MPa)	5987				

Sample I.D	Initial Test		Repeated Test		Mid Point
05-1725-10	1st	2nd	1st	2nd	
Stiffness (MPa)	5838	5230	5274	5028	
Differences (%)	10.4		4.7		
Mean (MPa)	5534		5151		

Sample I.D	Initial Test		Repeated Test		Mid Point
05-1791-10	1st	2nd	1st	2nd	
Stiffness (MPa)	7143	7156			
Differences (%)	-0.18				
Mean (MPa)	7150				

Sample I.D	Initial Test		Repeated Test		Mid Point
05-1792-10	1st	2nd	1st	2nd	
Stiffness (MPa)	6485	6230			
Differences (%)	3.9				
Mean (MPa)	6358				

Sample I.D	Initial Test		Repeated Test		Mid Point
05-1793-10	1st	2nd	1st	2nd	
Stiffness (MPa)	6090	6227			
Differences (%)	-2.2				
Mean (MPa)	6159				

Sample I.D	Initial Test		Repeated Test		Mid Point
05-1794-10	1st	2nd	1st	2nd	
Stiffness (MPa)	7245	6538			
Differences (%)	9.8				
Mean (MPa)	6892				

Sample I.D	Initial Test		Repeated Test		Mid Point
05-1795-10	1st	2nd	1st	2nd	
Stiffness (MPa)	5437	5623			
Differences (%)	-3.4				
Mean (MPa)	5530				

Sample I.D	Initial Test		Repeated Test		Mid Point
05-1796-10	1st	2nd	1st	2nd	
Stiffness (MPa)	7068	6823			
Differences (%)	3.5				
Mean (MPa)	6946				

Sample I.D	Initial Test		Repeated Test		Mid Point
05-1797-10	1st	2nd	1st	2nd	
Stiffness (MPa)	6092	5471	6113	5577	
Differences (%)	10.1		8.8		
Mean (MPa)	5781.5		5845		

Sample I.D	Initial Test		Repeated Test		Mid Point
05-1798-10	1st	2nd	1st	2nd	
Stiffness (MPa)	6727	6550			
Differences (%)					
Mean (MPa)	6639				

ITSM test results for vibratory compacted specimens (*D* = 150 mm)

Sample I.D	Initial Test		Repeated Test		Mid Point
05-1930-15	1st	2nd	1st	2nd	
Stiffness (MPa)	7641	7429			
Differences (%)	2.8				
Mean (MPa)	7535				

Sample I.D	Initial Test		Repeated Test		Mid Point
05-1931-15	1st	2nd	1st	2nd	
Stiffness (MPa)	8889	7724	8214	7488	
Differences (%)	13.1		8.8		
Mean (MPa)	8306.5		7851		

Sample I.D	Initial Test		Repeated Test		Mid Point
05-1932-15	1st	2nd	1st	2nd	
Stiffness (MPa)	8490	7875			
Differences (%)	7.2				
Mean (MPa)	8183				

Sample I.D	Initial Test		Repeated Test		Mid Point
05-1933-15	1st	2nd	1st	2nd	
Stiffness (MPa)	7518	7987			
Differences (%)	-6.2				
Mean (MPa)	7753				

Sample I.D	Initial Test		Repeated Test		Mid Point
05-1934-15	1st	2nd	1st	2nd	
Stiffness (MPa)	9026	7487	8546	7711	
Differences (%)	17		9.8		
Mean (MPa)	8256.5		8129		

Sample I.D	Initial Test		Repeated Test		Mid Point
05-1935-15	1st	2nd	1st	2nd	
Stiffness (MPa)	9598	9078			
Differences (%)	5.4				
Mean (MPa)	9338				

Sample I.D	Initial Test		Repeated Test		Mid Point
05-1936-15	1st	2nd	1st	2nd	
Stiffness (MPa)	7225	6986			
Differences (%)	3.3				
Mean (MPa)	7106				

Sample I.D	Initial Test		Repeated Test		Mid Point
05-1937-15	1st	2nd	1st	2nd	
Stiffness (MPa)	7810	8399			
Differences (%)	-7.5				
Mean (MPa)	8105				

Sample I.D	Initial Test		Repeated Test		Mid Point
05-1938-15	1st	2nd	1st	2nd	
Stiffness (MPa)	8654	7731	8618	7075	7532
Differences (%)	10.7		17.9		N/A
Mean (MPa)	8192.5		7846.5		7532

Sample I.D	Initial Test		Repeated Test		Mid Point
05-1939-15	1st	2nd	1st	2nd	
Stiffness (MPa)	8778	8625			
Differences (%)	1.7				
Mean (MPa)	8702				

Sample I.D	Initial Test		Repeated Test		Mid Point
05-1940-15	1st	2nd	1st	2nd	
Stiffness (MPa)	8661	9861	7363	7323	
Differences (%)	-13.9		0.5		
Mean (MPa)	9261		7343		

Sample I.D	Initial Test		Repeated Test		Mid Point
05-1941-15	1st	2nd	1st	2nd	
Stiffness (MPa)	9189	8664			
Differences (%)	5.7				
Mean (MPa)	8927				

ITSM test results for vibratory compacted specimens (*D* = 100 mm)

Sample I.D	Initial Test		Repeated Test		Mid Point
05-1930-10	1st	2nd	1st	2nd	
Stiffness (MPa)	8302	8152			
Differences (%)	1.8				
Mean (MPa)	8227				

Sample I.D	Initial Test		Repeated Test		Mid Point
05-1931-10	1st	2nd	1st	2nd	
Stiffness (MPa)	8115	7677	7522	7313	
Differences (%)	5.4		2.8		
Mean (MPa)	7896		7418		

Sample I.D	Initial Test		Repeated Test		Mid Point
05-1932-10	1st	2nd	1st	2nd	
Stiffness (MPa)	8057	7740			
Differences (%)	3.9				
Mean (MPa)	7899				

Sample I.D	Initial Test		Repeated Test		Mid Point
05-1933-10	1st	2nd	1st	2nd	
Stiffness (MPa)	7170	7280			
Differences (%)	-1.5				
Mean (MPa)	7225				

Sample I.D	Initial Test		Repeated Test		Mid Point
05-1934-10	1st	2nd	1st	2nd	
Stiffness (MPa)	7875	8379			
Differences (%)	-6.4				
Mean (MPa)	8127				

Sample I.D	Initial Test		Repeated Test		Mid Point
05-1935-10	1st	2nd	1st	2nd	
Stiffness (MPa)	8340	8215			
Differences (%)	1.5				
Mean (MPa)	8278				

Sample I.D	Initial Test		Repeated Test		Mid Point
05-1936-10	1st	2nd	1st	2nd	
Stiffness (MPa)	6807	6433			
Differences (%)	5.5				
Mean (MPa)	6620				

Sample I.D	Initial Test		Repeated Test		Mid Point
05-1937-10	1st	2nd	1st	2nd	
Stiffness (MPa)	7615	7367			
Differences (%)	3.3				
Mean (MPa)	7491				

Sample I.D	Initial Test		Repeated Test		Mid Point
05-1938-10	1st	2nd	1st	2nd	
Stiffness (MPa)	6313	6997	6313	6223	
Differences (%)	-7.3		1.4		
Mean (MPa)	6655		6268		

Sample I.D	Initial Test		Repeated Test		Mid Point
05-1939-10	1st	2nd	1st	2nd	
Stiffness (MPa)	8009	7300			
Differences (%)	8.9				
Mean (MPa)	7655				

Sample I.D	Initial Test		Repeated Test		Mid Point
05-1940-10	1st	2nd	1st	2nd	
Stiffness (MPa)	7089	7053			
Differences (%)	0.5				
Mean (MPa)	7071				

Sample I.D	Initial Test		Repeated Test		Mid Point
05-1941-10	1st	2nd	1st	2nd	
Stiffness (MPa)	7116	6761			
Differences (%)	5.0				
Mean (MPa)	6939				

ITSM test results for slab compacted specimens (*D* = 100 mm Z-direction)

Sample I.D	Initial Test		Repeated Test		Mid Point
05-2103A-10	1st	2nd	1st	2nd	
Stiffness (MPa)	6041	5663			
Differences (%)	6.3				
Mean (MPa)	5852				

Sample I.D	Initial Test		Repeated Test		Mid Point
05-2104B-10	1st	2nd	1st	2nd	
Stiffness (MPa)	7287	6686			
Differences (%)	8.2				
Mean (MPa)	6987				

Sample I.D	Initial Test		Repeated Test		Mid Point
05-2105C-10	1st	2nd	1st	2nd	
Stiffness (MPa)	6606	6343			
Differences (%)	4.0				
Mean (MPa)	6475				

Sample I.D	Initial Test		Repeated Test		Mid Point
05-2106D-10	1st	2nd	1st	2nd	
Stiffness (MPa)	7844	7252			
Differences (%)	7.5				
Mean (MPa)	7548				

Sample I.D	Initial Test		Repeated Test		Mid Point
05-2107A-10	1st	2nd	1st	2nd	
Stiffness (MPa)	5037	4859			
Differences (%)	3.5				
Mean (MPa)	4948				

Sample I.D	Initial Test		Repeated Test		Mid Point
05-2108B-10	1st	2nd	1st	2nd	
Stiffness (MPa)	6086	5686			
Differences (%)	6.6				
Mean (MPa)	5886				

Sample I.D	Initial Test		Repeated Test		Mid Point
05-2109C-10	1st	2nd	1st	2nd	
Stiffness (MPa)	6857	6247			
Differences (%)	8.9				
Mean (MPa)	6552				

Sample I.D	Initial Test		Repeated Test		Mid Point
05-2110D-10	1st	2nd	1st	2nd	
Stiffness (MPa)	7559	7109			
Differences (%)	6.0				
Mean (MPa)	7334				

Sample I.D	Initial Test		Repeated Test		Mid Point
05-2111A-10	1st	2nd	1st	2nd	
Stiffness (MPa)	6769	6298			
Differences (%)	7.0				
Mean (MPa)	6533.5				

Sample I.D	Initial Test		Repeated Test		Mid Point
05-2112B-10	1st	2nd	1st	2nd	
Stiffness (MPa)	6264	6067			
Differences (%)	3.1				
Mean (MPa)	6166				

Sample I.D	Initial Test		Repeated Test		Mid Point
05-2113C-10	1st	2nd	1st	2nd	
Stiffness (MPa)	7124	6730			
Differences (%)	5.5				
Mean (MPa)	6927				

Sample I.D	Initial Test		Repeated Test		Mid Point
05-2114D-10	1st	2nd	1st	2nd	
Stiffness (MPa)	7913	7513			
Differences (%)	5.1				
Mean (MPa)	7713				

ITSM test results for slab compacted specimens (*D* = 100 mm Y-direction)

Sample I.D	Initial Test		Repeated Test		Mid Point
05-2083A-10	1st	2nd	1st	2nd	
Stiffness (MPa)	5702	5844			
Differences (%)	-2.5				
Mean (MPa)	5773				

Sample I.D	Initial Test		Repeated Test		Mid Point
05-2084A-10	1st	2nd	1st	2nd	
Stiffness (MPa)	5722	5273			
Differences (%)	7.8				
Mean (MPa)	5498				

Sample I.D	Initial Test		Repeated Test		Mid Point
05-2085A-10	1st	2nd	1st	2nd	
Stiffness (MPa)	5991	5652			
Differences (%)	5.7				
Mean (MPa)	5822				

Sample I.D	Initial Test		Repeated Test		Mid Point
05-2086B-10	1st	2nd	1st	2nd	
Stiffness (MPa)	6996	6721			
Differences (%)	3.9				
Mean (MPa)	6859				

Sample I.D	Initial Test		Repeated Test		Mid Point
05-2087B-10	1st	2nd	1st	2nd	
Stiffness (MPa)	5265	5444			
Differences (%)	-0.03				
Mean (MPa)	5355				

Sample I.D	Initial Test		Repeated Test		Mid Point
05-2088B-10	1st	2nd	1st	2nd	
Stiffness (MPa)	5324	5099			
Differences (%)	4.2				
Mean (MPa)	5212				

Sample I.D	Initial Test		Repeated Test		Mid Point
05-2089A-10	1st	2nd	1st	2nd	
Stiffness (MPa)	5922	5819			
Differences (%)	1.7				
Mean (MPa)	5871				

Sample I.D	Initial Test		Repeated Test		Mid Point
05-2090A-10	1st	2nd	1st	2nd	
Stiffness (MPa)	5954	5616			
Differences (%)	5.7				
Mean (MPa)	5785				

Sample I.D	Initial Test		Repeated Test		Mid Point
05-2091A-10	1st	2nd	1st	2nd	
Stiffness (MPa)	5618	5427			
Differences (%)	3.4				
Mean (MPa)	5523				

Sample I.D	Initial Test		Repeated Test		Mid Point
05-2092B-10	1st	2nd	1st	2nd	
Stiffness (MPa)	6295	6101			
Differences (%)	3.1				
Mean (MPa)	6198				

Sample I.D	Initial Test		Repeated Test		Mid Point
05-2093B-10	1st	2nd	1st	2nd	
Stiffness (MPa)	6245	5946			
Differences (%)	4.8				
Mean (MPa)	6096				

Sample I.D	Initial Test		Repeated Test		Mid Point
05-2094B-10	1st	2nd	1st	2nd	
Stiffness (MPa)	6447	6411			
Differences (%)	0.6				
Mean (MPa)	6429				

ITSM test results for slab compacted specimens (*D* = 100 mm X-direction)

Sample I.D	Initial Test		Repeated Test		Mid Point
05-2115A-10	1st	2nd	1st	2nd	
Stiffness (MPa)	5091	4818			
Differences (%)	5.4				
Mean (MPa)	4955				

Sample I.D	Initial Test		Repeated Test		Mid Point
05-2116A-10	1st	2nd	1st	2nd	
Stiffness (MPa)	4545	4148			
Differences (%)	8.7				
Mean (MPa)	4347				

Sample I.D	Initial Test		Repeated Test		Mid Point
05-2117A-10	1st	2nd	1st	2nd	
Stiffness (MPa)	5222	4733			
Differences (%)	9.4				
Mean (MPa)	4978				

Sample I.D	Initial Test		Repeated Test		Mid Point
05-2118B-10	1st	2nd	1st	2nd	
Stiffness (MPa)	5497	5019			
Differences (%)	8.7				
Mean (MPa)	5258				

Sample I.D	Initial Test		Repeated Test		Mid Point
05-2119B-10	1st	2nd	1st	2nd	
Stiffness (MPa)	4816	4417			
Differences (%)	8.7				
Mean (MPa)	4617				

Sample I.D	Initial Test		Repeated Test		Mid Point
05-2120B-10	1st	2nd	1st	2nd	
Stiffness (MPa)	5136	5126			
Differences (%)	0.2				
Mean (MPa)	5131				

Sample I.D	Initial Test		Repeated Test		Mid Point
05-2121A-10	1st	2nd	1st	2nd	
Stiffness (MPa)	5147	5152			
Differences (%)	-0.1				
Mean (MPa)	5150				

Sample I.D	Initial Test		Repeated Test		Mid Point
05-2122A-10	1st	2nd	1st	2nd	
Stiffness (MPa)	5377	4765	5054	4665	
Differences (%)	11.4		7.7		
Mean (MPa)	5071		4860		

Sample I.D	Initial Test		Repeated Test		Mid Point
05-2123A-10	1st	2nd	1st	2nd	
Stiffness (MPa)	5409	5239			
Differences (%)	3.1				
Mean (MPa)	5324				

Sample I.D	Initial Test		Repeated Test		Mid Point
05-2124B-10	1st	2nd	1st	2nd	
Stiffness (MPa)	5545	5198			
Differences (%)	6.3				
Mean (MPa)	5372				

Sample I.D	Initial Test		Repeated Test		Mid Point
05-2125B-10	1st	2nd	1st	2nd	
Stiffness (MPa)	4850	4533			
Differences (%)	6.5				
Mean (MPa)	4692				

Sample I.D	Initial Test		Repeated Test		Mid Point
05-2126B-10	1st	2nd	1st	2nd	
Stiffness (MPa)	4858	4444			
Differences (%)	8.5				
Mean (MPa)	4651				

APPENDIX-D

VSA slope for all specimens (All particles orientation for 150 mm, 100 mm and computer trimmed 100 mm diameter specimens)

Gyratory compacted specimens (*D* = 150 mm All particles)

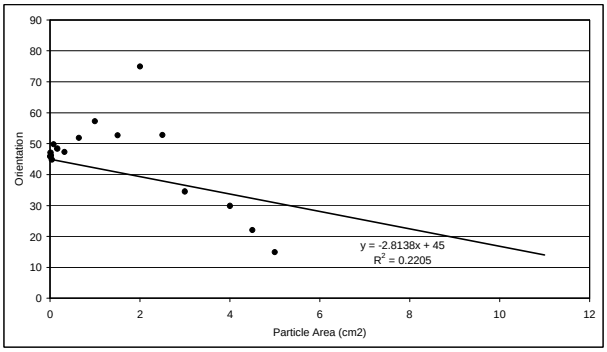

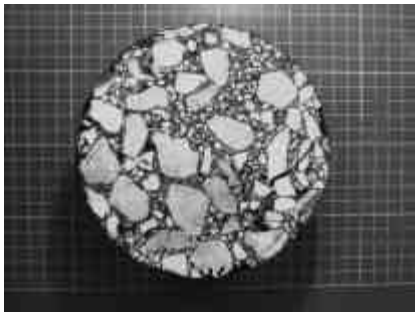

05-1722 Top

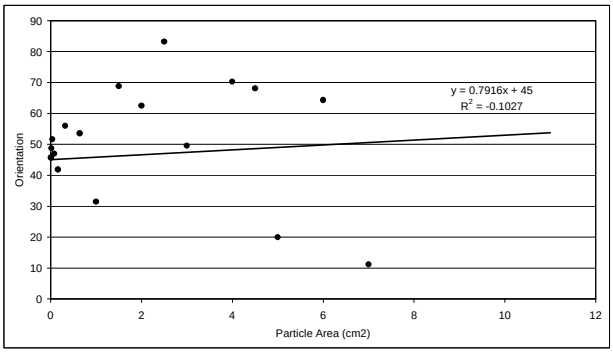

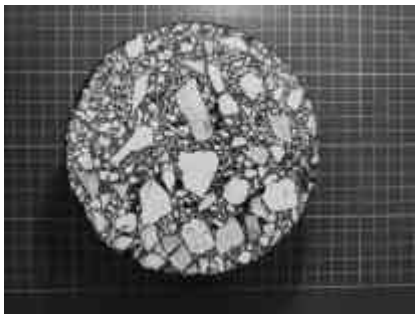

05-1722 Bottom

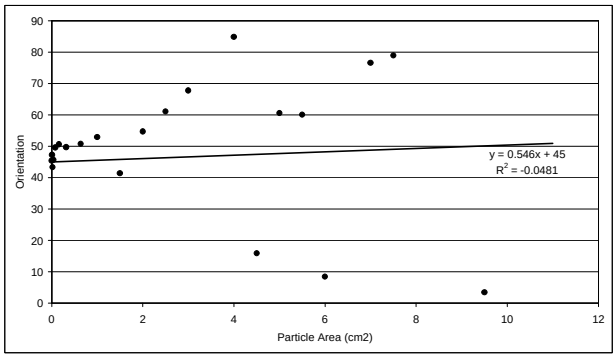

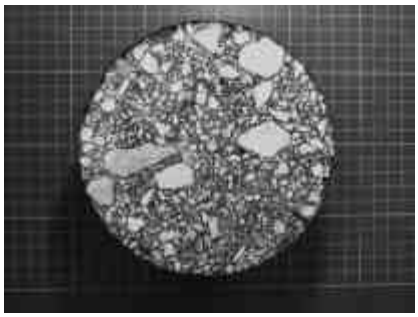

05-1723 Top

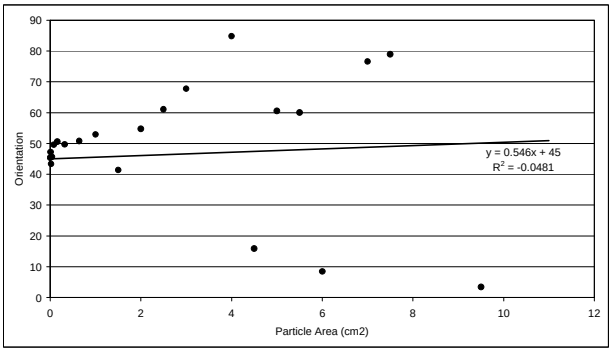

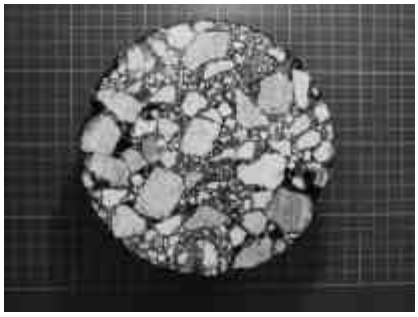

05-1723 Bottom

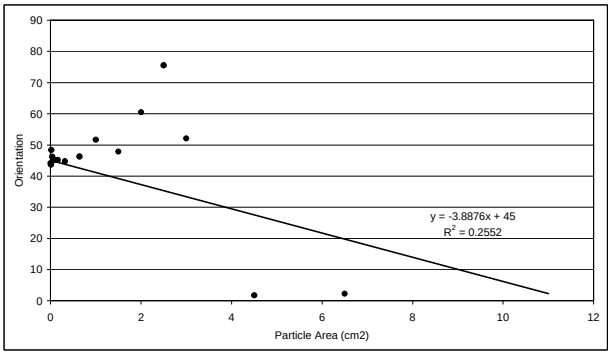

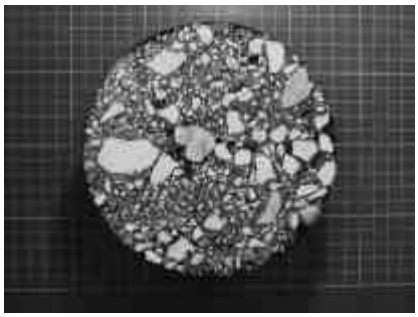

05-1724 Top

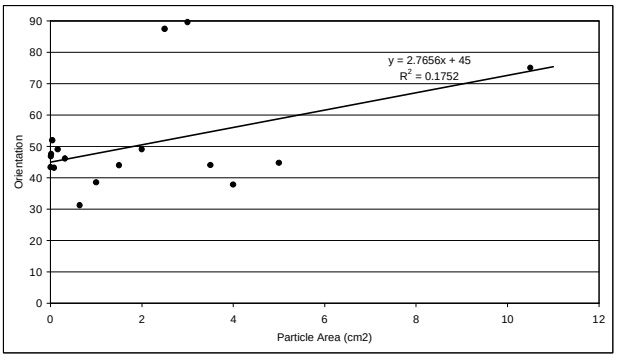

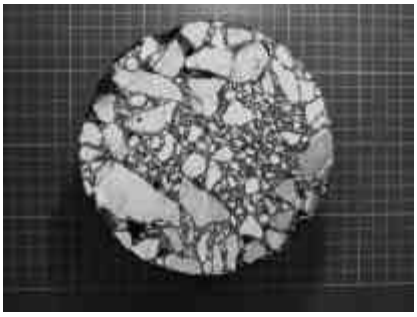

05-1724 Bottom

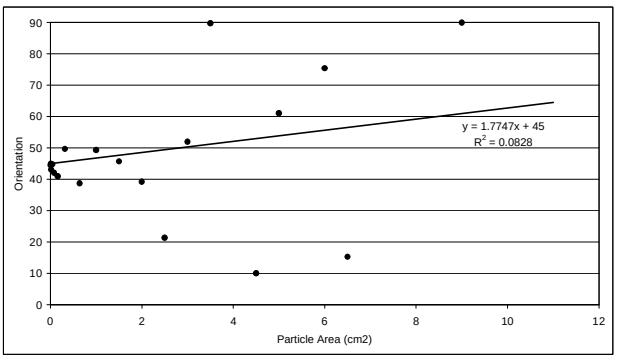

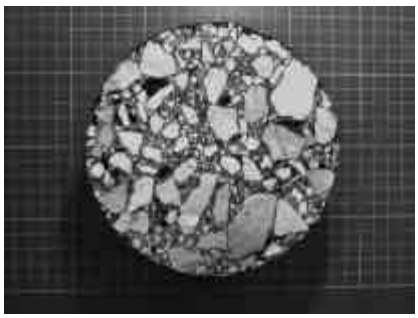

05-1725 Top

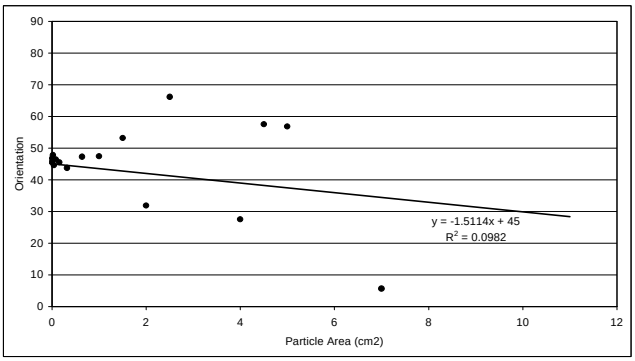

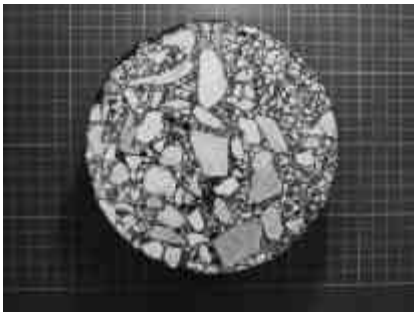

05-1725 Bottom

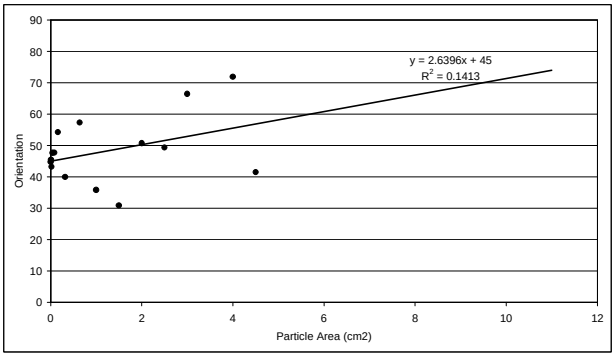

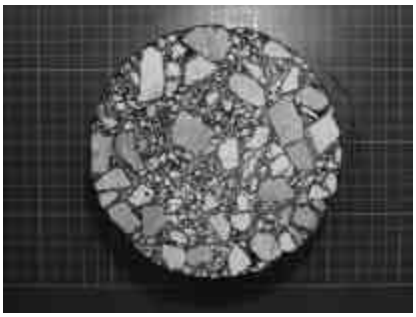

05-1791 Top

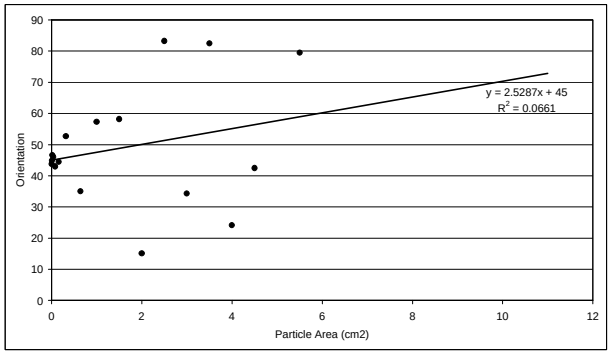

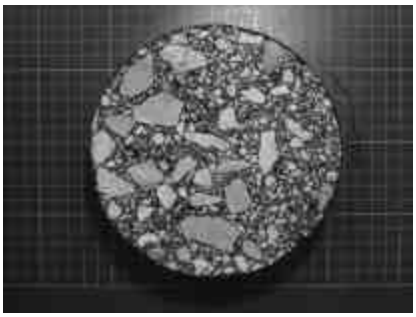

05-1791 Bottom

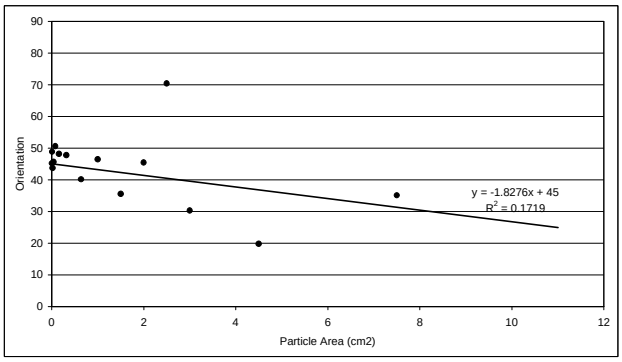

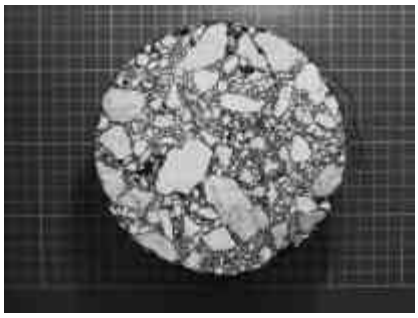

05-1792 Top

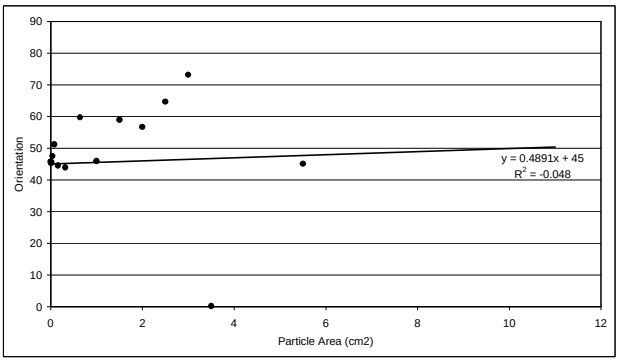

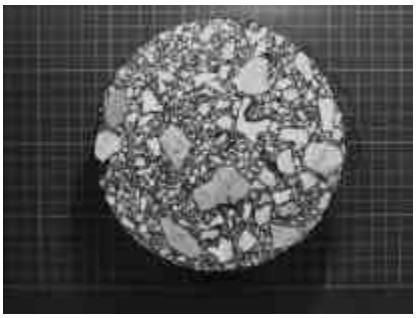

05-1792 Bottom

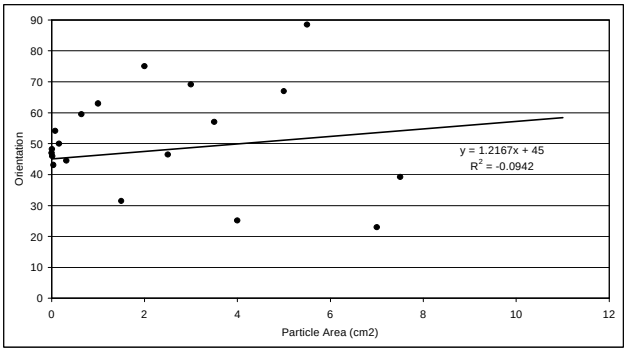

05-1794 Top

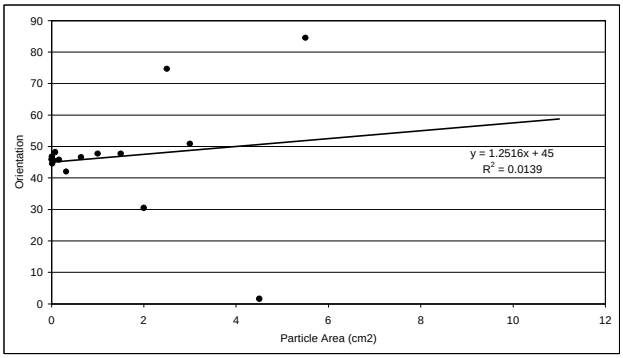

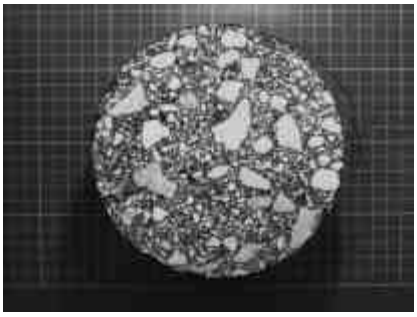

05-1794 Bottom

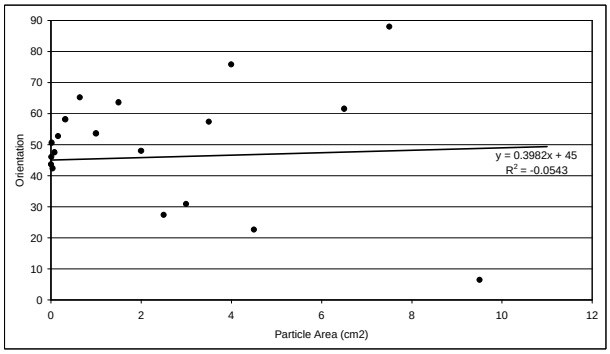

05-1795 Top

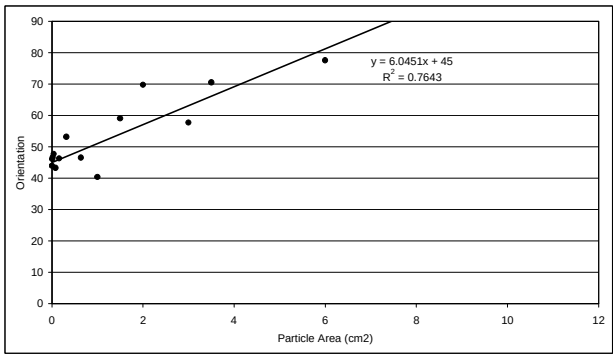

05-1795 Bottom

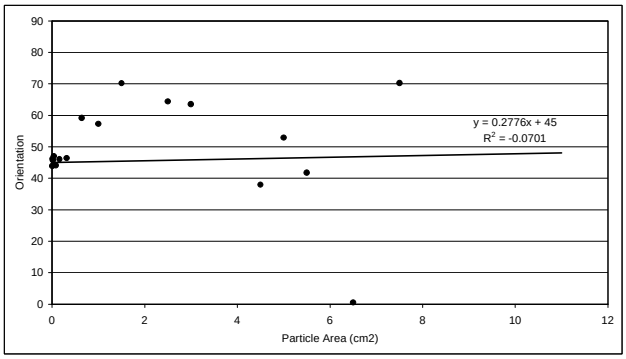

05-1796 Top

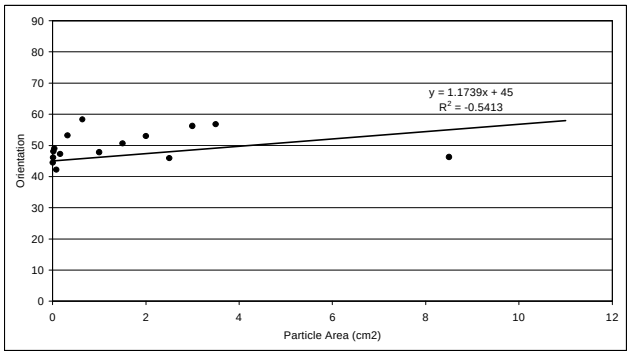

05-1796 Bottom

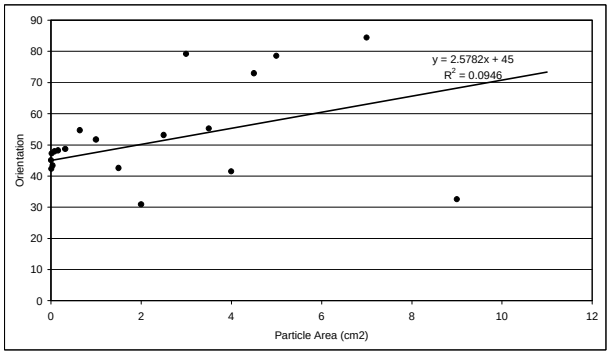

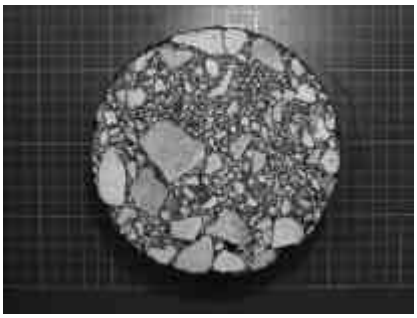

05-1797 Top

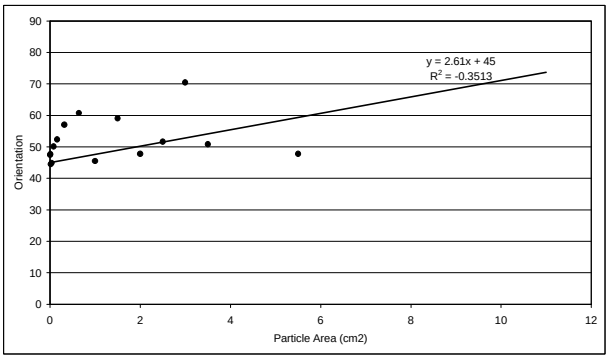

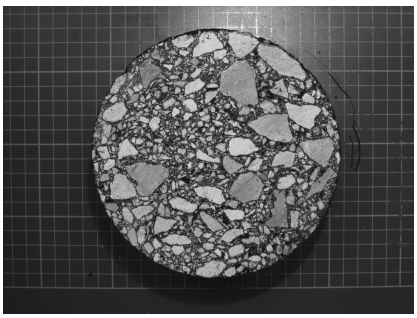

05-1797 Bottom

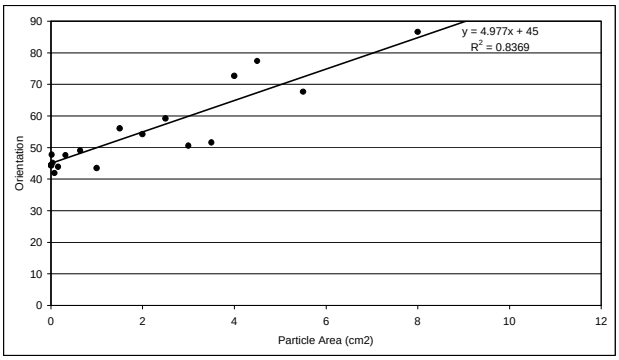

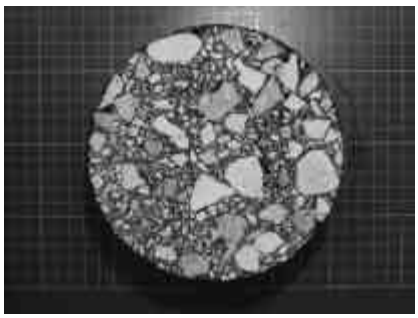

05-1798 Top

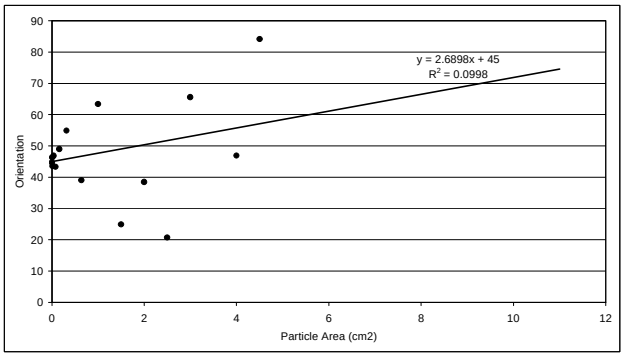

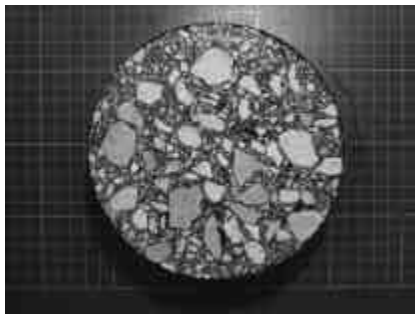

05-1798 Bottom

Gyratory compacted specimens (*D* = 100 mm)

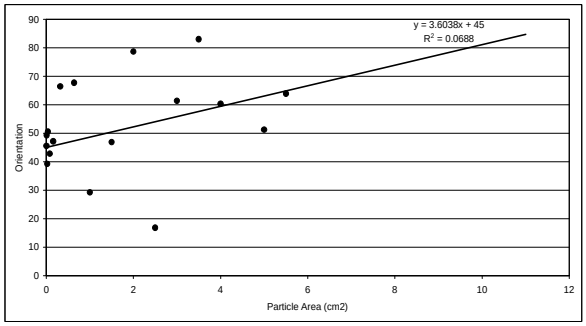

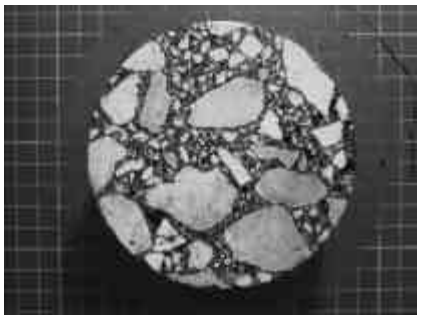

05-1722 Top

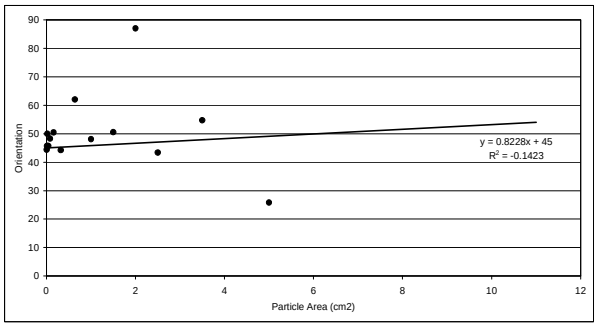

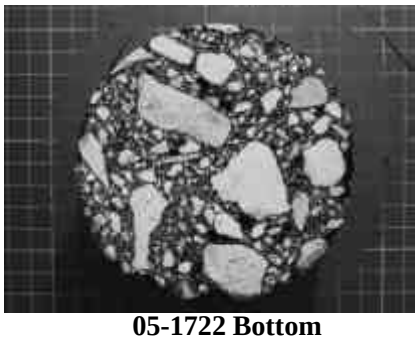

05-1722 Bottom

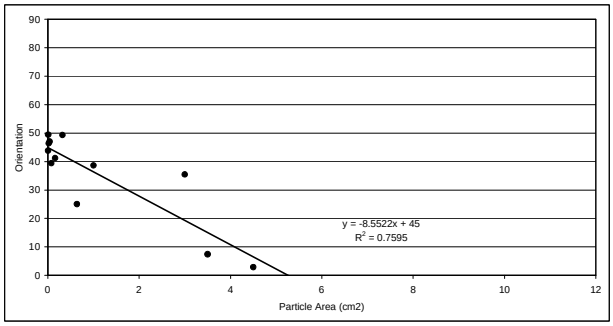

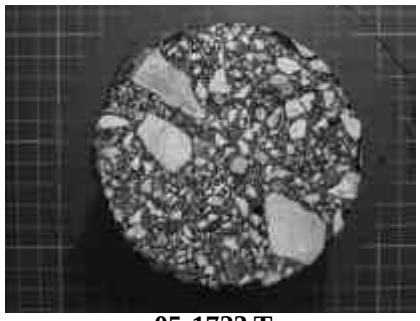

05-1723 Top

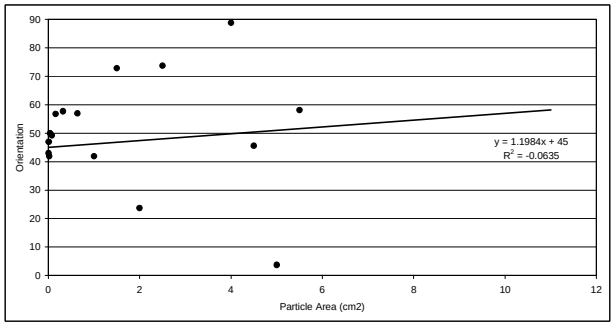

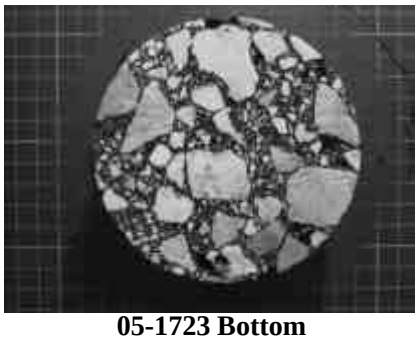

05-1723 Bottom

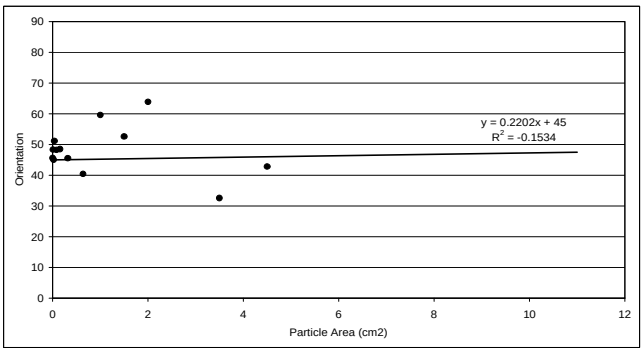

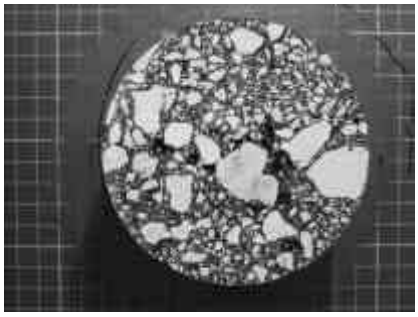

05-1724 Top

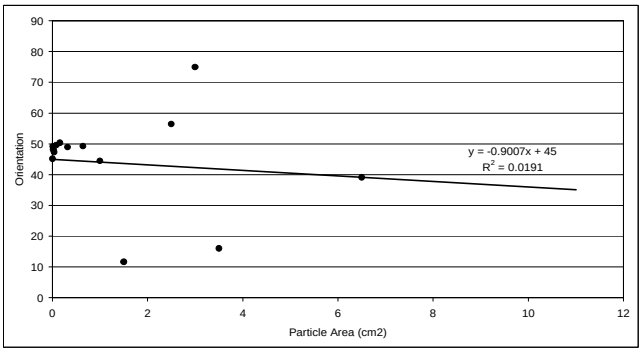

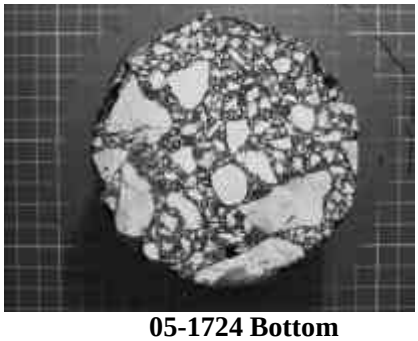

05-1724 Bottom

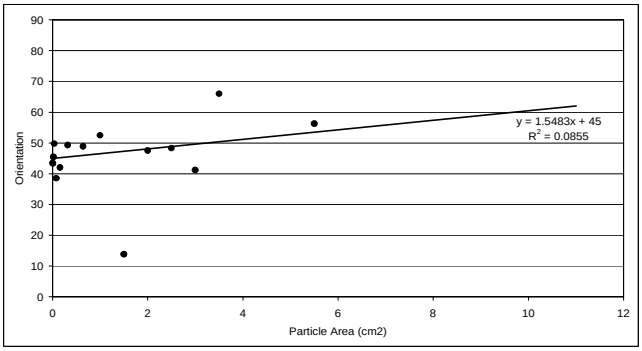

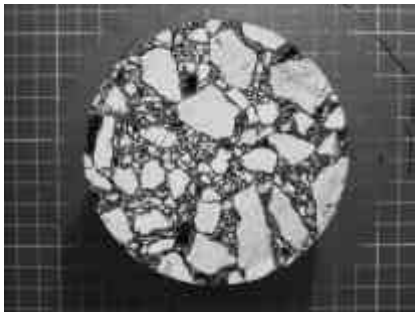

05-1725 Top

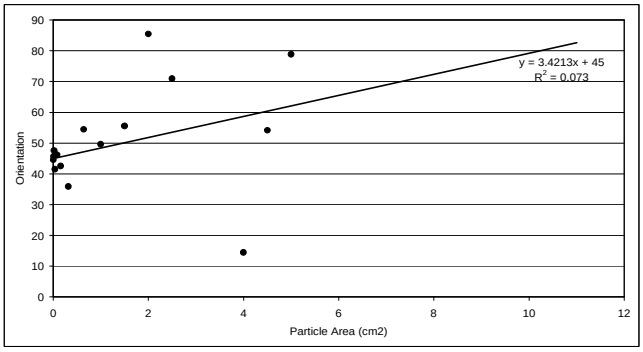

05-1725 Bottom

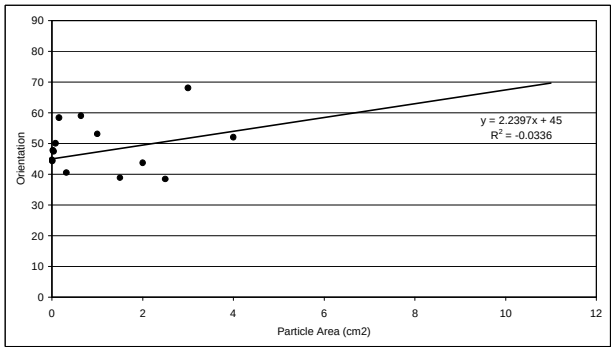

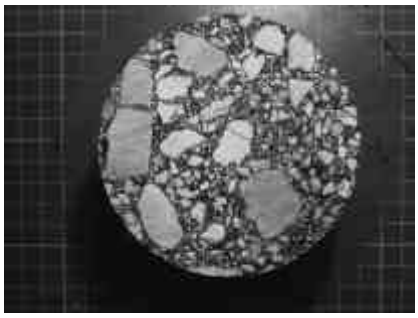

05-1791 Top

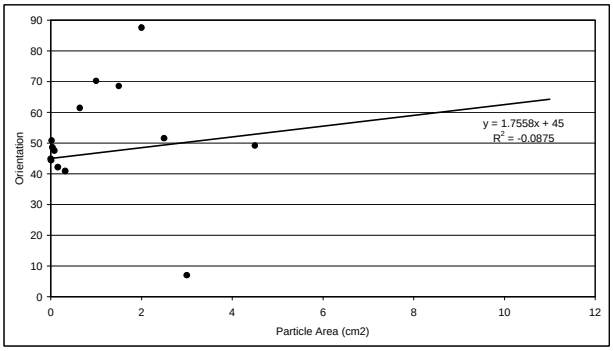

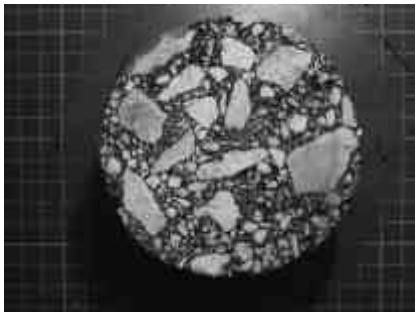

05-1791 Bottom

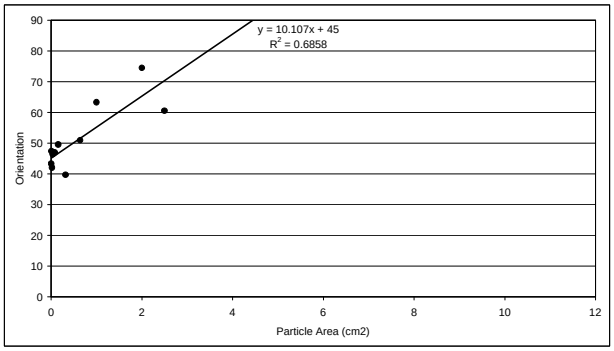

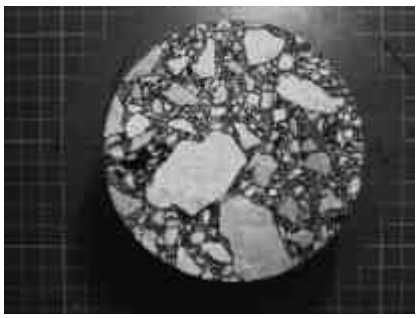

05-1792 Top

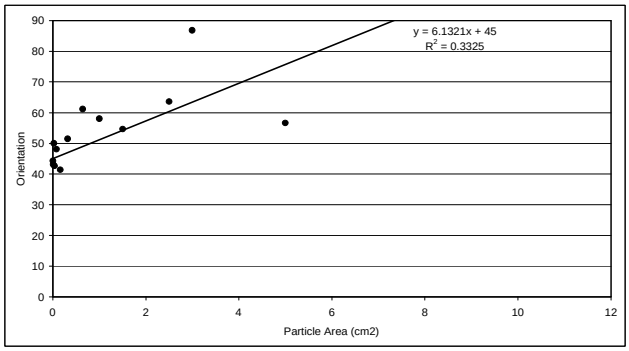

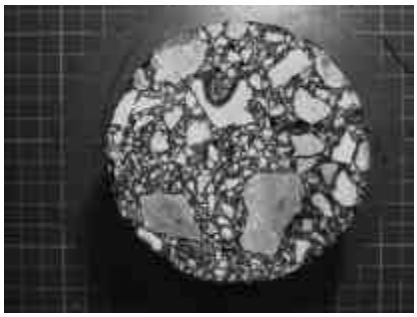

05-1792 Bottom

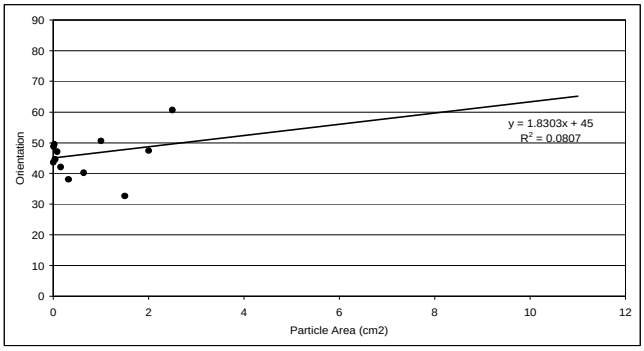

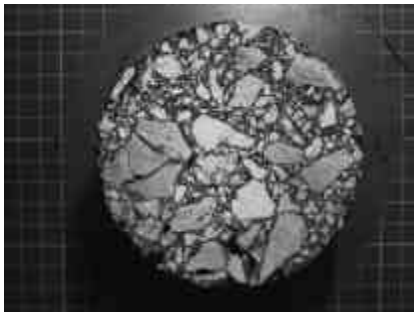

05-1793 Top

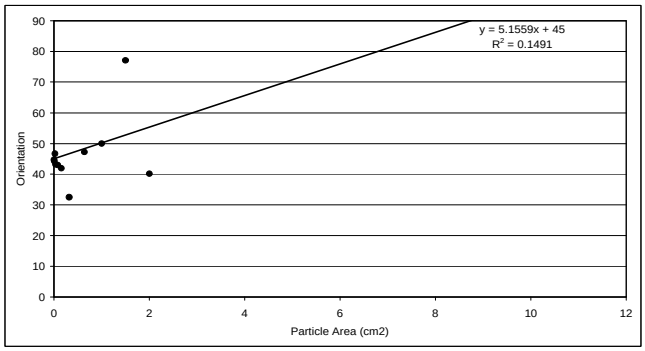

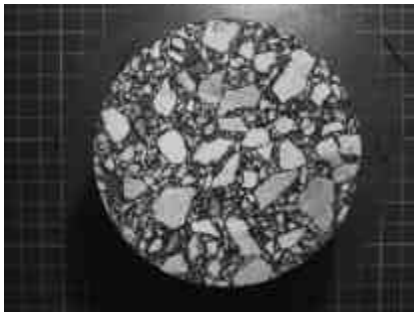

05-1793 Bottom

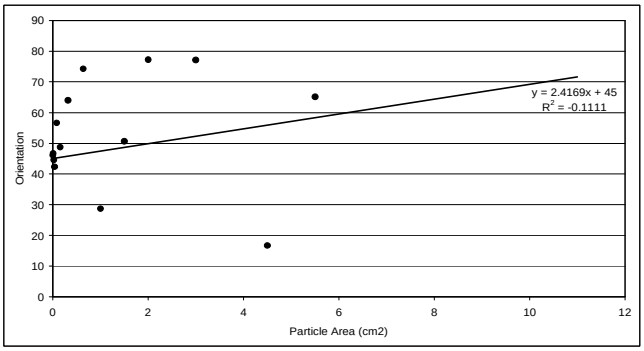

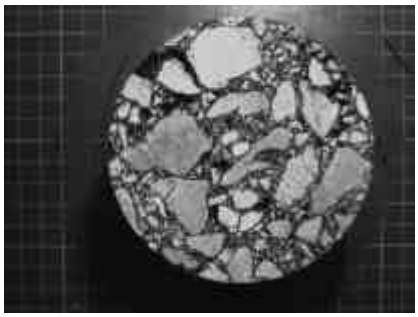

05-1794 Top

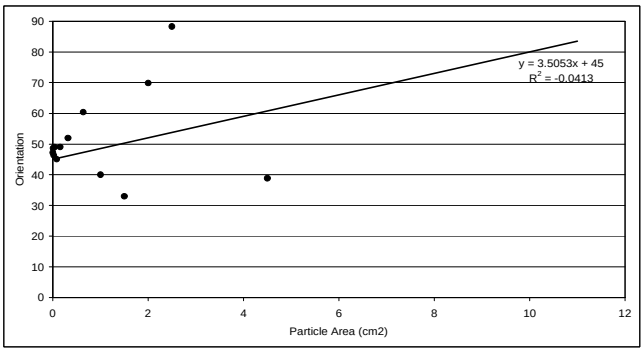

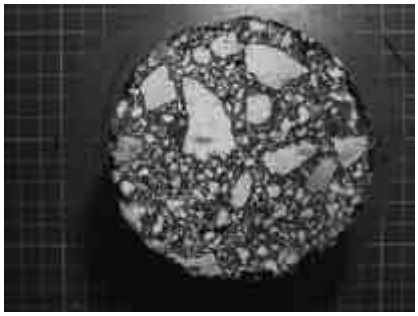

05-1794 Bottom

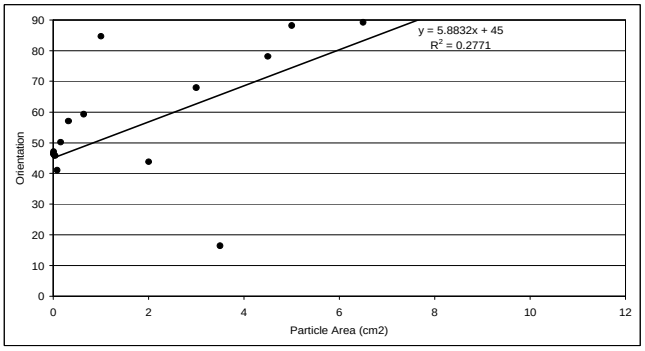

05-1795 Top

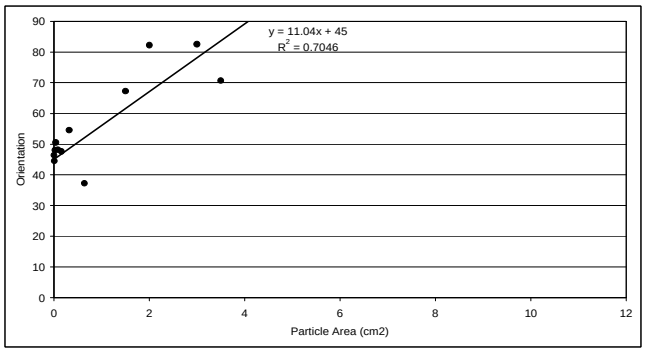

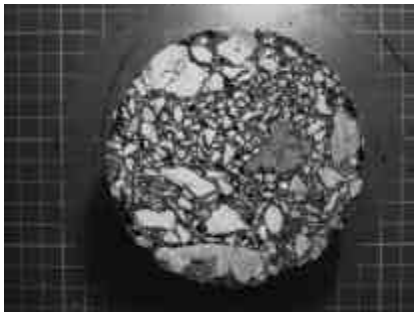

05-1795 Bottom

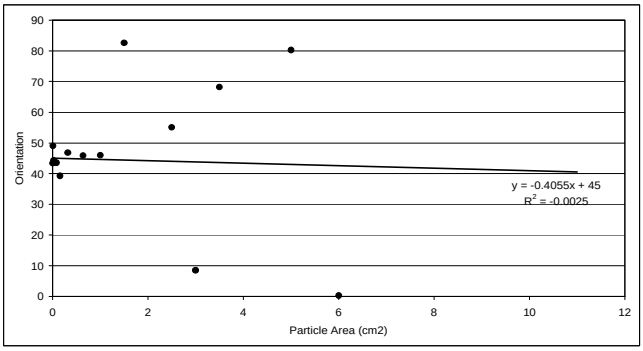

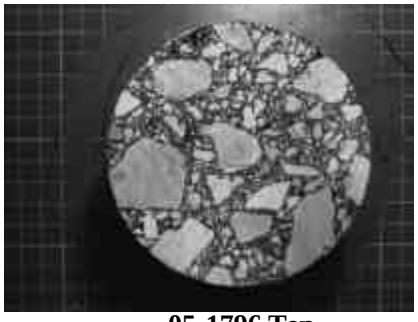

05-1796 Top

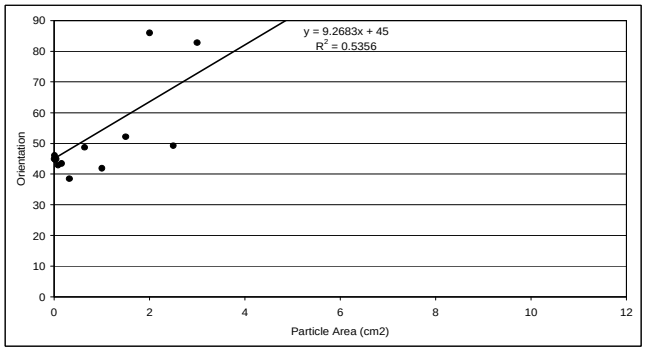

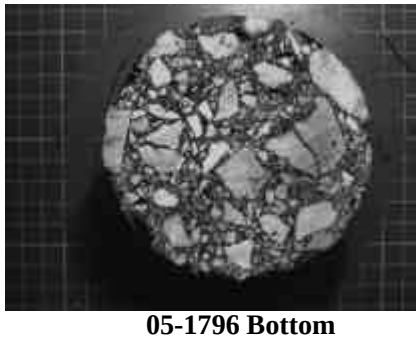

05-1796 Bottom

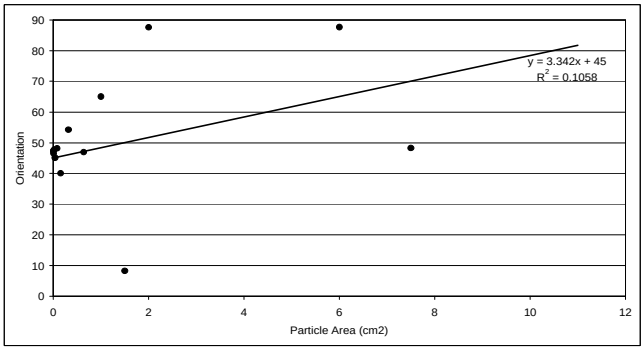

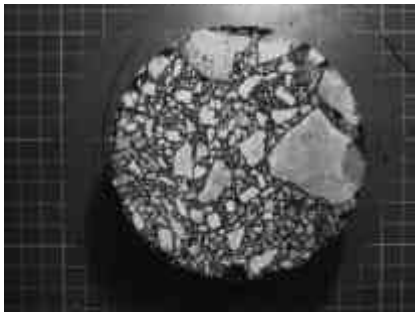

05-1797 Top

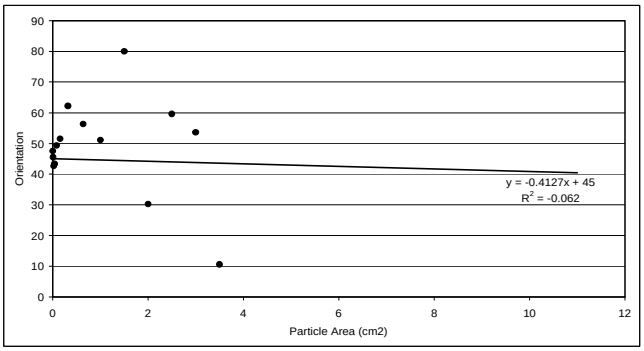

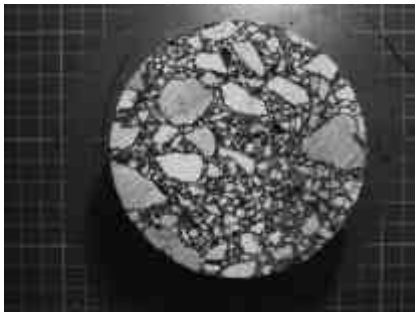

05-1797 Bottom

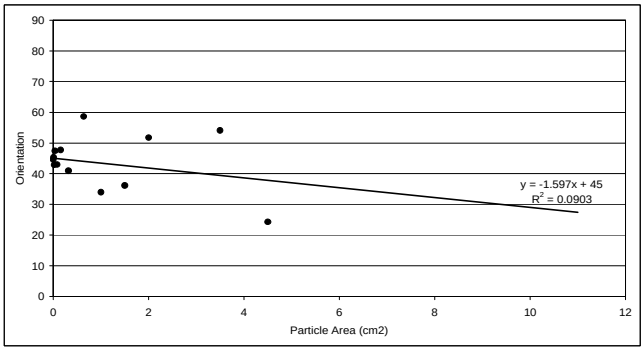

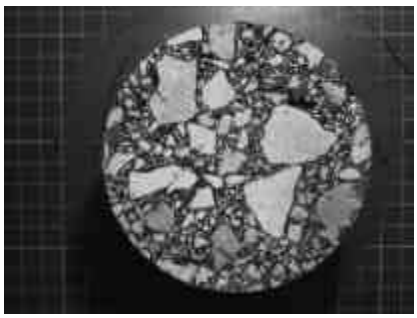

05-1798 Top

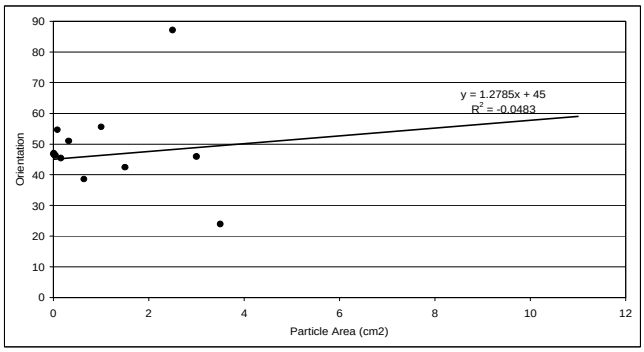

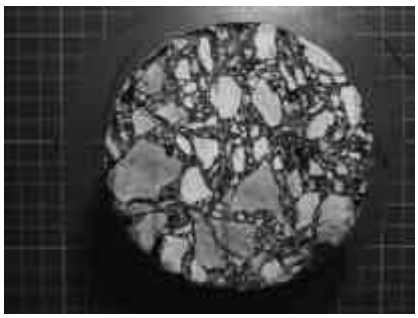

05-1798 Bottom

Gyratory compacted specimens (*D* = 150 mm Computer trimmed all particles)

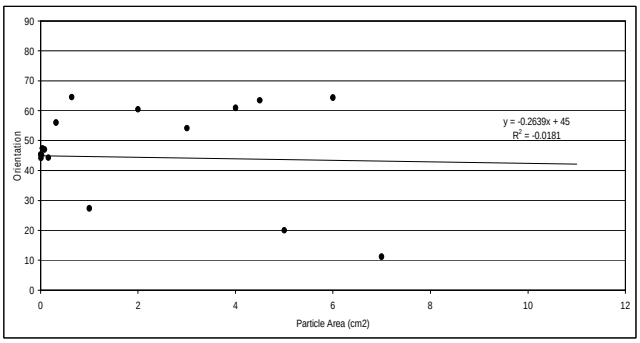

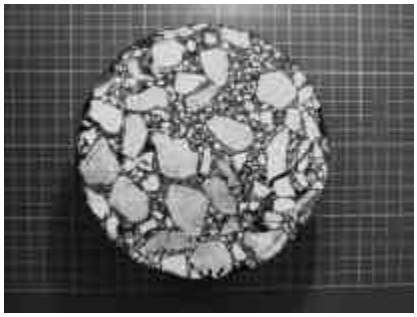

05-1722 Top

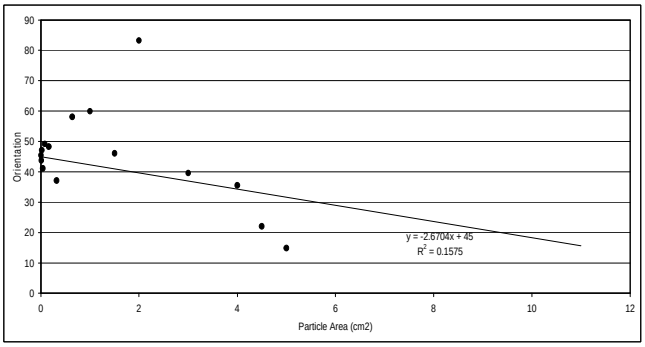

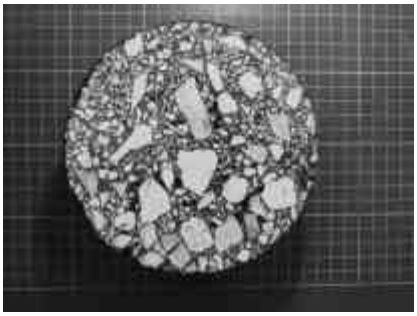

05-1722 Bottom

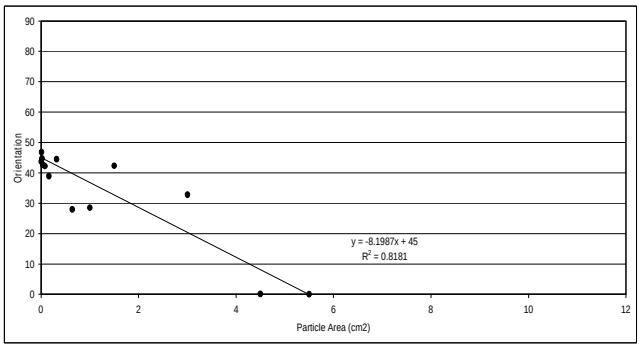

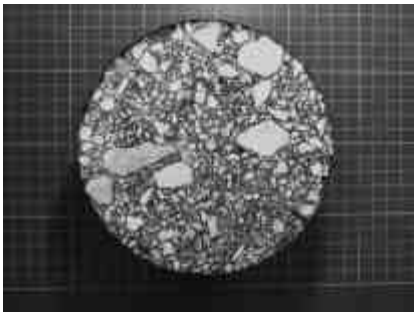

05-1723 Top

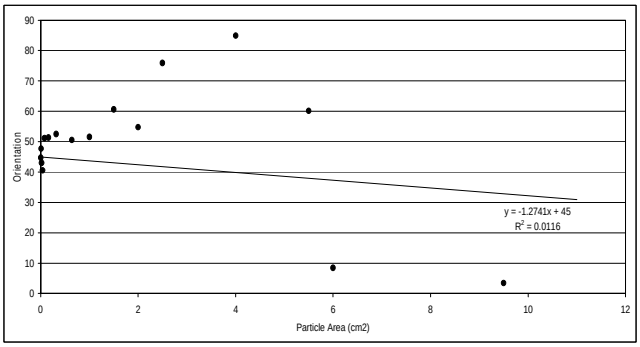

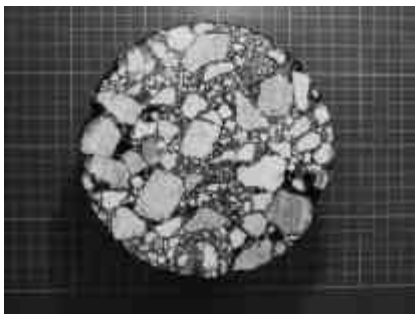

05-1723 Bottom

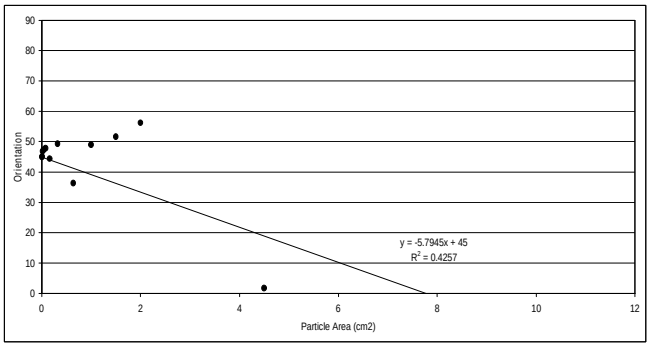

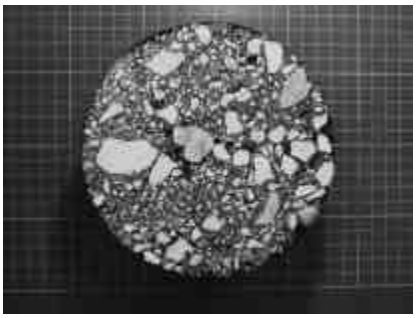

05-1724 Top

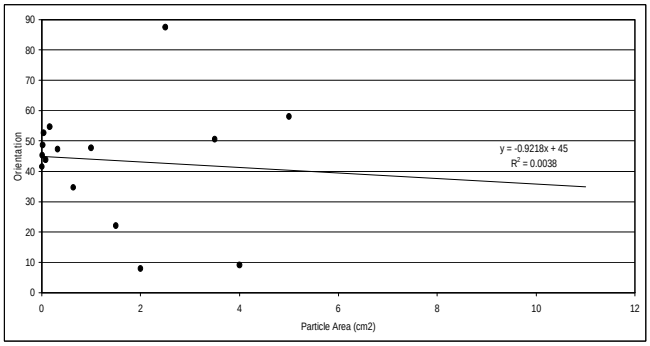

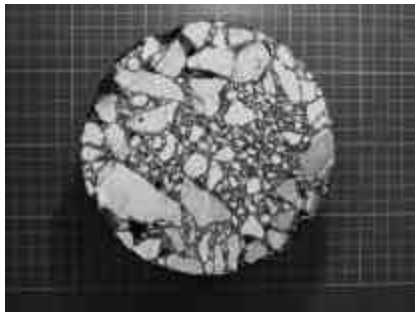

05-1724 Bottom

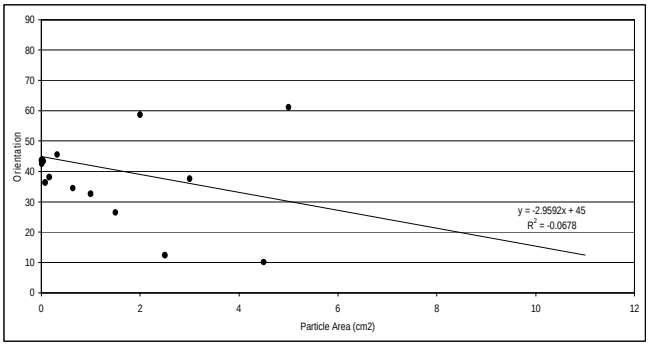

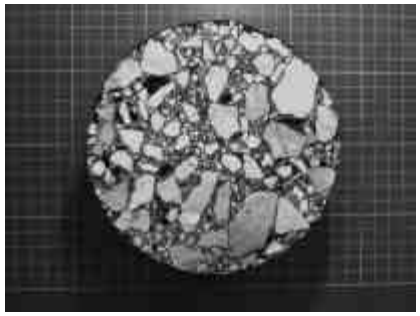

05-1725 Top

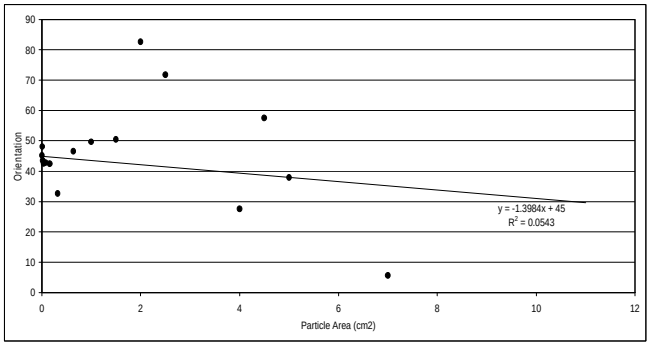

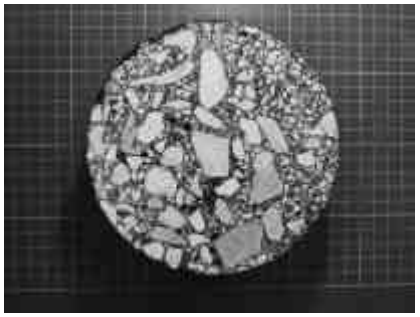

05-1725 Bottom

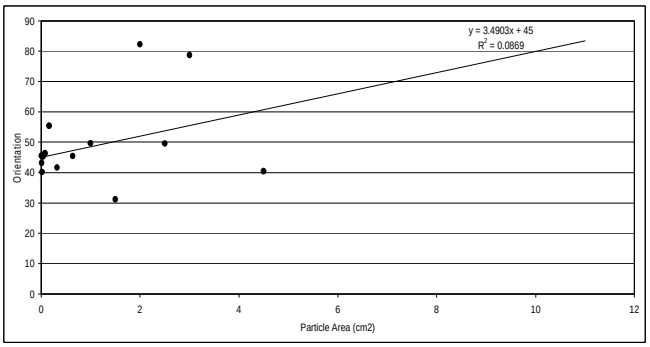

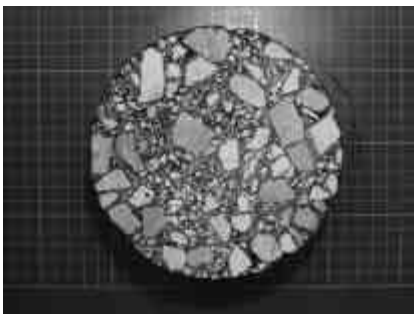

05-1791 Top

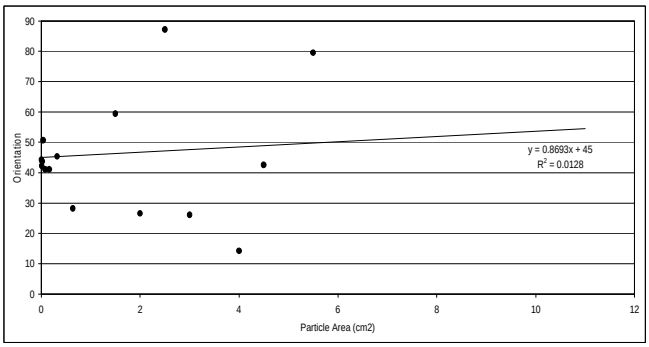

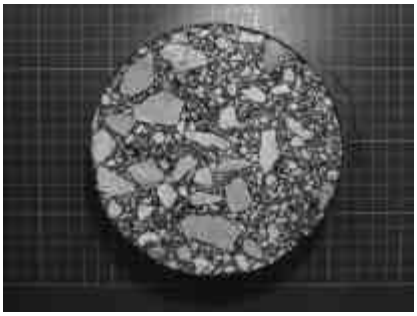

05-1791 Bottom

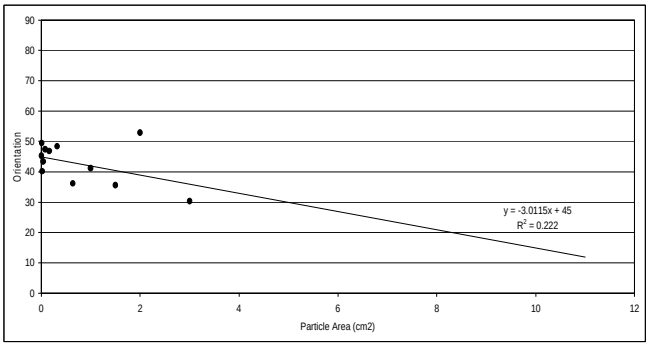

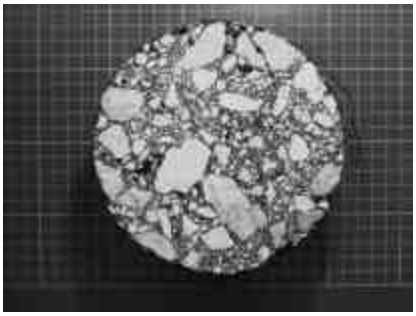

05-1792 Top

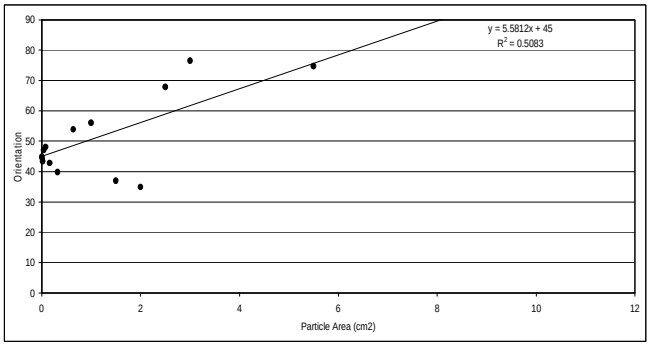

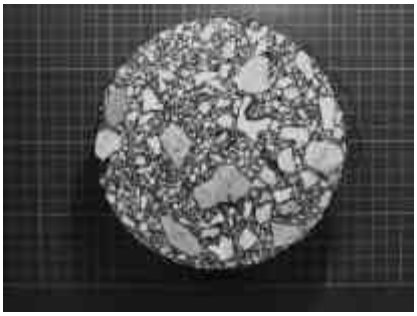

05-1792 Bottom

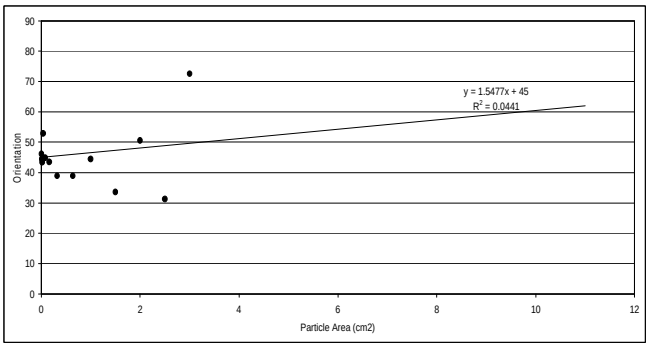

05-1793 Top

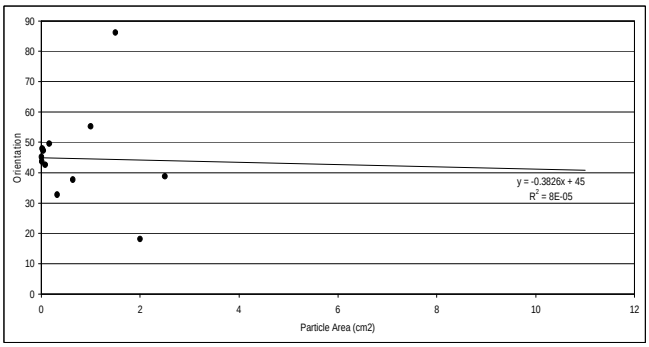

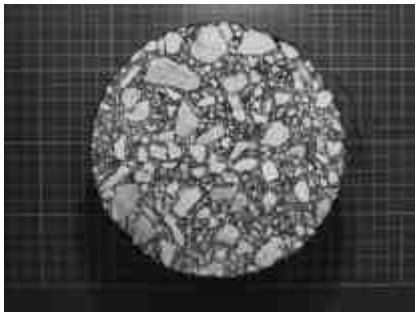

05-1793 Bottom

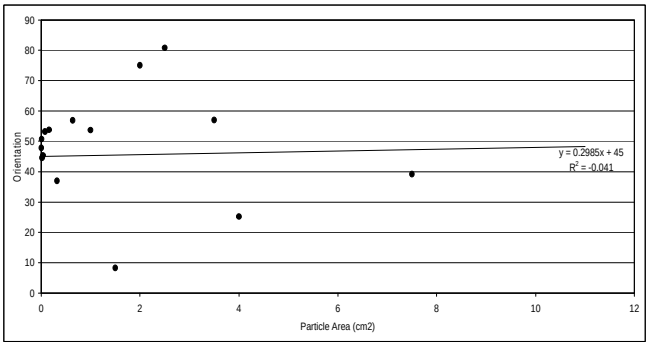

05-1794 Top

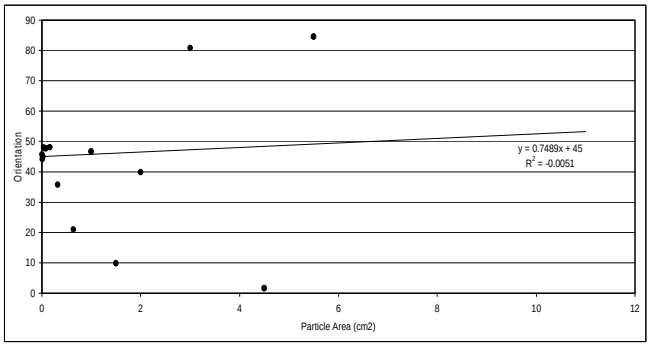

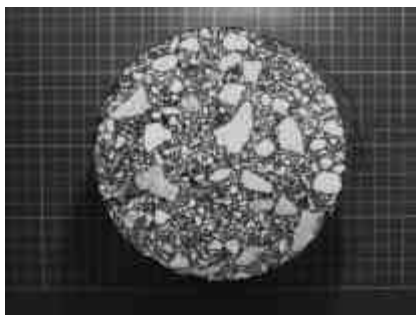

05-1794 Bottom

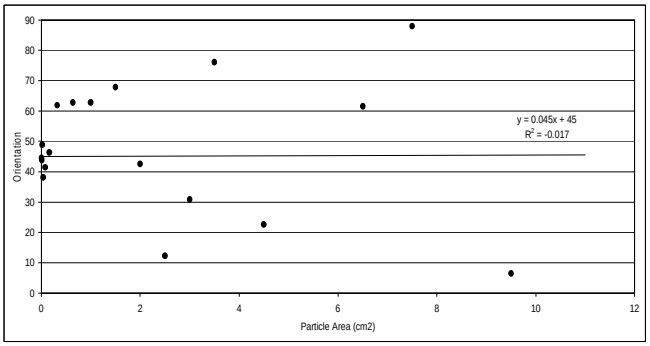

05-1795 Top

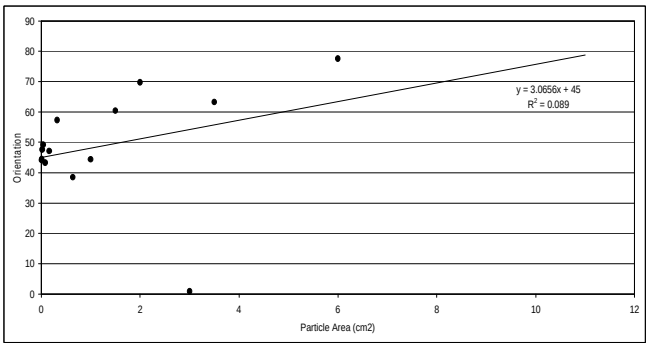

05-1795 Bottom

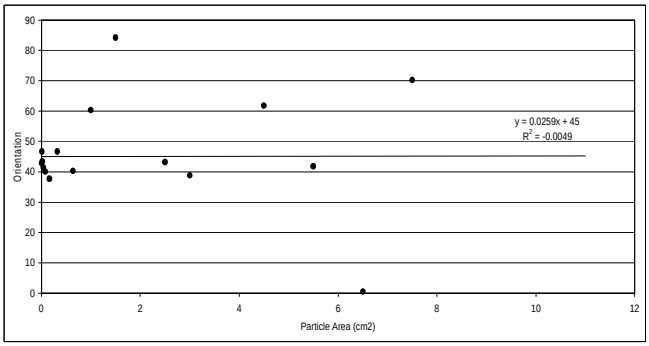

05-1796 Top

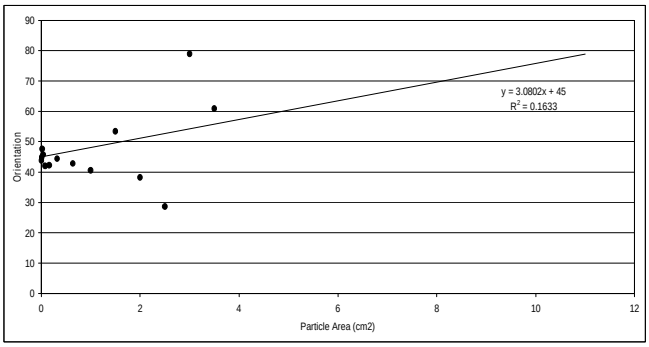

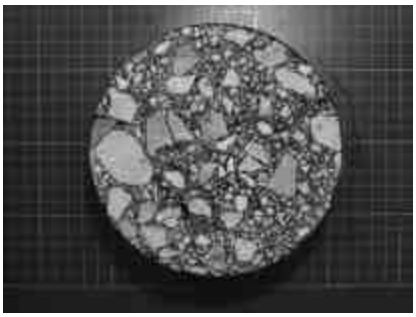

05-1796 Bottom

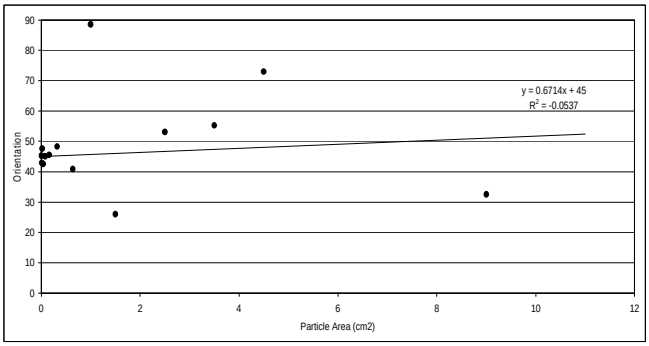

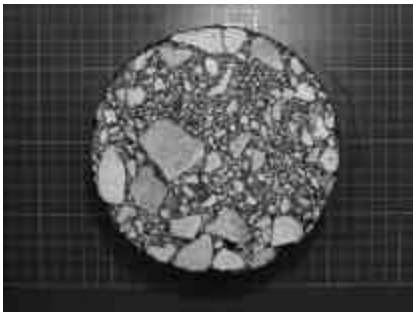

05-1797 Top

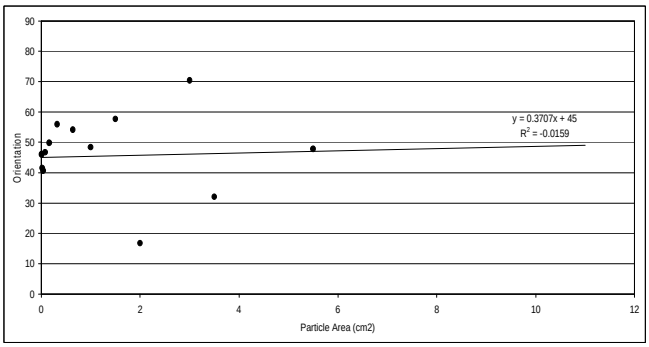

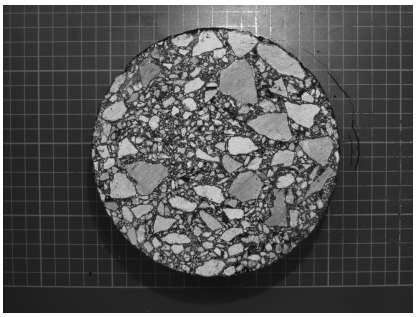

05-1797 Bottom

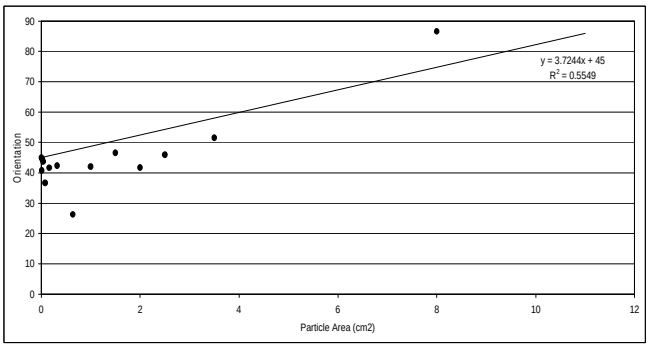

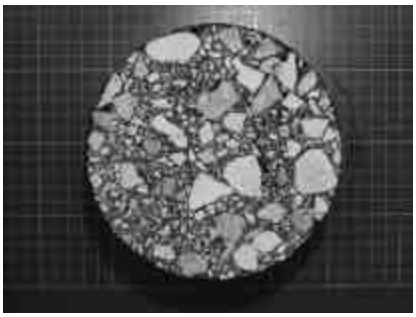

05-1798 Top

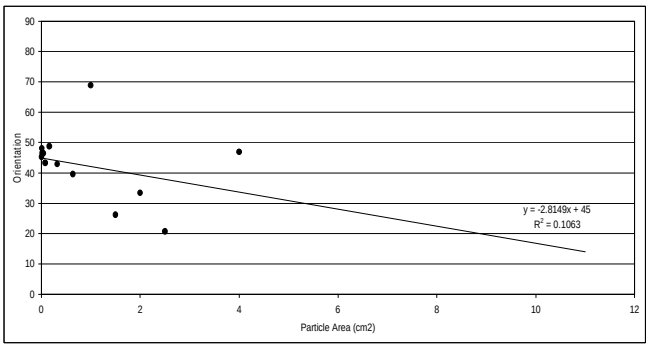

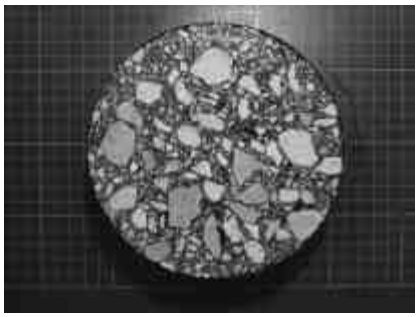

05-1798 Bottom

Vibratory compacted specimens (*D* = 150 mm All particles)

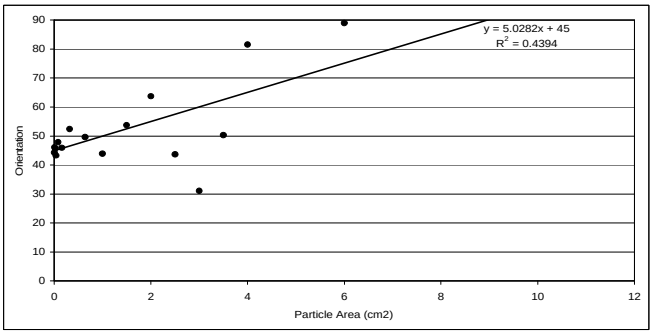

05-1930-Top

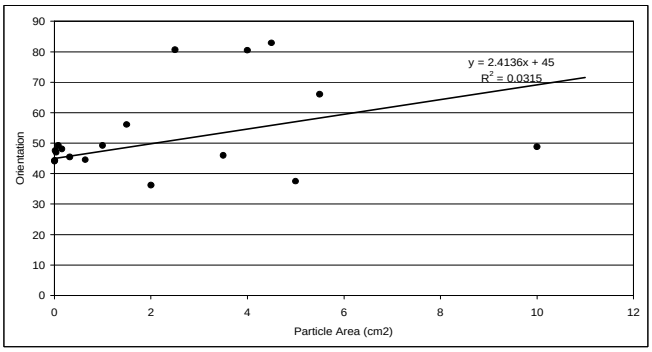

05-1930-Bottom

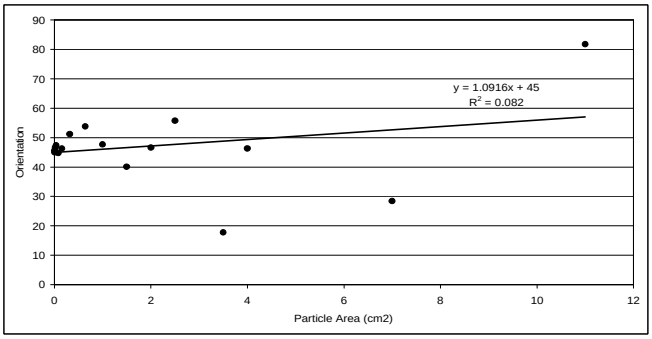

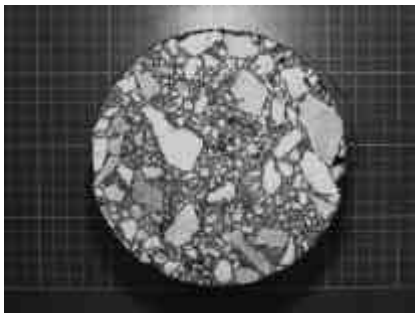

05-1931-Top

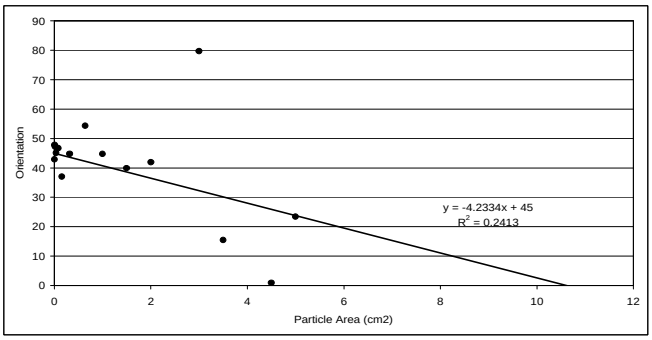

05-1931-Bottom

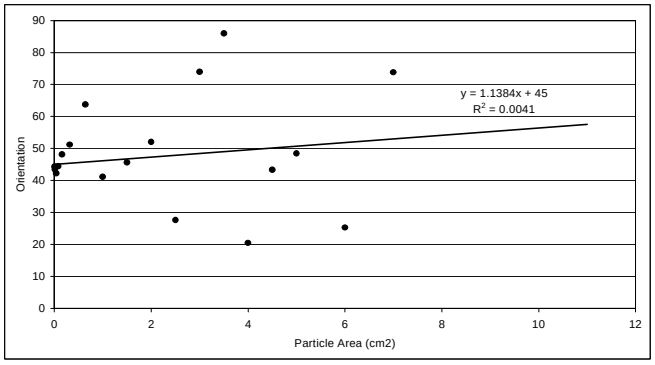

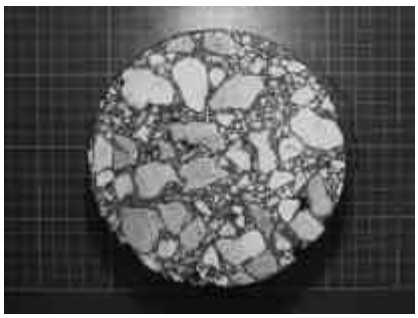

05-1932 Top

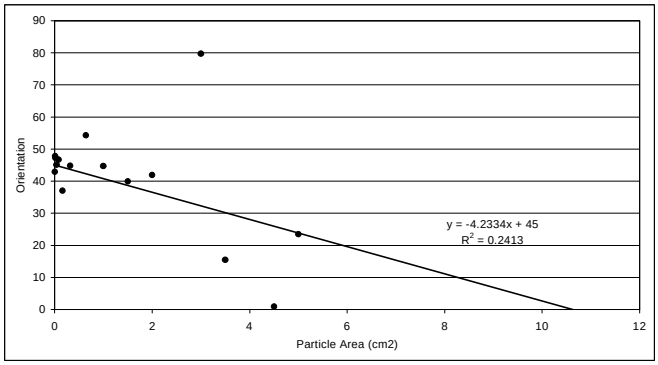

05-1932 Bottom

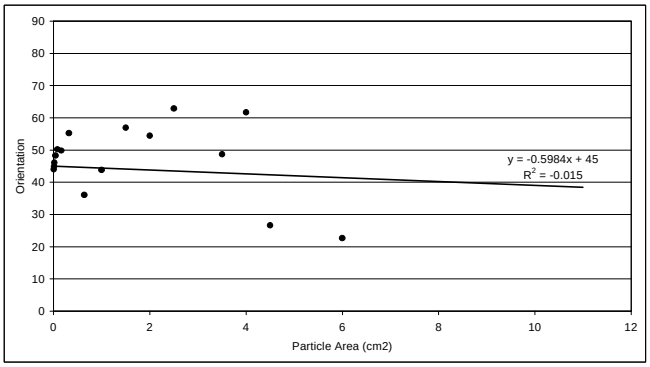

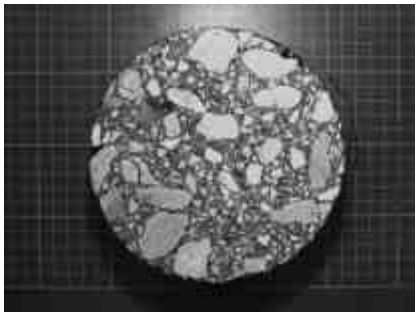

05-1933 Top

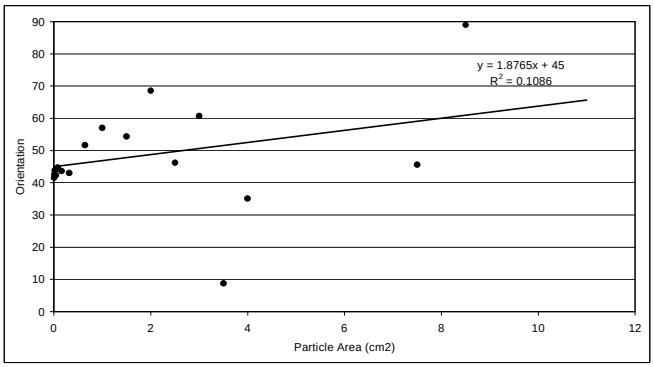

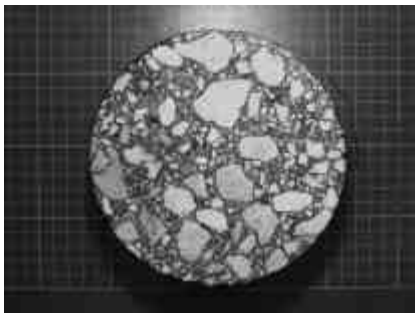

05-1933 Bottom

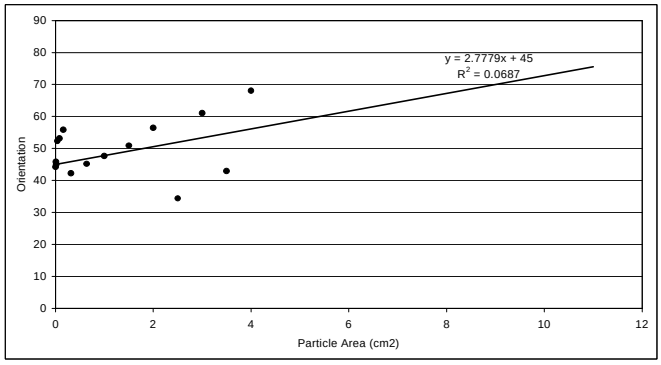

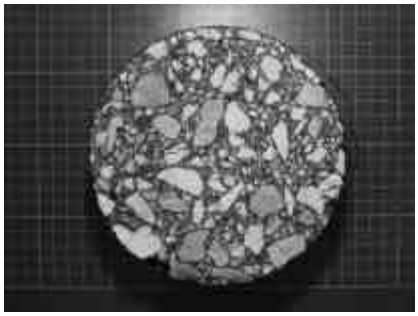

05-1934 Top

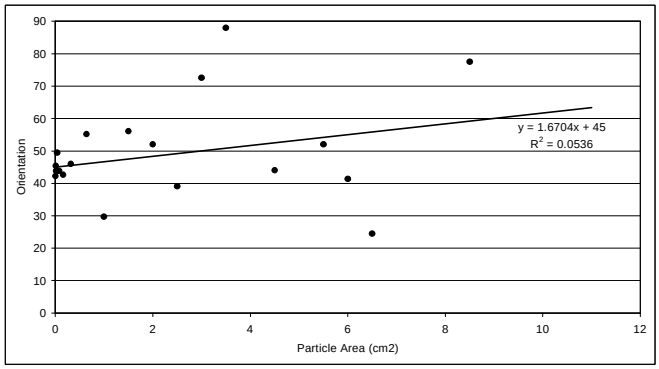

05-1934 Bottom

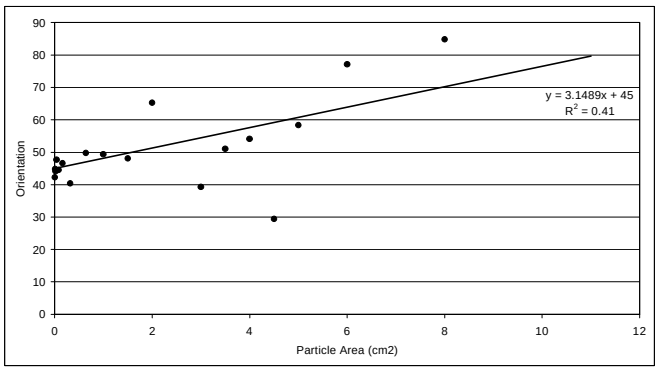

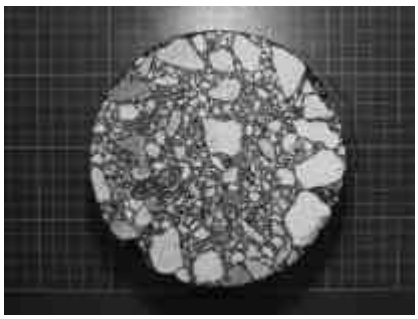

05-1935 Top

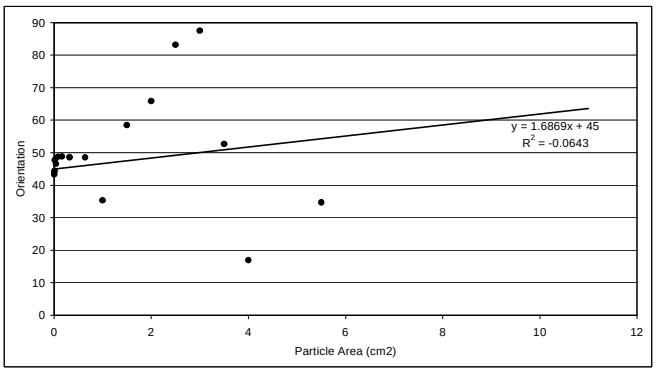

05-1935 Bottom

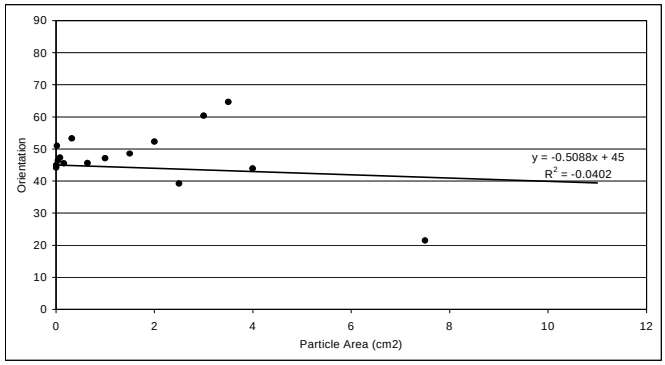

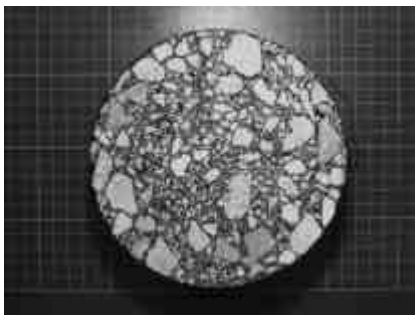

05-1936 Top

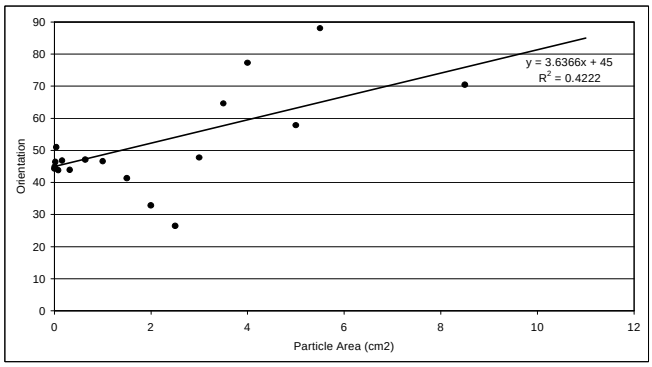

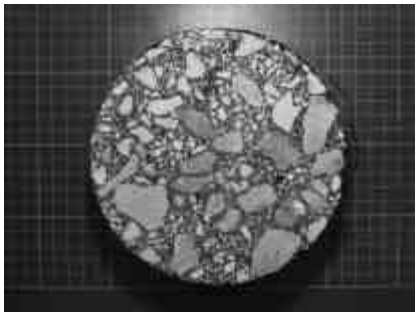

05-1936 Bottom

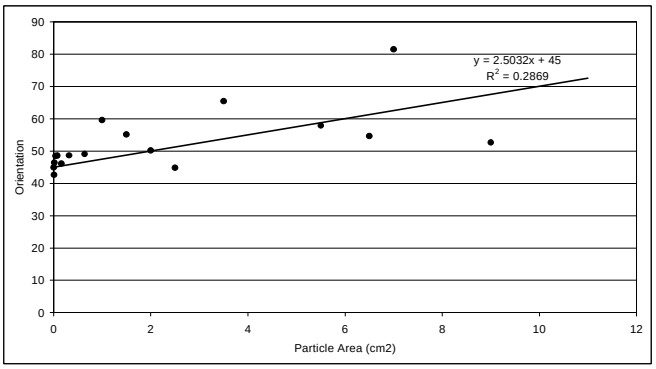

05-1937 Top

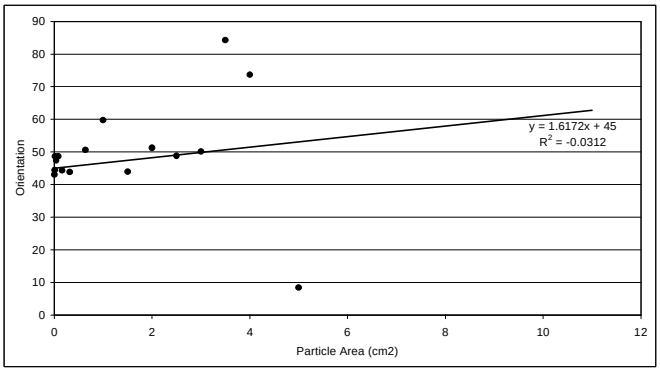

05-1937 Bottom

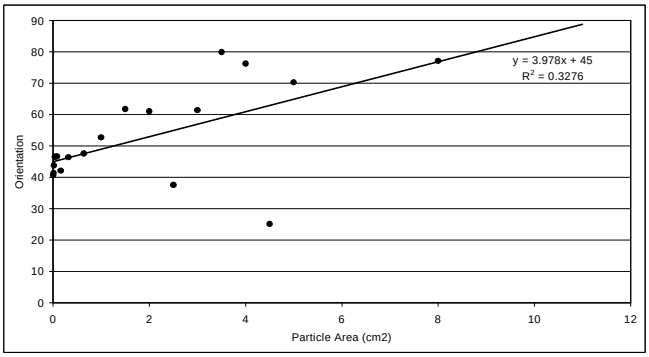

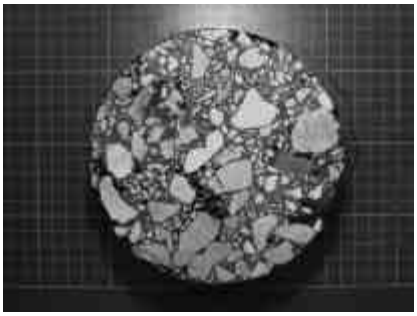

05-1938 Top

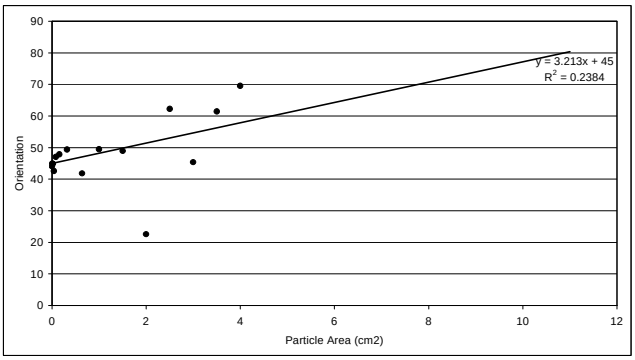

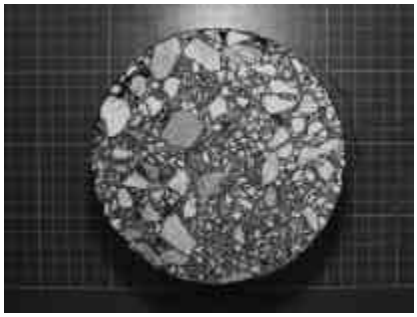

05-1938 Bottom

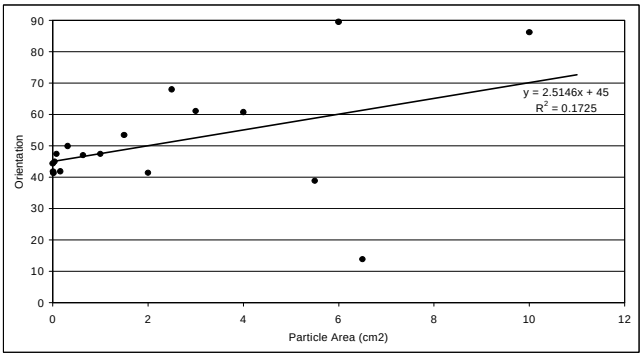

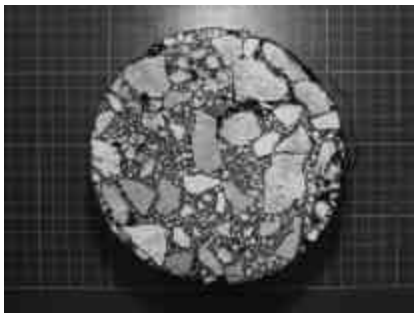

05-1939 Top

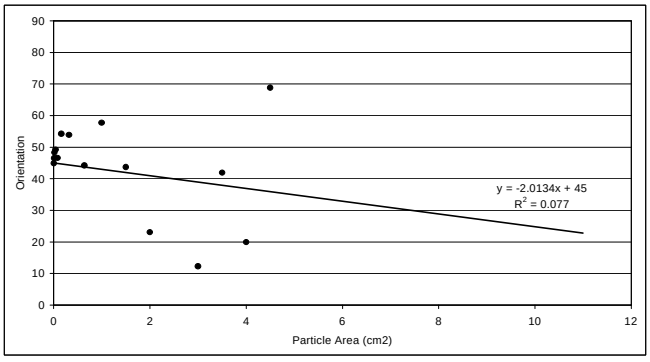

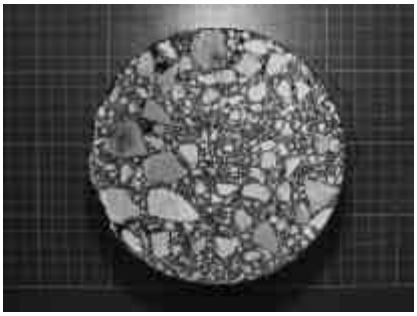

05-1939 Bottom

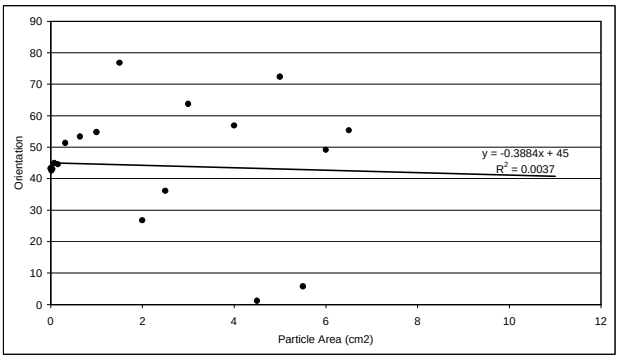

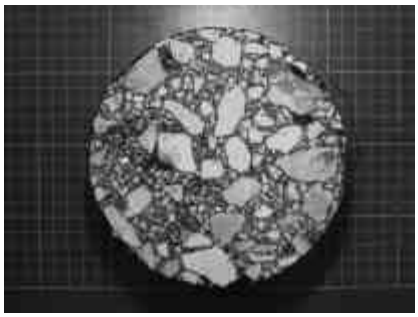

05-1940 Top

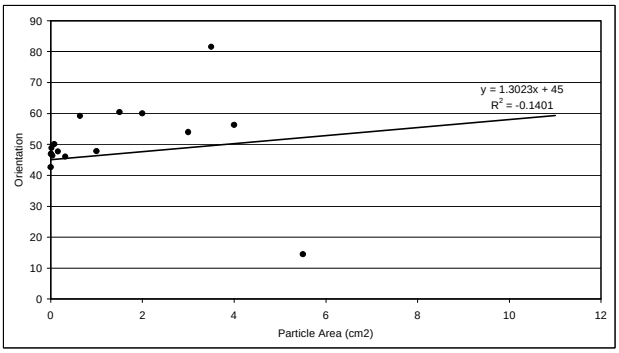

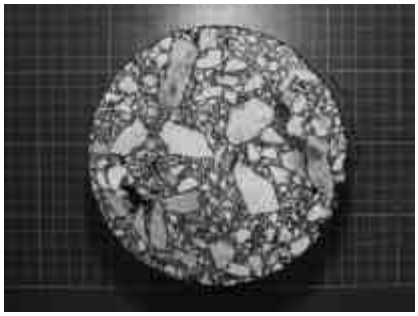

05-1940 Bottom

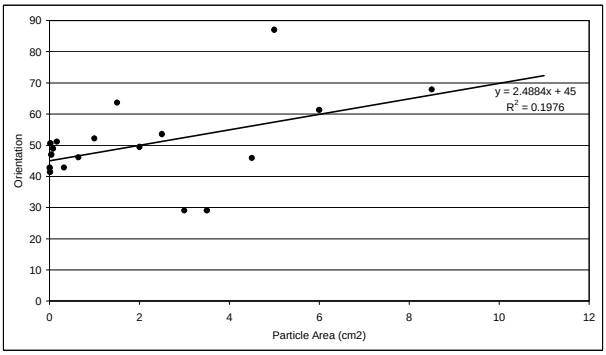

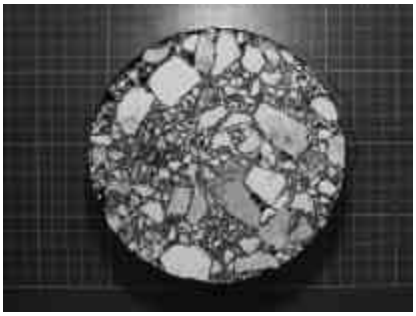

05-1941 Top

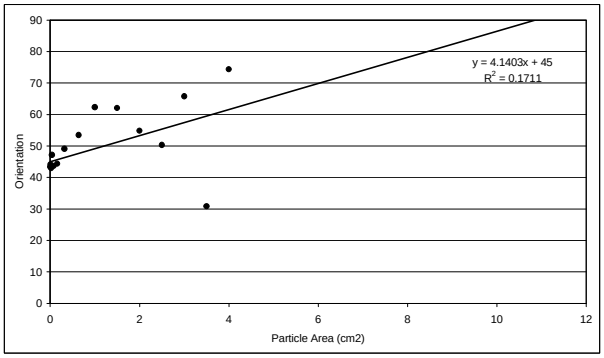

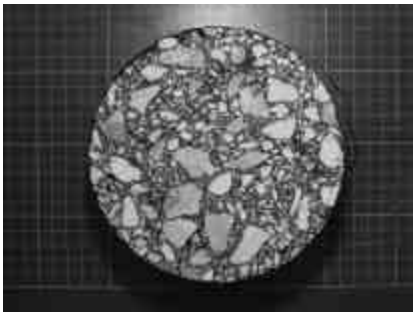

05-1941 Bottom

Vibratory compacted specimens (*D* = 100 mm All particles)

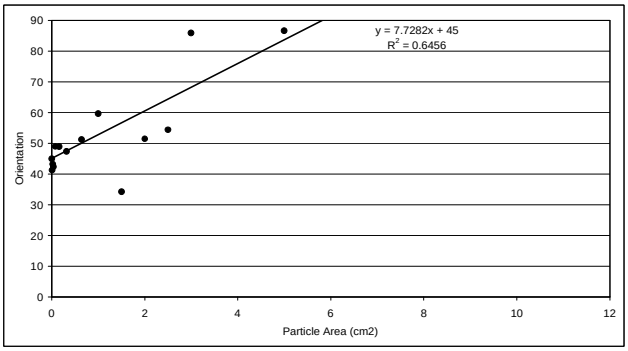

05-1930 Top

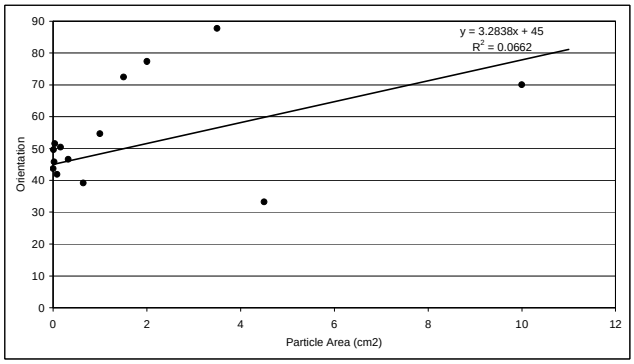

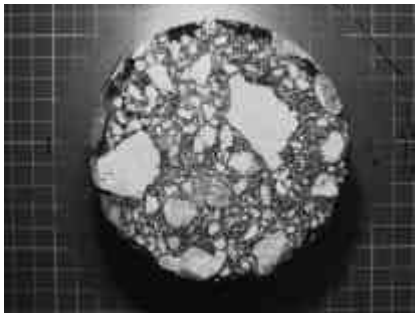

05-1930 Bottom

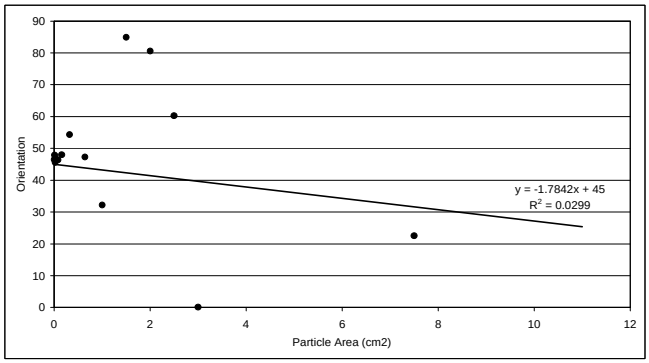

05-1931 Top

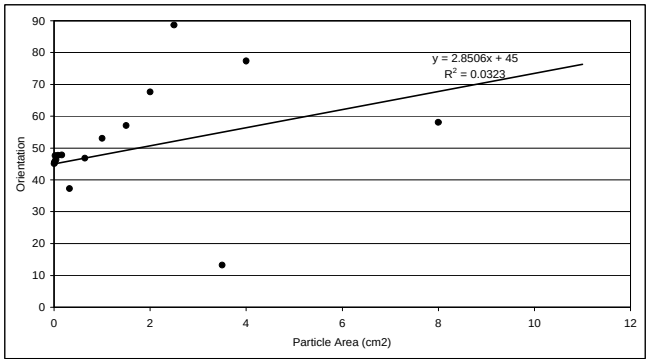

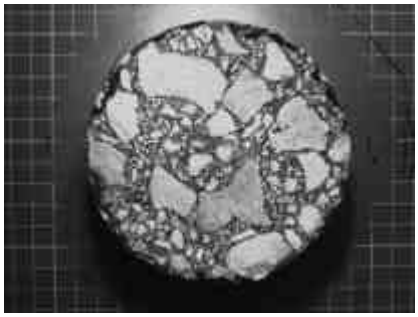

05-1931 Bottom

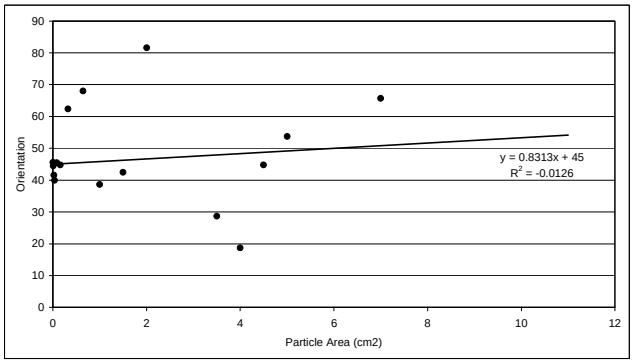

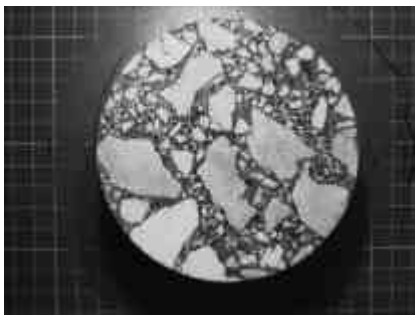

05-1932 Top

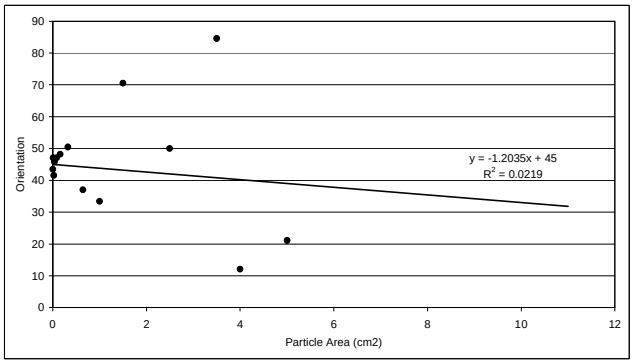

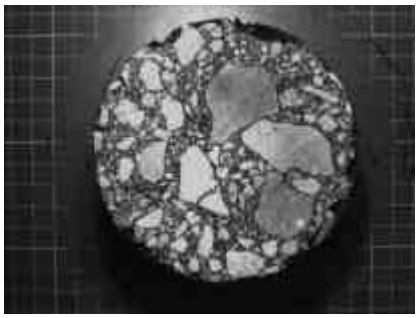

05-1932 Bottom

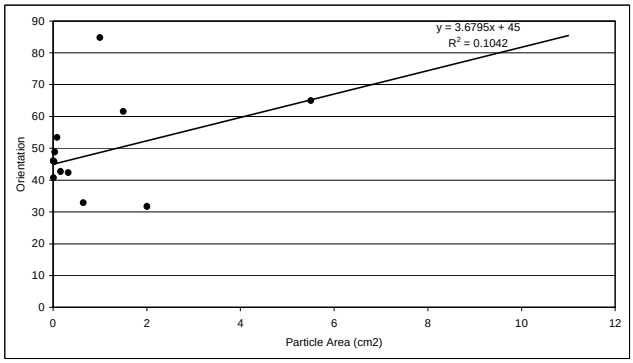

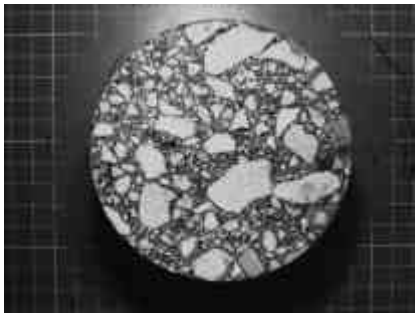

05-1933 Top

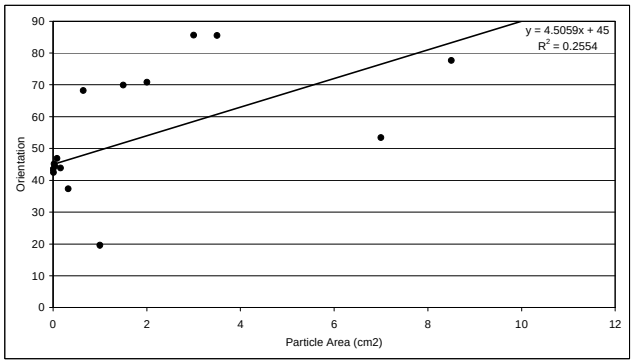

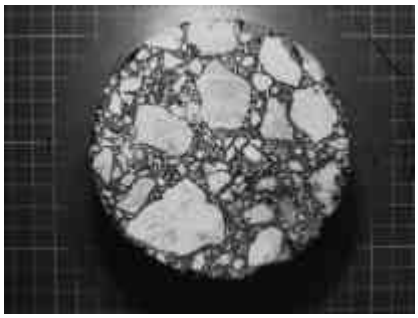

05-1933 Bottom

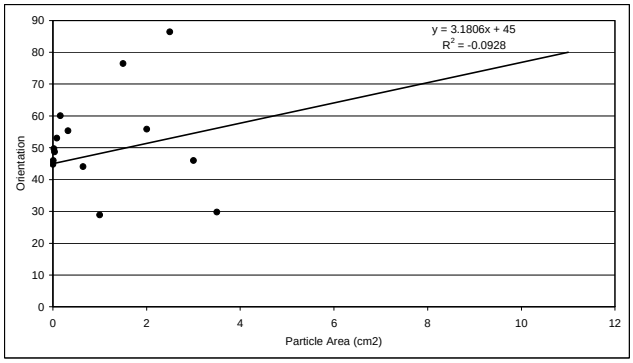

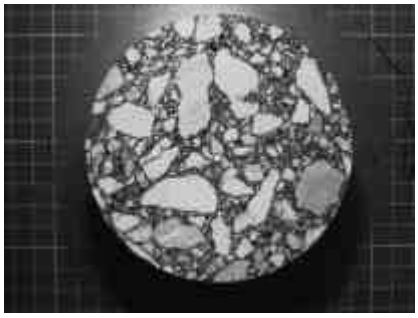

05-1934 Top

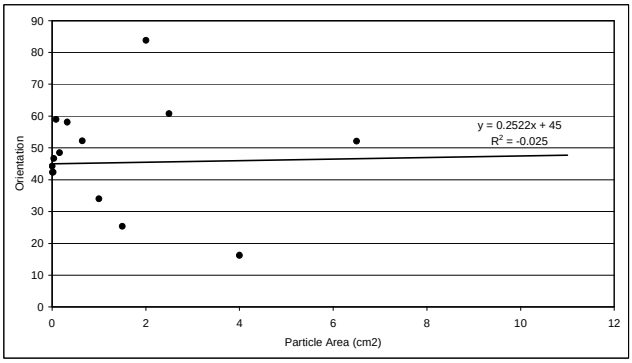

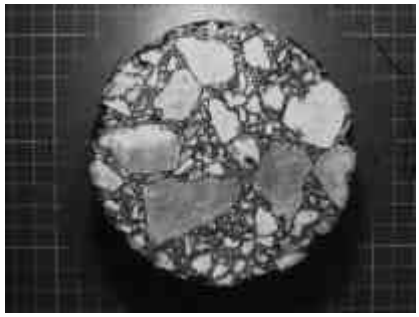

05-1934 Bottom

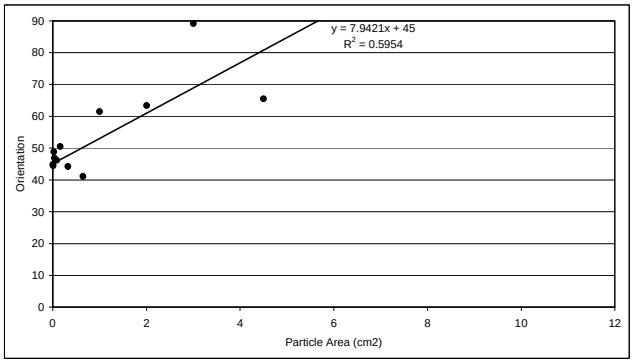

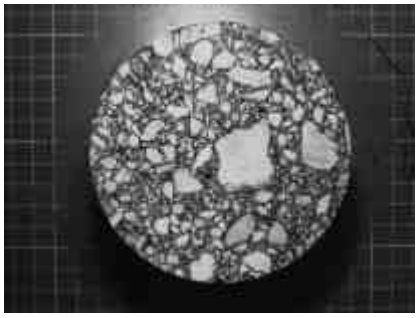

05-1935 Top

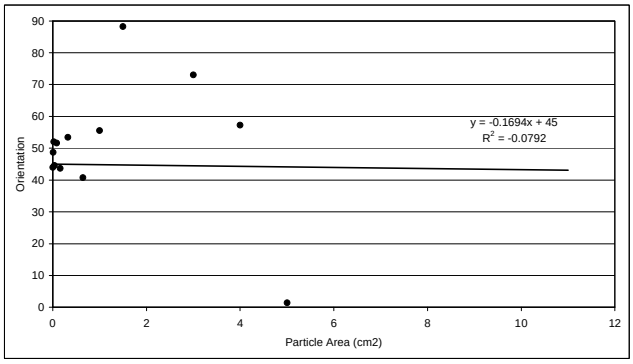

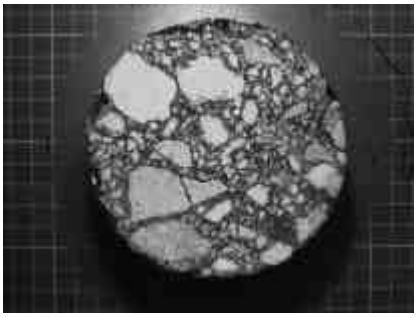

05-1935 Bottom

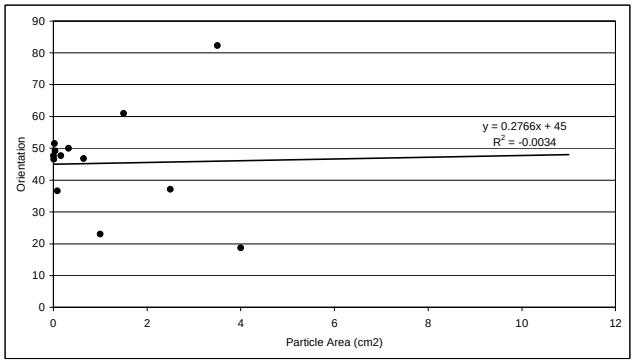

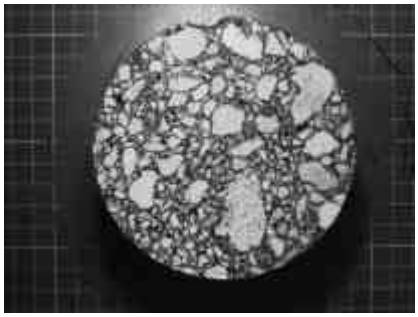

05-1936 Top

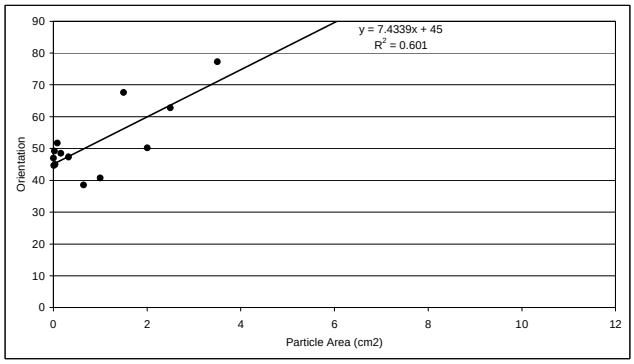

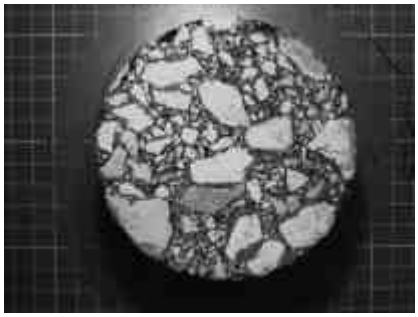

05-1936 Bottom

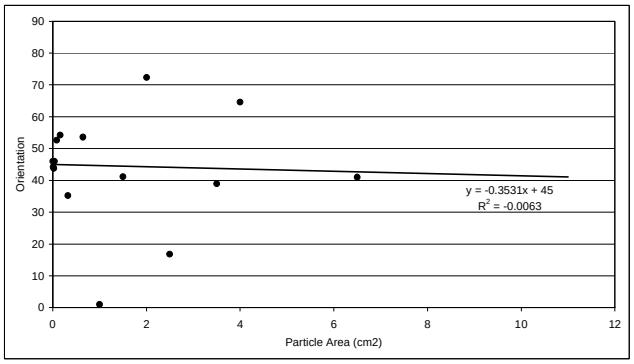

05-1937 Top

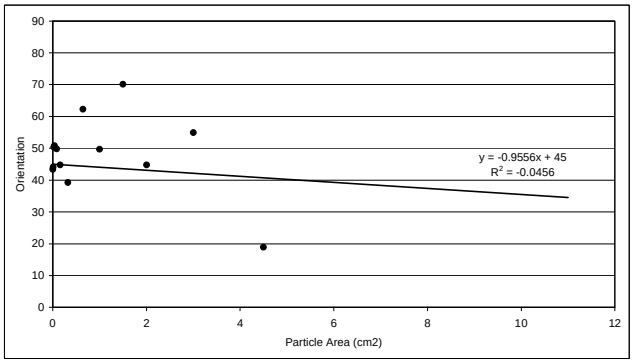

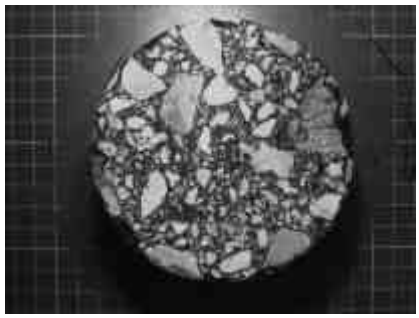

05-1937 Bottom

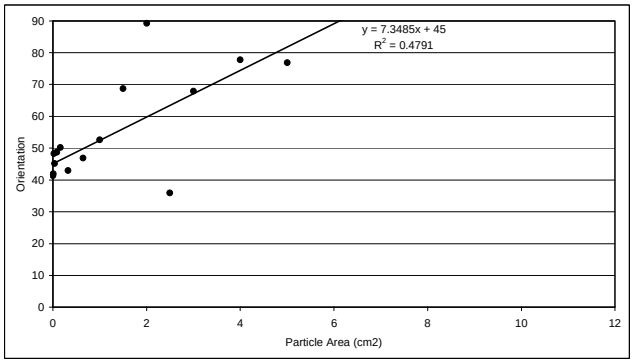

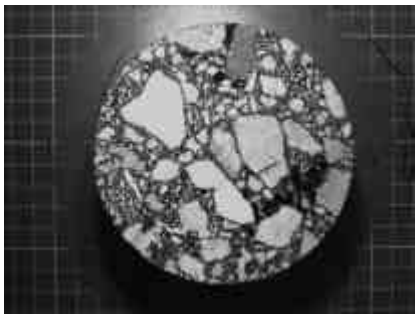

05-1938 Top

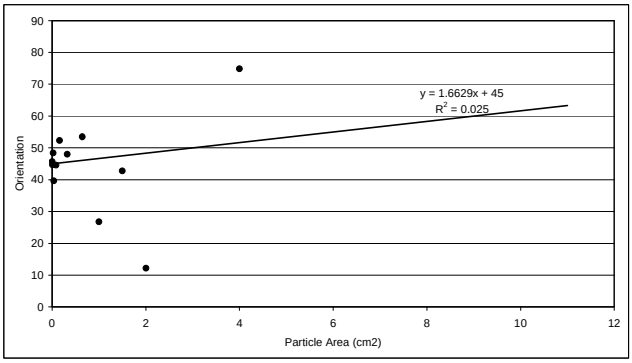

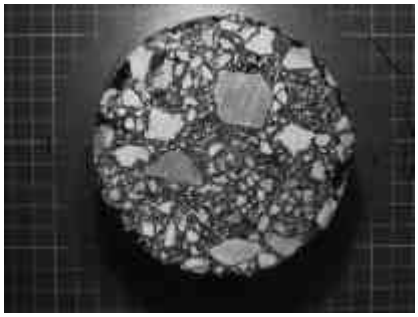

05-1938 Bottom

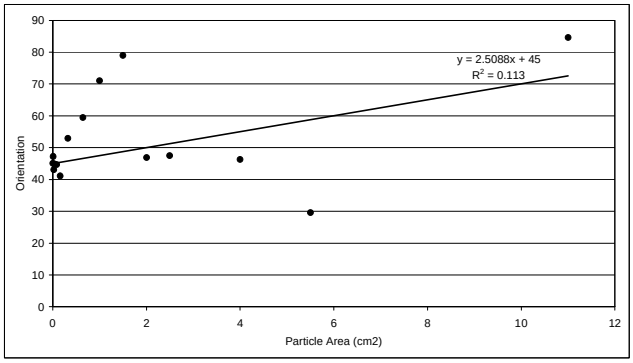

05-1939 Top

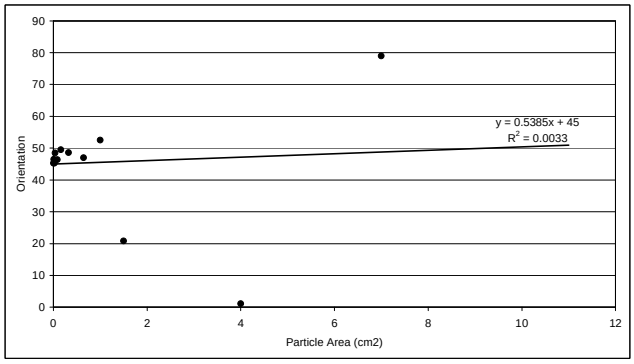

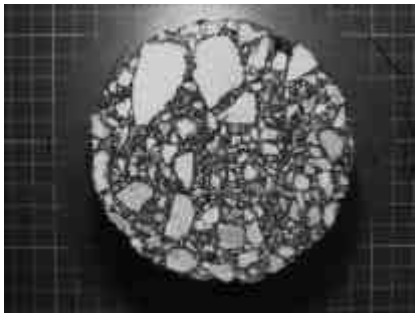

05-1939 Bottom

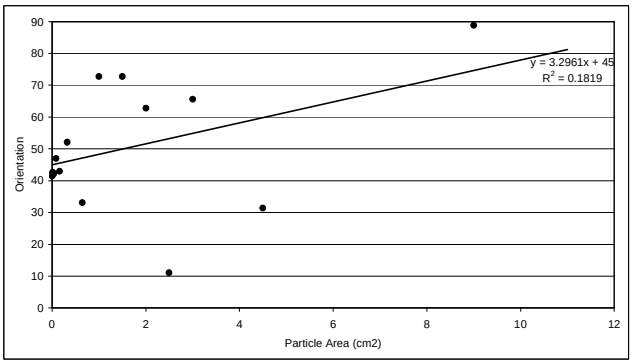

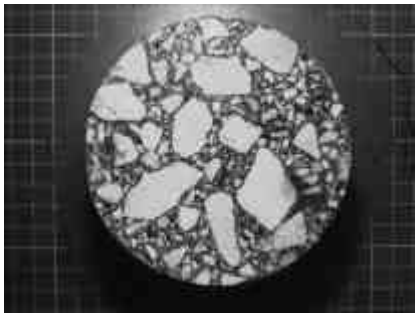

05-1940 Top

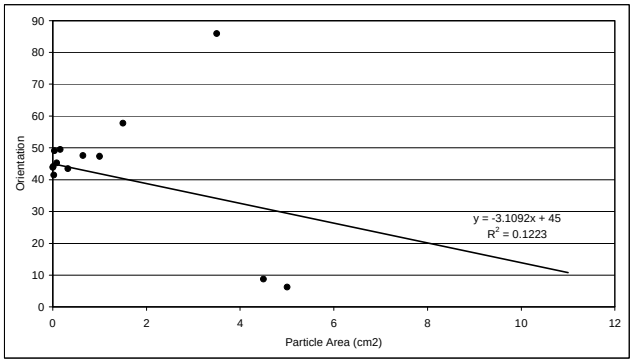

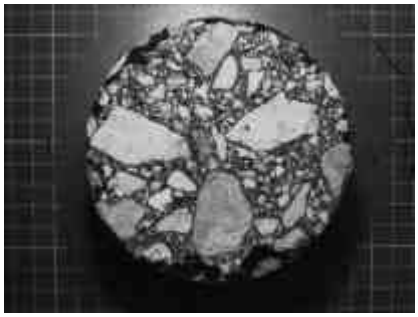

05-1940 Bottom

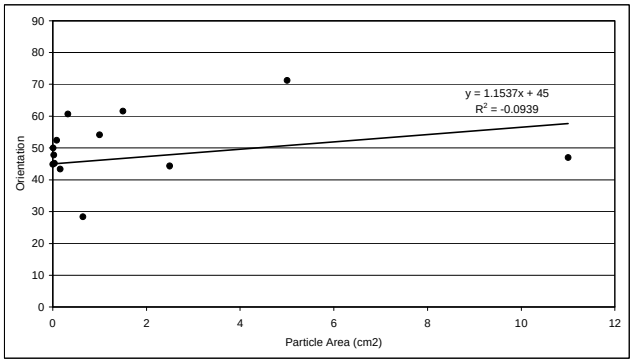

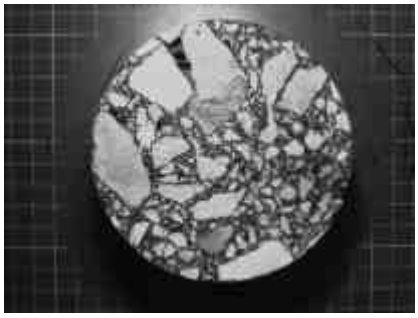

05-1941 Top

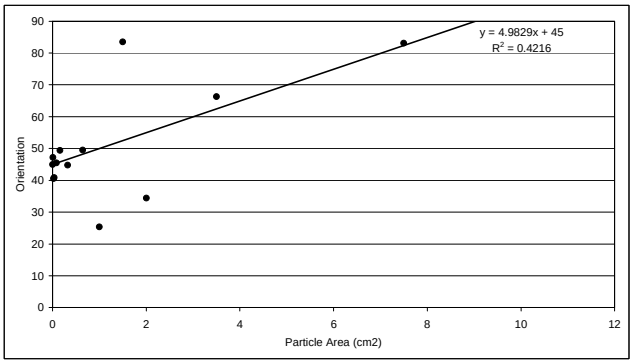

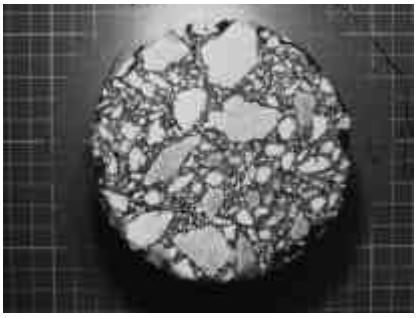

05-1941 Bottom

Vibratory compacted specimens (*D* = 150 mm Computer trimmed all particles)

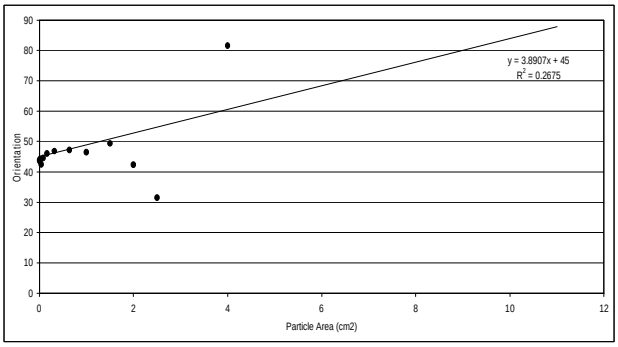

05-1930-Top

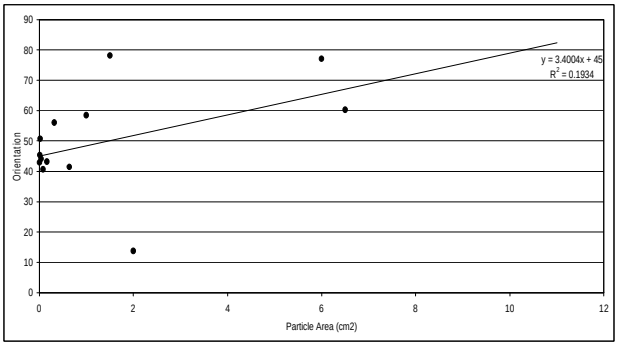

05-1930-Bottom

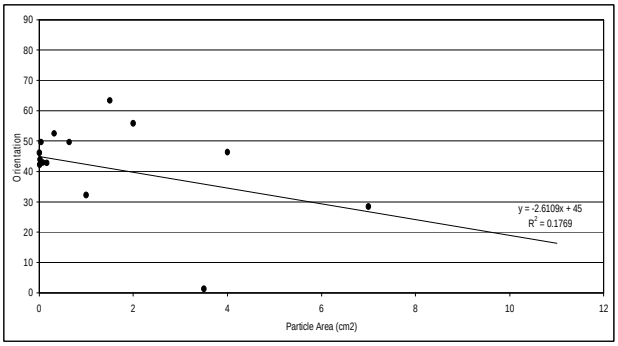

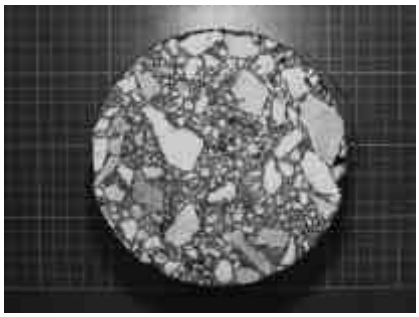

05-1931-Top

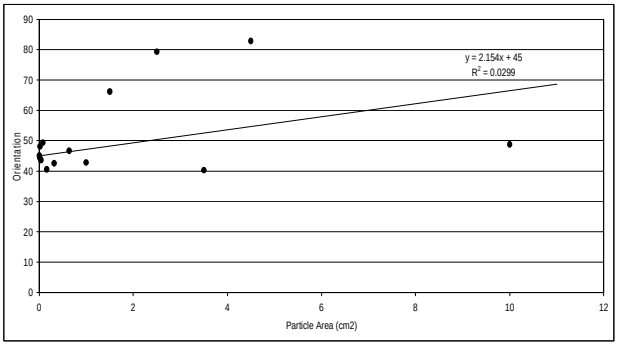

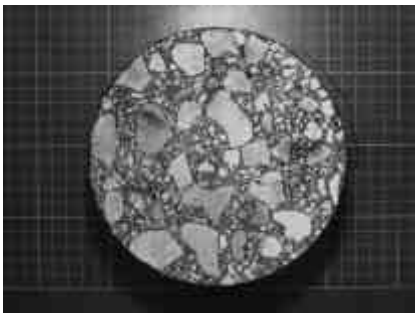

05-1931-Bottom

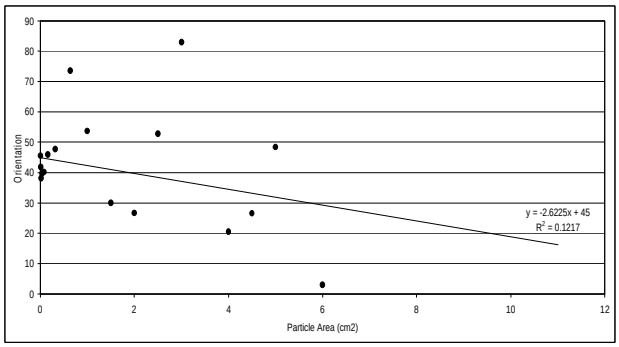

05-1932 Top

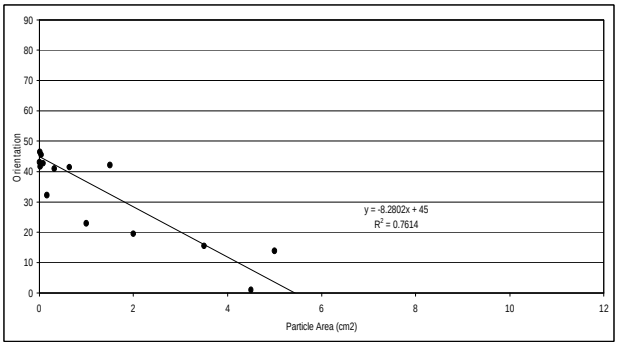

05-1932 Bottom

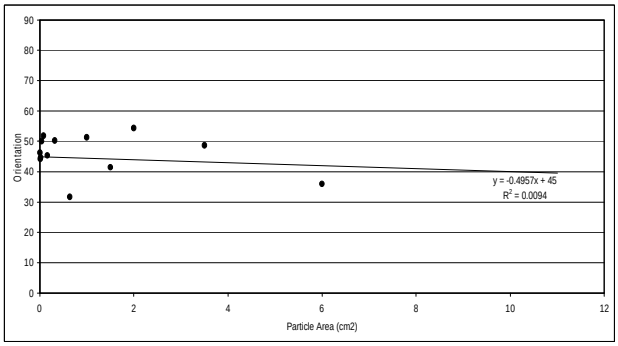

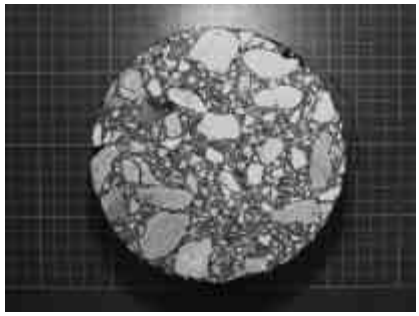

05-1933 Top

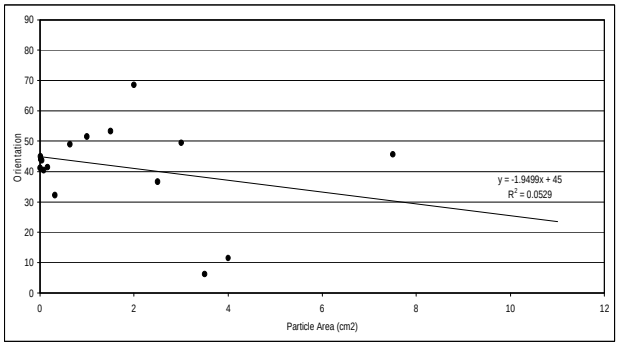

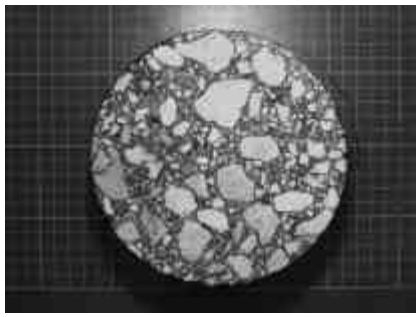

05-1933 Bottom

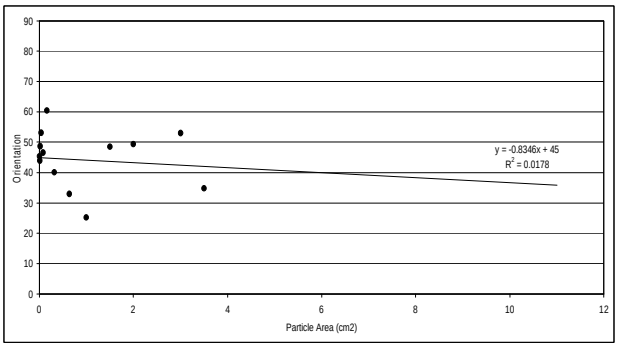

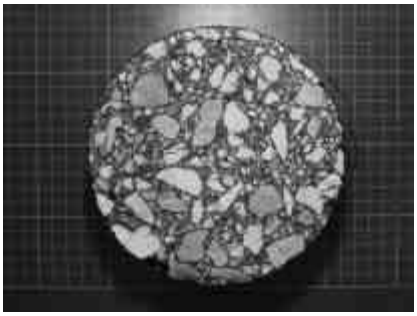

05-1934 Top

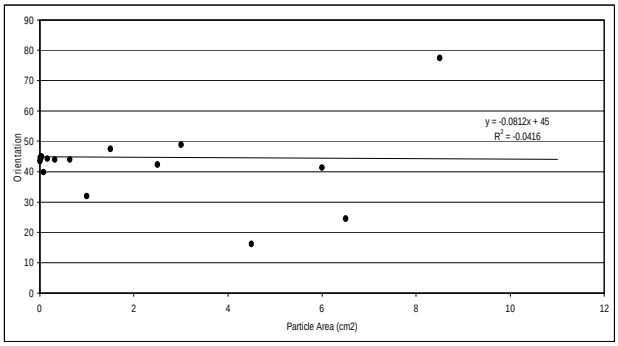

05-1934 Bottom

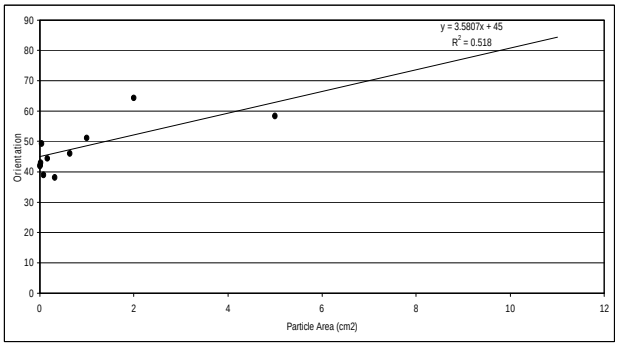

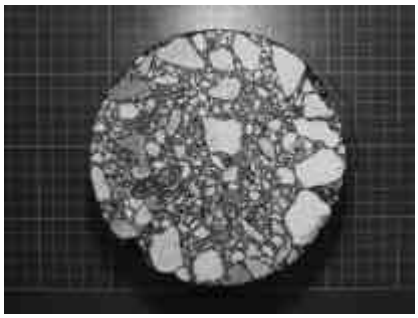

05-1935 Top

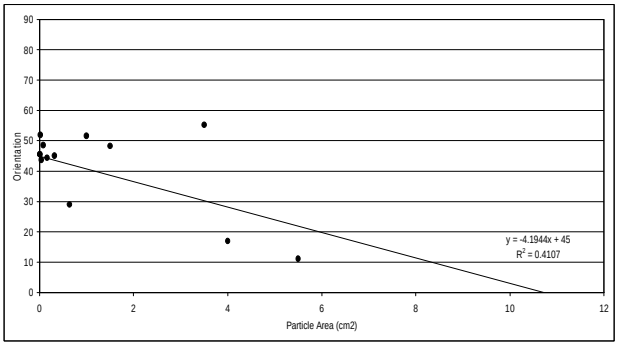

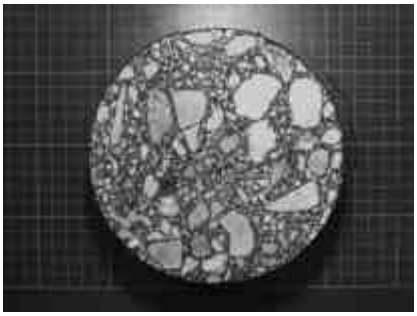

05-1935 Bottom

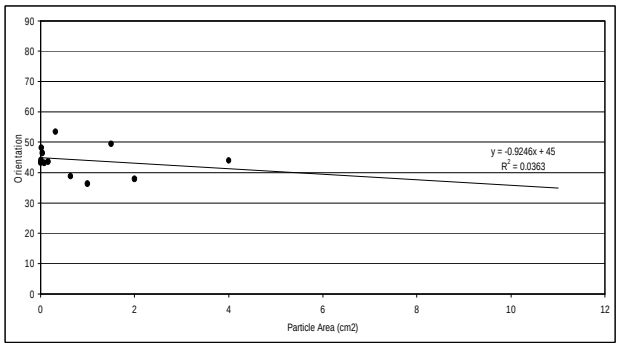

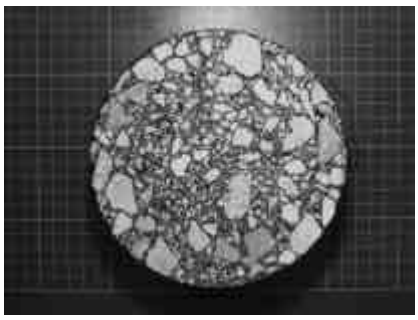

05-1936 Top

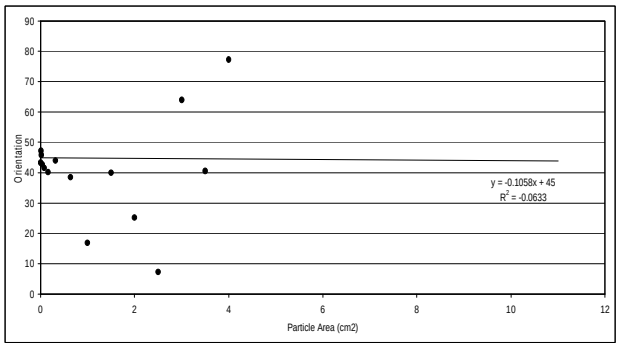

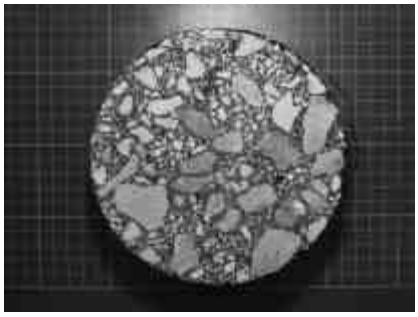

05-1936 Bottom

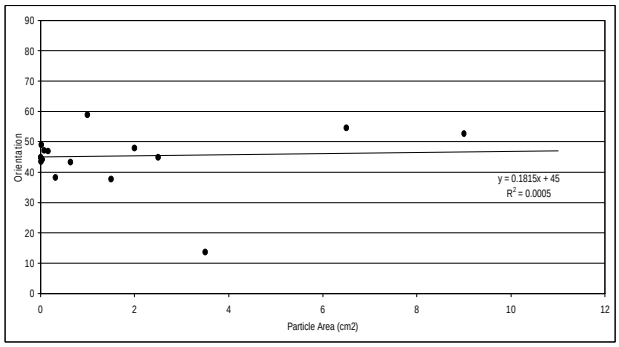

05-1937 Top

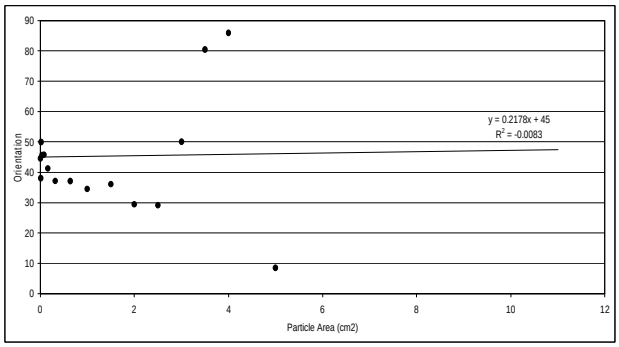

05-1937 Bottom

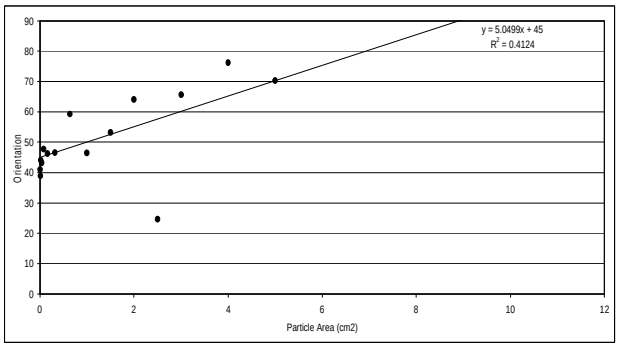

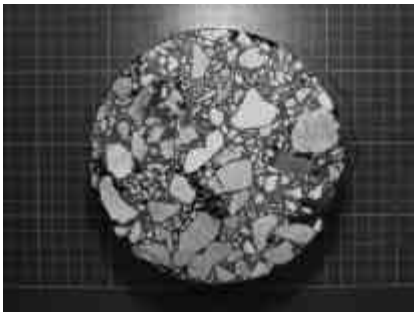

05-1938 Top

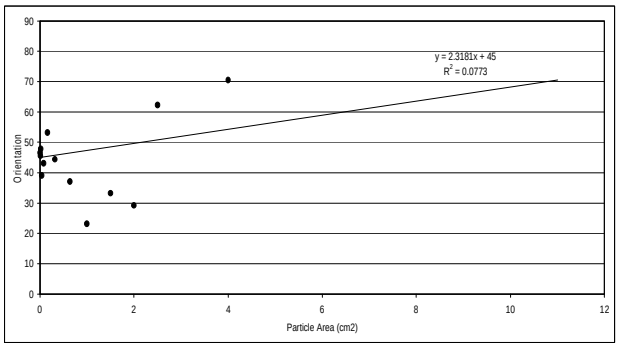

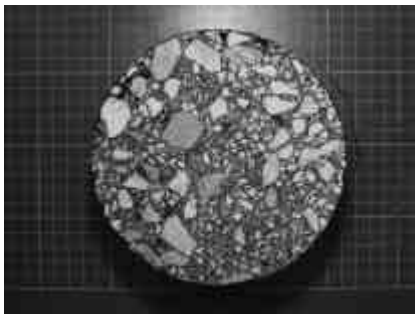

05-1938 Bottom

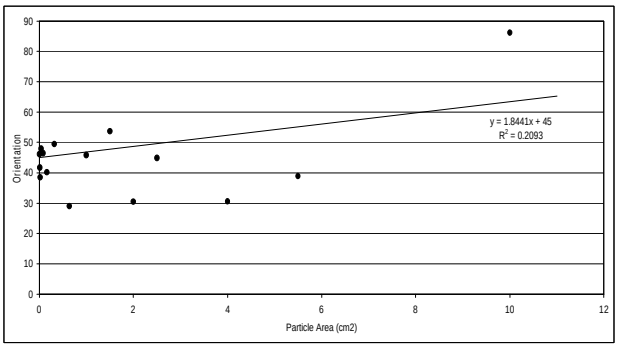

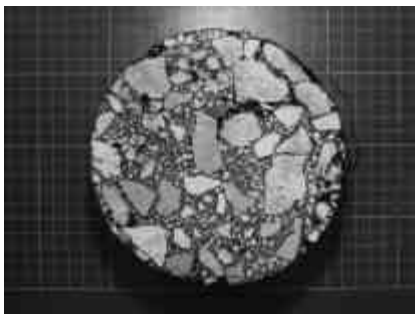

05-1939 Top

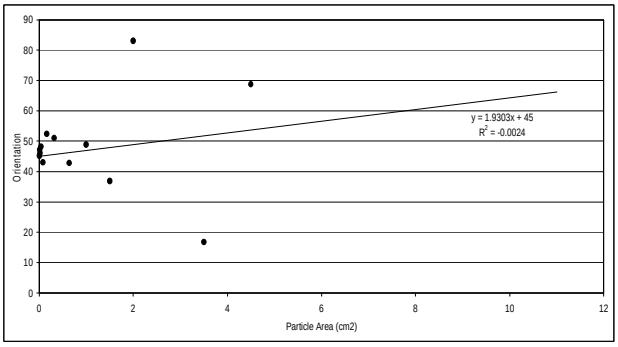

05-1939 Bottom

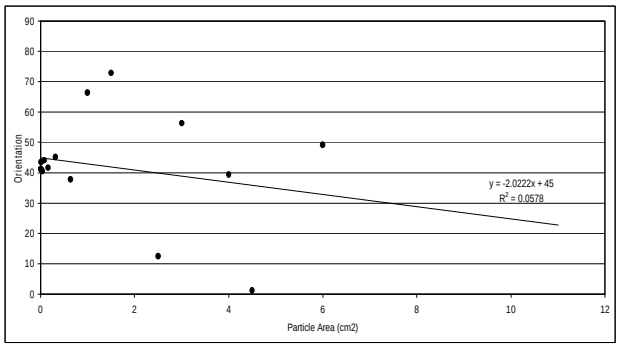

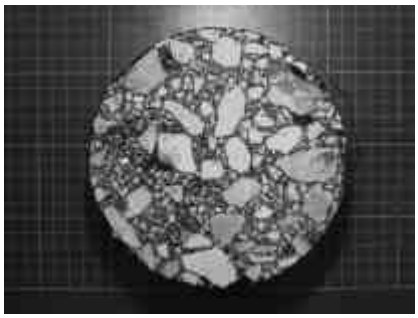

05-1940 Top

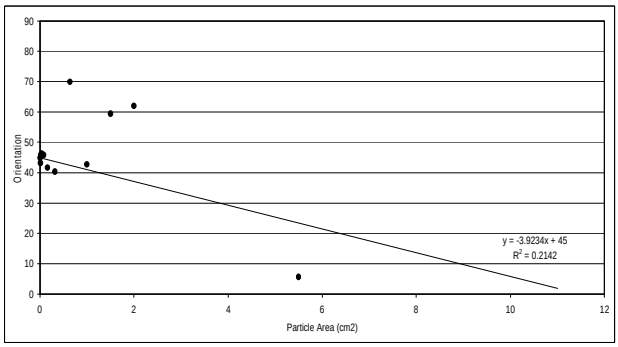

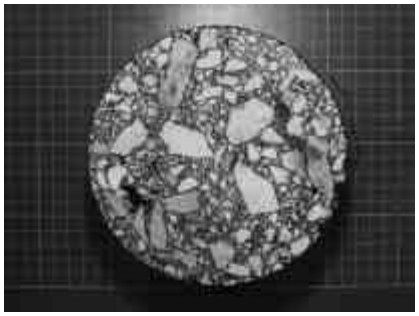

05-1940 Bottom

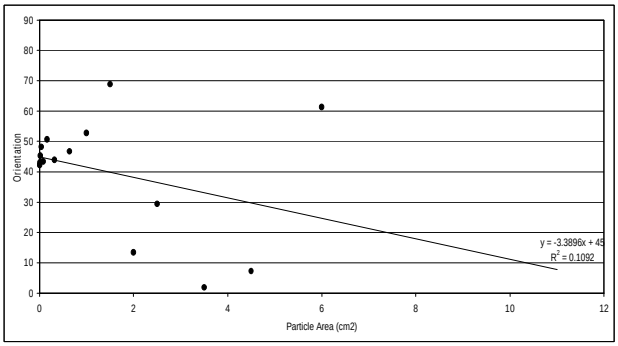

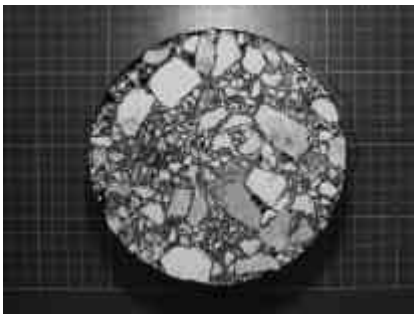

05-1941 Top

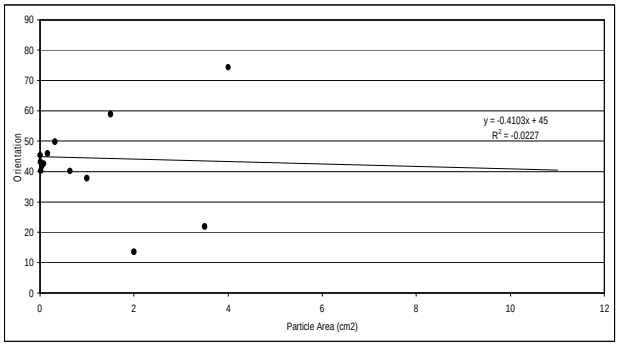

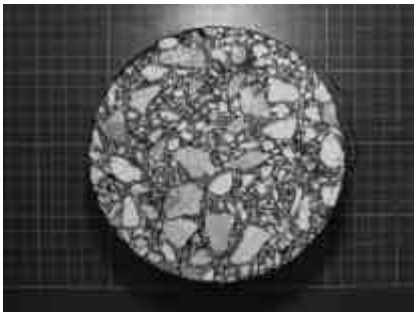

05-1941 Bottom

Slab compacted specimens Z-direction (*D* = 100 mm All particles)

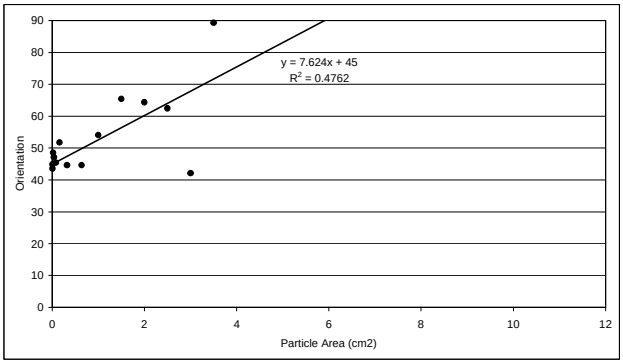

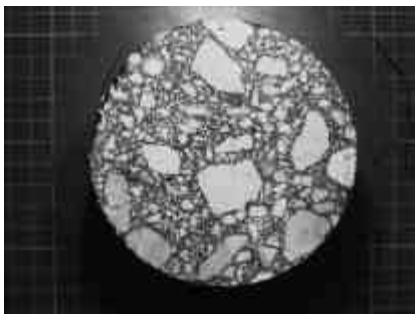

05-2103-A Top

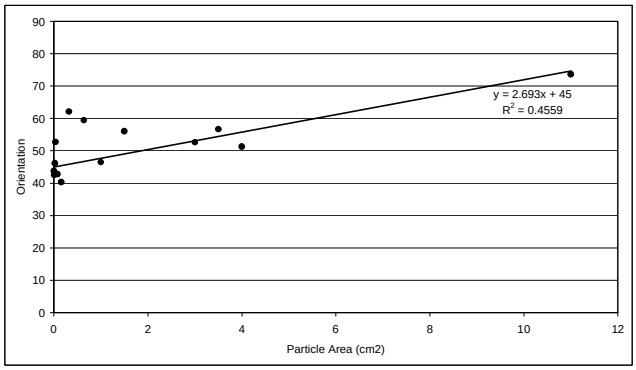

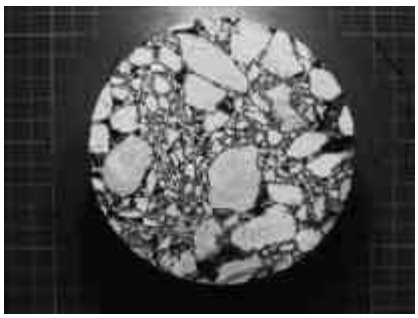

05-2103-A Bottom

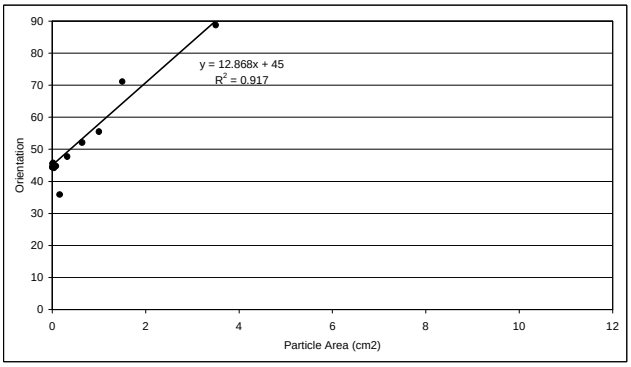

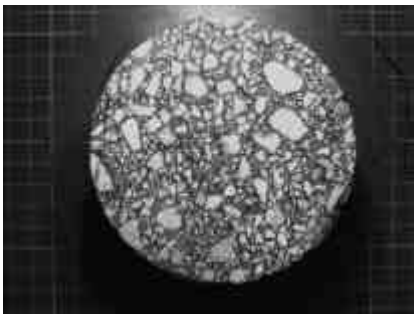

05-2104-B Top

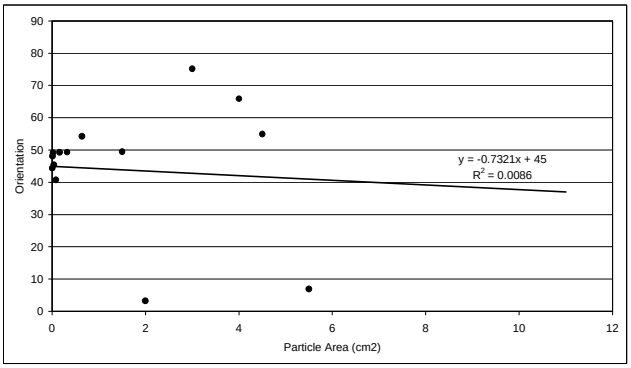

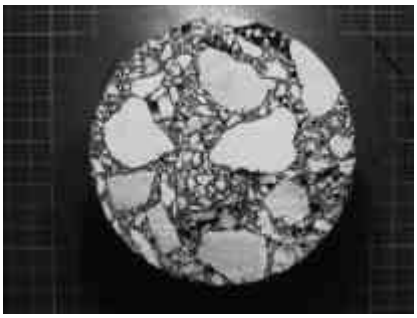

05-2104-B Bottom

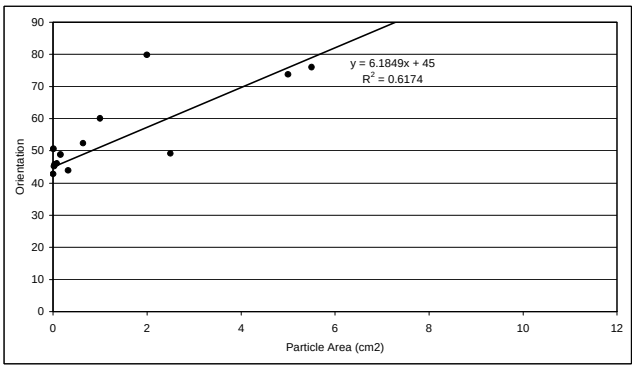

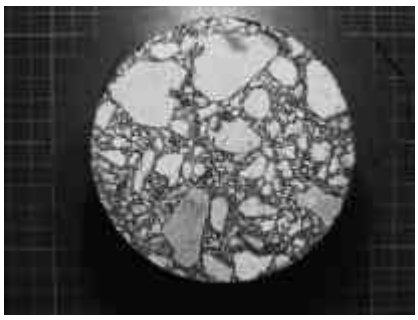

05-2105-C Top

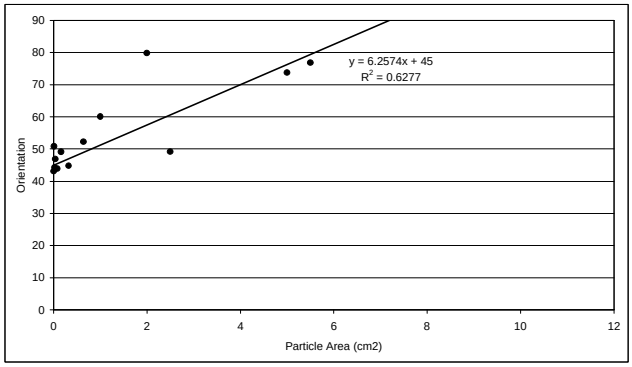

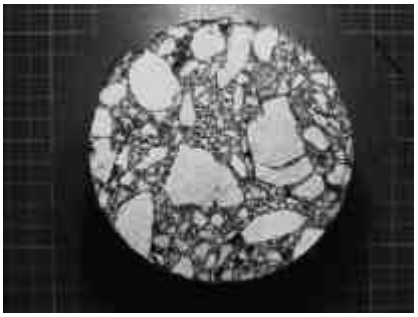

05-2105-C Bottom

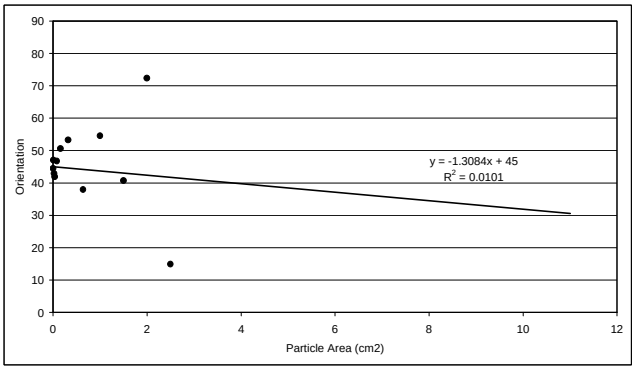

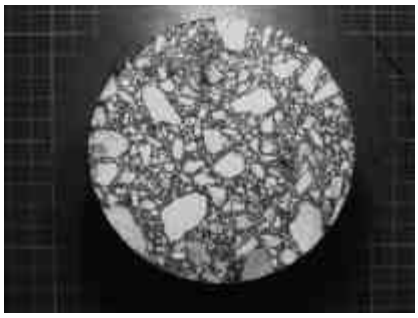

05-2106-D Top

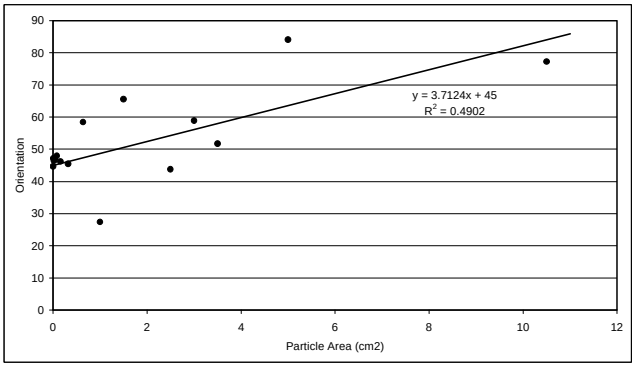

05-2106-D Bottom

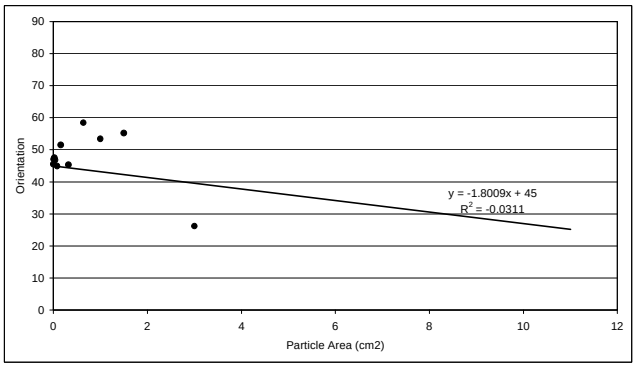

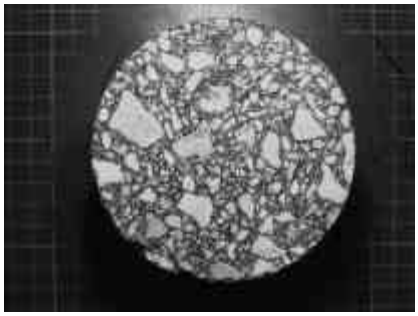

05-2107-A Top

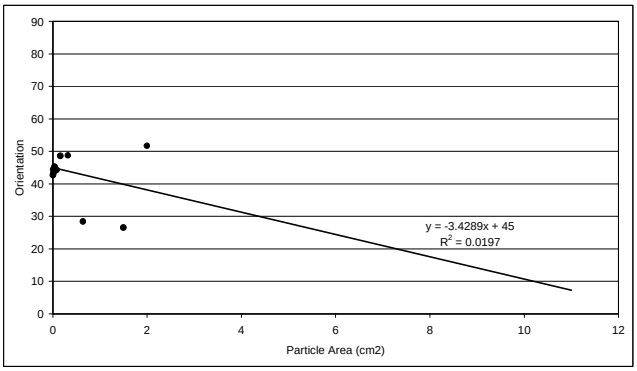

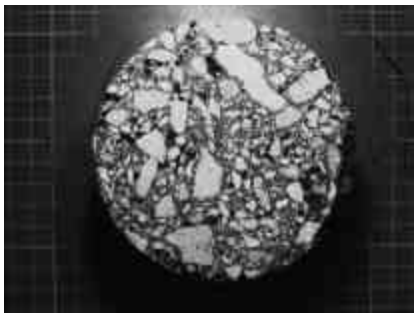

05-2107-A Bottom

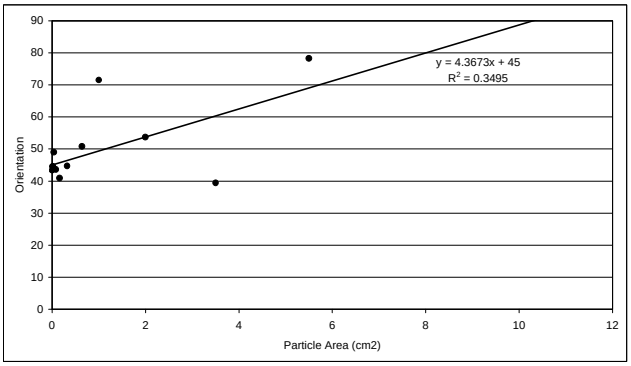

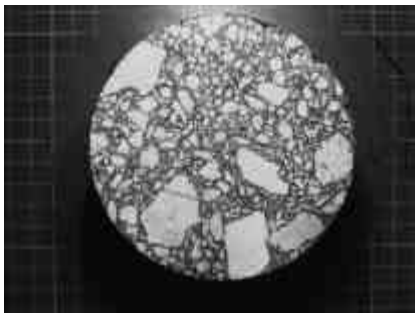

05-2108-B Top

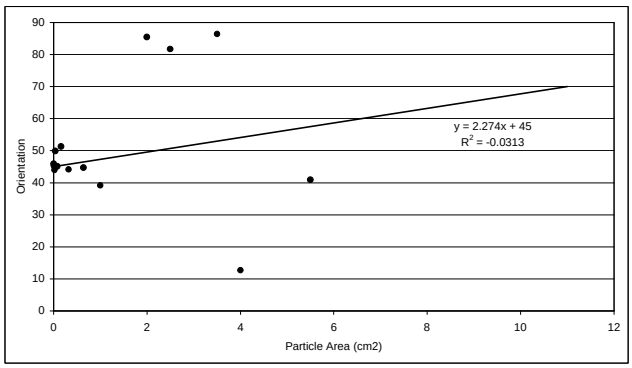

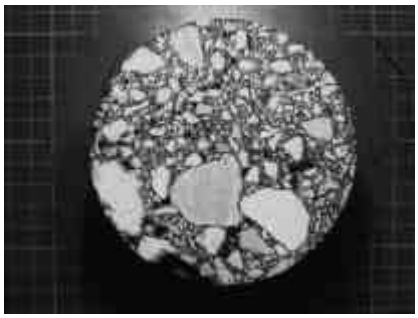

05-2108-B Bottom

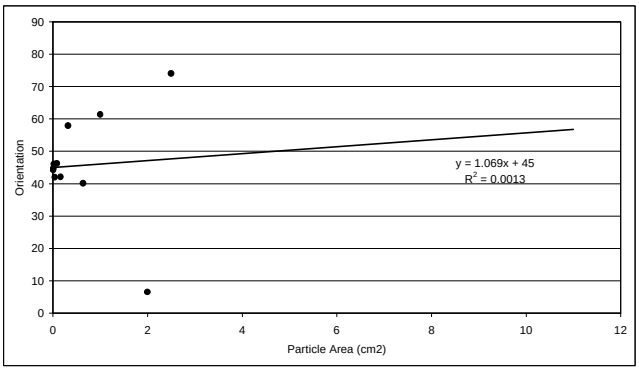

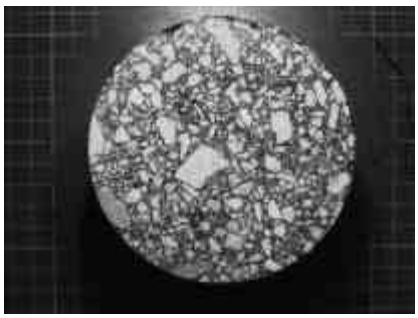

05-2109-C Top

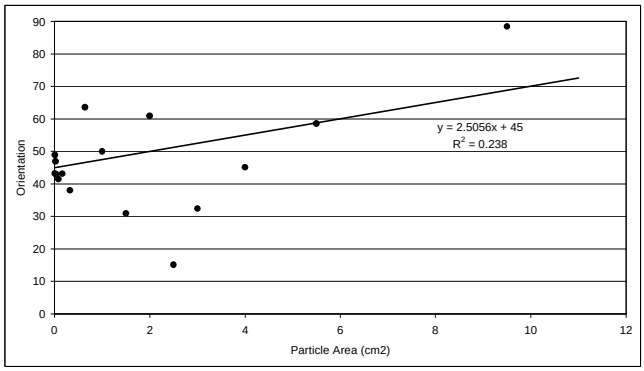

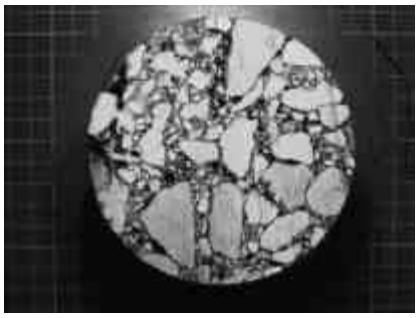

05-2109-C Bottom

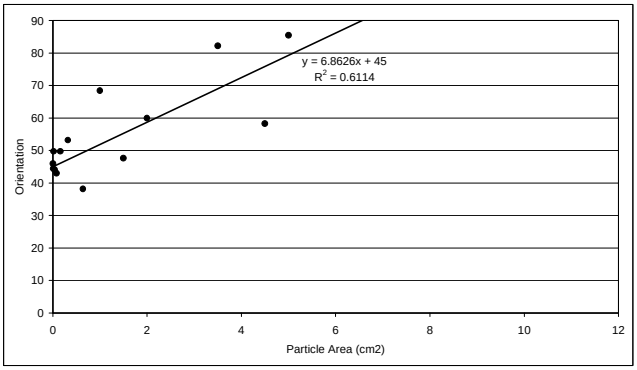

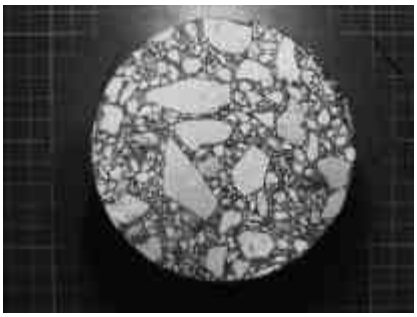

05-2110-D Top

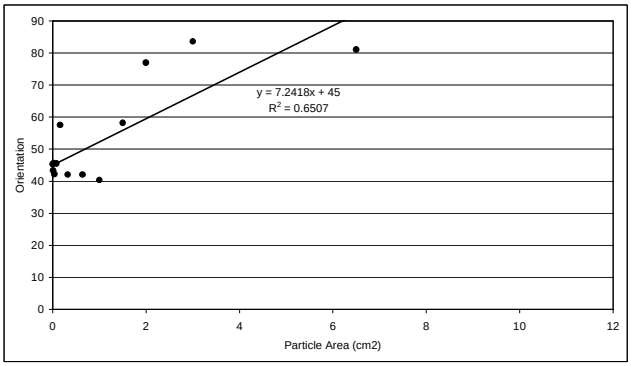

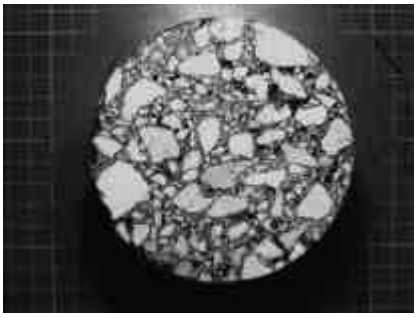

05-2110-D Bottom

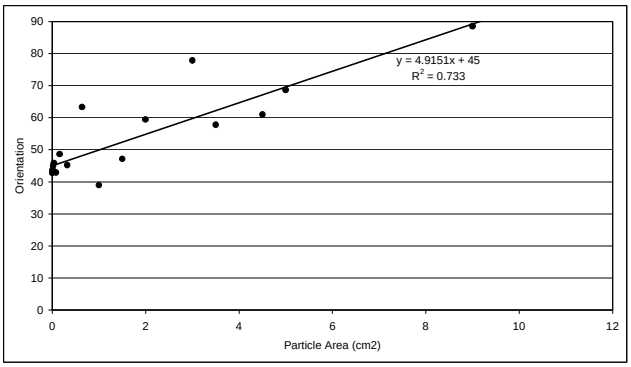

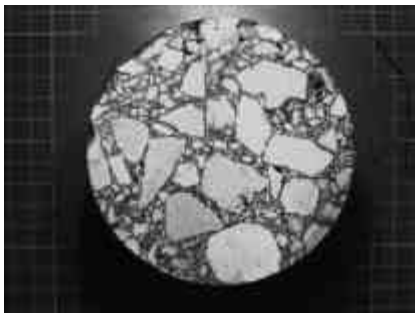

05-2111-A Top

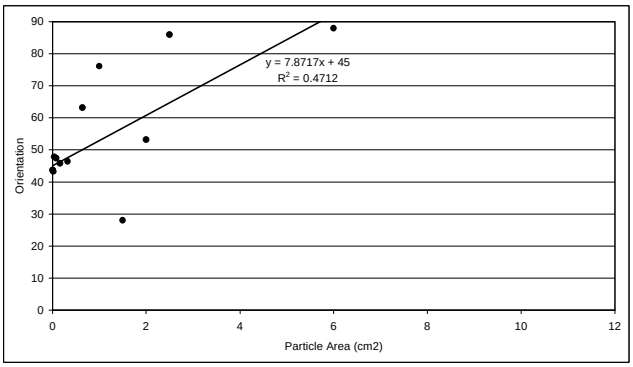

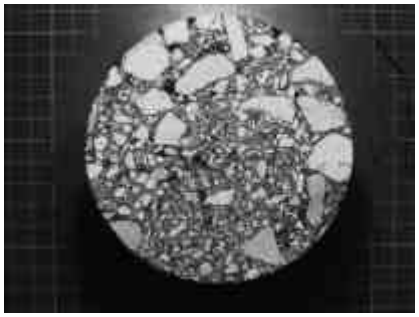

05-2111-A Bottom

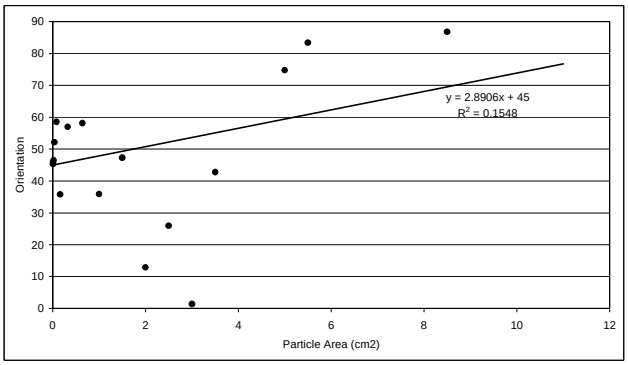

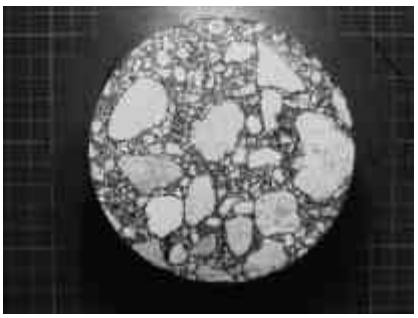

05-2112-B Top

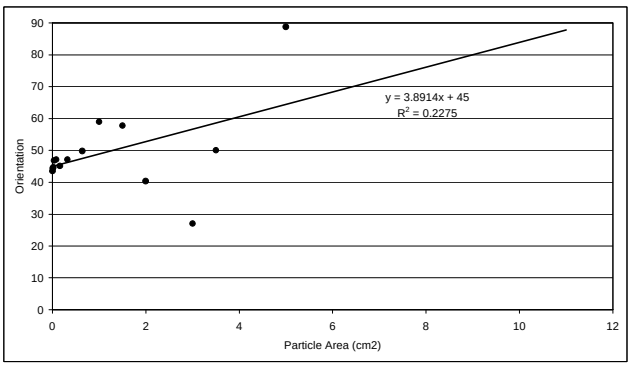

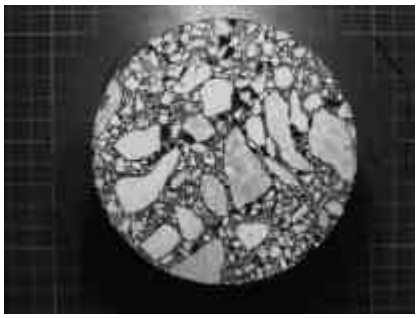

05-2112-B Bottom

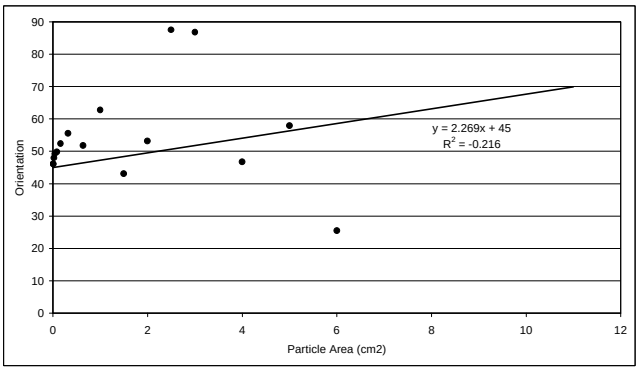

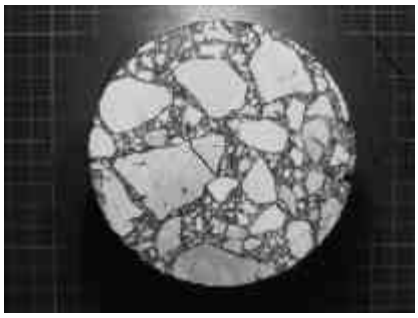

05-2113-C Top

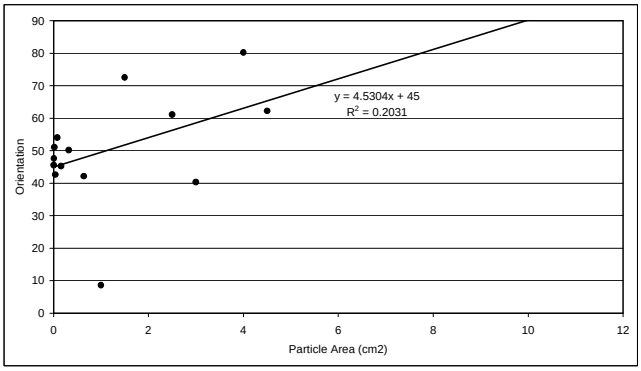

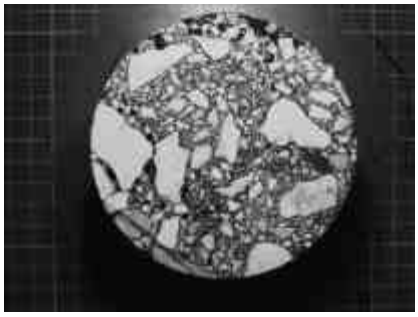

05-2113-C Bottom

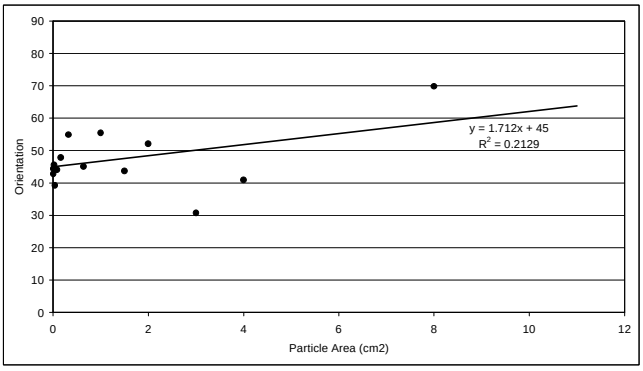

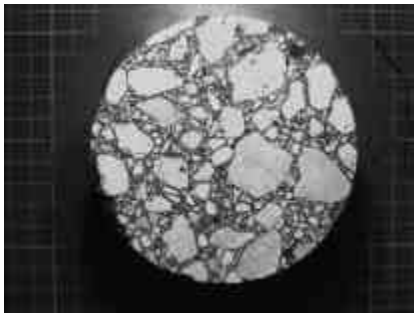

05-2114-D Top

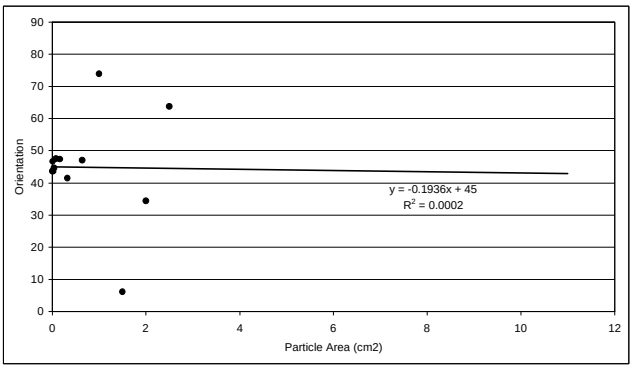

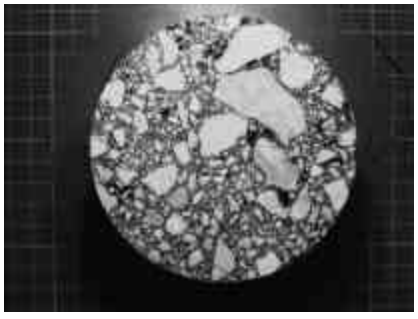

05-2114-D Bottom

Slab compacted specimens Y-direction (*D* = 100 mm All particles)

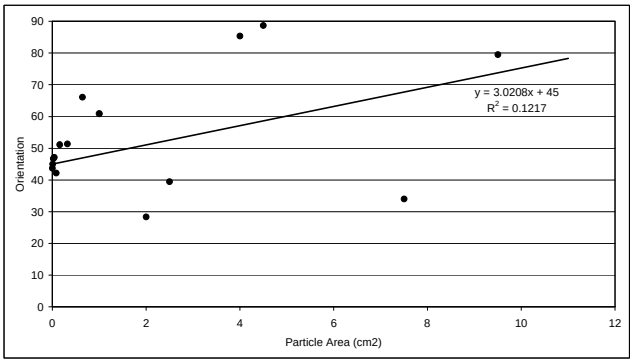

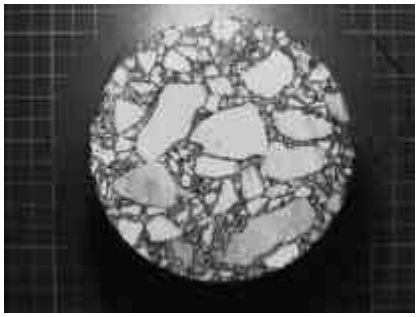

05-2083-A Top

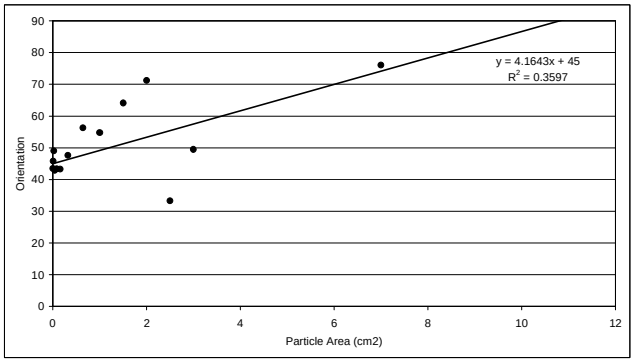

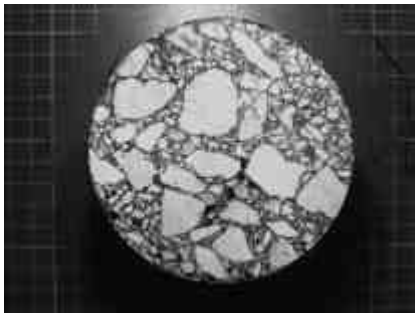

05-2083-A Bottom

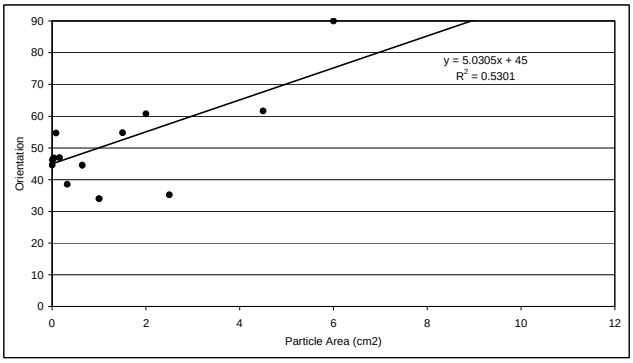

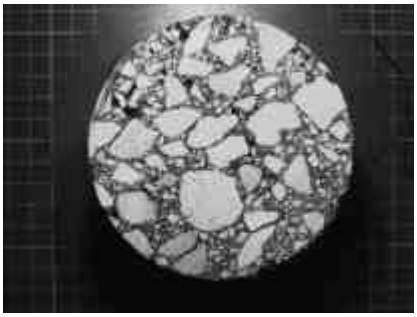

05-2084-A Top

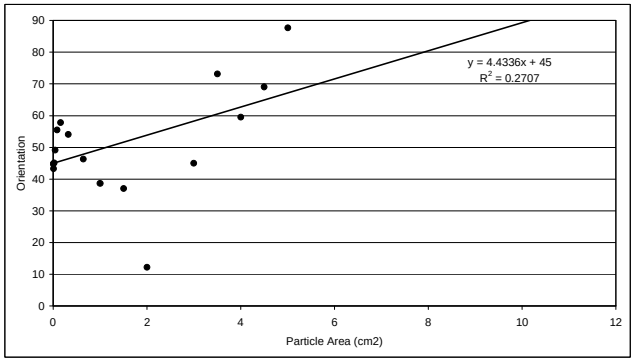

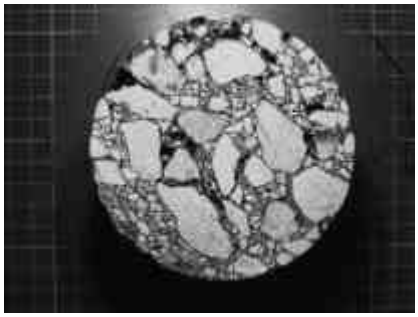

05-2084-A Bottom

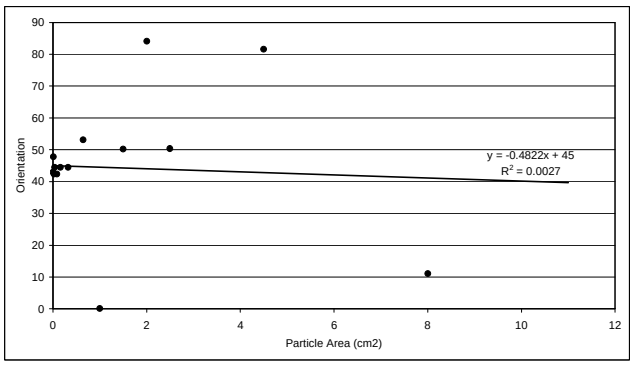

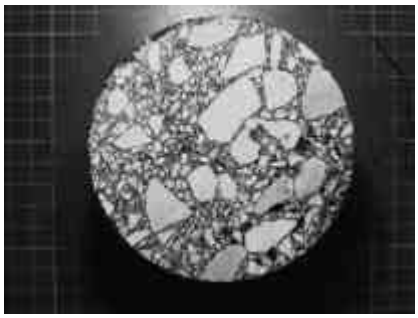

05-2085-A Top

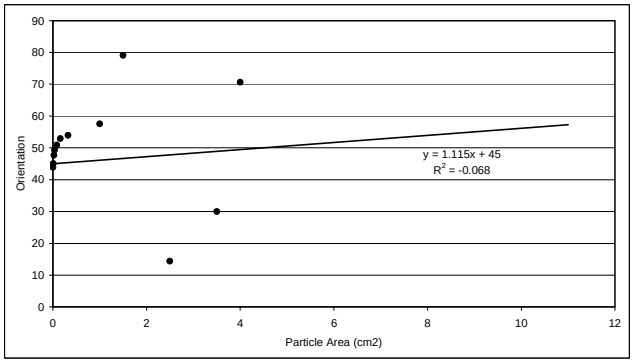

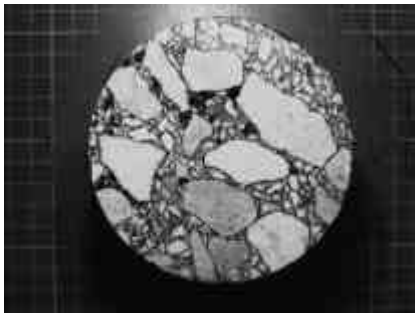

05-2085-A Bottom

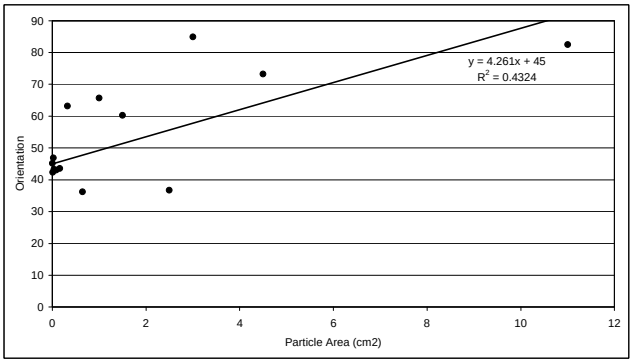

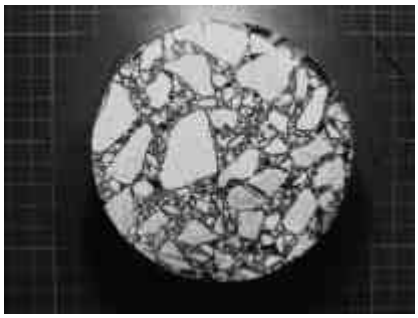

05-2086-B Top

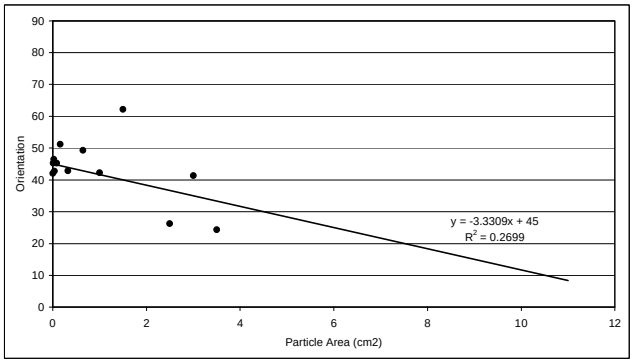

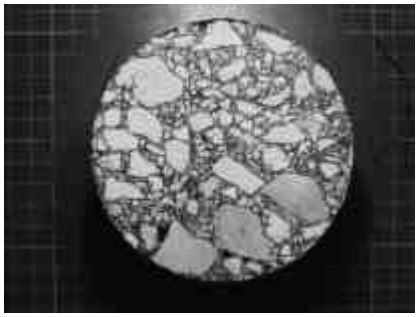

05-2086-B-Bottom

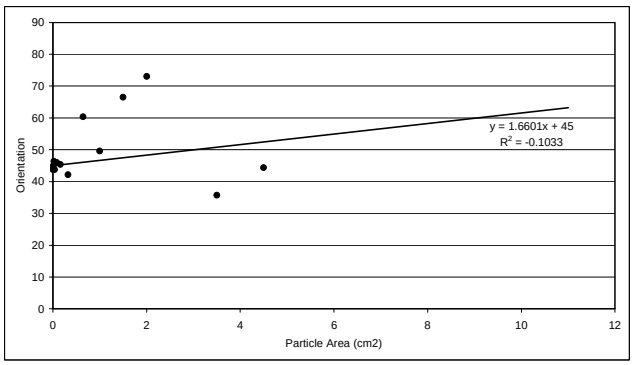

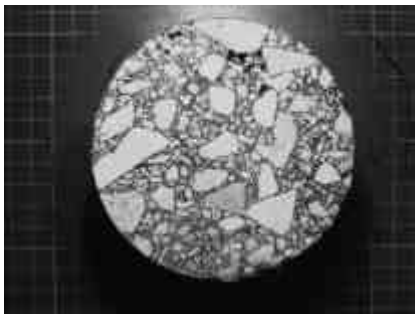

05-2087-B-Top

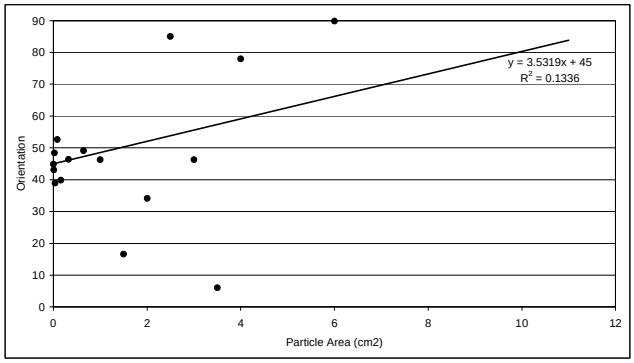

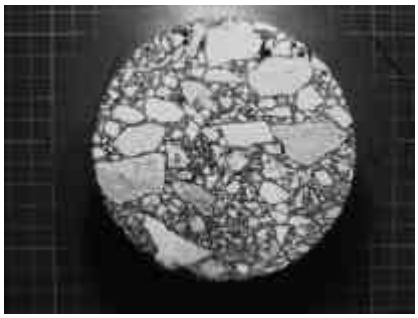

05-2087-B-Bottom

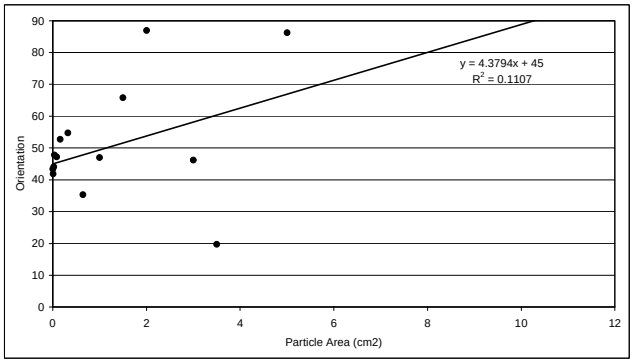

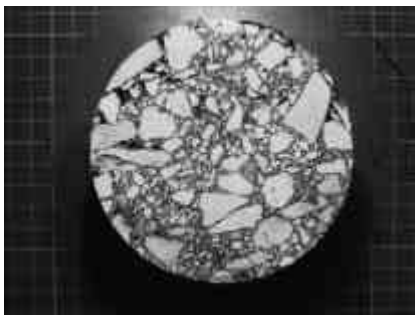

05-2088-B-Top

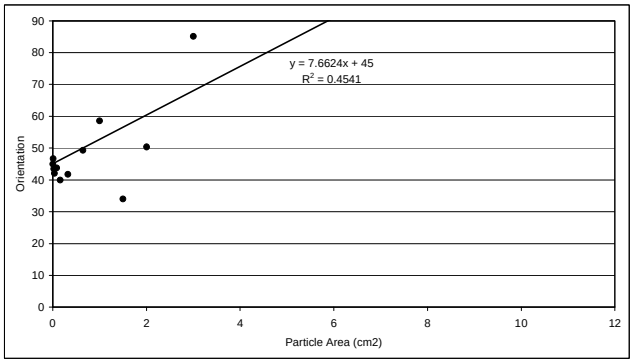

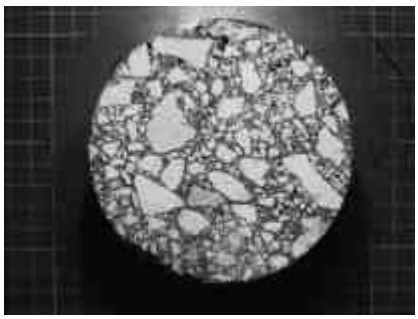

05-2088-B-Bottom

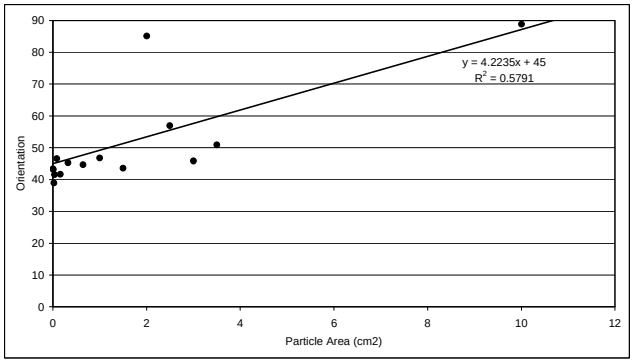

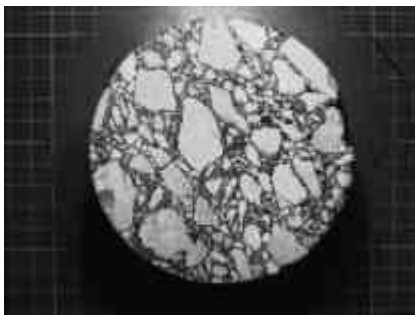

05-2089-A-Top

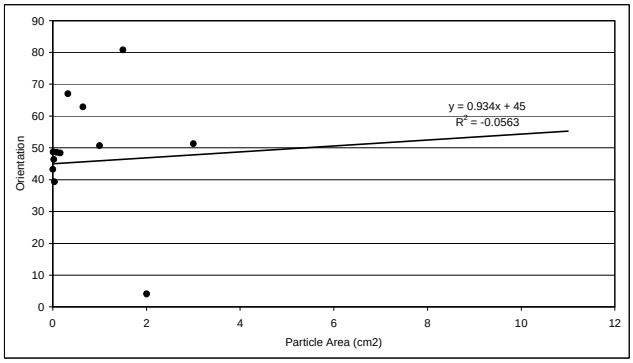

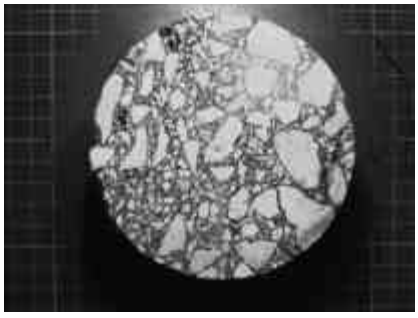

05-2089-A-Bottom

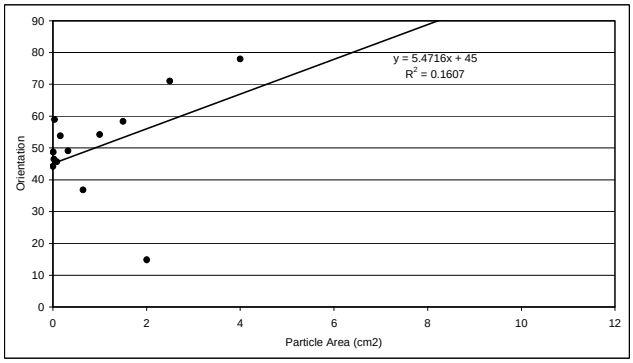

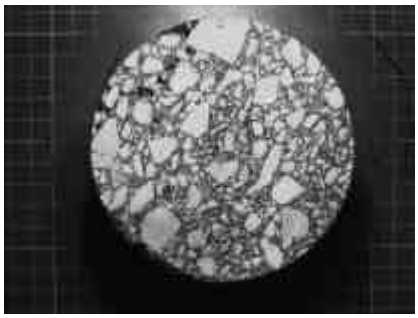

05-2090-A-Top

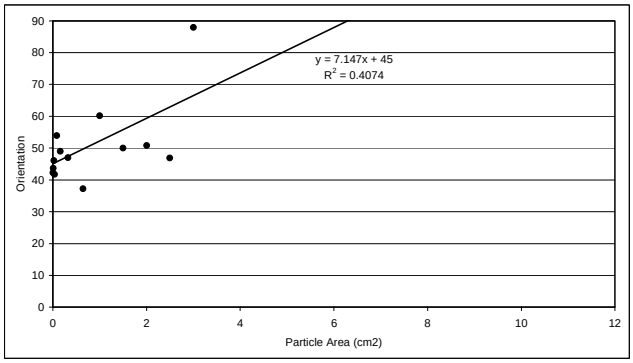

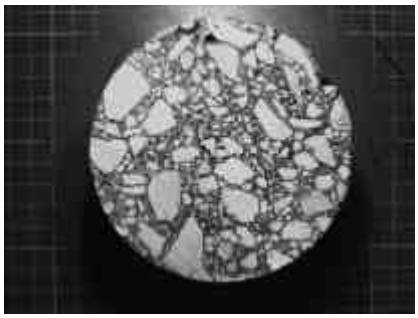

05-2090-A-Bottom

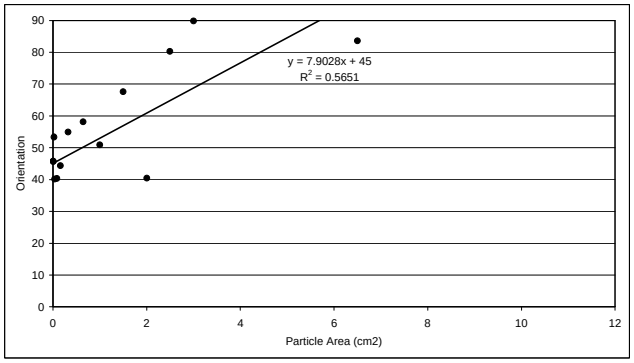

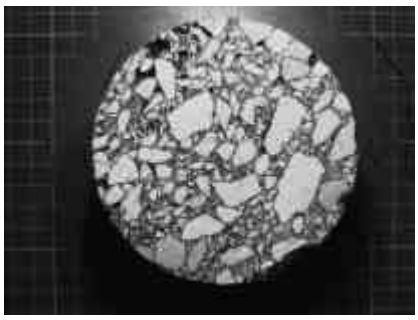

05-2091-A-Top

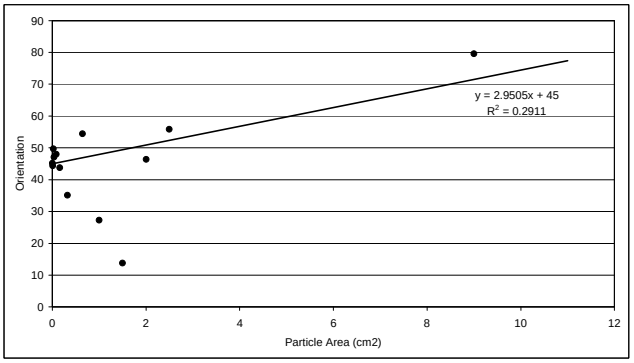

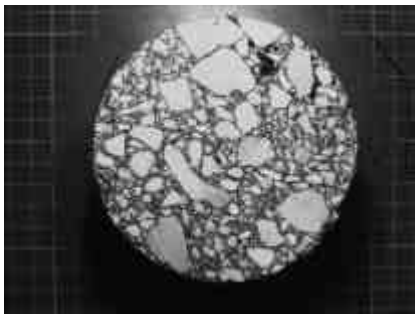

05-2091-A-Bottom

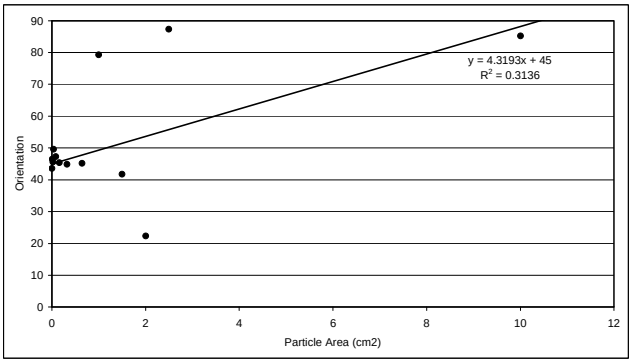

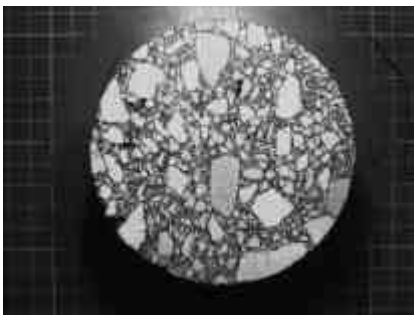

05-2092-B-Top

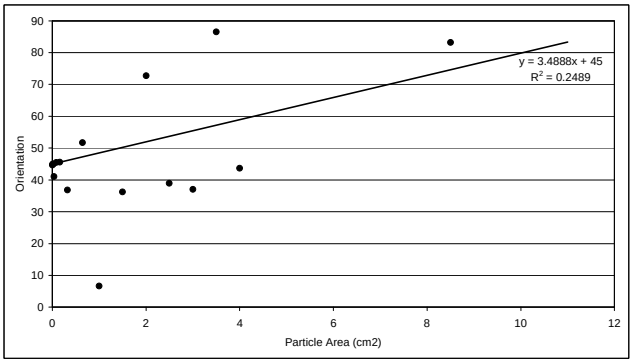

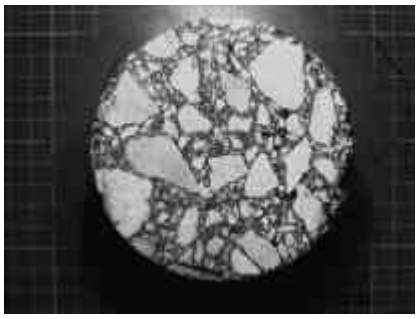

05-2092-B-Bottom

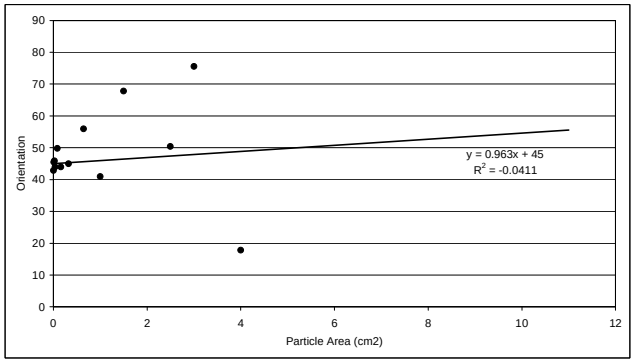

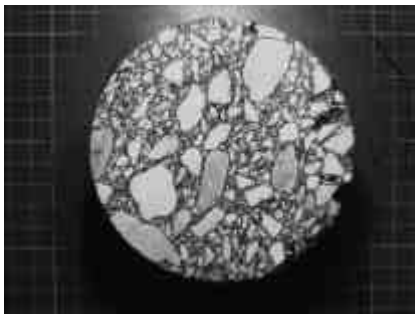

05-2093-B-Top

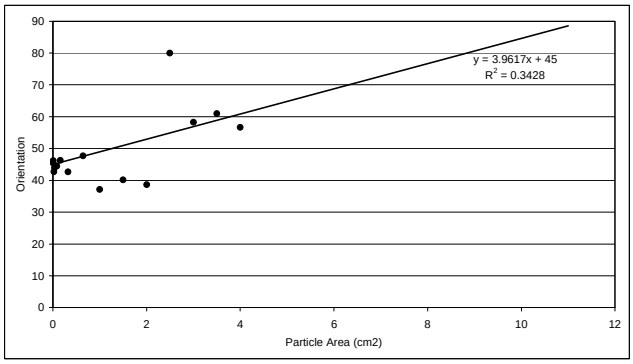

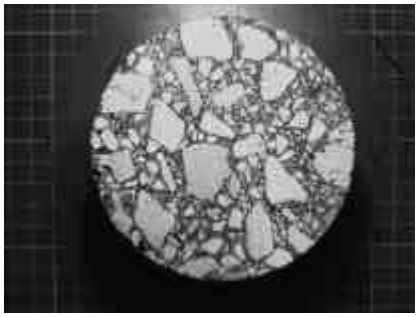

05-2093-B-Bottom

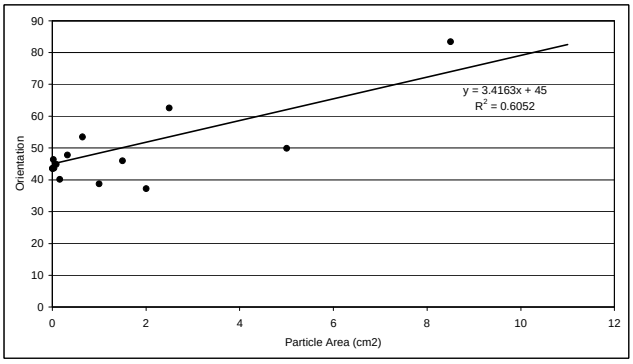

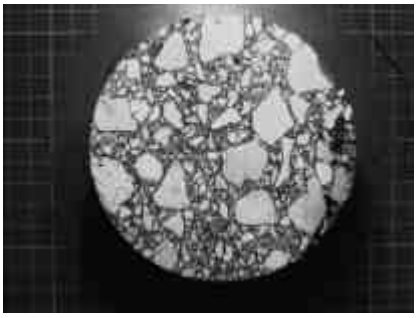

05-2094-B-Top

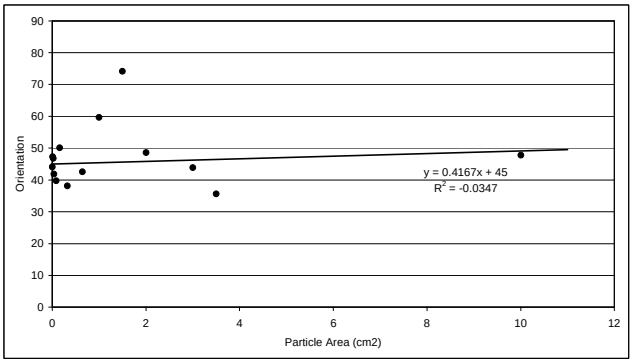

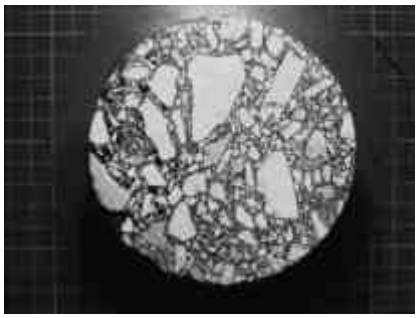

05-2094-B-Bottom

Slab compacted specimens X-direction (*D* = 100 mm All particles)

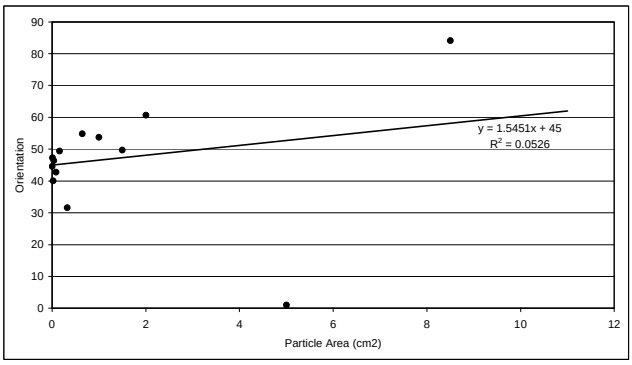

05-2115-A Top

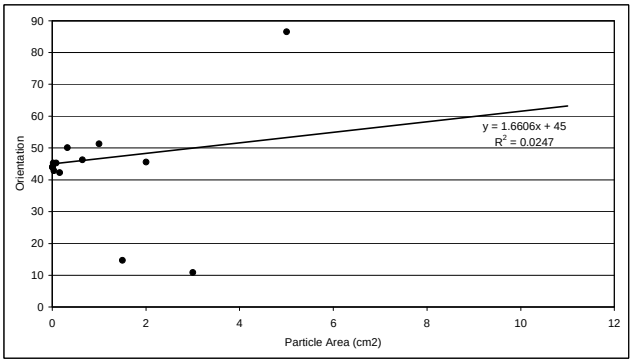

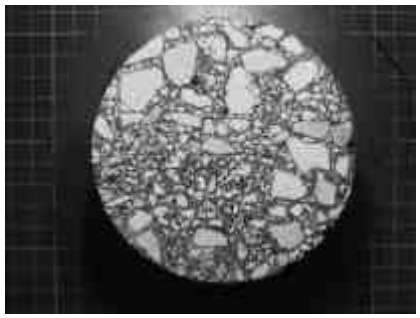

05-2115-A Bottom

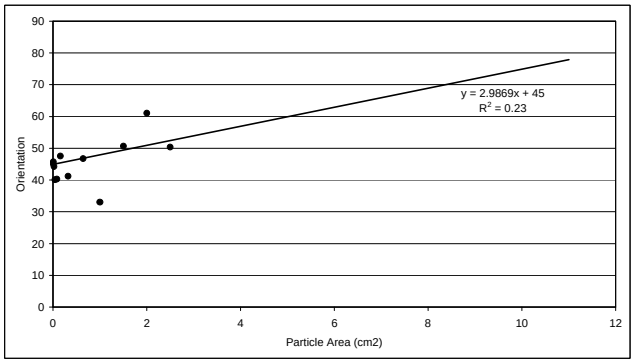

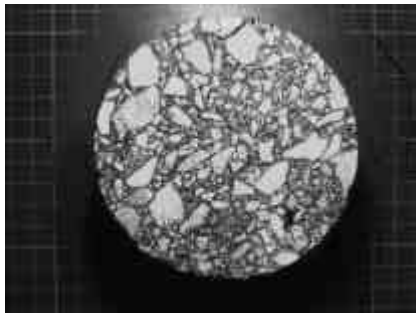

05-2116-A Top

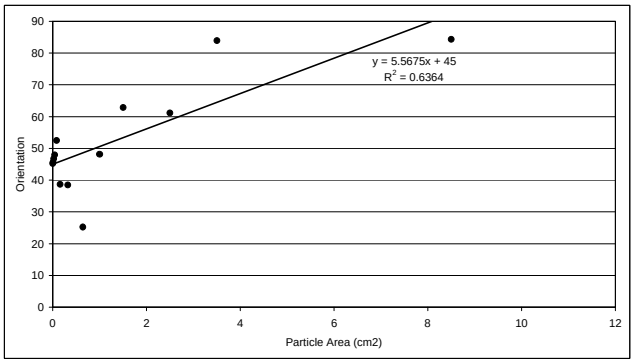

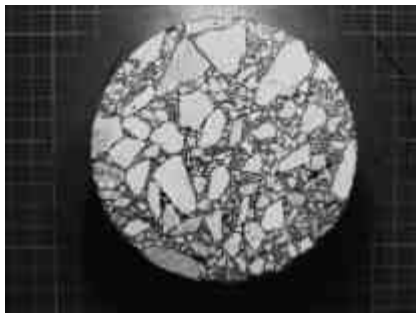

05-2116-A Bottom

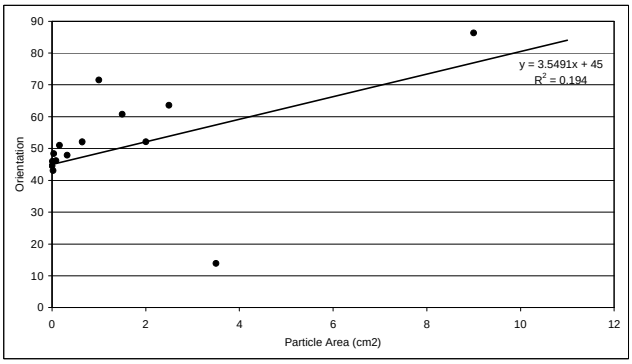

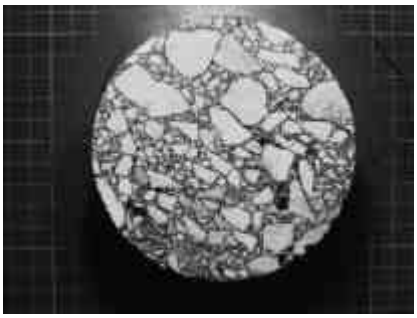

05-2117-A Top

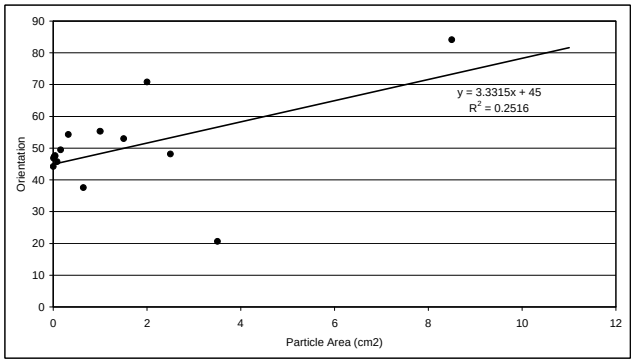

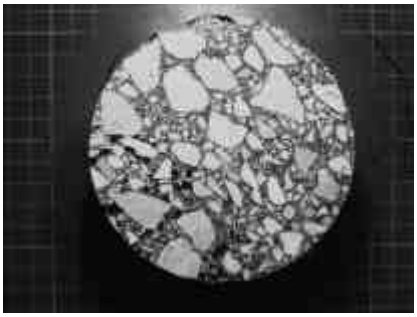

05-2117-A Bottom

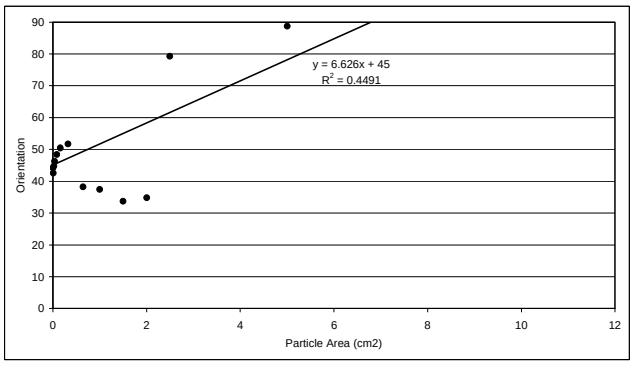

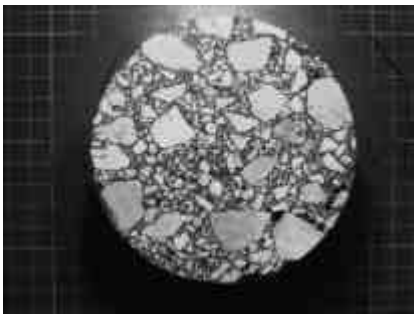

05-2118-B Top

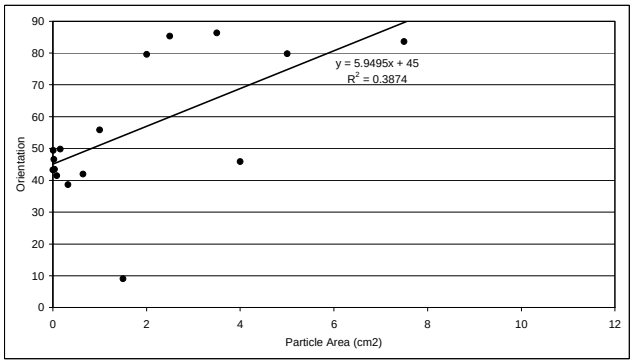

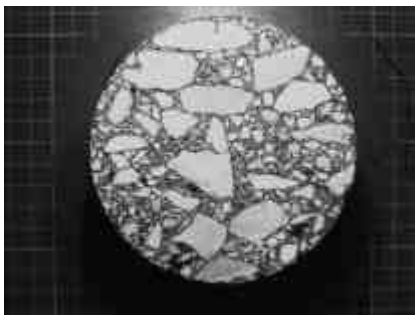

05-2118-B-Bottom

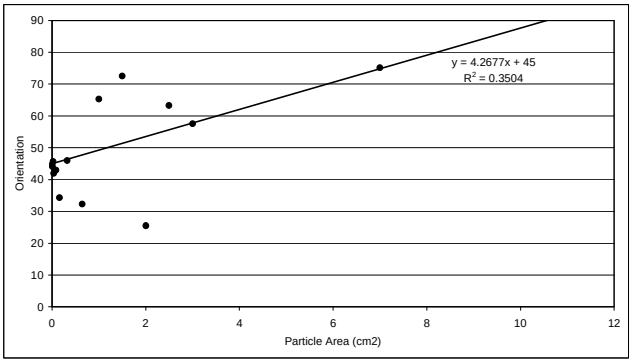

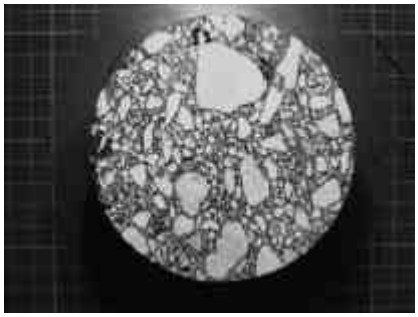

05-2119-B-Top

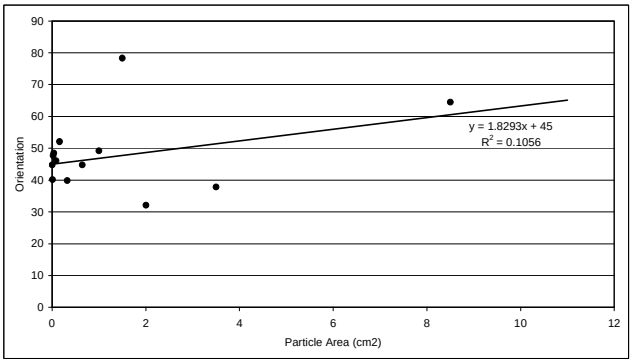

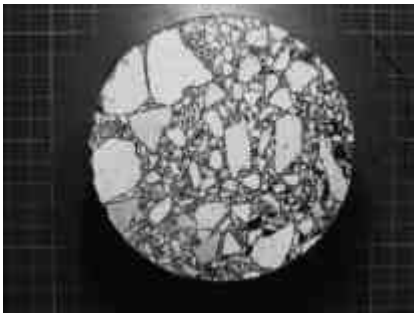

05-2119-B-Bottom

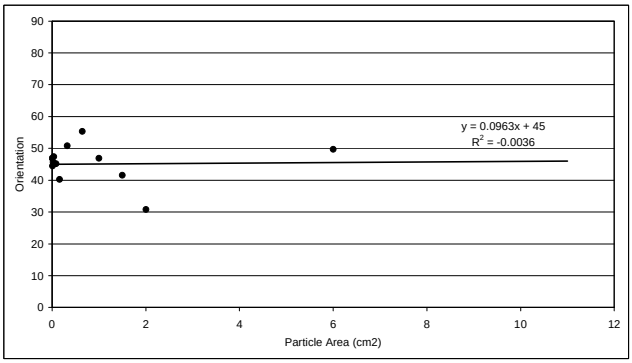

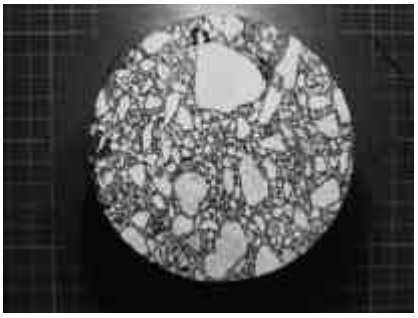

05-2120-B-Top

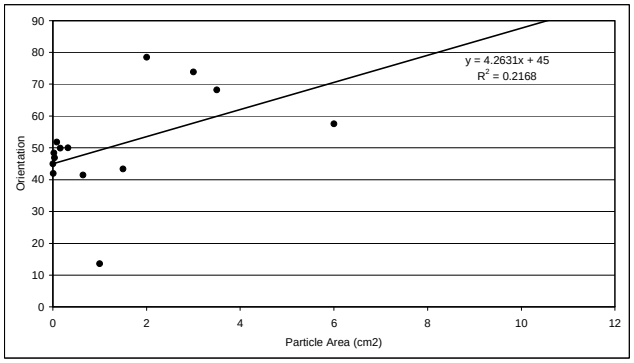

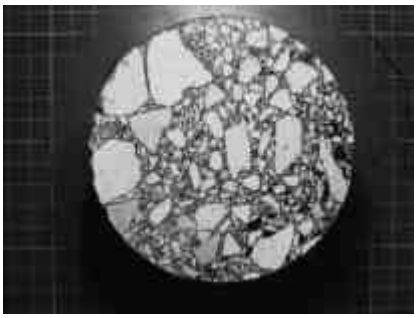

05-2120-B-Bottom

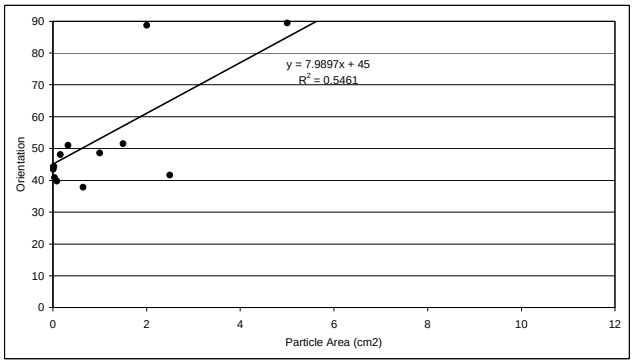

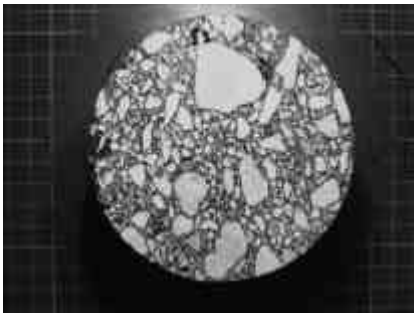

05-2121-A-Top

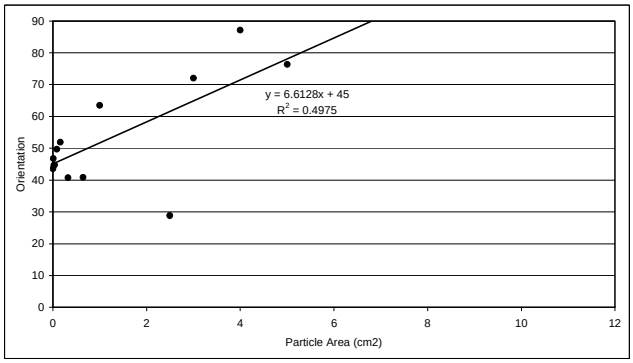

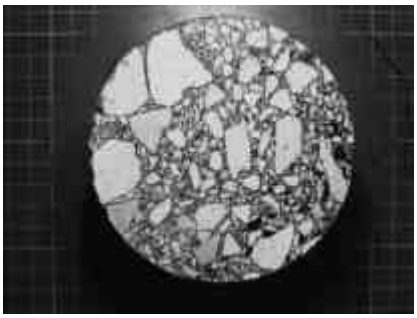

05-2121-A-Bottom

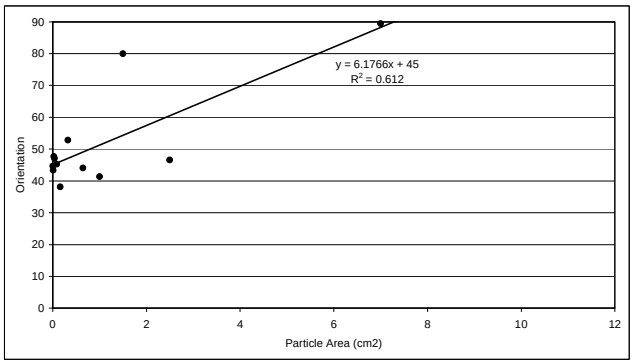

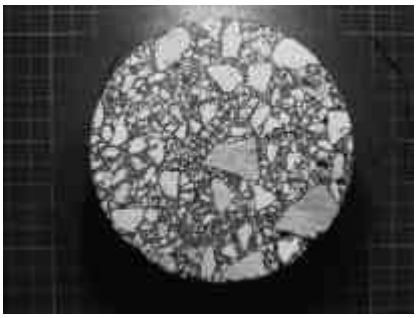

05-2122-A-Top

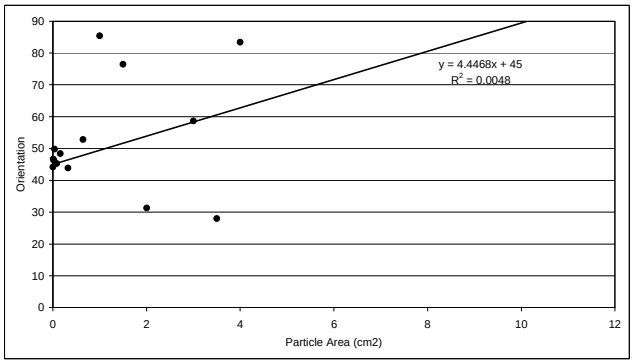

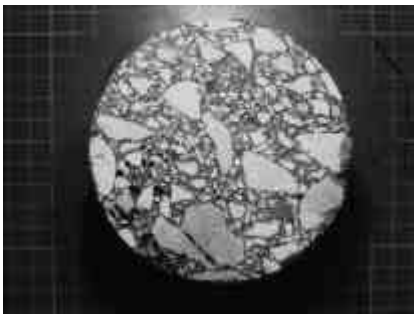

05-2122-A-Bottom

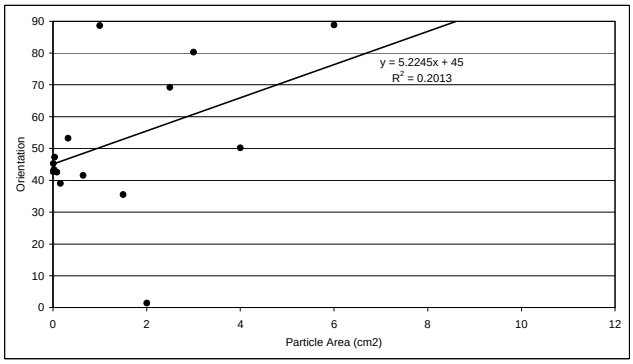

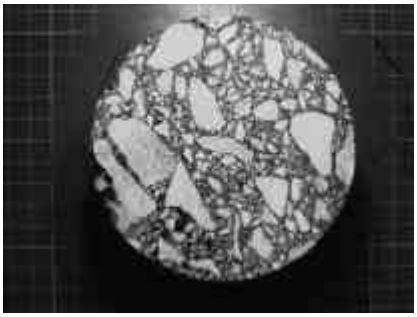

05-2123-A-Top

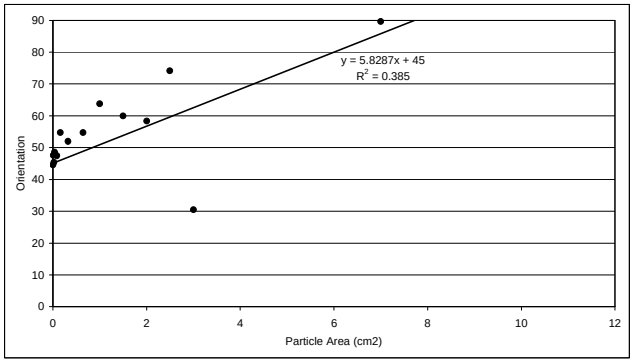

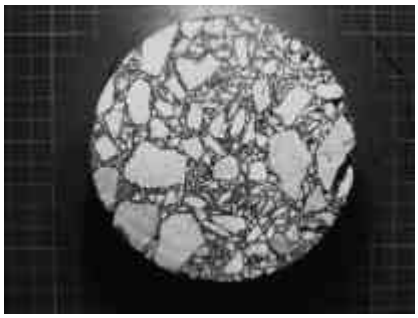

05-2123-A-Bottom

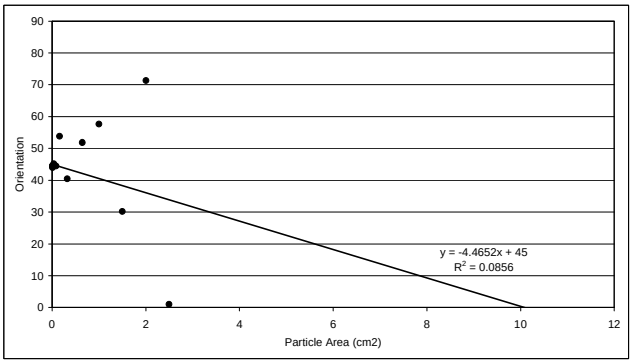

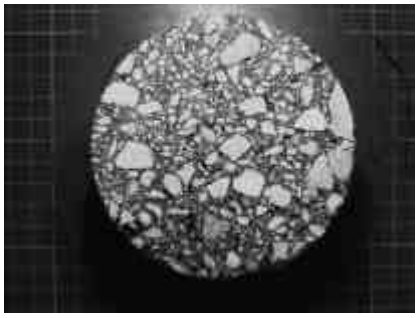

05-2124-B-Top

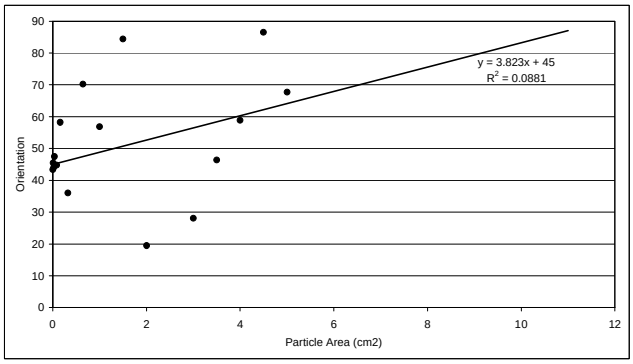

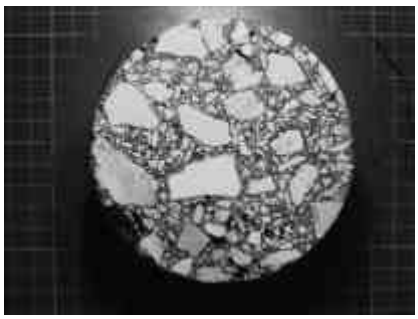

05-2124-B-Bottom

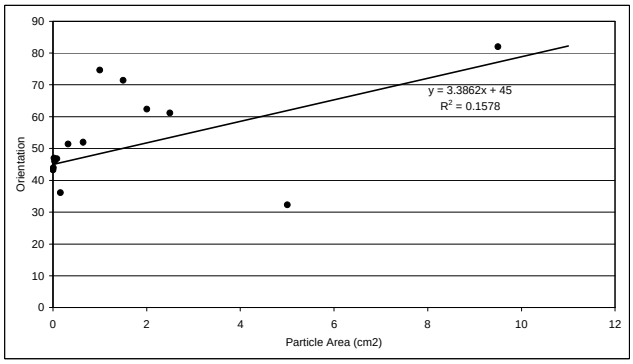

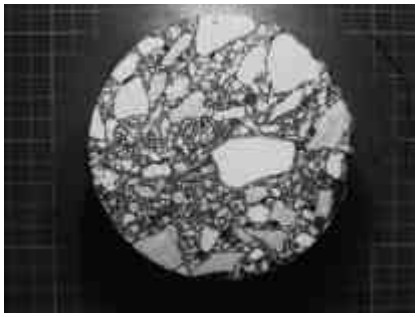

05-2125-B-Top

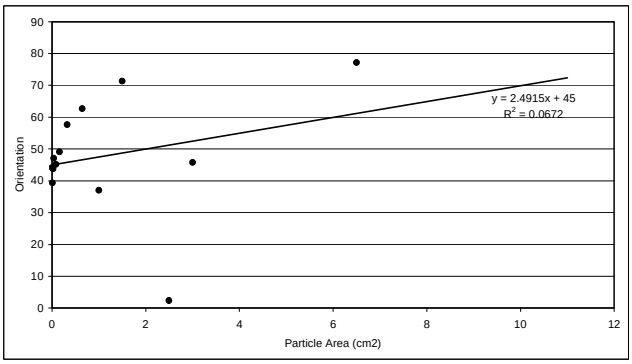

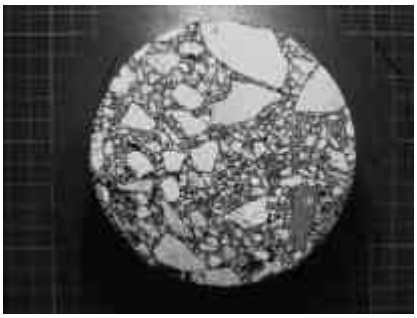

05-2125-B-Bottom

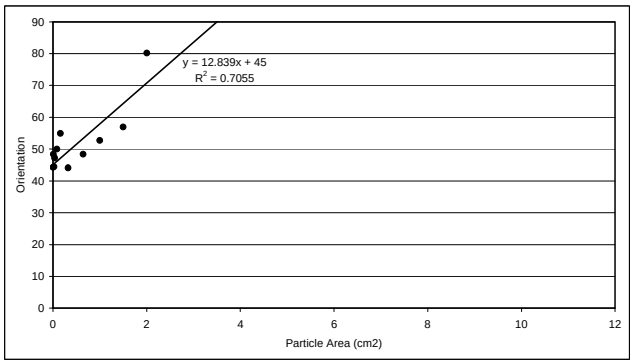

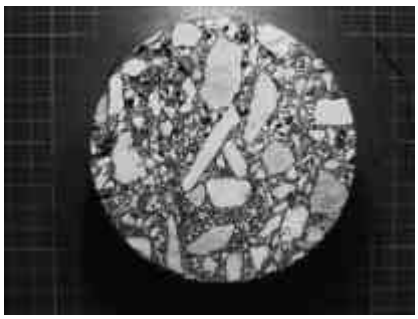

05-2126-B-Top

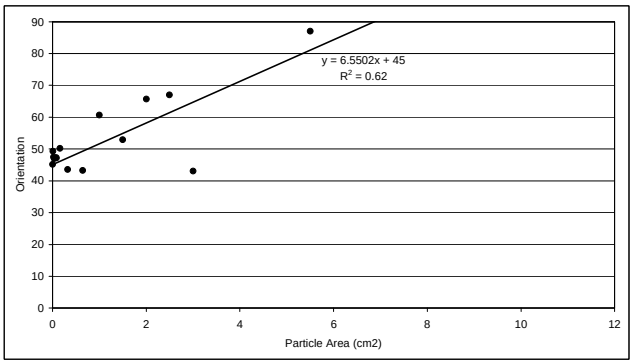

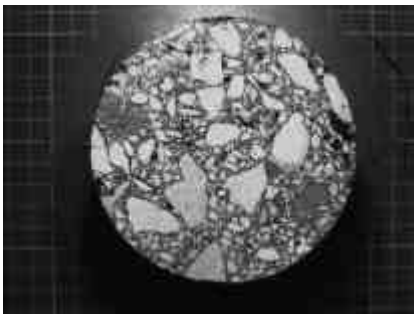

05-2126-B-Bottom